2013

The Critical Role of Mechanism-Based Models for Understanding and Predicting Liposomal Drug Loading, Binding and Release Kinetics

Sweta Modi
University of Kentucky, modisweta2@gmail.com

STUDENT AGREEMENT:

I represent that my thesis or dissertation and abstract are my original work. Proper attribution has been given to all outside sources. I understand that I am solely responsible for obtaining any needed copyright permissions. I have obtained and attached hereto needed written permission statements(s) from the owner(s) of each third-party copyrighted matter to be included in my work, allowing electronic distribution (if such use is not permitted by the fair use doctrine).

I hereby grant to The University of Kentucky and its agents the non-exclusive license to archive and make accessible my work in whole or in part in all forms of media, now or hereafter known. I agree that the document mentioned above may be made available immediately for worldwide access unless a preapproved embargo applies.

I retain all other ownership rights to the copyright of my work. I also retain the right to use in future works (such as articles or books) all or part of my work. I understand that I am free to register the copyright to my work.

REVIEW, APPROVAL AND ACCEPTANCE

The document mentioned above has been reviewed and accepted by the student's advisor, on behalf of the advisory committee, and by the Director of Graduate Studies (DGS), on behalf of the program; we verify that this is the final, approved version of the student's dissertation including all changes required by the advisory committee. The undersigned agree to abide by the statements above.

Sweta Modi, Student

Dr. Bradley D. Anderson, Major Professor

Dr. Jim Pauly, Director of Graduate Studies

THE CRITICAL ROLE OF MECHANISM-BASED MODELS FOR UNDERSTANDING AND PREDICTING LIPOSOMAL DRUG LOADING, BINDING AND RELEASE KINETICS

DISSERTATION

A dissertation submitted in partial fulfillment of the
requirements for the degree of Doctor of Philosophy in the
College of Pharmacy
at the University of Kentucky

By
Sweta Modi

Lexington, Kentucky

Director: Dr. Bradley D. Anderson, Professor of Pharmaceutical Sciences

Lexington, Kentucky

2013

ABSTRACT OF DISSERTATION

THE CRITICAL ROLE OF MECHANISM-BASED MODELS FOR UNDERSTANDING AND PREDICTING LIPOSOMAL DRUG LOADING, BINDING AND RELEASE KINETICS

Liposomal delivery systems hold considerable promise for improvement of cancer therapy provided that critical formulation design criteria can be met. The main objective of the current project was to enable quality by design in the formulation of liposomal delivery systems by developing comprehensive, mechanism-based mathematical models of drug loading, binding and release kinetics that take into account not only the therapeutic requirement but the physicochemical properties of the drug, the bilayer membrane, and the intraliposomal microenvironment.

Membrane binding of the drug affects both drug loading and release from liposomes. The influence of bilayer composition and phase structure on the partitioning behavior of a model non-polar drug, dexamethasone, and its water soluble prodrug, dexamethasone phosphate, was evaluated. Consequently, a quantitative dependence of the partition coefficient on the free surface area of the bilayer, a property related to acyl chain ordering, was noted.

The efficacy of liposomal formulations is critically dependent on the drug release rates from liposomes. However, various formulation efforts to design optimal release rates are futile without a validated characterization method. The pitfalls of the commonly used dynamic dialysis method for determination of apparent release kinetics from nanoparticles were highlighted along with the experimental and mathematical approaches to overcome them. The value of using mechanism-based models to obtain the actual rate constant for nanoparticle release was demonstrated.

A novel method to improve liposomal loading of poorly soluble ionizable drugs using supersaturated drug solutions was developed using the model drug AR-67 (7-t-butyldimethylsilyl-10-hydroxycamptothecin), a poorly soluble camptothecin analogue. Enhanced loading with a drug to lipid ratio of 0.17 was achieved and the rate and extent of loading was explained by a mathematical model that took into account the chemical equilibria inside and outside the vesicles and the transport kinetics of various permeable species across the lipid bilayer and the dialysis membrane.

Tunable liposomal release kinetics would be highly desirable to meet the varying therapeutic requirements. A large range of liposome release half-lives from 1 hr to 892 hr were obtained by modulation of intraliposomal pH and lipid composition using dexamethasone phosphate as a model ionizable drug. The mathematical models developed were successful in accounting for the change in apparent permeability with change in intraliposomal pH and bilayer free surface area. This work demonstrates the critical role of mechanism-based models in design of liposomal formulations.

KEYWORDS: Liposomes, Membrane Binding, Loading, Release Kinetics, Models, Dexamethasone

Sweta Modi

2013

THE CRITICAL ROLE OF MECHANISM-BASED MODELS FOR UNDERSTANDING AND PREDICTING LIPOSOMAL DRUG LOADING, BINDING AND RELEASE KINETICS

By

SWETA MODI

Prof. Brad Anderson
(Director of Dissertation)

Dr. Jim Pauly
(Director of Graduate Studies)

2013

Dedicated To

My Parents and My Husband

For their faith, support, and unconditional love

ACKNOWLEDGEMENTS

This dissertation is the outcome of guidance and support from numerous individuals throughout the course of my graduate life and it is my pleasure to express my heartfelt gratitude towards them. First and foremost, I would like to sincerely thank my mentor and research advisor, Dr. Bradley Anderson, for giving me an opportunity to join his lab and help me evolve as an independent scientist. His enormous and deep technical understanding of the subject was an enriched source of learning and I greatly appreciate his patience and perseverance in problem solving. The lessons I have learned from his enthusiasm and passion for science will guide me throughout my life, both as a scientist and as a person.

I would like to thank Dr. Tian-Xiang Xiang for his perpetual guidance and helpful discussions and especially for his help with the development of mathematical models. I would also like to thank my committee members, Dr. Paul Bummer, Dr. Markos Leggas and Dr. Zach Hilt for their valuable time and helpful discussions throughout my graduate studies. I would like to thank Pharmaceutical Sciences Graduate Program for giving me an opportunity to be part of this program and for financial assistance. I pay my appreciation to Catina Rossoll, who has always been there and helped in every possible way.

I would like to extend my thanks to Dr. John Rinehart from Markey Cancer Centre for the financial support and the scientific discussions on Dexamethasone work. I would like to thank American Foundation for Pharmaceutical Education (AFPE) and the PhRMA foundation for believing in me and awarding with the pre-doctoral fellowships.

I am thankful to my lab members Michael, Dhaval and Kyle who made this journey smooth, joyful and memorable. Spending long years in graduate life without good and supportive friends is not possible. Thanks to Suvid for innumerable coffee hours and all the non-sense discussions. Thanks to Apurv and Anwesha for their friendship and making this journey memorable. I am thankful to my friendship with Rutooj and Sarita for all the cherished moments spent together. I am glad to have friends like Abhijit, Nikhil, Sumesh and the whole Lex family for making this an enjoyable voyage.

On a personal note, I am grateful to my parents, in-laws, my sisters (Anshu and Swati), my brother (Deep), Anand and Kranthi who always stood by my side and infused me with love and strength to keep going. Last but certainly not the least, I have no words to express my love and thankfulness for my husband (Janu), without whom, this was never possible. He was the source of inspiration and motivation every single day of my graduate life, thanking him for his unconditional love and support. I owe this to him.

TABLE OF CONTENTS

LIST OF TABLES

LIST OF FIGURES

CHAPTER ONE

Statement of Aims

A major gap in the progress of liposomal delivery systems is that the loading and release kinetics are generally found empirically without the use of mechanistic models to guide the liposome design. This conventional approach turns out to be an arduous and time-consuming process that retards the pace of advancement of the delivery systems into the clinic. Hence, the ultimate goal in this field should be to develop a global, uniform mechanistic model that would enable design of nanoparticle delivery systems that have predictable and reproducible in vitro characteristics that also lead to predictable and reproducible in vivo performance. This work, in particular, focuses on models to characterize the in vitro performance (loading, partitioning and release kinetics) in an attempt to contribute towards the ultimate goal while stimulating further research with more diverse compounds.

The central hypothesis is that mathematical models that take into account the thermodynamics (ionization, membrane binding, complexation), intraliposomal microenvironment and permeability of the drug molecule across the bilayer are the keys for prediction of loading and release kinetics in liposomal formulations. The major driving force for the transport of a drug across a liposome is typically the activity gradient of the free unionized species, which is governed by the physicochemical properties of the drug. Another determining factor, among others, in the partitioning and transport of drug across liposomes is the bilayer barrier properties which can be described in terms of order parameter or free surface area. The model compounds explored in this study represent typical problem drug candidates that are likely encountered repeatedly by

those trying to develop delivery systems for antitumor agents. Two of the model compounds, 7-t-butyldimethylsilyl-10-hydroxycamptothecin (AR-67) and dexamethasone (Dex), represent drugs with low aqueous solubility and hydrophobic nature while the other, dexamethasone phosphate (Dex-P), is an amphipathic, water soluble molecule. Highly hydrophobic molecules are difficult to retain inside liposomes leading to premature leakage, while hydrophilic molecules are retained for a very prolonged period of time, failing to achieve therapeutic concentrations at the site of action. In addition, high drug loading in liposomes is critical for the maximum usefulness of its therapeutic potential. The aim with the liposomal delivery of any agent is to encapsulate the drug to the maximum possible extent and retain the drug inside the liposomes for long enough while in circulation but release the drug at an optimum rate once at the site of action. In other words, there is a need for tailored release kinetics to meet the various therapeutic requirements. The following specific aims have been explored to understand the various processes (loading, partitioning and release) in liposomes:

a) Determine the membrane partitioning behavior of dexamethasone and its 21-phosphate prodrug as a function of bilayer composition, temperature and pH and explore the inter-relationship between solute structure, bilayer chain ordering and membrane binding

The loading and release of a drug from liposomes is profoundly influenced by the nature and extent of partitioning of the drug in the bilayer. Experimental conditions that facilitate the accurate determination of the membrane/water partition coefficient of the drug are important to obtain a true value which will additionally facilitate the

mathematical modeling of the loading and release processes. The influence of bilayer composition and phase structure on the partitioning behavior of dexamethasone and its phosphate prodrug are studied in chapter three. A quantitative relationship between membrane water partition coefficient of these drugs and the bilayer order parameter (free surface area) is also developed.

b) Overcoming the pitfalls of dynamic dialysis, a commonly used method for determination of release kinetics from nanoparticles

Dynamic dialysis has been widely used, though often uncritically, for the determination of release kinetics from nanoparticles. The lack of proper understanding of the underlying principles and inaccurate data interpretation can lead to false conclusions regarding sustained release behavior. The pitfalls of dynamic dialysis are demonstrated in chapter four using model lipophilic drug-loaded liposomes varying in lipid composition to provide variations in bilayer permeability and membrane binding affinities. A mathematical model is proposed that can aid in deconvoluting the rate constant for drug release from the apparent kinetics in cases where drug binding effects and/or dialysis membrane transport may be partially contributing.

c) Explore the use of supersaturated solutions to enhance active liposomal loading using AR-67 as a model "problem" drug candidate

Active loading method is the method of choice for loading of ionizable drugs to achieve a higher encapsulated drug to lipid ratio. The loading is dependent on the trans-bilayer activity gradient of the drug, its permeability coefficient and the extraliposomal drug concentration. The low aqueous solubility of AR-67 limits its extraliposomal concentration for loading resulting in a very low drug to lipid ratio upon encapsulation. A

novel method of supersaturating the drug for active loading by the pH-gradient method is proposed in chapter five. A mathematical model taking into account the various intra- and extra-liposomal ionic and binding equilibria and permeability coefficients was developed to predict the rate and extent of active drug loading.

d) Optimize the liposome release kinetics of dexamethasone phosphate based on pH and lipid composition

Dexamethasone has been shown to act as a chemotherapy adjuvant to increase the uptake of chemotherapeutic agents. However, its use is limited by the requirement of frequent high doses owing to the high clearance of the drug and serious side-effects. There is a need for controlled and tailored release kinetics for extracting the maximum therapeutic benefits of the drug. Dexamethasone phosphate, the water soluble prodrug of dexamethasone and an ionizable compound, was used for the formulation development. Previous studies have shown that the differences in permeability of the free and ionized forms can be several orders of magnitude. The pH-dependent permeability was explored for Dex-P to obtain the range of release kinetics possible with a change in intraliposomal pH and the corresponding change in the neutral, permeable fraction. The permeability as a function of bilayer order parameter was evaluated by studying the release rate of Dex-P in liposomes varying in lipid composition and a quantitative relationship was established between bilayer permeability and free surface area in chapter six.

CHAPTER TWO

Introduction

Nanotechnology in Cancer

Nanotechnology is an emerging field that can have an enormous positive impact on human health, especially in cancer treatment (1). The application of nanoparticles in drug delivery has the incredible potential of revolutionizing cancer therapy. Current cancer therapy is faced with numerous challenges including non-specific distribution of antitumor agents, inadequate drug concentrations at the tumor site, multiple drug resistances and limited ability to monitor therapeutic responses (2-7). Nanoparticles have come a long way in cancer chemotherapy, radically changing the diagnosis and treatment of cancers. Tremendous amounts of research being conducted for the development of nano-based therapies have advanced the field of cancer treatment significantly, with several nano-based products now on the market (8). The unique physical and chemical properties of these three dimensional nanostructures allows great flexibility in designing drug delivery systems. They may be tailored to provide several desired properties such as the ability to deliver poorly water soluble drugs, overcome biological barriers and carry the drug selectively to the target site while protecting it from degradation. One of the greatest advantages of nanotechnology over conventional therapies is their multifunctionality; in diagnosis, imaging, monitoring and therapeutics (9-13).

Nanoparticles are sub-micron sized colloidal particles made of polymer, lipids or metals with drug either encapsulated within the matrix or conjugated on the surface. The primary reason for the ideal suitability of nanocarriers for the delivery of chemotherapeutics in

cancer treatment is their ability to take advantage of the EPR (Enhanced Permeation and Retention) effect, whereby the nanoparticles preferentially accumulate at the tumor site owing to the leaky, fenestrated vasculature and are retained there due to the underdeveloped lymphatic drainage system (14-17). Blood vessels in normal tissues have tight endothelial junctions preventing the entry of foreign particles while angiogenic blood vessels in tumor tissues, unlike those in normal tissues, have gaps as large as 600–800 nm between adjacent endothelial cells. Poorly developed, fenestrated tumor blood vessels coupled with poor lymphatic drainage induces the EPR effect, which enables nanoparticles to extravasate through these gaps into extravascular spaces and remain in tumor tissue (14-17). Nanoparticles have been explored for both passive targeting via the EPR effect and active targeting. Active targeting involves incorporation of a targeting ligand on the surface of nanoparticles that specifically binds to a receptor, which is either unique or overly expressed on tumor cell surfaces (18, 19). Passive or active targeting of therapeutics to tumor tissues is the main arena of nanoparticle use in cancer therapy, as it reduces side effects, increases efficacy and reduces systemic drug exposure. Liposomes, polymer nanospheres, nanorods, carbon nanotubes, solid lipid nanoparticles, fullerenes, nanocrystals, dendrimers etc. are some of the nanoparticles being widely explored for delivery of cancer chemotherapeutics. A more quantitative understanding of the properties of nanoparticles both in vitro and in vivo will be key to their clinical success.

Liposomal Drug Delivery

Over several decades, liposomes have evolved from simple model membrane systems to sophisticated drug delivery systems for a large number of therapeutic agents (20-23).

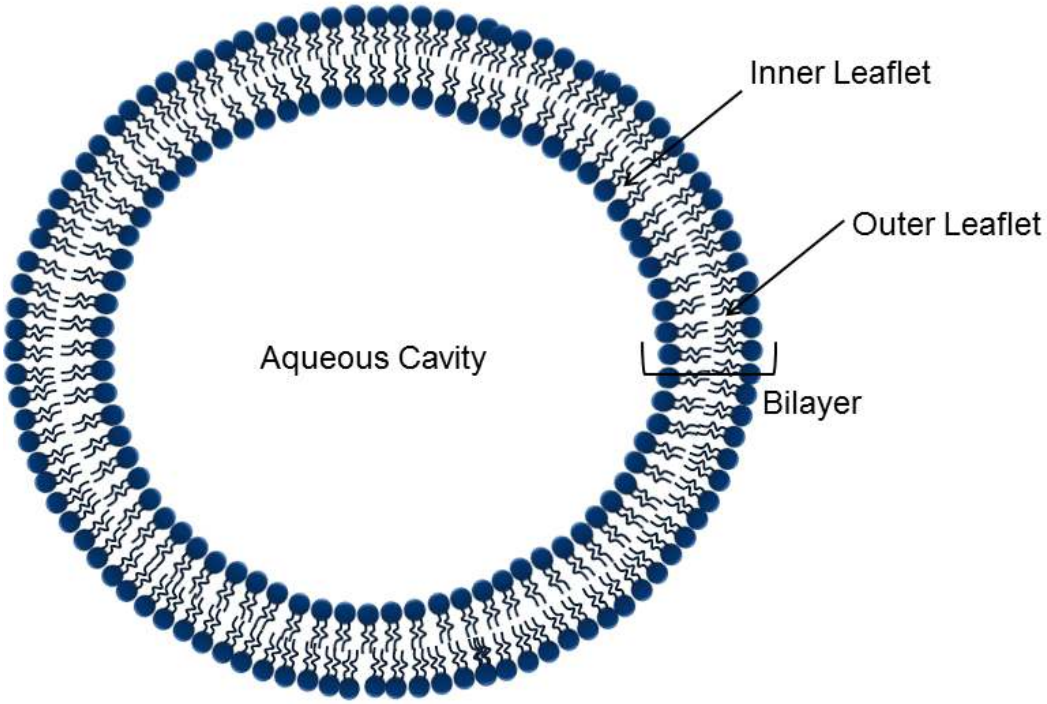

Figure 2.1 Schematic of a liposome

Liposomal nanoparticles represent an advanced class of drug delivery systems, with many formulations on the market and several in clinical trials. Liposomes are nanoparticles comprising one or more concentric lipid bilayers enclosing an aqueous interior (Figure 2.1). The typical size range for large unilamellar (consisting of one bilayer) liposomes is ~50-200 nm. Liposomes are unique in their versatility as they can incorporate both hydrophobic and hydrophilic agents either in the membrane phase or in the enclosed aqueous compartment, respectively (24-26). Liposomes composed of natural lipids are biodegradable, non-immunogenic and they have limited intrinsic toxicity. The manifold applications of liposomes have been to enhance the drug solubility and stability, avoid rapid degradation, reduce drug toxicity, and improve unfavorable pharmacokinetics. They can function as controlled release systems as per the therapeutic requirement. Stealth liposomes are pegylated liposomes, designed to evade recognition by the immune system and thereby elongate the in vivo circulation half-life (27-29). The attainment of longer circulation times in vivo ($t_{1/2}$~24 hrs) by polymer coating has led to the clinical success of several liposomal products (30-33).

Liposomes are particularly useful in cancer chemotherapy because of their ability to increase the therapeutic efficacy and reduce the side effects of a given drug by the well-known EPR effect. The potential benefit from a liposomal carrier depends on the nature of the drug, the desired pharmacological intervention and the site of application. The current pharmaceutical preparations of liposome based therapeutic agents mainly result from our understanding of membrane-drug interactions and liposome disposition kinetics. Despite the significant advances with liposomes as drug delivery systems, there is a big gap in the amount of research efforts invested and the clinical successes of the liposomal

formulations (33). This can be majorly attributed to the lack of quantitative mechanism based approaches in formulation design (34, 35). Other factors are poor understanding of the physical and chemical stability of the lipids, mechanisms affecting liposome clearance in vivo, scale-up issues and cost prohibitiveness of the lipids for large scale manufacturing of liposome formulations (36-38).

The ability to entrap as much drug as possible, retain the drug inside the liposomes as long as they are in circulation, and subsequently release the drug content at an optimum rate once at the tumor site will be preeminent to the clinical success of any liposomal formulation. Understanding the physicochemical factors affecting the loading and release of a liposomal drug and developing mechanism-based models for quantifying and predicting these processes are the principal objectives of this thesis.

Loading Methodologies

One of the major challenges in the advancement of liposomes into clinical products has been the achievement of a high level of loading of the therapeutic agent in the liposome. The tiny intraliposomal volume (about 0.002 femtoliter for 150 nm liposome) demands a very efficient loading method in order to achieve meaningful drug concentrations at the site of action (39). Inadequate drug loading essentially defies the purpose of a targeted delivery vehicle and renders it insufficient. The two most common methods of loading are discussed below.

(i) Passive Loading

In the passive loading method, drug incorporation takes place while the liposomes are being formed. It is mainly driven by the water solubility and membrane water partition coefficient or hydrophobicity of the drug (40-42). For a highly water soluble drug, the

extent of drug loading will depend on the entrapped aqueous volume while for a highly hydrophobic drug, about 50% drug will be associated with the intraliposomal leaflet and the remaining 50% with the extraliposomal leaflet. In either case, only part of the drug will be encapsulated by the passive loading method. Thus, although it is a simple method, the drug to lipid ratio achieved by this method is not very high.

(ii) Active Loading

Active loading is preferred for ionizable drugs, where the loading takes place in response to a trans-membrane chemical potential gradient (43, 44). Several marketed products have been launched based on this approach, the most notable being the doxorubicin formulation, Doxil®. The active loading method adopted for Doxil® is based on an ammonium sulfate gradient as demonstrated in Figure 2.2 (36, 45). In general, in this method, a trans-bilayer pH gradient is first established by creating a concentration gradient of the weak acid or base, which causes the diffusion of the weak acid or base from inside to outside the liposomes. After development of the pH gradient, the weakly acidic or basic drug is allowed to diffuse into the liposomes, once again, in response to the concentration gradient of the drug. Upon encapsulation, the drug ionizes due to the pH difference and is trapped in the membrane impermeable form, which drives further loading (46-48). However, the loading is limited by the availability of the extraliposomal drug, which is a function of its aqueous solubility. Thus, achieving a high drug to lipid ratio by active loading remains a challenge for poorly water soluble drugs.

Intraliposomal drug precipitates in the form of insoluble salts can significantly prolong the release half-life. The formulation may exhibit zero order kinetics until the drug concentration reaches below the saturation solubility of the drug in the aqueous entrapped

volume (49). However, with active loading methods based on pH-gradient, the maintenance or the collapse of the pH gradient *in vivo* can affect the drug release rate. Therefore, it would be desirable to evaluate the release kinetics of active loaded liposomes in physiologically relevant media to predict the in vivo performance (50).

Liposome Release Kinetics

Determination of the release kinetics of the encapsulated drug from liposomes is a critically important aspect of the formulation characterization. The rate of liposomal drug release will determine the extent of premature drug leakage from the liposomes while they are in the systemic circulation prior to reaching the target site. Once at the site of action, the drug needs to be released at an optimal rate as per the therapeutic requirement because rates that are either too slow or too fast can result in poor efficacy. Thus, the drug release rate potentially determines the therapeutic efficacy of the formulation. A bell-shaped curve can be expected between liposomal release rate and therapeutic effect in tumors (51-53). Profiles describing antitumor efficacy versus release rates are necessary in order to predict therapeutic outcome for a particular tumor type. Extensive physicochemical and medical characterization is needed for translation of these formulations into clinical products.

(i) Factors Controlling Liposome Release Kinetics

The kinetics of drug release from liposomes depends on the permeability of the solute and its concentration gradient across the bilayer. The permeability, in turn, is a function of the membrane-water partition coefficient of the drug, the diffusion coefficient of the permeable species and the nature of the bilayer (54). The major understanding of the

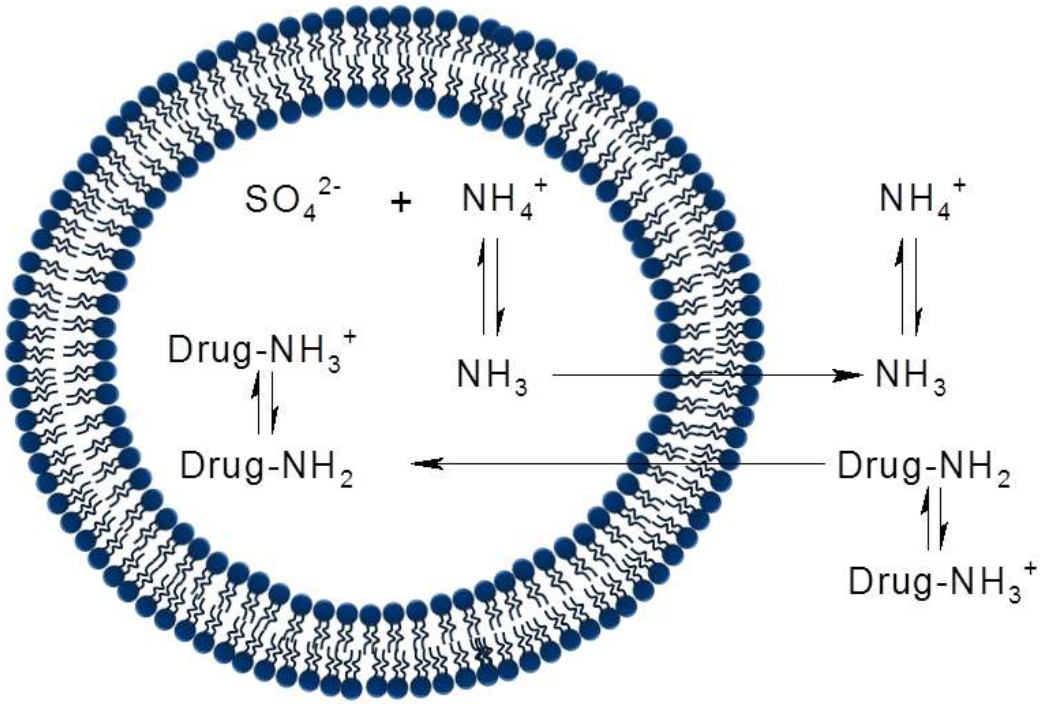

Figure 2.2 Schematic depicting the active loading into liposomes based on ammonium sulfate gradient method for weak bases.

barrier properties of liposomes comes from studies aimed at exploring the factors governing the bilayer permeability using liposomes as model membrane systems. Partitioning and permeability of solutes in lipid bilayers is dependent on the physical and chemical properties of the solute and the bilayer structure.

(a) Bilayer Phase Structure

Liposomes are most often made up of phospholipids, the most common being phosphatidylcholine (PC) molecules. Some of the phospholipids used in this study are shown in Figure 2.3. Phosphatidylcholines, owing to the double fatty acid chains, differ from other amphipathic molecules (e.g., detergents, lysolecithin) in having a preference to form bilayers rather than micellar structures. The structure of the bilayer is influenced by the phospholipid composition, acyl chain length of the phospholipid, its phase transition temperature and presence of cholesterol among some of the major factors (55-57). Although liquid crystalline bilayers are said to mimic the phase structure of most physiological membranes, in drug delivery the goal is to optimize the release rate of the entrapped drug and therefore gel and liquid–crystalline phases, both are explored. Solute permeability has been observed to be strongly dependent on the phase structure of the bilayer (58-63). For a long time, the passive transport of small molecules across membranes was explained by a bulk-phase solubility diffusion model (56, 64). However, with the increasing research interests and efforts in the field of bilayer permeability, the role of lipid chain packing in the membranes on the permeability was realized. Owing to the physical and chemical heterogeneity of lipid bilayers, its treatment as a bulk solvent

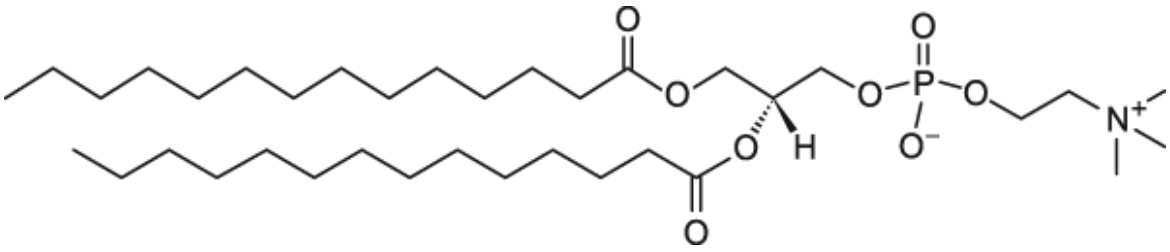

1,2-Dimyristoyl-sn-glycero-3-phosphocholine (DMPC)

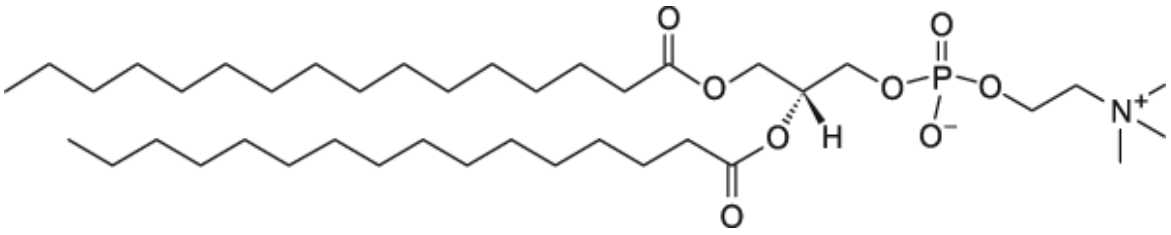

1,2-Dipalmitoyl-sn-glycero-3-phosphocholine (DPPC)

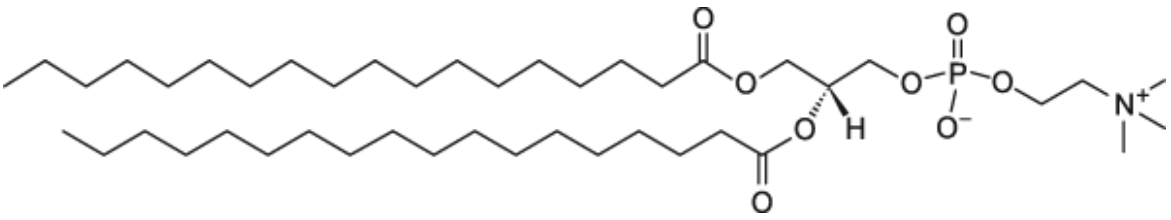

1,2-Distearoyl-sn-glycero-3-phosphocholine (DSPC)

Contd..

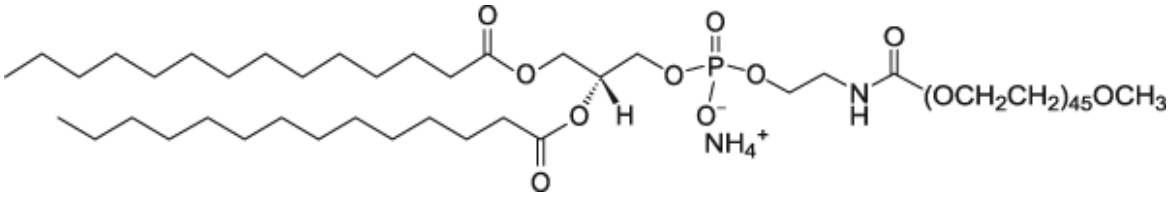

1,2-Dimyristoyl-sn-glycero-3-phosphoethanolamine-N-[methoxy(polyethylene glycol)-2000] (ammonium salt) (mPEG-DMPE)

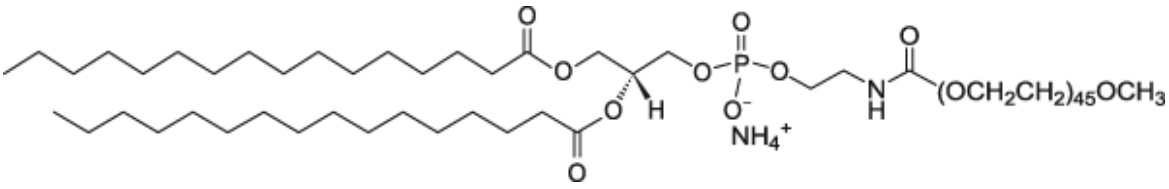

1,2-Dipalmitoyl-sn-glycero-3-phosphoethanolamine-N-[methoxy(polyethylene glycol)-2000] (ammonium salt) (mPEG-DMPE)

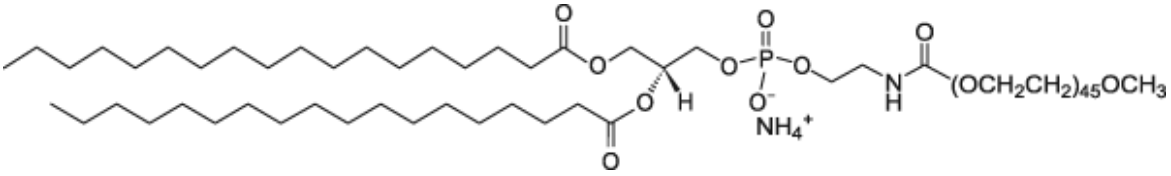

1,2-Distearoyl-sn-glycero-3-phosphoethanolamine-N-[methoxy(polyethylene glycol)-2000] (ammonium salt) (mPEG-DMPE)

Figure 2.3 Chemical structures of the phospholipids employed in this study.

was not sufficient. Dramatic increases in bilayer permeability on transitioning from a gel to liquid crystalline phase emphasized the more ordered nature of the gel phase due to tighter lipid chain packing and reduced lateral motions in lipid bilayers. Xiang and Anderson proposed the barrier-domain model whereby they introduced a permeability decrement factor to account for the decrease in permeability from that predicted by solubility diffusion theory owing to chain ordering in lipid bilayers (61, 65).

(b) <u>Solute Size and Structure</u>

Lipid bilayer permeability has been shown to be sensitive to the solute size, attributed to the effect of lipid chain ordering which cannot be explained by the bulk solubility diffusion theory. The sensitivity of the permeability coefficient of solutes to bilayer chain packing was shown to exhibit linear dependence on the minimum cross-sectional area of the permeants (using seven short-chain monocarboxylic acids) (61). It was suggested that the permeants prefer to orient with their long principal axis along the bilayer normal and correlate better with the permeant cross sectional area rather than molecular volume. The size selectivity for transport across lipid bilayers may be credited to size dependent effects on both partitioning and diffusion in lipid bilayers.

The preferred site for solute partitioning is dependent on the hydrophobicity of the solute. Hydrophilic solutes or compounds having polar functional groups may reside preferentially at the bilayer interface while hydrophobic nonpolar solutes may locate in the interior of the bilayer upon partitioning. Similarly, amphipathic solutes may orient at the interface to maximize the interaction of their polar groups with the aqueous region and the non-polar parts with the hydrocarbon region of the bilayer. The chemical nature of the solute (i.e., functional groups, number of $-CH_2$ groups, hydrogen bonding

potential) impacts its release kinetics across the bilayer (61). For example, in the more ordered gel phase bilayer, the permeability coefficient decreased with increasing chain length for short-chain monocarboxylic acids from formic acid to propionic acid, followed by a reversal in the trend at higher chain lengths whereas in liquid crystalline bilayer, an approximately monotonic increase in permeability coefficient with permeant chain length was observed. The results suggested the interplay of both the lipophilicity of the permeant and the chain ordering within the membrane and that the unfavorable steric interactions associated with the addition of a methylene group may dominate over the accompanying increase in lipophilicity (61).

The ionization potential of the solute also has an important role in its permeability across the bilayer. For ionizable solutes, the apparent permeability changes with a change in pH and the corresponding change in fraction unionized. This is largely based on experimental evidence accumulated over several years indicating that neutral species are often orders-of-magnitude more permeable than their ionized counter-parts (60, 61, 64-67). The pH dependent permeability of ionizable compounds has been used successfully in the active loading of several weak bases and few acids in the liposomes to achieve high drug to lipid ratios. In this work, the use of intravesicular pH to modulate the release kinetics of an ionizable drug, dexamethasone phosphate (Dex-P) was demonstrated.

(ii) <u>Methods Used to Assess Liposome Release Kinetics</u>

There are several methods used for the determination of drug release rates from nanoparticles. Each method has its own advantages and disadvantages. One of the methods is to dilute the nanoparticles with buffer and then separate the carrier from drug at different time points. For separation by ultrafiltration, the issue is that some

nanoparticles (e.g. liposomes) being non-solid flexible structures may pass through the filter membranes. Separations using ultracentrifugation may alter release rates due to the high centrifugal force (68). The reverse dialysis method, (69) where the nanoparticle formulation is diluted in the large volume to maintain sink conditions and free drug is sampled from the dialysis tubes immersed in the sink solution, requires a highly sensitive analytical method for quantitative determination of the drug. In dynamic dialysis, one of the most commonly used methods, the nanocarrier dispersion is suspended inside a dialysis tube/cassette of semipermeable membrane having a particular molecular weight cut off and dialyzed in a large volume of sink medium (70). During the kinetic study, the free drug is separated from the carrier by the dialysis membrane and does not require a separate separation step at each time point. Unfortunately, there exists an inadequate understanding of the dynamic dialysis method leading in some cases to a false notion of sustained release behavior from nanoparticles. Owing to the popularity of nanoparticle drug delivery systems, there is a critical need to understand the processes underlying the dynamic dialysis method and use the method appropriately to obtain reliable estimates of nanoparticle release rates.

Camptothecins

Camptothecin and its related analogues constitute an important class of drugs that gained considerable interest for their anti-tumor activity and unique mechanism of action (71, 72). Camptothecins form non-covalent complexes with the topoisomerase I-DNA cleaved complex and thereby interfere with the DNA unwinding step of DNA replication. Prolonged exposure of replicating cells to camptothecins results in double strand breaks and consequently cell death (73, 74). One of the characteristics of this class is the pH

dependent chemical hydrolysis of the α-hydroxy δ-lactone ring (E-ring) moiety to form a ring-opened camptothecin carboxylate. The lactone moiety is thought to be the therapeutically active form and therefore, ring opening to form the carboxylate leads to diminished *in vivo* activity (73).

Two compounds of this class, topotecan (Hycamptin®) and irinotecan (Camptosar®) have received FDA approval. In addition, several analogues are in clinical trial. One such analogue is AR-67 (7-t-butyldimethylsilyl-10-hydroxycamptothecin), which was synthesized in an attempt to improve its lactone stability in blood by promoting the binding of the lactone form to red blood cell membranes (75-78). The substitution of nonpolar groups imparted hydrophobicity to the compound resulting in a very low water solubility. Liposomal delivery of AR-67 was pursued to increase the solubility and stability of the compound along with the targeting potential of the nanosized liposomes to enhance the overall efficacy of the drug and reduce its systemic toxicity (79, 80). Besides, a prolonged schedule of camptothecin administration given continuously at low doses or frequently fractionated appeared to be more effective clinically (81-83). However, owing to the high lipophilicity, AR-67 has a high permeation rate across the liposome bilayer and therefore rapidly leaks from vesicles. In addition, the low aqueous solubility poses a challenge in achieving high encapsulation of the drug by the active loading method. Consequently, a novel strategy to enhance the encapsulated drug to lipid ratio of this and other poorly water soluble compounds by the active loading method was proposed and evaluated in this thesis.

Glucocorticoids

Glucocorticoids are a class of steroidal agents that bind to glucocorticoid receptors and are mainly known for their anti-inflammatory and immunosuppressive responses (84, 85). Dexamethasone is a prominent member of the synthetic group of this class and one of the most widely used. In addition to its anti-inflammatory action, it has been used as an adjuvant in chemotherapy. In some of the recent pre-clinical and clinical trials, pre-treatment with dexamethasone was shown to reduce the toxicity associated with chemotherapeutic agents and even increase the efficacy (86-89). This is potentially attributed to the down-regulation of pro-inflammatory cytokines (e.g., vascular endothelial growth factor (VEGF), interleukin 1β (IL-1β)) by dexamethasone and as a consequence, a reduction in the interstitial fluid pressure within tumors. Reduced intratumoral pressure facilitates the uptake and diffusion of chemotherapeutic agents (90-92). Despite the beneficial effects of dexamethasone, its use is limited by substantial side effects. In addition, due to its rapid clearance from the body, frequent high doses are required to achieve efficacy which in turn causes serious side effects (84). To better exploit the therapeutic potential of dexamethasone, targeted delivery systems with tailored release kinetics are desirable (86, 87, 93).

CHAPTER THREE

Bilayer Composition, Temperature and Speciation Effects on Partitioning of Dexamethasone and its 21-phosphate: The Role of Bilayer Chain Ordering

INTRODUCTION

The partitioning of drugs into lipid bilayers and biological membranes is a significant factor governing their tissue distribution and bioaccumulation (94-97). These properties, in turn, directly influence efficacy or toxicity when the mode of drug action involves interaction with membrane components (98, 99) and may also affect efficacy and toxicity indirectly through their role in modulating drug delivery, pharmacokinetics, metabolism and clearance (100, 101). As drug candidates have become more lipophilic and less water soluble there is a greater need for rapid and reliable screening methods and/or computational approaches to allow pharmaceutical scientists to select lead candidates based on their developability, as indicated by properties such as their potential to exhibit good oral bioavailability (102, 103). Guided by the perception originating in Overton's rule and the solubility-diffusion model that the equilibrium membrane-water partition coefficient should correlate with permeability across biomembranes (102, 104, 105) numerous researchers have attempted to devise experimental systems and computational models that link drug permeation to membrane affinity. As yet, however, there are no models that can quantitatively predict either biomembrane partitioning or transport solely from a knowledge of the structure of the drug and composition of the membrane.

For decades, it has been a common practice to predict membrane-water partitioning of drugs and also in vivo absorption based on various bulk solvent-water partition coefficients (103, 106, 107). Although different bulk solvents have been used to

determine the partition coefficient, octanol has been the most referenced system (106). However, with time, deficiencies of bulk solvents as models for membranes have become more widely appreciated. Conceptually, these deficiencies mainly reflect the fact that bulk solvents are homogeneous and isotropic while lipid bilayer membranes are anisotropic interfacial phases with properties that vary as a function of internal distance from the bilayer-water interface (57, 108-110). One striking experimental discrepancy noted in several recent publications is that linear free energy relationships based on bulk solvent/water partitioning fail to predict lipid bilayer/water partitioning. This has been particularly apparent in the lack of correlation between octanol/water partition coefficients and membrane water partition coefficients for drugs containing ionizable substituents (102, 111-113). Ionized solutes may have higher affinity for lipid bilayer membranes than octanol due to the anisotropy of lipid bilayers, their high surface area-to-volume ratios, and electrostatic interactions of ionized solutes with charged moieties in the bilayer headgroups (111, 112, 114-116). Within the anisotropic microenvironment of the bilayer interface, solutes preferentially adopt conformations and orientations that maximize hydrophobic and van der Waals interactions between non-polar regions of the solute and acyl chains within the bilayer interior while retaining electrostatic interactions with the polar head groups and water molecules (117-120). The complexity of factors leading to that preferred solute conformation, orientation, and position within the bilayer that constitutes a minimum in free energy appears to have no close correlate in bulk solvent/water partitioning.

Another discrepancy between lipid bilayer/water versus bulk solvent/water partitioning is the well-known dependence of lipid bilayer/water partition coefficients on bilayer phase

behavior and chain ordering. For example, decreasing the temperature below the phase transition temperature, inclusion of cholesterol in the bilayer, or elongating the phospholipid chain length, cause significant decreases in partition coefficient values (55, 121, 122) that are not easily rationalized using only bulk solvent models for the partitioning process.

In addition to their importance in drug delivery, liposomes are widely used as model membrane systems for studying the partitioning behavior of drugs (57, 98, 123-125). Determination of the liposome/water partition coefficient is essential for characterizing drug loading and the driving force governing release kinetics from liposomal delivery systems (126-128). More generally, such information can contribute to an understanding of several biological phenomena including passive transport and biodistribution (103, 129).

A unified quantitative mathematical model that could predict the membrane-water partition coefficient as a function of drug structure, membrane composition, and the local aqueous microenvironment would be valuable both from a practical standpoint in assessing drug developability and for understanding drug biodistribution, clearance, efficacy, and toxicity. Such a model would need to take into account the concentrations of the various neutral and ionized drug species that may exist as a function of the pH of the aqueous microenvironment; the hydrophobic regions of the solute, the nature and location of various polar functional groups in the solute molecule and its conformational flexibility; and the surface charge, chain ordering and phase behavior, and other properties of the bilayer that in turn depend on lipid composition and the temperature, pH and ionic strength of the solution.

In the present study, the influence of bilayer composition and phase structure on the partitioning behavior of the anti-inflammatory steroid dexamethasone (Dex) was explored. These studies demonstrate a quantitative dependence of the partition coefficient of dexamethasone on the free surface area of the bilayer, a property related to acyl chain ordering that is modulated by changes in bilayer composition and temperature. Comparison of the present results to previous literature studies of drug partitioning into lipid bilayers suggests that this concept may have general applicability, as it has been previously shown for drug permeability across lipid bilayer membranes (122, 130, 131). Phosphorylation of dexamethasone to produce the water soluble prodrug dexamethasone 21-phosphate (Dex-P) complicates its membrane binding behavior. The dependence of the apparent partition coefficient of Dex-P, as a function of pH after correction for drug concentration effects, was determined in order to generate species-specific partition coefficients. Comparison of these species-specific partition coefficients for Dex-P to that for Dex in bilayers varying in lipid composition suggests that the influence of chain ordering as quantified by free surface area on partitioning behavior affects both nonpolar and polar solutes similarly.

MATERIALS AND METHODS

Phospholipids including DSPC (1,2-distearoyl-sn-glycero-3-phosphatidylcholine, >99% purity), DPPC (1,2-dipalmitoyl-*sn*-glycero-3-phosphocholine, >99% purity)**,** DMPC (1,2-dimyristoyl-*sn*-glycero-3-phosphocholine, >99% purity), m-PEG DSPE (1,2-distearoyl-sn-glycero-3-phosphoethanolamine-N-[methoxy (polyethylene glycol)-2000]), m-PEG DPPE (1,2-dipalmitoyl-*sn*-glycero-3-phosphoethanolamine-N-[methoxy(polyethylene glycol)-2000]) and m-PEG DMPE (1,2-dimyristoyl-*sn*-glycero-3-phosphoethanolamine-

N-[methoxy(polyethylene glycol)-2000]) were purchased as powders from Avanti Polar Lipids (Alabaster, AL). Dexamethasone (Dex) (≥98%, powder) was purchased from Sigma-Aldrich Co., St. Louis, MO. Dexamethasone sodium phosphate (Dex-P), USP, was from Spectrum Chemical Mfg. Corp., New Brunswick, NJ. Dialysis flat sheets (Spectra/Por® RC Membrane, MWCO: 3.5 kD) were purchased from Spectrum Laboratories (Rancho Dominguez, CA). HPLC grade solvents and other chemicals were purchased from Fisher Scientific (Florence, KY). Deionized water was used for all experiments.

Liposome Preparation

Blank liposomes were prepared based on a previously reported method (127). Briefly, DMPC: mPEG DMPE, DPPC: mPEG DPPE and DSPC: mPEG-DSPE (95:5 mol%, 120 mg) were separately dissolved in 2 mL of chloroform. The solvent was evaporated under a stream of nitrogen while rotating the container and the resulting film was dried overnight in a vacuum oven. For determination of partition coefficient of Dex in different lipid systems, the lipid film was hydrated with 2 mL of phosphate buffered saline (PBS) (pH 7.4) and for Dex-P; 20 mM acetate buffer (pH 4) was used. For pH-dependent partition coefficient of Dex-P in DMPC liposomes, several buffers at different pH were used (20 mM KCl-HCl buffer, pH 1.5; 20 mM glycine buffer, pH 2; 20 mM acetate buffer, pH 4 and 5; 20 mM MES buffer, pH 6; 20 mM phosphate buffer, pH 8). To uniformly suspend the lipid, the suspension was alternately vortexed and heated in a water bath at a temperature above the phase transition temperature of the respective lipids. The lipid suspension was then extruded 10 times through two stacked 100 nm polycarbonate membranes (GE Water and Process Technologies, Trevose, PA) using an

extrusion device (Liposofast®, Avestin, Canada) at 30, 50 and 60 °C for DMPC, DPPC and DSPC, respectively, to obtain unilamellar liposomes. Liposomes were allowed to cool to room temperature for 3 hr and stored at 4 °C until further use. Particle sizes of blank liposomes were measured at 25 °C by dynamic light scattering (DLS) using a Delsa™ Nano submicron particle size analyzer (Beckman Coulter Inc., Brea, CA). The liposomes were diluted in the same buffer as that used in their preparation.

Lipid Analysis

Lipid concentrations in the liposomal suspensions were determined by high performance liquid chromatography (HPLC) using an evaporative light scattering detector (ELSD) as reported previously for DSPC liposomes (132). Briefly, separation was achieved using an Allsphere™ Silica Column (Grace Davison Discovery Sciences, Deerfield, IL) (5 µ, 4.6 x 150 mm) with a guard column (Allsphere silica, 5 µ, 7.5 x 4.6 mm). A linear gradient method was employed starting with 100% (v/v) mobile phase A (80% chloroform:19.5% methanol:0.5% (v/v) ammonium hydroxide solution (30%) and changing to 80% mobile phase A:20% mobile phase B (80% methanol:19.5% water:0.5% (v/v) ammonium hydroxide solution (30%)) over 3 min. This composition was maintained from 3- 7 min followed by a return to 100% mobile phase A by 14 min. The total run time was 15 min at a flow rate of 1 mL/min with the ELSD setting at a gain of 8, pressure of 3.4 bar, and temperature of 40 °C. The sample compartment temperature was set at 4 °C and the column was at ambient temperature. Standards of DSPC, DPPC and DMPC were prepared in mobile phase A and linearity was observed between log concentration and log peak area.

Aliquots of liposomal suspension (10 µL) were dried under nitrogen and reconstituted in mobile phase A for lipid analysis before the start of each experiment. Since 95% of the phospholipid content in the liposomes was non-pegylated and the chain lengths for the pegylated and non-pegylated components were same, the liposomes were assumed to contain 100% DMPC, DPPC or DSPC, respectively, for the determination of lipid content. Lipid stability was assessed under two representative conditions (Dex-P, pH 1.5 and 6, DMPC liposomes). Stability samples were withdrawn at different time points during dialysis for lipid analysis.

Determination of Membrane-Water Partition Coefficients

Equilibrium Dialysis Method

Membrane-water partition coefficients of Dex and Dex-P (Figure 3.1) were determined at 25 °C and varying lipid concentrations in three different liposomal systems (DMPC, DPPC and DSPC) by equilibrium dialysis using one mL Teflon® cells (Equilibrium Dialyzer (Spectrum Labs)). A liposome stock suspension of 60 mg/ml was diluted to varying concentrations and mixed with a drug solution having a fixed concentration. One ml of this mixture was introduced into one compartment (donor) of the equilibrium dialyzer and one ml of the corresponding blank buffer was added to the other compartment (receiver). The dialyzer, which consists of five pairs of one mL cells, was then placed in an incubator at 25 °C and allowed to equilibrate. Aliquots (100-150 µL) were withdrawn at 24, 48 and 72 hours from each compartment, diluted in 900 µL methanol and analyzed by HPLC. Equilibrium was considered to have been established when two subsequent time points yielded constant values. Partition coefficients of Dex

were also determined in DPPC liposomes at 37 °C and 45 °C following the same procedure.

Equilibrium Solubility Method

Partition coefficients of Dex in DMPC, DPPC and DSPC liposomes were also determined by the equilibrium solubility method. Excess solid (Dex) was equilibrated with blank liposomes at different lipid concentrations at 25 °C. After equilibration, samples were filtered through 0.45 µ PVDF filters and the filtrates were analyzed for drug concentration by HPLC after a 10-fold dilution in methanol. Errors due to filter adsorption were eliminated by analyzing successive aliquots of the filtrate to attain constant values. Aliquots of filtrate (10 µL) were dried under nitrogen and reconstituted in mobile phase for lipid analysis.

Simultaneous Determination of Dex and Dex-P by HPLC

A new isocratic HPLC method was developed and validated for the simultaneous determination of Dex and Dex-P with UV detection at 240 nm. Four independent standards for Dex-P (100-800 µM) in water and Dex (100-800 µM) in methanol were prepared. A Waters Alliance 2695 Separations Module coupled to a UV detector (Waters 996, Photodiode Array Detector) at 240 nm was employed. A Waters Symmetry® C18 column (5 µm, 3.9 x 150 mm) and guard column (3.9 x 20 mm) were used at an injection volume of 10 µL with a mobile phase composition of 32% acetonitrile and 68% (v/v) pH 5.5 triethylamine acetate (2%) buffer. The retention times for Dex-P and Dex at a flow rate of 1 mL/min were 2.5 and 6.4 min, respectively. The stability of Dex-P during equilibrium dialysis was monitored using this method as it allowed the simultaneous determination of Dex and Dex-P. The HPLC response was linear within the range of

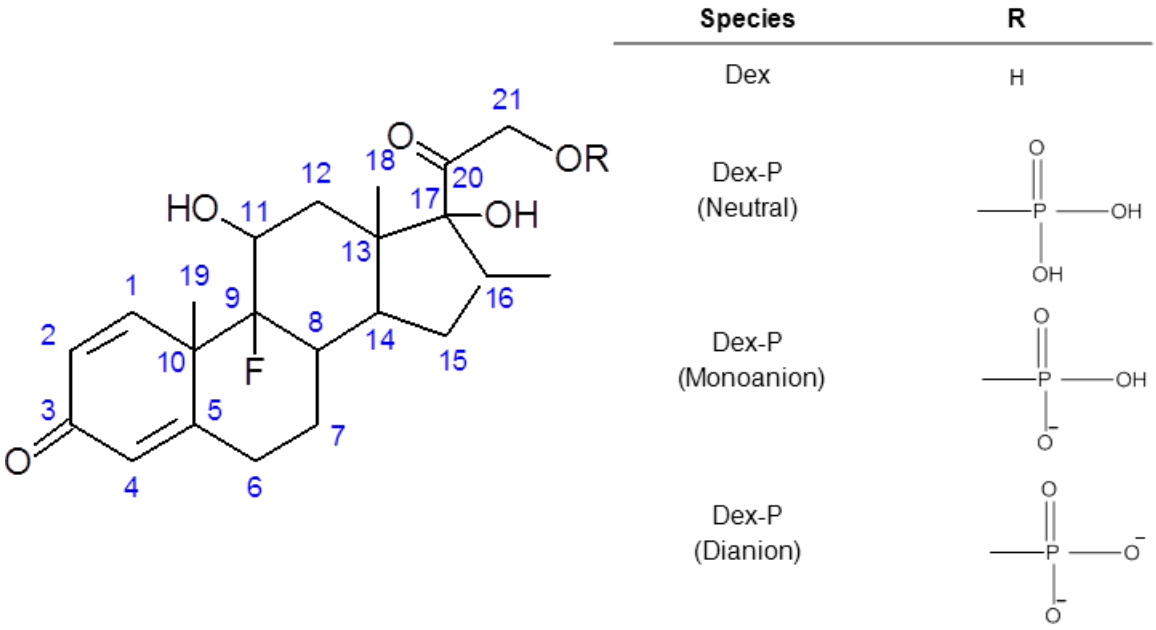

Figure 3.1 Structures of Dex and Dex-P with different ionization states of the 21-phosphate.

100-800 μM for both Dex and Dex-P. The response factor for both analytes yielded a coefficient of variation less than 3% intraday and interday.

THEORY

Membrane-Water Partition Coefficient

At equilibrium, the total mass of drug in the donor (liposomal) compartment is the sum of the masses in the bilayer membrane and the aqueous phase:

$$C_d V_d = C_w V_w + C_m V_m \qquad Eq\ 3.1$$

where C_d is the total drug concentration in the donor compartment, C_m and C_w are the drug concentrations in the lipid and aqueous phases, respectively, and V_d, V_m, V_w are the respective volumes. The aqueous concentration in the donor compartment (C_w) should equal the aqueous concentration in the receiver compartment (C_r) at equilibrium.

The volume based partition coefficient can then be defined by

$$K_p = \frac{C_m}{C_w} = \frac{C_d V_d - C_w V_w}{C_w V_m} = \frac{C_d V_d - C_r V_w}{C_r V_m} \qquad Eq\ 3.2$$

Saturable Binding Correction for Neutral Dex-P

The concentrations of membrane bound Dex divided by the lipid concentration were proportional to the free drug concentration in solutions approaching infinite dilution. However, deviations from linearity were observed for Dex-P partitioning at pH 1.5 and 2, necessitating a correction for membrane saturation. At pH 1.5 and 2, membrane bound Dex-P exists predominantly as the neutral species (the reported first pKa of Dex-P in aqueous solution is 1.9 (133)). Therefore, the following equation was employed to fit the,

the ratios of bound drug to lipid concentration (B) as a function of the free drug concentration (C_u):

$$B = \frac{K_p^{app} C_u}{1 + Const. C_u} \qquad Eq\ 3.3$$

where K_p^{app} is the partition coefficient at infinite dilution at the solution pH specified.

Gouy-Chapman Correction for the Partition Coefficient of Bound Monoanion

For membrane binding of ionized molecules, the partition coefficient decreases with the adsorbed concentration and needs to be adjusted to infinite dilution using Gouy-Chapman theory (134-139). At pH 4 - 6 in this study, the membrane bound drug was assumed to be predominantly monoanionic. Monoanion binding contributes to the development of a charge on the membrane surface, which in turn changes the surface potential as given by Gouy-Chapman equation:

$$\sigma^2 = 2000\epsilon_0\epsilon_r RT \sum C_i \left(\exp\left(\frac{-Z_i F \Phi_0}{RT}\right) - 1\right) \qquad Eq\ 3.4$$

where σ is the surface charge density, ϵ_0 is the permittivity of vacuum, ϵ_r is the relative permittivity of water, R is the gas constant, C_i is the molar concentration of the ith electrolyte in the bulk solution, Z_i is the signed charge number of that electrolyte, F is the Faraday constant and Φ_0 is the surface potential in volts.

Based on the number of moles bound per mole of lipid and the surface area of the phospholipids, σ was calculated and then using eq. 3.4 the surface potential, Φ_0, was calculated. The apparent partition coefficient at infinite dilution K_p^{app} was calculated from observed K_p^{obs} by the following equation,

$$K_p^{app} = K_p^{obs} \exp\left(\frac{-Z_D F \Phi_0}{RT}\right) \qquad Eq\ 3.5$$

where Z_D is the signed charge number of the drug.

pH Dependence of the Partition Coefficient (for Dex-P)

The apparent partition coefficient of Dex-P obtained at each pH value can be related to the concentrations of species D (unionized), D^- (monoanion) and D^{2-}(dianion) (Figure 3.1) in the membrane and aqueous phases as follows,

$$K_p^{app} = \frac{D_m + D_m^- + D_m^{2-}}{D_w + D_w^- + D_w^{2-}} \qquad Eq\ 3.6$$

$$K_p^{app} = \frac{K_{p1} + K_{p2}K_{a1}/H^+ + K_{p3}K_{a1}K_{a2}/(H^+)^2}{1 + K_{a1}/H^+ + K_{a1}K_{a2}/(H^+)^2} \qquad Eq\ 3.7$$

where the subscripts *m* and *w* refer to the membrane and aqueous phases, respectively, K_{a1} and K_{a2} are the two ionization constants of Dex-P; and K_{p1}, K_{p2} and K_{p3} are the intrinsic partition coefficients of the three species D , D^- and D^{2-}, respectively. Over the pH range of interest in this study (pH 1.5-8) the properties of the DMPC bilayer itself were assumed to be independent of pH because the intrinsic pKa of the phosphatidylcholine head group of 0.8 (140) is still well below pH 1.5.

Bilayer Surface Density/ Free Surface Area

The normalized surface density is a parameter related to relative acyl chain ordering in the bilayer. It is defined as $\sigma = A_0/A$, where A is the area occupied per phospholipid molecule and A_0 is its area in the crystal (40.8 Å^2) (55, 121, 131). The normalized surface density varies from 0-1 with the value of 1 representing a completely ordered crystalline state. In the present study, the surface density values for the various liposome compositions were taken from a single compilation in the literature (131) and quantitatively related to the generated partitioning data.

Xiang and Anderson (131) related the surface density to the free surface area a_{free} of the bilayer by the following equation:

$$a_{free} = A - A_0 = A_0(1/\sigma - 1) \qquad Eq\ 3.8$$

They showed that the free surface area ($A_0/a_{free} = \sigma/(1-\sigma)$) served as a unified fundamental molecular packing parameter in lipid bilayers for describing the permeability of solutes across both liquid crystalline and gel phases of the bilayer. An observed dependence of the lipid bilayer permeability coefficient on the inverse of free surface area was attributed, at least in part, to the sensitivity of solute partitioning into the interior hydrocarbon barrier domain of the bilayer to chain ordering as expressed by the following equation (131):

$$K_p = K_0 \exp(-a^*/a_{free}) \qquad Eq\ 3.9$$

K_p in Eq. 3.9 refers to the barrier domain/water partition coefficient, not the overall bilayer/water partition coefficient that is of interest in this study, and K_0 is the partition coefficient for the same solute in a bulk solvent (e.g., a hydrocarbon) that was found to most closely mimick the chemical selectivity of the bilayer barrier domain and water. Xiang and Anderson (130) later examined the lipid bilayer permeability coefficients of a series of mono-carboxylic acids varying in the size of their alkyl portion to probe the dependence of bilayer transport on molecular size. When relative bilayer permeability coefficient measurements were ascribed to relative changes in apparent partitioning of the permeant into the barrier domain with increasing solute size, the quantity a^* in Eq. 3.9 was demonstrated to be proportional to the minimum cross-sectional area of the solute. Thus, sensitivity of lipid bilayer permeability coefficients to free surface area of the bilayer is a function of the permeant size.

A few previous studies of small molecule partitioning into lipid bilayers have revealed correlations between partition coefficients and the normalized surface density (55, 121, 122). However, the solutes employed in previous studies (i.e., hexane, benzene, and acetic acid) are hardly representative of typical drug molecules either in terms of their size or complexity. Herein, whether or not a dependence of the partition coefficient on bilayer free surface area is a more general phenomenon applicable to a broader array of drug molecules was examined.

RESULTS

Liposome Characterization

Blank liposomes of DMPC, DPPC and DSPC, prepared for partitioning studies, had the particle size in the range of 85-100 nm, with a polydispersity index in the range of 0.05-0.09, indicating monodisperse formulations. The extrusion procedure employed in this study was previously shown by ^{31}P-NMR to produce unilamellar vesicles (141).

A simple analytical method using gradient HPLC and ELSD for evaluation of lipid concentration was developed for three different lipids DMPC, DPPC and DSPC. Figure 3.2 shows the chromatograms of the three lipids with retention times for DSPC, DPPC and DMPC being 7.9, 8.0 and 8.2 min, respectively. Lipid concentrations were determined from log-log plots of peak area versus concentration which were linear over the concentration ranges of 150-800 μM for DMPC, 100-400 μM for DPPC, and 150-400 μM for DSPC.

Lipid concentrations in the liposomal samples were analyzed prior to equilibrium dialysis and used for calculation of volume based partition coefficients. The analyzed lipid concentrations were typically 25-35% lower than the theoretical concentrations indicating

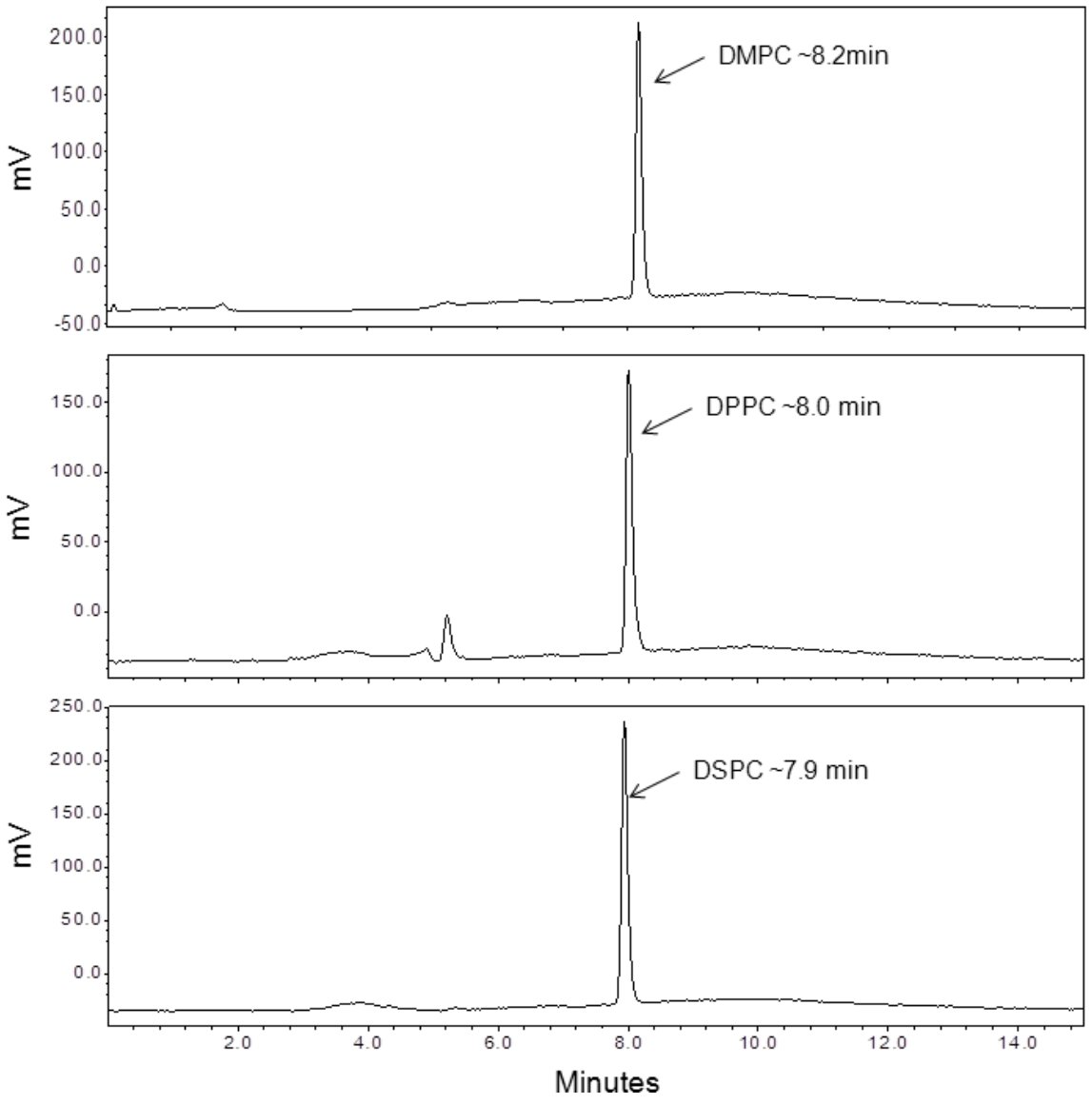

Figure 3.2 Representative chromatograms of DPPC, DMPC and DSPC obtained by HPLC with ELSD (Evaporative Light Scattering Detection) detection.

some lipid loss during the extrusion process. This highlights the necessity for analyzing the lipid concentration in order to obtain reliable partition coefficient values rather than just assuming no lipid loss. In order to assess lipid stability during the time required for equilibration (48 hr), lipid concentrations were analyzed versus time for up to 72 hr in representative experiments in DMPC liposomes (Dex-P) at pH 1.5 and 6 (Figure 3.3). No significant change was observed in lipid concentration as judged by the 95% confidence interval of the slope from a first-order fit at pH 6. However, some degradation of the lipid was detected at pH 1.5, with a first-order rate constant of 0.006±0.0003 h^{-1} corresponding to a half-life of 115 ± 5 hr, consistent with previous evidence that phospholipid hydrolysis is acid catalyzed (142, 143). Importantly, no change in partition coefficients was discernible with time after equilibration indicating that a small percentage of lipid hydrolysis did not alter the lipid volume within the liposomes or the membrane affinity for the solute.

Membrane-Water Partition Coefficients

Dexamethasone

The membrane-water partition coefficient of Dex in DMPC, DPPC and DSPC liposomes at 25 °C was determined at varying lipid concentrations by two different methods – equilibrium dialysis and equilibrium solubility. In the equilibrium dialysis experiments, the total drug concentrations were kept low and approximately constant with increasing lipid concentration (drug to lipid ratios varied from 0.0006 to 0.0052) to determine the partition coefficient in the linear region of binding isotherm (Figure 3.4). The bound drug to lipid ratios increased linearly with increasing unbound drug concentration (Figure 3.4 inset) and the partition coefficients (705 ± 24 in DMPC, 106 ± 11 in DPPC and 58 ± 9 in

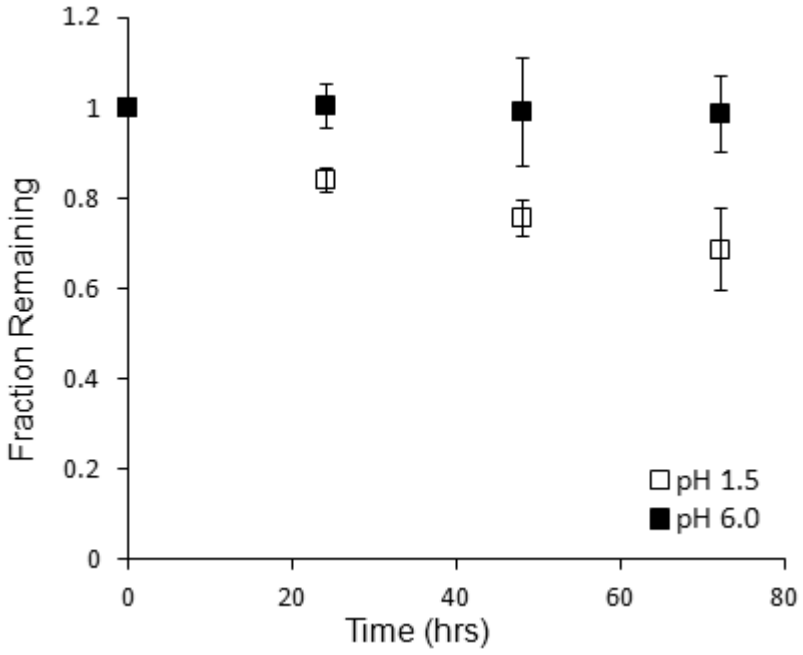

Figure 3.3 Fraction of DMPC remaining vs. time during equilibrium dialysis experiments at pH 1.5 and 6. Each data point is the average of five different concentrations and the error bars are the standard deviations.

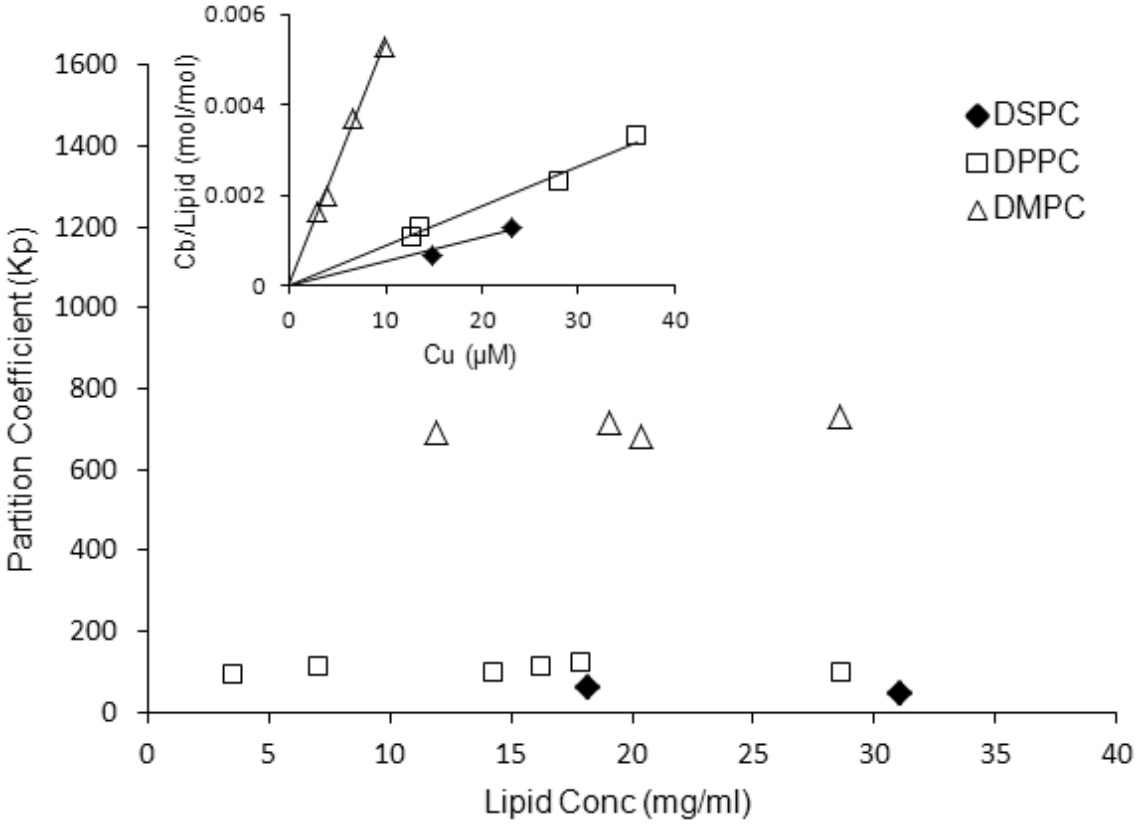

Figure 3.4 DMPC, DPPC and DSPC membrane-water partition coefficients of Dex in PBS buffer at pH 7.4 as a function of lipid concentration determined by equilibrium dialysis at 25 °C. Inset shows the corresponding binding isotherms.

DSPC liposomes) were constant in the lipid concentration range studied. In the equilibrium solubility method, excess solid Dex was equilibrated with liposomes resulting in linear increases in solubility as a function of lipid concentration for DMPC, DPPC and DSPC liposomes (Figure 3.5). The membrane-water partition coefficients determined from the equilibrium solubility method were also independent of the lipid concentration (Figure 3.5 inset).

Partition coefficients of Dex in all three lipid systems determined by the equilibrium dialysis and solubility methods were combined in Figure 3.6 to examine the effect of drug-to-lipid ratio on the partition coefficient, since the drug-to-lipid ratios at equilibrium were significantly higher in the equilibrium solubility method relative to the equilibrium dialysis method. In DPPC and DSPC liposomes, no significant differences in partition coefficients were observed at low vs high drug/lipid ratios as judged by the overlap of 95% confidence intervals for the average values from two methods. However, the drug-to-lipid ratios for Dex in DMPC liposomes were substantially higher for the equilibrium solubility method (~0.07) than those employed in equilibrium dialysis (<0.01), and in this case the partition coefficients differed significantly between the two methods.

The dependence of the partition coefficients on temperature was determined in DPPC liposomes using the equilibrium dialysis method, as shown in Figure 3.7. Partition coefficients increased with temperature, varying from 106 ± 11 at 25 °C to 478 ± 20 at 45 °C (Figure 3.7A). Linear binding isotherms were observed (Figure 3.7A inset) in all cases, indicating that the partition coefficients represent the infinitely dilute region. The slope of a linear least squares fit of the van't Hoff plot shown in Figure 3.7B yielded the

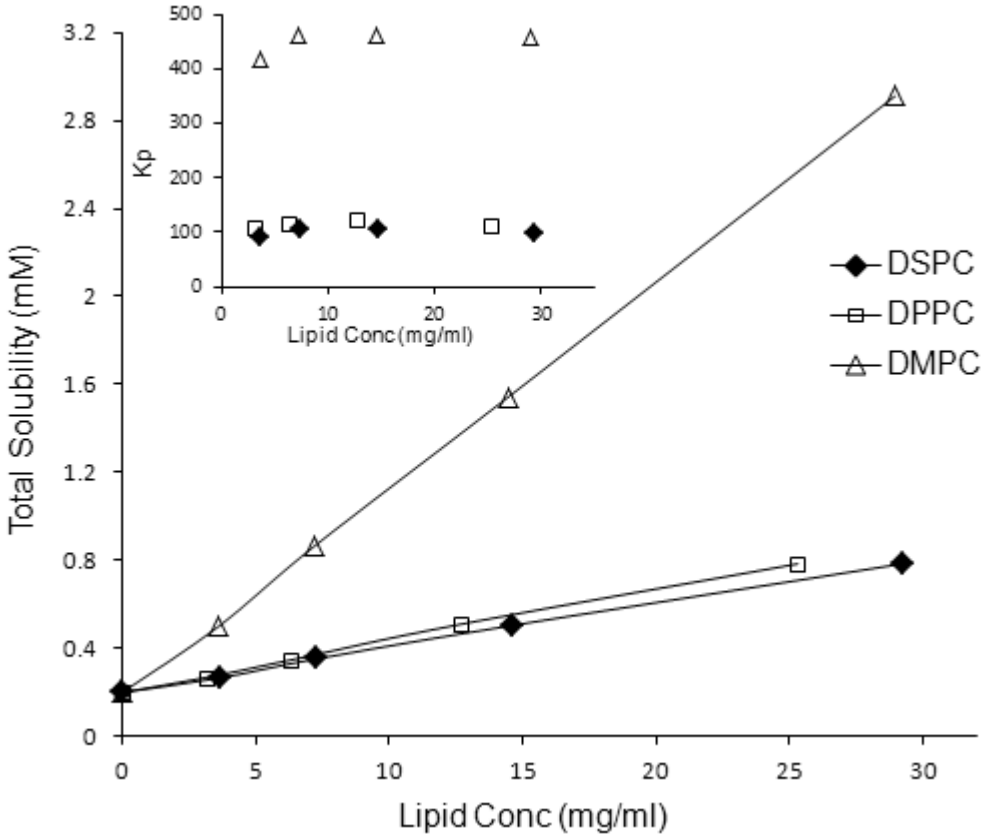

Figure 3.5 Relationship between total equilibrium solubility of Dex and the lipid concentration in DMPC, DPPC, and DSPC liposomes at 25 °C. Inset shows the effect of lipid concentration on the partition coefficients.

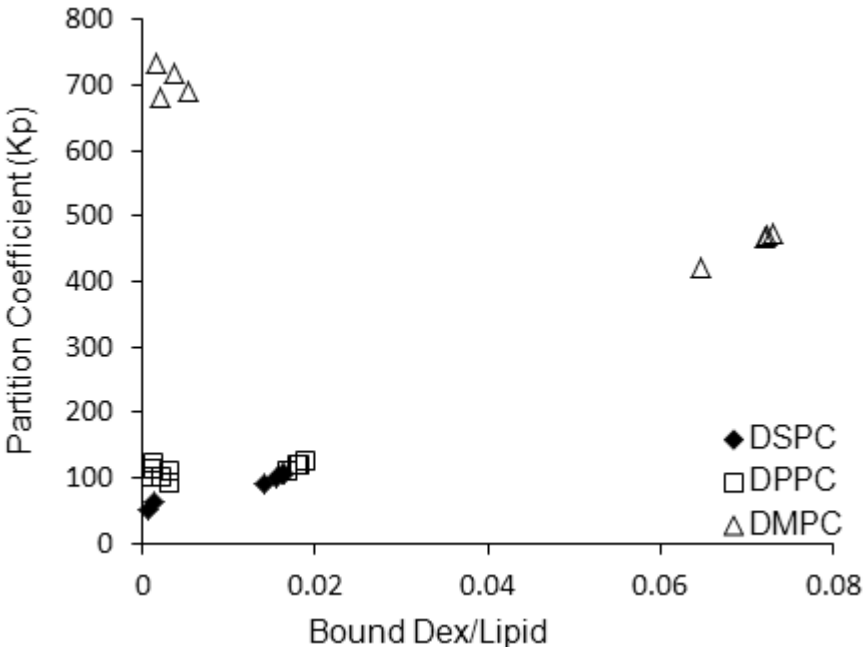

Figure 3.6 DMPC, DPPC and DSPC liposomal membrane-water partition coefficients of Dex at 25 °C vs. the bound drug-to-lipid ratios. The partition coefficients at bound Dex/lipid ratios below 0.01 were obtained by equilibrium dialysis and those above 0.01 were obtained by equilibrium solubility.

molar enthalpy (ΔH°=58.6 kJ/mol) and entropy of transfer (ΔS°=235.1 J/mol.K) of Dex from water to DPPC liposomes.

Dexamethasone Phosphate

The 21-phosphate prodrug of Dex is ionizable and therefore partition coefficients of Dex-P were generated in DMPC liposomes at 25 °C as a function of aqueous solution pH from 1.5-8.0 to study the species dependence of its partitioning behavior. The partition coefficients generated at a fixed concentration of Dex-P and at various pH values are plotted versus lipid concentration in Figure 3.8. At pH 1.5 and 2, systemic increases in the partition coefficients with increasing lipid concentration are evident. In this pH region, neutral Dex-P is the predominant bound species present because, although the first pKa of Dex-P is 1.9 (133), preferential binding of the neutral species relative to the monoanion results in a pKa shift for the membrane bound drug of approximately one unit. The binding isotherms (drug/lipid (mol/mol) ratio versus unbound drug concentration) for the data at pH 1.5 and 2 displayed in the inset to Figure 3.8 suggest that membrane saturation may have been responsible for the decreasing partition coefficients with increasing unbound drug concentrations that accompany a decrease in liposome concentration. The solid lines in Figure 3.8 (inset) represent fits of the data at pH 1.5 and 2 to Eq. 3.3. K_p^{app}, respresenting the partition coefficient at infinite dilution at the solution pH of interest, could be obtained from the linear portion of these fitted lines.

The partition coefficients at pH 4-6 are nearly constant with increases in lipid concentration (Figure 3.8), though a slight upward drift is discernible at pH 4. In this pH region, the predominant membrane bound species is Dex-P monoanion. This conclusion

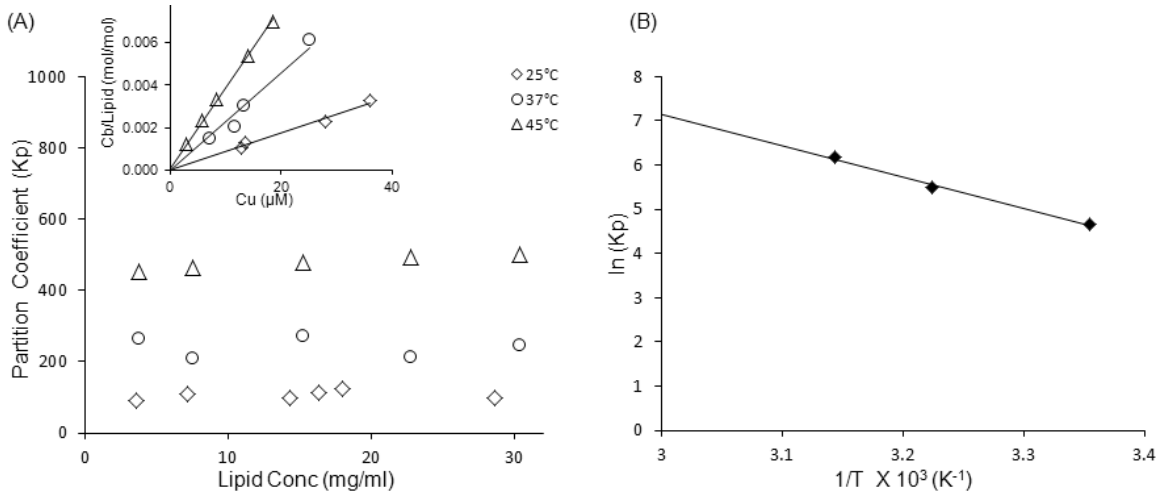

Figure 3.7 (A) Influence of lipid concentration on the DPPC membrane-water partition coefficients of Dex at different temperatures. Inset shows the corresponding binding isotherms. (B) Van`t Hoff plot of the DPPC membrane-water partition coefficients for Dex.

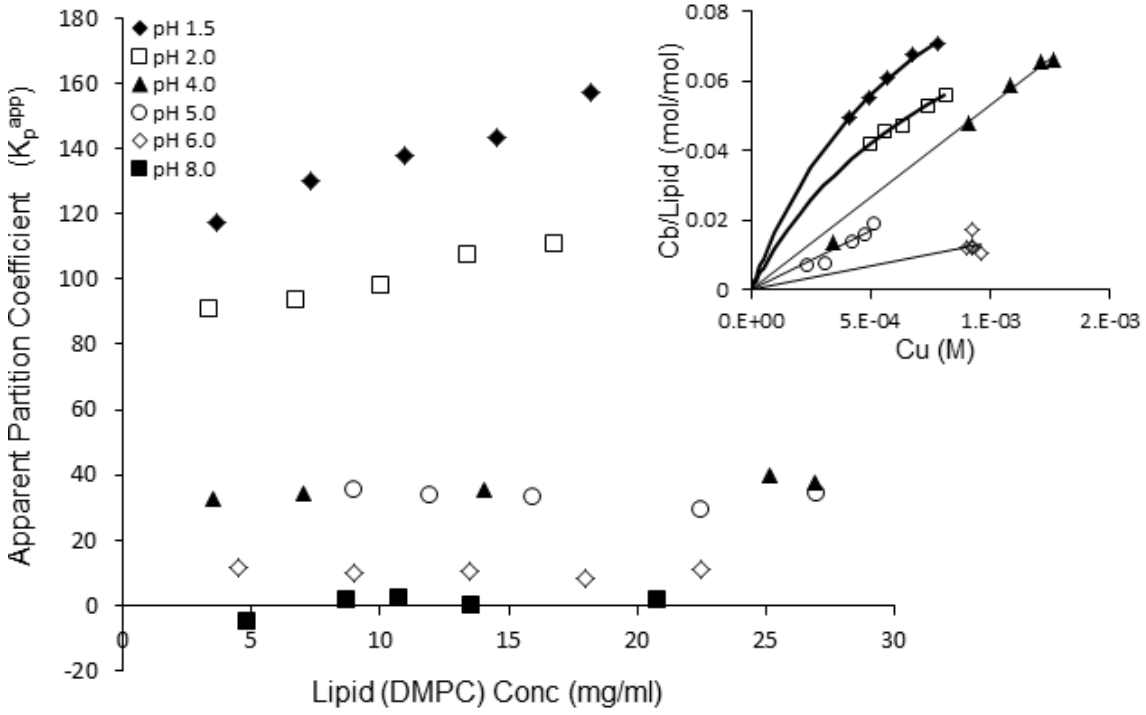

Figure 3.8 Effect of lipid concentration on the apparent DMPC membrane-water partition coefficients of Dex-P at different pH values (25 °C). Inset shows the binding isotherms (bound drug/lipid ratio versus unbound aqueous drug conc.) for data at pH 1.5, 2, 4, 5 and 6. The solid curves at pH 1.5 and 2 represent non-linear least-squares fits of the data to Eq. 3. Data at pH 4, 5 and 6 were corrected using the Gouy-Chapman equation (Eq. 5).

is based on the experimentally determined pKa_2 value for Dex-P of 6.27 ± 0.13 (pH solubility method, our unpublished data) in aqueous solution combined with the observation in Figure 3.8 that the partition coefficient for Dex-P at pH 8 is not significantly different from zero indicating that the concentration of Dex-P dianion in the membrane between pH 4-6 should be negligible. Anion partitioning to neutral phospholipid membranes imparts a negative charge to the membrane that increases with the bound drug/lipid ratio. Typically, the Gouy-Chapman theory can be employed to correct for the effects of charge repulsion on the activity coefficient of the membrane bound anion in order to obtain a partition coefficient at infinite dilution (134-139). Such a correction, as described in Eqs. 4 & 5, was applied to the monoanion partitioning data at pH 4-6 resulting in the plots of drug/lipid ratio versus unbound drug concentration shown in the Figure 3.8 inset.

After the appropriate corrections, K_p^{app} values for each pH applicable at infinite dilution were obtained and plotted in Figure 3.9. These data were fit to Eq. 3.7 by nonlinear regression to generate the solid curve shown. For this analysis, pKa_1 and pKa_2 were fixed at their previously determined solution values of 1.9 and 6.27, respectively, and the partition coefficient for Dex-P dianion was assumed to be equal to zero. The partition coefficient for the neutral species was estimated to be 241 ± 38 (95% C.I.) and for the monoanion, it was 48 ± 9 (95% C.I).

Membrane water partition coefficients of Dex-P (at pH 4) were determined in DMPC, DPPC and DSPC liposomes as a function of lipid concentration by equilibrium dialysis (25 °C) as shown in Figure 3.10. The highest partitioning was observed in DMPC

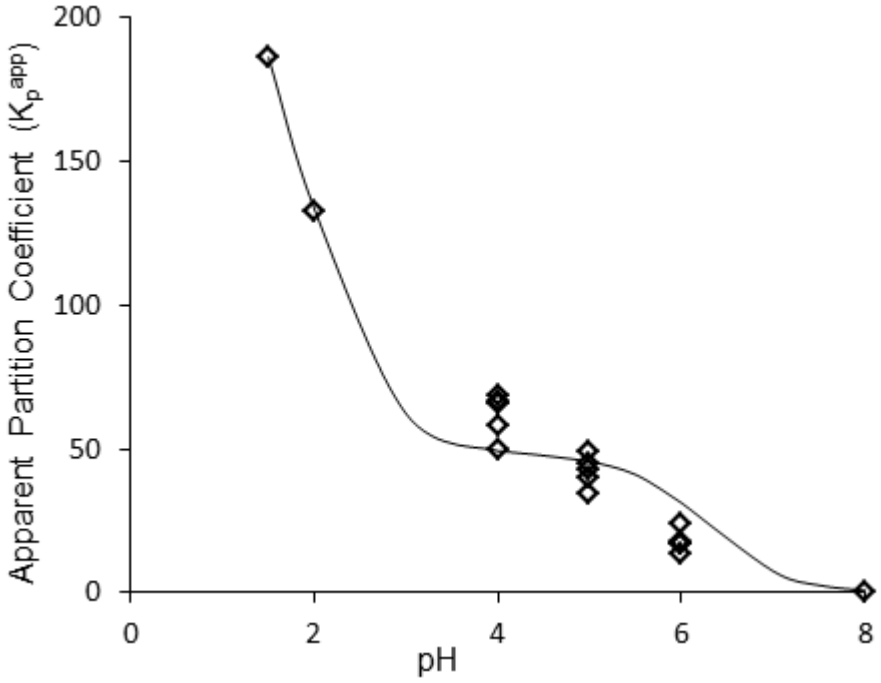

Figure 3.9 Effect of pH on apparent partition coefficients of Dex-P in DMPC liposomes. The solid curve represents the best fit of Eq. 7 to the data by nonlinear least-squares regression analysis.

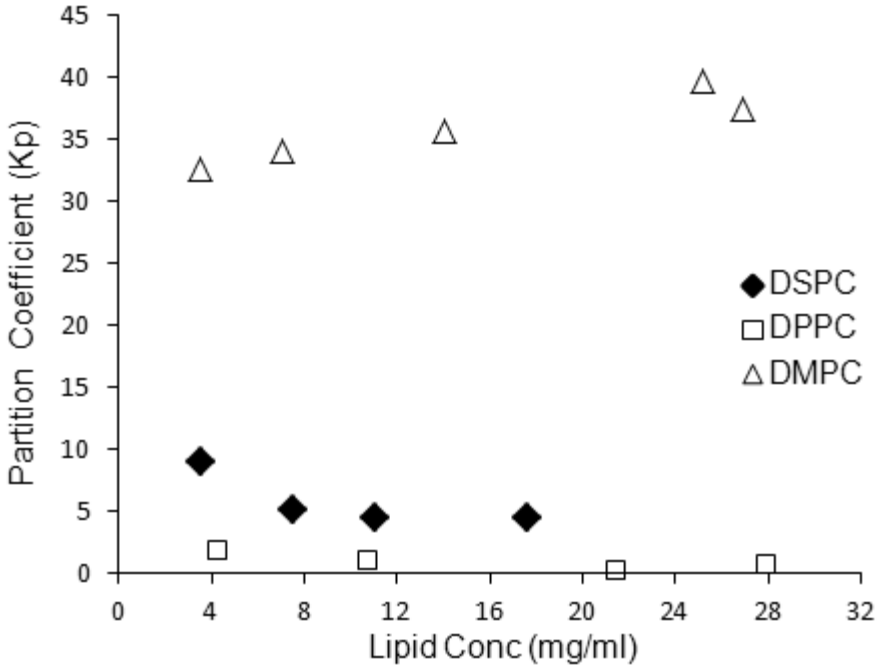

Figure 3.10 DMPC, DPPC and DSPC liposomal membrane-water partition coefficients of Dex-P at pH 4 and 25 °C determined by equilibrium dialysis versus lipid concentration.

liposomes (62 ± 8 in DMPC (after Gouy-Chapman correction) while the values were dramatically lower in DPPC (2 ± 4) and DSPC liposomes (6 ± 2).

Effect of Bilayer Free Surface Area on Membrane-Water Partition Coefficients

The membrane water partition coefficients were significantly higher in DMPC liposomes as compared to DPPC and DSPC liposomes for both Dex and Dex-P (at pH 4). At 25 °C DMPC, with a gel->liquid crystalline phase transition, Tm, of 23 °C is liquid crystalline while both DPPC (Tm=41 °C) and DSPC (Tm=55 °C) are in their gel states. Therefore, the acyl chain region in DPPC and DSPC bilayers is more highly ordered at 25 °C in comparison to those in DMPC. To quantitatively probe the dependence of the partition coefficient on the degree of bilayer chain ordering, the natural logarithms of the partition coefficients (K_p) are plotted versus the inverse of free surface area as suggested by Eq. 3.9. For Dex, a linear relationship was observed between $ln(K_p)$ and free surface area of the bilayer ($1/a_{free} = \sigma/(1-\sigma)$) as illustrated in Figure 3.11. In one of the partitioning system (Dex in DPPC liposomes), the free surface area of the bilayer was altered by varying the temperature from 25 °C to 45 °C, through phase transition temperature (41 °C) of DPPC. Figure 3.11 shows the combined data for Dex partition coefficients when free surface area was varied either by varying phospholipid chain length (DMPC, DPPC, and DSPC) or varying temperature (DPPC, 25-45 °C). The Dex-P partition coefficients at pH 4 appear to show a similar trend though the number of data points and poor precision of the values in DPPC and DSPC do not allow one to assess linearity. There are numerous studies in the literature that have reported lipid bilayer/water partition coefficients of various solutes in similar fully saturated

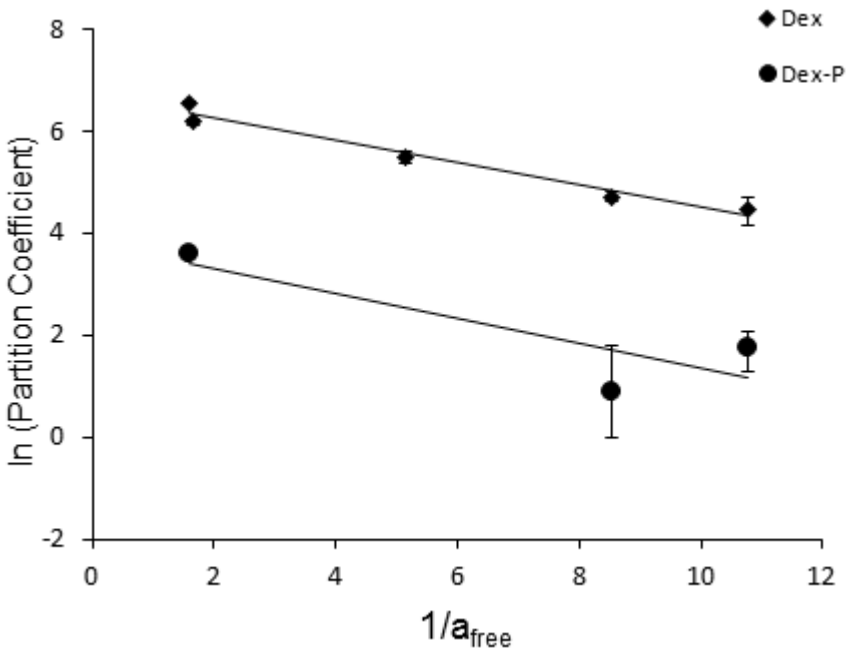

Figure 3.11 Natural logarithms of the liposomal membrane-water partition coefficients of Dex and Dex-P versus the inverse of the bilayer free surface area, a measure of chain ordering as altered by phospholipid chain length and temperature.

phospholipids as a function of either phospholipid chain length or temperature. Some representative examples taken from the literature (55, 141, 144-146) conducted in liposomal systems for which surface density data were available from the same source used in the present study (131) are plotted in Figure 3.12 along with the partition coefficients generated for Dex and Dex-P in the present study versus the inverse of free surface area. In all cases explored, a similar trend of decreasing partition coefficient versus the inverse of bilayer free surface area was found with slopes in the plots of ln (K_p) vs.$1/a_{free}$ (see Figure 3.12 legend) varying over a narrow range of approximately -0.2 to -0.3.

DISCUSSION

Liposomal partitioning studies appear to offer clear advantages in predicting the biodistribution of drugs because ordered lipid bilayers more accurately mimic biological membranes than bulk solvents. These advantages are particularly apparent for ionizable compounds (111, 112, 114). Additionally, a quantitative understanding of liposomal partitioning is essential for designing liposomal drug delivery systems with predictable loading and tunable release characteristics (126, 127, 132, 147). However, the interfacial nature of lipid bilayers adds complexity both in terms of generating reliable experimental data and in interpreting the values obtained. Proper correction for surface charge effects on binding of ionized species (134) and saturation phenomena for neutral species (138, 148) may be necessary with increasing drug concentration. For ionizable drug molecules, quantitative mathematical models describing the contributions of neutral and ionized drug species are needed to account for the pH dependence of membrane partitioning. Finally, the experimental partitioning system employed in terms of liposome composition (e.g.,

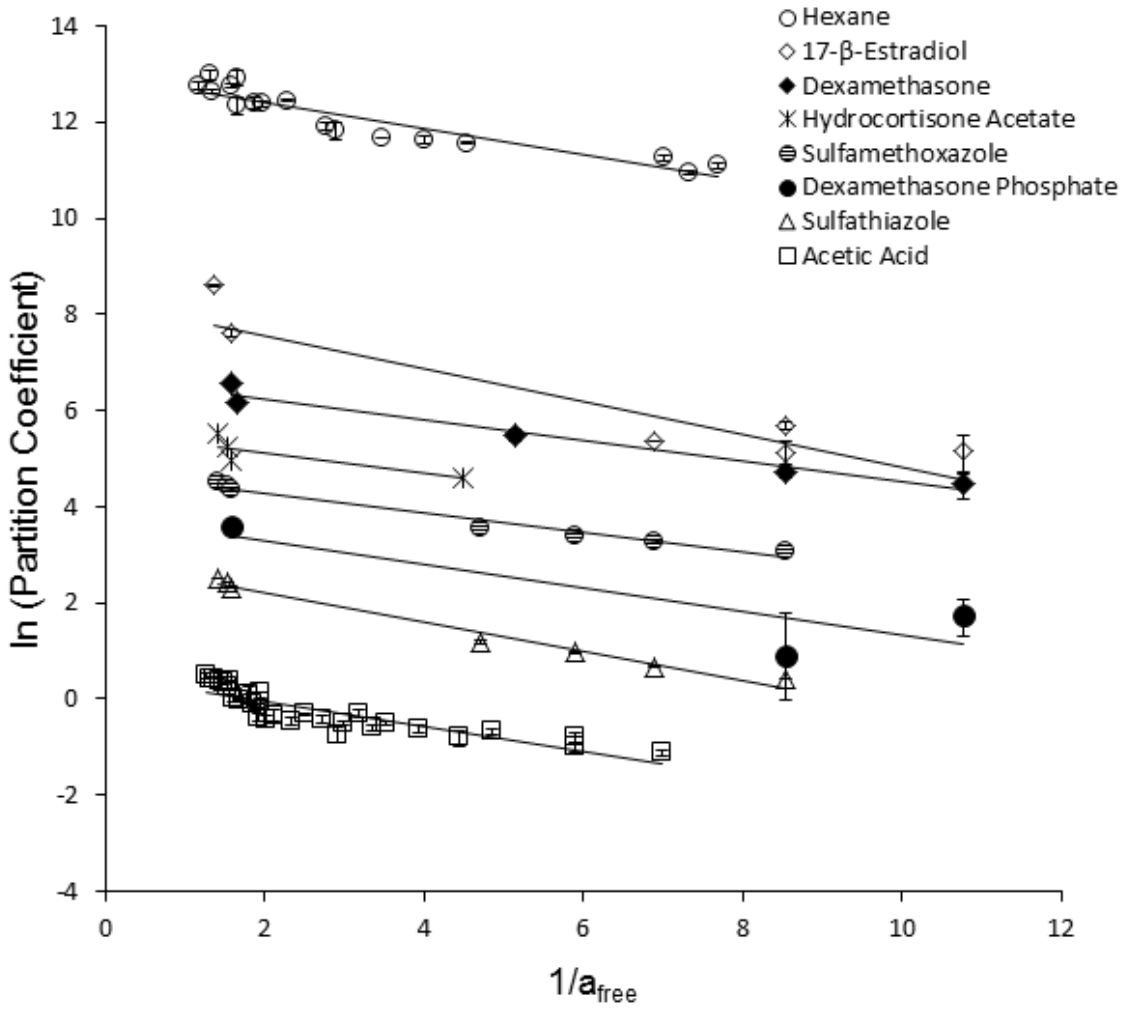

Figure 3.12 Natural logarithms of membrane-partition coefficients for various solutes versus the inverse of free surface area (1/afree).

Key: hexane (55) (○,slope=-0.28); 17-β-estradiol (149) (◊,slope=-0.34); Dex (♦,slope=-0.22); hydrocortisone acetate (145) (✳,slope=-0.21); sulfamethoxazole (144) (◍,slope=-0.21); Dex-P (●,slope=-0.24); sulfathiazole (144) (Δ,slope=-0.17); and acetic acid (122) (□,slope=-0.26). (The partition coefficient values are in mole fraction for hexane and in molarity for the other solutes).

head group, acyl chain length, degree of unsaturation, presence of cholesterol, etc.), size and lamellarity, temperature, and the like can be significant factors in determining the results obtained. Presently, a different LFER equation is required for each lipid system (146), highlighting the need for unifying relationships that could quantitatively predict membrane-water partitioning from a knowledge of drug structure, membrane composition, and the environmental conditions.

Some of the pioneering work on bilayer/water partitioning has revealed that factors such as decreasing the temperature below the phase transition temperature, inclusion of cholesterol in the bilayer, or elongating the phospholipid chain length cause decreases in partition coefficients that can be correlated with order parameters such as surface density of the bilayer chains (55, 121) or free surface area of the bilayer (122). The solutes typically employed in these studies have been simple, small molecules such as benzene, hexane, and acetic acid. Whether or not such relationships exist for larger and more structurally complex drug molecules has not been established. The present study of the partitioning behavior of Dex and Dex-P provides an opportunity to begin to explore the hypothesis that the bilayer free surface area is a "universal" variable useful in relating membrane-water partition coefficients to bilayer composition.

Factors Governing the Membrane-Water Partition Coefficient

Drug Concentration & Drug-to-Lipid Ratio

An important factor in the determination of reliable membrane-water partition coefficients is the bound drug-to-lipid ratio at equilibrium. As noted by De Young and Dill, it is very important to extrapolate partitioning data to infinite dilution for their proper interpretation. Unlike adsorption to solids that might be construed as having a

fixed number of binding sites, solute binding to bilayer membranes may involve partial or complete insertion into the membrane with accompanying changes in both bilayer surface area and the chemical nature of the surface, with an increase in the bound drug/lipid ratio. These alterations with increasing solute uptake may lead to either increases or decreases in the apparent partition coefficient with drug concentration (121, 136, 150, 151). Alternatively, self-association of drug molecules with each other at high aqueous drug concentrations may reduce the activity of the free available drug for the partitioning (152).

The importance of determining partition coefficients at concentrations approaching infinite dilution is evident from the difference in the partition coefficients obtained for Dex from the two different methods employed in this study. In the equilibrium dialysis method, the drug-to-lipid ratio could be varied with values approaching infinite dilution (~0.001) (Figure 3.4 inset) whereas in the equilibrium solubility method, the drug to lipid ratio in DMPC was constant at 0.07 (±0.004) even with varying lipid concentration as dictated by the equilibrium solubility of Dex and the DMPC-water partition coefficient. The equilibrium solubility method could not be used to probe DMPC partitioning in a concentration region approaching infinite dilution and therefore the values obtained using this method differed from those obtained by equilibrium dialysis (Figure 3.6). This was not the case for Dex partitioning in DPPC and DSPC where the drug-to-lipid ratios at equilibrium were <0.02 using the solubility method. For DPPC and DSPC, the partition coefficients were the same by either method.

While generally higher drug-to-lipid ratios are possible for neutral molecules in comparison to ionized compounds before deviations from linearity in sorption isotherms

become apparent, the borderline appears to vary with the compound and lipid. Escher found no deviations from linearity in neutral compound sorption isotherms up to drug-to-lipid ratios of 0.1 (116) while Austin et al. suggested that the ratio of lipid to bound neutral compound should be greater than 60 (111) which would translate to a drug-to-lipid ratio of <0.017. As noted above, a significant deviation was found in the partition coefficient for Dex at a drug-to-lipid ratio of 0.07 but using equilibrium dialysis at drug-to-lipid ratios <0.007 the partition coefficients were independent of drug-to-lipid ratio (Figure 3.4 & 3.7 insets).

Deviations in the sorption isotherms for Dex-P at pH conditions where the bound drug is neutral were clearly evident at drug-to-lipid ratios above 0.04. Eq. 3.3 was therefore used to extrapolate these results to infinite dilution. Langmuir-type adsorption models are commonly employed to account for saturation effects in membrane partitioning of drug molecules (153, 154). While the assumption of a fixed number of binding sites may not accurately reflect the nature of the binding of molecules to flexible bilayer membranes, it might be justifiable for drugs that bind predominantly at the membrane surface (137). Changes in partitioning at high drug concentration are more likely due to changes in the membrane or in the affinity of the drug molecule for the modified membrane surface rather than a depletion of binding sites (136). However, at infinite dilution, partitioning and association models are equivalent.

Sorption isotherms for ionized molecules become non-linear mainly because of the repulsive forces between the charged species upon membrane binding (134, 135, 137-139, 148). Austin et al suggested that for ions also, a ratio of lipid to bound ion >60 should be sufficient to render surface charge effects insignificant (111), although the

Gouy-Chapman theory can be used to correct for surface charge effects at higher drug concentrations (Figure 3.8 inset) (109, 116, 134, 135, 137, 138, 148, 155, 156).

Temperature Dependence of Partition Coefficients

The fundamental driving force for transfer of nonpolar solutes from water to a lipid environment is generally assumed to be the hydrophobic effect but specific solute interactions with the ordered bilayer structure modulate the overall thermodynamics of the process (157, 158). The dependence of the membrane-water partition coefficient of Dex was measured in DPPC liposomes as a function of temperature from 25-45 °C, a range that crosses the gel->liquid crystalline transition temperature of 41 °C. These results are displayed in the van't Hoff plot in Figure 3.7B. The standard free energy change ($\Delta G°$) upon transfer of Dex from water to DMPC liposomes was negative at all temperatures indicating an energetically favorable process, driven by a positive entropy ($\Delta H°$=58.6 kJ/mol and $\Delta S°$=235.1 J/mol.K). The thermodynamic parameters for the transfer of Dex compare reasonably well qualitatively with values reported elsewhere for corticosteroid transfer into DMPC bilayers both above and below its Tm, supporting the observations of an entropy driven process for the partitioning of steroids into saturated phospholipids (145, 159). One contribution to the positive entropy is that associated with the removal of the steroids from water (57, 159, 160).

Kwon et al obtained the enthalpy and entropy changes for partitioning of several endocrine disruptors between water and liposomes formed from DOPC, POPC, DMPC, DPPC, and DSPC at temperatures ranging from 11 – 37°C (149). Over this temperature range DOPC and POPC liposomes are liquid crystalline and DPPC and DSPC liposomes are in a gel phase. DMPC undergoes a phase transition within the middle of this

temperature range at 23 °C. Generally, they found negative enthalpies of solute transfer from water to liquid crystalline bilayers consisting of unsaturated lipids and positive enthalpies for the transfer of solutes from water to gel phase membranes composed of saturated phospholipids. Others have reported similar findings (161, 162). Such disparities illustrate the greater complexity of the membrane binding process relative to that for solute partitioning from water to bulk solvents.

Xiang and Anderson (131) determined that apparent energies of activation for acetic acid permeability across liquid crystalline bilayer membranes increase in a dramatic fashion with increases in chain ordering, with an Ea value of only 13 kcal/mol in DLPC containing 20% cholesterol increasing to 20 kcal/mol in DMPC, and 37 kcal/mol in DPPC. The enthalpy of transfer of acetic acid from water to decane, a bulk solvent that mimics the chemical selectivity of phospholipid bilayers toward permeants, is only 4.8 kcal/mol (122). Thus, the elevated apparent energies of activation for acetic acid transport were attributed largely to an increase in enthalpy for acetic acid insertion into the bilayer barrier domain (i.e., the ordered acyl chain bilayer interior) with increases in chain ordering. This unfavorable enthalpic contribution should be less important for solute partitioning in comparison to transbilayer permeation because most drug molecules are likely to be only partially inserted into the ordered chain region of the bilayer at equilibrium, but this factor may nevertheless contribute to the positive enthalpies generally observed for solute transfer from water into gel phase bilayers as observed by Kwon et al. and others (144, 149, 163). On the other hand, the liquid crystalline bilayers such as the DOPC and POPC systems explored by Kwon et al are highly disordered. For such systems, the enthalpy associated with partial solute insertion into the acyl chain

region likely consists of a small positive hydrophobic contribution that is often more than compensated for by the negative enthalpic contribution accompanying hydrogen bonding interactions or other electrostatic interactions between polar functional groups within the solute and polar phospholipid head groups.

The thermodynamic driving force for the interaction may vary depending on the location of binding, nature and structure of the solute and physical state of the bilayer (149, 163). Removal of a hydrophobic solute from water and partitioning presumably into the hydrophobic core of the membranes is entropically driven. Whereas, if a drug is preferentially bound to the interface due to electrostatic interactions between the charged drug and phospholipid headgroups, favorable enthalpy may dominate over the entropy, example, cationic drugs have exothermic partitioning as compared to neutral (114). Thus, the relative contribution of entropy driven hydrophobic effect and enthalpy driven hydrophobic and electrostatic interaction between drug and membranes to the overall free energy of transfer will really determine the thermodynamic driving force.

Structure-Partitioning Relationships – 21-Phosphate Group Contribution & Ionization

As reported in Table 3.1, the Kp value for Dex at 25 °C varies from 705 ± 24 in liquid crystalline DMPC to 106 ± 11 in DPPC and 58 ± 9 in DSPC bilayers, both of which are in their gel state at room temperature. These results illustrate the dramatic effect that simply changing the chain length of the phospholipid can have on the partition coefficient. Given such differences, it is understandable that a different LFER equation is required for each lipid system (146).

The contribution of the polar phosphate group at the 21-position of dexamethasone to the free energy of transfer from water to DMPC depends on its state of ionization. Fitting the

K_p^{app} vs. pH data in Figure 3.9 to the model described in Eq. 3.7 generated values of K_p for the neutral and monoanion forms of Dex-P of 241 ± 38 (95% C.I.) and 48 ± 9 (95% C.I.), respectively. Comparing the neutral K_p values for Dex vs. Dex-P, phosphorylation of Dex reduces its partition coefficient by only 3-fold, giving a group contribution for the unionized phosphate residue to the transfer free energy from water to DMPC of only $\Delta(\Delta G°)$ = 2.66 kJ/mol (0.64 kcal/mol). Monoanion formation reduces K_p by another 5-fold and dianion formation leads to a further decrease such that at pH 8, K_p is close to zero.

Several reports indicate that amphiphilic molecules orient themselves at the interphase of bilayers such that charged or polar groups interact with lipid head groups while their non-polar regions are embedded in the hydrocarbon region of the bilayer (119, 164-166). Vijayan et al. (166) conducted MD simulations of the location and orientation of cortisone, a corticosteroid similar in structure to Dex, in a model lipid bilayer. They observed that, unlike cholesterol which aligns itself approximately parallel to the bilayer chains, cortisone adopts an orientation that is nearly parallel to the bilayer surface such that its polar groups are able to maximize favorable contacts in the heterogeneous bilayer interface region. With the increase in charge and hydrogen bonding potential accompanying 21-phosphorylation, the molecule is likely pulled further towards the interface such that particularly the phosphate monoanion residue remains solvated by water. The reduction in the partition coefficient reflects the greater amount of energy needed to break the hydrogen bonds and remove the hydrophobic portions of the solute from water (112, 167).

Effect of Bilayer Free Surface Area

Unlike bulk solvents, lipid bilayers are interfacial phases having properties that depend on surface density or free surface area. The acyl chain in bilayers are more highly ordered near the headgroups and the order diminishes with distance towards the bilayer center (61). The free surface area and the length of the phospholipid acyl chains are the principal independent variables that determine the chain organization (55). We studied the effect of changes in free surface area by altering the phospholipid acyl chain lengths and by varying temperature.

In the current study, DMPC was in liquid crystalline state at 25 °C, DPPC was in gel state at 25 and 37 °C and in liquid crystalline state at 45 °C and DSPC in a gel phase at 25 °C. Irrespective of the ordering mechanism (temperature or lipid composition), the partition coefficient of Dex was found to be negatively dependent on the inverse of free surface area (Figure 3.11). A linear relationship was obtained between $ln(K_p)$ and the inverse of free surface area ($1/a_{free} = \sigma/(1- \sigma)$) for Dex (slope=-0.22). Dex-P at pH 4.0 exhibited a similar dependence on free surface area with a similar slope (=-0.24). Dex-P, the prodrug of Dex having the same steroidal parent structure and differing only in the presence of a phosphate at the 21-position, is predominantly monoanionic at pH 4.0. The similarity in slopes indicates that the two molecules, one neutral and one anionic, have nearly equal sensitivities to bilayer chain ordering as quantified by the free surface area parameter.

There are numerous reports in the literature of decreases in membrane partition coefficients of various solutes with increases in alkyl chain length of the phospholipids, changes in the degree of chain unsaturation, decreases in temperature, or incorporation of cholesterol into liquid crystalline bilayers (55, 121, 122, 145, 146, 151). Yamamoto and

Liljestrand (146) observed a 20-fold decline in the room temperature partition coefficient of estradiol when the liposome composition was changed from POPC to DPPC. This substantial effect of lipid composition on solute partitioning was attributed to the influence of chain saturation on the main transition temperature. At room temperature POPC liposomes exist as a liquid crystalline phase while DPPC is in a gel phase.

The lattice theory developed by Marqusee and Dill (108) suggests that solute partitioning will decrease with increasing surface density due to the increasingly unfavorable entropy associated with solute insertion as orientational ordering of the phospholipid chains is increased. Experimentally, correlations have been observed between the partition coefficient for small molecules (hexane, benzene and acetic acid) and surface density of the lipid bilayer (55, 121, 122). Xiang and Anderson combined statistical mechanical theory with molecular dynamic simulation to show that the lateral pressure in a bilayer increases steeply with surface density and that increased lateral pressure results in higher local order and exclusion of solutes from the interphase (110). In other words, increased chain-chain interaction at higher chain density inhibits solute incorporation (146, 151, 152, 168).

These results suggest that solute exclusion accompanies chain ordering but the magnitude of the effect may be solute dependent. To explore whether a general, quantitative relationship can be found between bilayer chain ordering and membrane-water partition coefficients, the natural logarithms of the bilayer-water partition coefficients of several drugs from studies published by other labs against the inverse of free surface area, $1/a_{free}$ was plotted in Figure 3.12. These studies employed similar phospholipids as those in the present study. The average of the slopes was -0.26 with a 95% confidence interval of -

0.22 to -0.29, emphasizing the negative relationship between the partition coefficient and inverse of free surface area of the bilayers.

Xiang and Anderson (131) previously determined both partition coefficients and permeability coefficients for acetic acid as a function of surface density. A slope of -0.26 for the natural logarithm of the partition coefficient of acetic acid versus the inverse of free surface area was found in Figure 3.12 which compares to a much steeper slope (-0.71) when their permeability data for acetic acid are plotted in the same manner, a 2.7-fold difference. This is attributed to the requirement for passage of the solute across the bilayer barrier region for permeation whereas partitioning involves only partial insertion into the interfacial region of the bilayer for acetic acid (122, 131). In all cases, there is a dependence of the partitioning on the available free surface area, as demonstrated by Figure 3.12 for several different solutes varying in size and chemical properties. Generally, drug molecules having both polar and hydrophobic residues may bind in the interfacial region of bilayers with only portions of their structures embedded into the ordered alkyl chain region depending on their lipophilicity. The similarity of the slopes obtained for all of the representative solutes illustrated in Figure 3.12 suggests that the dependence of partitioning on chain ordering is not highly sensitive to either the overall size or chemical structure of the solute. The relatively uniform but modest dependence of membrane binding on bilayer free surface area may reflect the availability of hydrophobic surface area on the membrane, which is the surface property that increases with an increase in free surface area. While the above relationship appears to be valid for partitioning to a sub-set of bilayers composed of saturated phospholipids both above and

below their phase transition temperatures, further studies in a more diverse set of membranes are necessary to determine the universality of this relationship.

CONCLUSIONS

The partition coefficient of a drug in bilayer is dependent upon several factors such as the bound drug-to-lipid ratio, pH, temperature, membrane composition, etc. Appropriate corrections for neutral and ionized species at high concentrations are required in order to determine a reliable partition coefficient value (at infinite dilution). The membrane-water partition coefficient of Dex at infinite dilution was studied in liposomes of varying composition. Increasing the negative charge of Dex-P gradually reduced the partition coefficient, ultimately overcoming the hydrophobic contribution to membrane insertion provided by the steroid rings. In order to explore the possible existence of a relationship between membrane-water partition coefficients and bilayer chain ordering, the partition coefficients were related to the inverse of bilayer free surface area. For both, Dex and Dex-P, the natural logarithms of the partition coefficients in liposomes decreased linearly with the inverse of free surface area in the bilayer as modulated by increasing phospholipid chain length or decreasing temperature. Inclusion of membrane partitioning data in saturated lipid systems for other solutes from the literature, showed a similar dependence on the free surface area. These results may be useful in the development of more comprehensive quantitative models relating membrane-water partition coefficients of drug molecules to bilayer properties.

CHAPTER FOUR

Determination of Drug Release Kinetics from Nanoparticles: Overcoming Pitfalls of the Dynamic Dialysis Method

INTRODUCTION

Interest in nanoparticle drug delivery systems has grown dramatically in recent years due to their manifold potential applications in solubilizing poorly soluble drug candidates, reducing drug toxicity, prolonging circulation times, controlling drug release kinetics, drug targeting, and monitoring drug delivery to enhance therapeutic efficacy (1-3, 169-171). Nanoparticles have been particularly attractive in cancer because of their passive targeting potential through the enhanced permeability and retention (EPR) effect (172-174) and the perception that with the right size, shape, and cell surface properties, nanoparticles can circulate systemically for a prolonged period, accumulate in tumor tissue and release drug locally to cancer cells (20, 45, 175, 176). To maximize the effectiveness of nanoparticle targeting, drug release from nanoparticles needs to be slow enough to avoid substantial drug loss before the carrier reaches the site of action thereby reducing toxicity (177, 178). After nanoparticle accumulation at the target site, optimizing efficacy will require tunability of the drug release rate (51, 52, 126). Thus, the kinetics of drug release from nanoparticles should be an essential feature of their design and a property monitored for the quality control of nanoparticle formulations. Reliable determination of *in vitro* release kinetics is also a prerequisite for establishing *in vitro - in vivo* correlations which in turn define the formulation performance *in vivo*.

Dynamic dialysis is one of the most commonly used methods for the determination of release kinetics from nanoparticles. Very recently, Zambito *et al*. pointed out that out of

90 literature reports on *in vitro* drug release from nanoparticles surveyed in the year 2011, nearly 40 used dynamic dialysis to measure the release kinetics (70). The reason for the popularity of dynamic dialysis over other methods (e.g., ultracentrifugation and ultrafiltration) is that the additional step of separating nanoparticles from the free drug at various time points during the kinetic study is eliminated. The external pressure applied for separation in other methods can disturb the equilibrium and incomplete separation can lead to significant measurement errors (68, 179).

In dynamic dialysis, the appearance of drug in the "sink" receiver compartment is the result of diffusion from the nanoparticles followed by diffusion across the dialysis membrane, though it is generally treated as a simple first-order process. Experimentally, either disappearance of drug from the donor compartment containing the nanoparticles or appearance in the receiver compartment can be measured. Because the apparent release rate is the net result of drug transport across two barriers in series, the rate constant obtained may not necessarily reflect the rate of drug release from the nanoparticles. Both, the barrier properties of the dialysis membrane and the driving force for drug transport across that membrane must be considered. The latter quantity, the driving force, is not the total drug concentration in the nanoparticle dispersion but the free aqueous drug concentration, a quantity that is of critical importance but never measured directly. Therefore, assessment of the reliability of rate constants determined by dynamic dialysis demands a careful consideration of the pitfalls in interpreting apparent release data.

Some authors have recognized the potential sources of error in data generated using dynamic dialysis for the determination of release rates from nanoparticles. As mentioned above, the inherent barrier properties of the dialysis membrane itself may impose a limit

on the rate constant of release from nanoparticles that can be measured (180, 181). Others have highlighted the issue of drug partitioning between the phases present in dispersed systems and their influence on the driving force for drug transport across the dialysis membrane (70, 182-184). Reversible drug binding to the nanocarrier reduces the driving force governing drug transport across the dialysis membrane which may alter the overall apparent rate of release. Currently, there is not only a lack of general agreement on the reliability of the dynamic dialysis method, but also uncertainty as to the lower limit of nanoparticle release half-lives that can be accurately determined using this method.

In this paper, the practical limitations of the commonly used dynamic dialysis method for determination of apparent release kinetics was highlighted along with the value of using mechanism-based models both to obtain the actual rate constant for nanoparticle release and to estimate its level of certainty. The experiments utilize liposomes as representative nanocarriers and two model hydrophobic drugs, one of which is ionizable. A comprehensive analysis of the interplay of the critical factors (membrane/water partition coefficient, lipid concentration, and liposomal and dialysis membrane permeability coefficients) that govern the apparent release kinetics illustrates the potential pitfalls underlying this method. The mathematical models and their utility in extracting reliable rate constants for drug release are demonstrated in cases where drug binding effects and/or dialysis membrane transport may be partially contributing to the apparent release kinetics. There are situations where dynamic dialysis can be safely used with simple first-order treatment of the data and situations requiring detailed, mechanistic modeling of the data.

MATERIALS AND METHODS

AR-67 (7-t-butyldimethylsilyl-10-hydroxycamptothecin) was provided by Novartis Pharmaceuticals Corporation (East Hanover, NJ). Dexamethasone (Dex) (≥98%, powder) was purchased from Sigma-Aldrich Co., St. Louis, MO. Lipids (DSPC (1,2-distearoyl-sn-glycero-3-phosphatidylcholine, >99% purity), DPPC (1,2-dipalmitoyl-*sn*-glycero-3-phosphocholine, >99% purity), DMPC (1,2-dimyristoyl-*sn*-glycero-3-phosphocholine, >99% purity), m-PEG DSPE (1,2-distearoyl-sn-glycero-3-phosphoethanolamine-N-[methoxy (polyethylene glycol)-2000]), m-PEG DPPE (1,2-dipalmitoyl-*sn*-glycero-3-phosphoethanolamine-N-[methoxy(polyethylene glycol)-2000]) and m-PEG DMPE (1,2-dimyristoyl-*sn*-glycero-3-phosphoethanolamine-N-[methoxy(polyethylene glycol)-2000])) were purchased as powders from Avanti Polar Lipids (Alabaster, AL). Sephadex® pre-packed (PD-10) size exclusion columns (GE Healthcare Bio-sciences Corporation (Piscataway, NJ)), containing about 8.3 ml of Sephadex G-25 M medium, were used for separation of free drug from encapsulated. Dialysis tubes (Float-A-Lyzer®, MWCO (Molecular Weight Cut Off): 100 kD) of 1 and 5 ml volumes were purchased from Spectrum Laboratories (Rancho Dominguez, CA). HPLC grade solvents and other chemicals were purchased from Fisher Scientific (Florence, KY). Deionized water was used for all experiments.

Liposome Preparation

Blank and drug loaded liposomes were prepared based on a previously reported method (127). Briefly, DMPC: mPEG DMPE, DPPC: mPEG DPPE and DSPC: mPEG-DSPE (95:5 mol%, 120 mg) were separately dissolved in about 2 ml of chloroform. The solvent

was evaporated under a stream of nitrogen and the resulting film was dried overnight in a vacuum oven.

AR-67 loaded liposomes

Drug loaded DSPC: mPEG-DSPE liposomes were prepared at pH 4.2 and 9.5. Blank liposomes at pH 4.2 were prepared by hydrating the dried lipid film in 85 mM acetate buffer (pH 4.2). Drug loading at pH 4.2 was accomplished by adding 10 µl of an AR-67 stock solution in DMSO (~80 µM) to 2 ml of blank liposomes and incubating at 60°C for about 2 hours. Drug loading at pH 9.5 was carried out by hydrating the dried lipid film in 2 ml of 100 mM borate buffer (pH 9.5) containing AR-67 (1.2 µM) by alternate vortexing and heating at 60°C. In all cases, the lipid suspensions were then extruded 10 times through two stacked 200 nm polycarbonate membranes (GE water and Process Technologies, Trevose, PA) using an extrusion device (Liposofast®, Avestin, Canada) at 60°C to obtain unilamellar liposomes.

Dexamethasone loaded liposomes

Blank DMPC, DPPC and DSPC liposomes were prepared by hydrating the dried lipid films in 2 ml of phosphate buffered saline (PBS, pH 7.4). Dexamethasone loaded liposomes were prepared by hydrating the dried lipid films in 2 ml of a PBS solution of dexamethasone (~0.05-0.06 mg/ml) to give a lipid concentration of 60 mg/ml. The suspensions were alternately vortexed and heated in a water bath to temperatures above the phase transition temperature of the respective lipid to uniformly suspend the lipid. The lipid suspensions were then extruded 10 times through two stacked 100 nm polycarbonate membranes using the extrusion device at 30°C, 50°C and 60°C for DMPC, DPPC and DSPC, respectively, to obtain unilamellar liposomes.

Blank and drug (AR-67 and Dex) loaded liposomes were allowed to cool to room temperature for 3 hours and stored at 4°C until further use. Particle sizes of the liposomes were measured by dynamic light scattering (DLS) using a Delsa™ Nano submicron particle size analyzer (Beckman Coulter Inc., Brea, CA) at 25°C. The liposomes were diluted in the same buffer as that used in their preparation.

Dynamic Dialysis Experiments

All drug loaded liposome suspensions were passed through a Sephadex® G25 column pre-equilibrated in the same buffer as that used in the preparation of liposomes in an attempt to separate free from entrapped drug. Aliquots (0.1-0.5 ml) of the drug loaded liposome suspensions were applied to the top of a Sephadex column and eluted with the same buffer as that used in the preparation in the increments of 1 ml. The eluent fraction containing liposomes was collected between 2.5 to 5 and analyzed for drug and lipid concentration. The residual extravesicular membrane bound fraction was determined from model fitting (*vide infra*). The eluent fraction containing drug loaded liposomes was diluted (if needed) in the same buffer to obtain a desired lipid concentration and introduced into the dialysis tube.

AR-67 loaded liposome suspensions were diluted to a lipid concentration of about 0.48 mg/ml before placing in the dialysis tube. Total drug concentration in the dialysis tube was monitored versus time for pH 4.2 drug loaded liposomes and blank liposomes spiked with drug (~75 nM) at 37°C after immersion in 1 L of acetate buffer (85 mM, pH 4.2) to provide sink conditions in the receiver solution. Dialysis experiments for drug loaded liposomes at pH 9.5 were conducted similarly after immersion of the dialysis tube in 1L of borate buffer (100 mM, pH 9.5). Aliquots (50 µl) withdrawn from inside the dialysis

tube at different time points were diluted with cold (−25 °C) 2:1 v/v methanol: acetonitrile and analyzed by HPLC.

Dynamic dialysis experiments for Dex loaded liposomes were conducted at high (~12-15 mg/ml) and low lipid concentrations (~4-5 mg/ml). Total drug concentration in the dialysis tube was monitored versus time after immersed in 1 L of PBS. Similar experiments were conducted using blank liposomes spiked with Dex (~20 µM for low and ~50 µM for high lipid concentration) and free Dex solution (100 µM) at 25°C. Dedicated dialysis tube was used for drug loaded, spiked and free drug profile in a particular lipid system in order to eliminate variability introduced by dialysis tubes. Aliquots (10-100 µl) withdrawn from inside the dialysis tube at various time points were diluted with an appropriate volume of methanol and analyzed by HPLC.

Drug Analyses

AR-67

Samples from release experiments were analyzed using a previously developed and validated isocratic high performance liquid chromatography (HPLC) method with fluorescence detection (126, 127). Both, lactone and carboxylate were monitored at pH 4.2 and 9.5. A Waters Alliance 2695 Separations Module coupled to a Waters Scanning Fluorescence Detector (M474) was employed with excitation and emission wavelengths at 380 and 560 nm, respectively. A Waters Symmetry® C18 column (5 µm, 3.9 X 150 mm) and guard column (3.9 X 20 mm) were used with a mobile phase composition of 48% acetonitrile and 52% (v/v) pH 5.5 triethylamine acetate (2%) buffer. Standards for AR-67 carboxylate (0.2-2 µM) were prepared in 10 mM sodium carbonate buffer (pH 10.4) and standards for AR-67 lactone (0.5-2.5 µM) were prepared in acidified methanol.

The retention times at an injection volume of 10 µl and a flow rate of 1 ml/min were 1.7 and 5.9 min for AR-67 carboxylate and lactone, respectively.

Dexamethasone

Samples from liposome release studies and partitioning experiments were analyzed using an isocratic HPLC method with UV detection. Four independent standards of dexamethasone (50-800 µM) in methanol were prepared and the relative standard deviation for the response factor was less than 3%. A Waters Alliance 2695 Separations Module coupled to a UV detector (Waters 996, Photodiode Array Detector) was employed at a wavelength of 240 nm. A Waters Symmetry® C18 column (5 µm, 3.9 X 150 mm) and guard column (3.9 X 20 mm) were used with a mobile phase composition of 32% acetonitrile and 68% (v/v) pH 5.5 triethylamine acetate (2%) buffer. The retention time for Dex at an injection volume of 10 µl and a flow rate of 1 ml/min was about ~6.4 min.

Lipid Analysis

Lipid concentrations in blank and drug loaded liposome dispersions were analyzed by HPLC using ELSD (Evaporative Light Scattering Detector), as reported previously (126). Briefly, an Allsphere™ Silica Column (Grace Davison Discovery Sciences, Deerfield, IL) (5 µ, 4.6X150 mm) and guard column (5µ, 7.5 X 4.6mm) were employed with a linear gradient method starting with 100% (v/v) mobile phase A (80% chloroform:19.5% methanol:0.5% (v/v) ammonium hydroxide solution (30%) and changing to 80% mobile phase A:20% mobile phase B (80% methanol:19.5% water:0.5% (v/v) ammonium hydroxide solution (30%)) over 3 min. Standards were made in mobile phase A and linearity was observed between log concentration and log area of the peak over the

concentration ranges of 150-800 µM for DMPC, 100-400 µM for DPPC, and 150-400 µM for DPPC. Aliquots of blank and drug loaded liposomes (10-20 µl) were transferred to test tubes, dried under nitrogen and stored at -20°C until further analysis. For analysis, the dried lipid films were re-constituted in mobile phase A.

MATHEMATICAL MODELING AND SIMULATIONS

Data fitting and simulations were done based on previously developed mathematical models (126, 127, 132). The models take into account the inner and outer aqueous volumes, the volumes of the inner and outer bilayer leaflets in the liposome suspension, and the membrane-water partition coefficient of drug to determine the fractions bound inside and outside the liposomes. The rate of bilayer transport of the encapsulated drug is determined by the concentration gradient of the unbound neutral drug concentration. The extravesicular unbound concentration is dictated by the partition coefficient and the rate of drug transport across the dialysis membrane into a large volume of the reservoir solution to provide sink conditions. Thus,

$$\frac{d(D_i)}{dt} = -k_m(D_i^w - D_o^w) \qquad (4.1)$$

$$\frac{d(D_i)}{dt} = -k_m(\alpha_i D_i - \alpha_o D_o) \qquad (4.2)$$

$$\frac{d(D_o)}{dt} = \frac{k_m}{x}(D_i^w - D_o^w) - k_d(D_o^w) \dots\dots x = \frac{V_o}{V_i} \qquad (4.3)$$

$$\frac{d(D_o)}{dt} = \frac{k_m}{x}(\alpha_i D_i - \alpha_o D_o) - k_d(\alpha_o D_o) \qquad (4.4)$$

$$where, \quad \alpha_i = \frac{ab}{b + aK_p}, \alpha_o = \frac{cd}{d + cK_p}; a = \frac{V_i}{V_i^w}, b = \frac{V_i}{V_i^m}, c = \frac{V_o}{V_o^w}, d = \frac{V_o}{V_o^m}$$

where, D_i and D_o are the total intravesicular and extravesicular (within the dialysis tube) drug concentrations respectively; a and b are volume ratios to account for the differences

in aqueous and membrane volumes with respect to the total intravesicular volume; c and d are volume ratios to account for the differences in aqueous and membrane volume with respect to the total extravesicular volume in the dialysis tube. V_i is the total liposomally entrapped aqueous volume plus the lipid volume in the inner bilayer leaflet of liposomes in the suspension, V_i^w and V_i^m are the volumes of the inner aqueous compartment and inner monolayer in each vesicle, respectively. V_o is the extravesicular aqueous volume along with the volume of lipid in the outer bilayer leaflet of suspended liposomes in the dialysis tube; V_o^m is the volume of the outer monolayer in each vesicle and V_o^w is the volume of the extravesicular aqueous compartment in the dialysis tube. K_p is the membrane-water partition coefficient, α_i and α_o are the factors that account for the binding of drug to lipid membrane and convert total intravesicular and extravesicular concentrations to the aqueous free concentrations, respectively; k_m and k_d are the rate constants for drug transport across the lipid bilayer and dialysis membrane respectively and x is the ratio of extravesicular to intravesicular volume in the dialysis tube.

To account for non-instantaneous drug binding to the dialysis membrane, modifications to the model were made to account for release profiles of Dex,

$$\frac{d(D_o)}{dt} = \frac{k_m}{x}(\alpha_i D_i - \alpha_o D_o) - (k_{on} + k_d)\alpha_o D_o + \frac{k_{on}}{K} D_m \qquad \left(K = \frac{k_{on}}{k_{off}}\right) \qquad (4.5)$$

$$\frac{d(D_m)}{dt} = k_{on}\alpha_o D_o - \frac{k_{on}}{K} D_m \qquad (4.6)$$

where, D_m is the drug concentration bound to the dialysis membrane and k_{on} and k_{off} are the association and dissociation constants, respectively, for binding of drug to the dialysis membrane.

Simulations were conducted to evaluate the impact of variations in the membrane-water partition coefficients of the drug and the lipid concentration inside the dialysis tube on the overall release profiles from liposomes at various k_m values. To determine the region of the variable space in which reliable rate constants for drug release could be obtained (in the absence of experimental variability), simulations were performed using the above detailed mathematical model assuming an intrinsic rate constant and then the simulated data were fit using a simple first order rate equation. For an assumed higher intrinsic rate constant, the apparent kinetics (k_{app}) can be slower at high partition coefficient because $k_{app}=k_m*\alpha i$ where αi is the factor that accounts for intravesicular binding. The effective rate constant was deemed to be determinable by dynamic dialysis and a first-order treatment if the fitted rate constant from first order model was within ± 20% of the input or assumed value.

RESULTS AND DISCUSSION

Liposome Characterization

The particle sizes of blank and AR-67 loaded DSPC liposomes (pH 4.2 and 9.5) were 180±15 nm, with polydispersity indices in the range of 0.04-0.07. Blank and Dex loaded DMPC, DPPC and DSPC liposome particle sizes were in the range of 90±20 nm, with polydispersity indices between 0.05-0.08, indicating monodisperse formulations. The extrusion procedure employed in this study was previously shown by ^{31}P-NMR to produce unilamellar vesicles (141).

In order to assess the impact of lipid concentration on the apparent release kinetics, it was important to analyze the actual lipid concentrations in blank and drug loaded liposomal suspensions used in release studies. Lipid concentrations were analyzed prior to release

experiments by gradient HPLC with evaporative light scattering detection and were typically 25-35% lower than the theoretical concentrations indicating some lipid loss during the extrusion process. The retention times of DMPC, DPPC and DSPC were 8.2, 8.0 and 7.9 min, respectively.

Determination of the particle size and actual lipid concentration of liposomal suspensions was critical for mathematical modeling of the release data as the calculation of α_i and α_o in Eqs. 4.2, 4.4, and 4.5 requires this information. The parameters a and b (internal volume ratios) needed to determine α_i are directly dependent on particle size while the parameters c and d (external volume ratios) necessary for the determination of α_o are dependent on both particle size and lipid concentration.

Factors Governing the Apparent Release Rate Constants using Dynamic Dialysis

As depicted for liposomal release in Figure 4.1, four major factors govern the determination of reliable release rate constants from nanoparticles by dynamic dialysis: 1) the effective drug concentration within the nanoparticle provides the driving force for release from the particle (*i.e.*, D_i^w in Figure 4.1); 2) the rate constant (k_m) for nanoparticle release reflects the properties of the barrier domain within the carrier (*i.e.*, for liposomes this is the ordered chain region of the bilayer); 3) drug binding/partitioning to the nanoparticles and the dialysis membrane influences D_o^w, the effective drug concentration within the dialysis tube that serves as the driving force for drug transport across the dialysis membrane once the drug is released from the nanoparticle; and 4) the dialysis membrane itself constitutes a second transport barrier as represented by k_d. The effective liposomal drug concentration, D_i^w, is the unbound intravesicular aqueous concentration of the permeable drug species. Referring to Eqns. 1-6, $D_i^w = \alpha_i D_i$ where

D_i is the total intravesicular drug concentration and α_i accounts for the binding of drug to the inner leaflet of the bilayer. The mathematical model treatment, developed based on the equilibrium and transport processes and described by Eqns. 4.1-4.6, is applicable to nonionizable drugs. For an ionizable drug where the neutral species is the permeant, D_i^w would be reduced by both membrane binding and ionization as demonstrated in previous work (126).

The rate of neutral drug release from nanoparticles that would be expected under true sink conditions, as would likely prevail in the systemic circulation in vivo, is reflected in the first term of Eqn. 4.2, $d(D_i)/dt = -k_m \alpha_i D_i$. Thus, the first two factors outlined above govern drug release under sink conditions while factors (3) and (4) come into play when release rates are monitored using dynamic dialysis. In dynamic dialysis all four factors are intertwined although one process may dominate over the others, depending upon the drug and nanoparticle properties, the nanoparticle concentration, drug loading, and the dialysis membrane selected. Herein, we demonstrate the effect of these factors on the determination of release rates using liposomes as representative nanoparticles, but the general principles should be more broadly applicable.

Release Kinetics of AR-67 from DSPC Liposomes at pH 4.2 and 9.5

The release kinetics of AR-67 from liposomes at pH 4.2 and 9.5 demonstrate two contrasting scenarios that may be encountered in determining release profiles by dynamic dialysis. The first and most straightforward situation to be presented is that for the release of AR-67 at a constant (intra- and extravesicular) pH of 9.5 as shown in Figure 4.2. AR-67 is a camptothecin analogue having a α-hydroxy-δ-lactone moiety that undergoes pH-dependent chemical hydrolysis to a ring-opened carboxylate form. In its lactone form, the

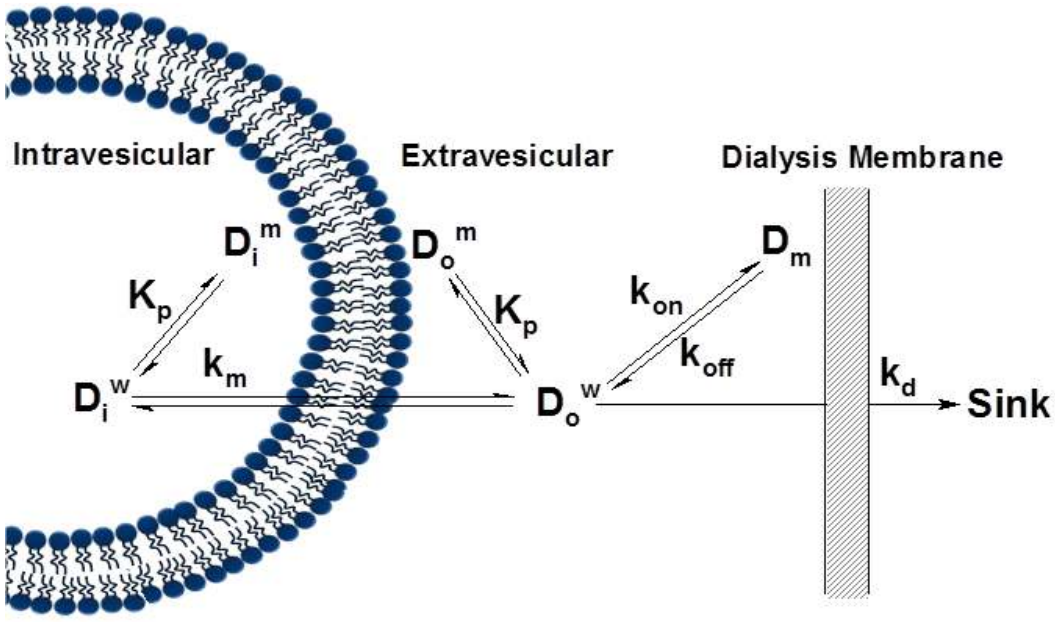

Figure 4.1 Schematic depicting the ionization and binding equilibria along with transport pathways representing the study of drug release kinetics from liposomes by dynamic dialysis method.

Diw and Dim are the intravesicular aqueous and membrane bound drug concentration respectively, Dow and Dom are the extravesicular aqueous and membrane bound drug concentration respectively. Dm is the dialysis membrane bound drug concentration. km and kd are the rate constants for permeation across the bilayer membrane and dialysis membrane respectively. kon and koff are the apparent association and dissociation constants for the binding of drug to the dialysis membrane.

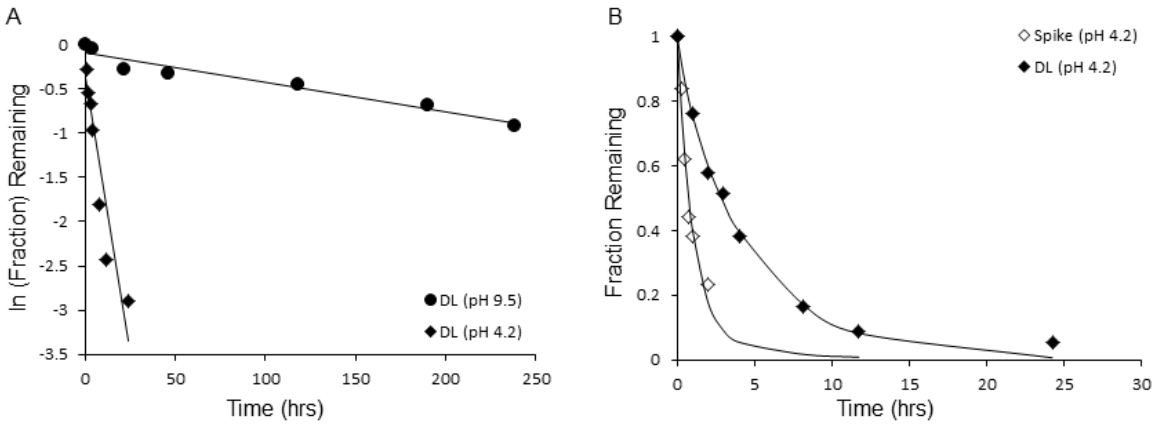

Figure 4.2 Fractions of initial amount of AR-67 remaining in dialysis tube versus time. (A) First order fits of release profiles of AR-67 loaded DSPC liposomes at pH 4.2 (lactone) and pH 9.5 (carboxylate). (B) Simultaneous model fitting of the AR-67 loaded (pH 4.2). DL stands for drug loaded liposomes.

predominant species at pH 4.2, this compound is highly hydrophobic with a cLogP=5.4±1.3. The aqueous solubility of the lactone form is extremely low at 0.11 µg/ml (127, 185). However, at pH 9.5, AR-67 exists predominantly in its membrane impermeable carboxylate form and the overall release rate is very slow due primarily to the small fraction of lactone present at that pH (126). In this case, the liposomal release is clearly rate-determining and a first-order fit of the observed concentration versus time profile generated in a dynamic dialysis experiment can reliably be used to obtain the effective release rate constant that would also be expected under true sink conditions at the same pH. The first-order rate constant for AR-67 transport from DSPC liposomes at 9.5 estimated from Figure 4.2A is 0.0034 h^{-1} corresponding to a half-life of 204 hr. (It should be noted that the actual release half-life achieved in plasma for the above pH 9.5 liposomes was dramatically reduced due to CO_2 mediated dissipation of the internal-external pH gradient (126). Such considerations have not been taken into account in the present analysis.)

At pH 4.2, however, the rate of AR-67 release from DSPC liposomes is much faster, with an apparent first-order rate constant of 0.123 h^{-1} corresponding to a half-life of 5.6 hr. Given the hydrophobic nature of this drug in its lactone form and its substantial binding affinity toward liposome membranes (132) the question arises as to whether or not this apparent half-life truly reflects the rate constant for nanoparticle release.

In order to explore the potential confounding effects of extravesicular membrane binding and dialysis membrane transport in the pH 4.2 release experiment, blank liposomes at pH 4.2 were spiked with AR-67 solution at the same concentration as that present in the drug-loaded liposomal suspensions and subjected to the same dialysis procedure, as

shown in Figure 4.2B. Eqns. 4.2 & 4.4 were then employed to simultaneously fit the two release profiles in Figure 4.2B. The intrinsic rate constant k_m obtained for nanoparticle AR-67 release at pH 4.2 was 44 ± 18 h^{-1} ($k_m.\alpha_i$ = 0.22 h^{-1}) corresponding to a half- life of 3.1 ± 0.9 hr, in close agreement with the value of 2.8 ± 0.3 hr reported previously when a similar simultaneous fit of spiked and loaded liposomes was conducted (132). The intrinsic rate constant for free drug transport across the dialysis membrane (k_d) obtained from the simultaneous model fitting in Figure 4.2B was 1.2 ± 0.2 h^{-1} corresponding to a half-life of 0.52 ± 0.07 hr. In the presence of liposomes, the half-life for AR-67 disappearance in a spiked experiment increased to 0.73 hr due to the effect of extravesicular drug binding to the outer leaflet of the liposome bilayers (*i.e.*, reduction in α_o). This example illustrates the importance of probing for drug binding to nanoparticles after release. It also highlights the potential value of conducting a spiking experiment at the same nanoparticle concentration in conjunction with simultaneously fitting the two release profiles to obtain a more reliable estimate of the true rate constant for drug release from the nanoparticles.

The Unencapsulated Initial Drug Concentration

In simultaneously fitting Equations 2 and 4 to drug loaded and spiked liposome release data such as those shown in Figure 4.2B, the fraction of unencapsulated drug present in drug-loaded liposomes at t=0 must be considered. In practice, a liposome/drug system is never completely free of unencapsulated drug (186). For blank liposomes, the term D_0 representing the extravesicular drug concentration can be assumed to represent 100% of the drug added at t=0 but for drug loaded liposomes, D_0 is unlikely to be zero despite attempts to separate free from entrapped drug by Sephadex column chromatography or

other techniques. In part, this is due to drug release from nanoparticles after the separation has been completed but prior to the start of a dialysis experiment. Another likely factor is that, depending on its binding affinity, drug bound reversibly to the nanoparticle may not be completely removed by separation on a Sephadex column. Shown in Figure 4.3A is an elution profile for the separation of liposome associated from free AR-67 on passage through a mini-Sephadex G-25 column such as that typically employed for separating free from encapsulated drug. The relatively small free drug peak (after 20 ml) compared to the drug peak in the liposome fraction eluting within 5 ml suggests that nearly all of the drug eluted in the liposome fraction. However, the passive loading technique used to prepare these liposomes should have led to no more than about 50% entrapment for a highly membrane bound drug, because approximately 50% of the bound drug should reside on the outer bilayer leaflet. Indeed, simultaneous fitting of the release data in Figure 4.2B indicated an initial unentrapped percentage in the drug-loaded liposomal suspension of 30 ± 14 %.

The efficiency of separation of free from encapsulated or membrane bound drug in a Sephadex column will be determined by several factors including the membrane/water partition coefficient, the sample load applied to the column, and the number of theoretical plates. Previously, Joguparthi *et al* obtained a value of K_p=2440 ± 230 for the partition coefficient of AR-67 with DSPC liposomes (187). To explore the possibility that external liposome binding may reduce separation efficiency, we conducted a spiking experiment using dexamethasone and DPPC liposomes. The partition coefficient for dexamethasone binding to DPPC liposomes is K_p=106 (188), much lower than that for AR-67 with DSPC liposomes. Blank DPPC liposomes were spiked with Dex solution and 0.5 ml of

this suspension was immediately added to a Sephadex column and eluted with PBS (pH 7.4). Figure 4.3B shows that about 40% of the added drug was associated with the liposome (first 5 ml) while the remaining drug continued to elute from the column over the next 15-20 min. Given that, as shown in the next sections, the half-life for Dex release from DPPC liposomes is ~ 4 hr, it is most likely that the high apparent concentration for entrapped Dex in this spiking experiment is due to binding to the outer leaflet of DPPC liposomes. These results justify the need to include a parameter to allow for an initial concentration of unencapsulated drug in fitting release data even after a Sephadex treatment.

Determination of Release Kinetics of Dex from DMPC liposomes

Dexamethasone is a non-ionizable corticosteroid having a log P= 2.03 and an aqueous solubility of 0.035 mg/ml (ACD/Labs V11.02). Initially, release kinetics of Dex encapsulated in DMPC liposomes were evaluated by dynamic dialysis in a manner similar to that described previously for AR-67 at pH 4.2. That is, drug loaded liposomal release was compared to that for blank liposomes spiked with Dex. A parallel experiment with an aqueous Dex solution was also included (Figure 4.4A). Unlike AR-67, the release profiles of Dex from loaded and spiked liposomes were virtually indistinguishable at a lipid concentration of ~13.9 mg/ml. A possible explanation for the similarity between drug loaded and spiked profiles was that entrapped drug release is relatively rapid. Simultaneously, the significant deviation of the spiked from free drug profile suggests that Dex binding to the liposomal bilayer reduces the driving force for Dex transport across the dialysis membrane.

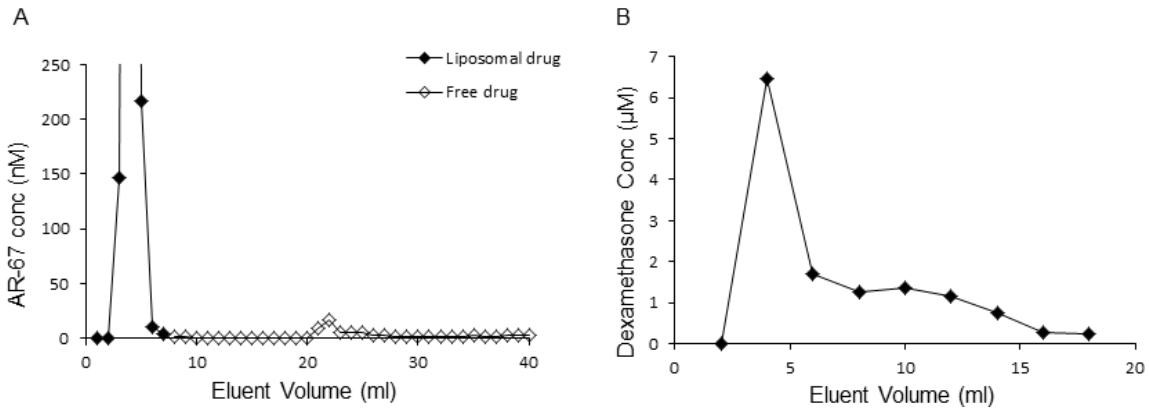

Figure 4.3 (A) Elution profiles of free and liposomal entrapped AR-67 (Kp=2440) as determined by HPLC after passing 0.1 ml through Sephadex G25 and eluted with acetate buffer (85 mM, pH 4.2). (B) Elution profile of blank liposome spiked with Dex (Kp=106) after passing 0.5 ml through Sephadex G25 and eluted with PBS (pH 7.4).

The influence of liposomal membrane binding on the apparent release kinetics can be minimized by reducing the lipid concentration. To probe this, release experiments were repeated at lower lipid concentrations (~4.6 mg/ml) in Figure 4.4B. This caused a significant increase in the apparent rates of drug release from both drug loaded and spiked liposomes. Also noteworthy, the concentration vs. time profiles for spiked liposomes and free drug solution nearly overlap with virtually identical terminal slopes. This suggests that the effect of drug binding to liposomes on the driving force for dialysis membrane transport has been minimized and nearly eliminated at this lower lipid concentration. Nevertheless, it is unclear from a visual examination of Figure 4.4B whether or not there is sufficient information content to enable a reliable estimation of the effective rate constant for liposomally entrapped drug release.

Before attempting to apply more sophisticated modeling to data such as those displayed in Figure 4.4, the rate constant for Dex transport across the dialysis membrane, k_d, was examined by determining the disappearance of free Dex from solution in six independent experiments with different dialysis tubes having a molecular weight cut-off of 100 kD (Figure 4.5). The observed biphasic profile obtained suggests non-instantaneous reversible binding or partitioning of the drug in the dialysis membrane, which was incorporated into the mathematical model by replacing Eqn. 4.4 with Eqns. 4.5 & 4.6. The data in Figure 4.5 highlight the potential importance of monitoring free drug disappearance over a sufficient time frame to capture the relevant contribution of the dialysis membrane transport and binding to the overall release processes of interest.

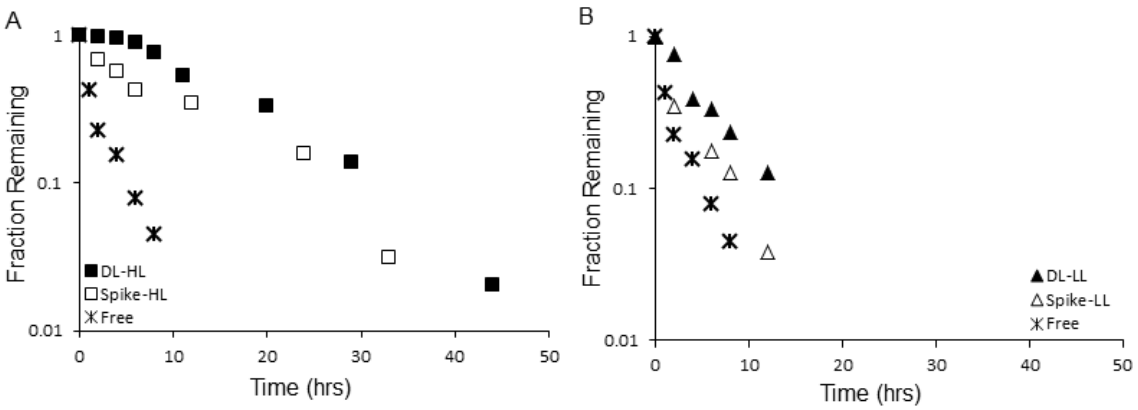

Figure 4.4 Release profiles of Dex in DMPC liposomes at 25°C using dynamic dialysis method. (A) Release profiles of drug loaded and blank liposomes spiked with Dex at high lipid concentration (~13.9 mg/ml) along with free drug profile (B) Release profiles of drug loaded and blank liposomes spiked with Dex at low lipid concentration (~4.6 mg/ml) along with free drug profile. DL stands for drug loaded liposomes. HL and LL represents high and low lipid concentrations respectively.

Comparison of Dex Binding and Release from DMPC, DPPC, and DSPC liposomes

While the impact of drug binding to the nanoparticle on the apparent release kinetics can be probed by the studies described above, the actual quantitative determination of binding constants might be best obtained separately to avoid introduction of another fitted parameter in the transport models described in Eqs. 4.1-4.6. To better understand and quantify the role of membrane binding in modulating the apparent release kinetics, the partition coefficients of Dex in DMPC, DPPC and DSPC liposomes was determined. The values obtained by equilibrium dialysis at 25°C were 705±24 in DMPC, 106±11 in DPPC and 57±9 in DSPC liposomes (188) as displayed graphically in Figure 4.6.

Further, the range of release rates from liposomes that can be reliably determined by dynamic dialysis was determined by including studies employing DPPC and DSPC to take advantage of the expected reduction in release rates accompanying the higher acyl chain ordering present in these longer chain lipids as detailed in the barrier domain model for lipid bilayer permeability previously (131, 189). Release profiles at 25°C generated by dynamic dialysis of Dex loaded liposomes and blank liposomes spiked with Dex at low (~4-5 mg/ml) and high lipid concentrations (~12-15 mg/ml) are compared with those from free Dex solution in Figure 4.7. The upper panel of Figure 4.7 shows the comparison of drug loaded liposomal release profiles at low and high lipid concentrations while the lower panel compares spiked profiles at low and high lipid concentrations in DMPC, DPPC and DSPC, respectively, along with the free drug profile.

Evident from Figure 4.7 (upper panel) is that differences between the release profiles from drug loaded liposomes at low and high lipid concentrations (*i.e.*, low vs high

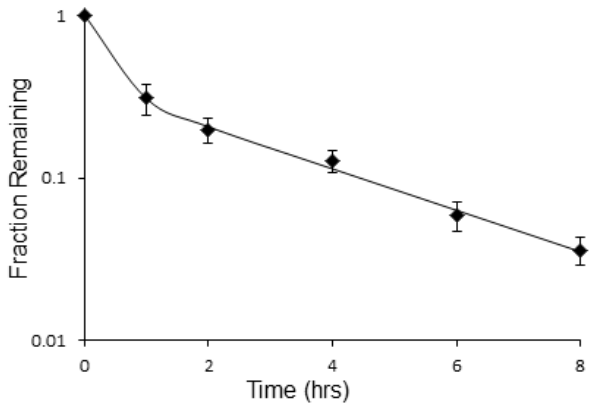

Figure 4.5 Release profile of free Dex solution across the dialysis membrane (MWCO: 100kD) at 25°C. Average of six independent profiles across six different tubes, error bars are the standard deviations.

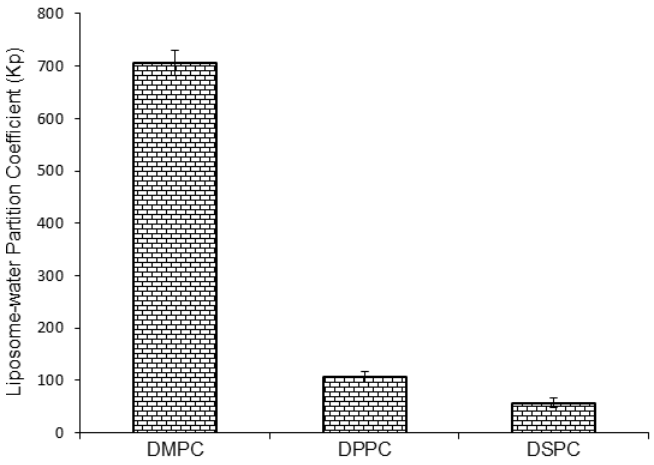

Figure 4.6 Liposome-water partition coefficient of Dex in DMPC, DPPC and DSPC liposomes determined by equilibrium dialysis at 25°C.

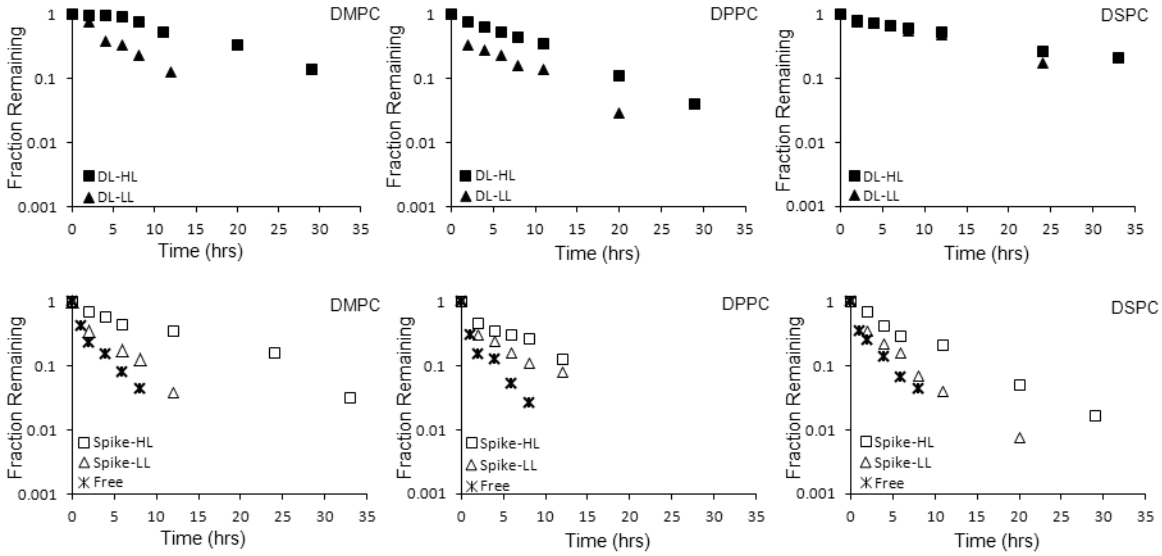

Figure 4.7 Release profiles of Dex loaded liposomes, blank liposomes spiked with Dex and free Dex solution at 25°C. The upper panel compares the release profiles of drug loaded (DL) DMPC, DPPC and DSPC liposomes at low and high lipid concentration. The lower panel compares the release profiles of free Dex solution in the absence and presence of low and high concentrations of liposomes. DL stands for drug loaded liposomes. HL stands for high lipid concentration (~12-15 mg/ml) and LL stands for low lipid concentration (~4-5 mg/ml) inside the dialysis tube.

nanoparticle concentrations) can be related to the partition coefficients observed in these systems. The largest partition coefficients prevalent in DMPC liposomes resulted in the greatest difference between the profiles at low and high lipid concentration, in both drug loaded and spiked liposomes. At high lipid concentrations, drug released from the DMPC liposomes undergoes relatively extensive external membrane binding inside the dialysis tube leading to a slower apparent release that is rate-limited by transport across the dialysis tube. Thus, a dynamic dialysis experiment performed at the highest DMPC concentration displayed in the upper left panel of Figure 4.7 would erroneously suggest a liposomal release half-life of ~ 10 hr when in fact it is at least 3-fold less than that. With a substantial decrease in partition coefficient, the apparent release kinetics become less sensitive to lipid concentration and in DSPC at a low lipid concentration no influence of lipid binding can be discerned. Particularly noteworthy, there is no influence of liposome concentration on the Dex release profiles from drug loaded DSPC liposomes (upper right panel, Figure 4.7) and the slopes are significantly smaller than those obtained from free drug solution or from spiked DSPC liposomes (lower right panel, Figure 4.7). These combined observations provide confidence that a reliable rate constant for Dex release from DSPC liposomes can be generated by dynamic dialysis.

The value of establishing the free drug permeation across the dialysis membrane in order to assess its contribution to the kinetic profiles obtained from drug loaded nanoparticles during dynamic dialysis has been well documented (66, 182, 190, 191) but this may not be a sufficient control. Although it has also been understood for decades that the rate of diffusion of small molecules through a dialysis membrane is proportional to the concentration of the unbound species (192, 193) systematic studies are seldom conducted

to account for both drug binding to the nanocarrier and its influence on dialysis membrane transport. The effect can be dramatic for the drugs having high affinity for the formulation and can be probed by varying the concentration of the carrier particles.

The release profiles from Dex loaded DMPC, DPPC and DSPC liposomes at low and high lipid concentration were fit simultaneously to the mathematical model represented by Figure 4.1 and Eqs. 4.2 & 4.5-4.6. The DPPC and DSPC results are shown in Figure 4.8. As discussed earlier, the percentage of unencapsulated drug at time t=0 was included as a fitted parameter for each system in the model fitting. The values obtained were 31 % and 53 % at high and low DPPC concentrations, respectively, and 15 % and 20 % at high and low DSPC concentrations, respectively. To test the reproducibility of the release profiles generated by dynamic dialysis and to confirm that the variation observed in release profiles with changes in lipid concentration was not due to variability of the method, the release profiles from Dex loaded DPPC liposomes were determined in triplicate, at both low and high lipid concentrations along with free drug. Six drug loaded profiles in DPPC when fitted simultaneously gave an intrinsic rate constant (k_m) of 2.13 ± 0.43 h^{-1} (95% confidence interval) while that obtained from simultaneous fitting of average profiles at high and low lipid concentrations was 2.08 ± 0.36 h^{-1}. The effective rate constant for liposomal release that takes into account the effect of intravesicular binding on the driving force ($k_m\alpha_i$) was 0.17 h^{-1} corresponding to the half-life of 4.2 hrs for release from DPPC liposomes. Similarly, the intrinsic rate constant obtained from simultaneous fitting of profiles of Dex loaded DSPC liposomes was 0.43 ± 0.08 h^{-1} and $k_m\alpha_i$ was 0.05 h^{-1}, yielding a half-life of 13.6 hrs. While the same modeling approach

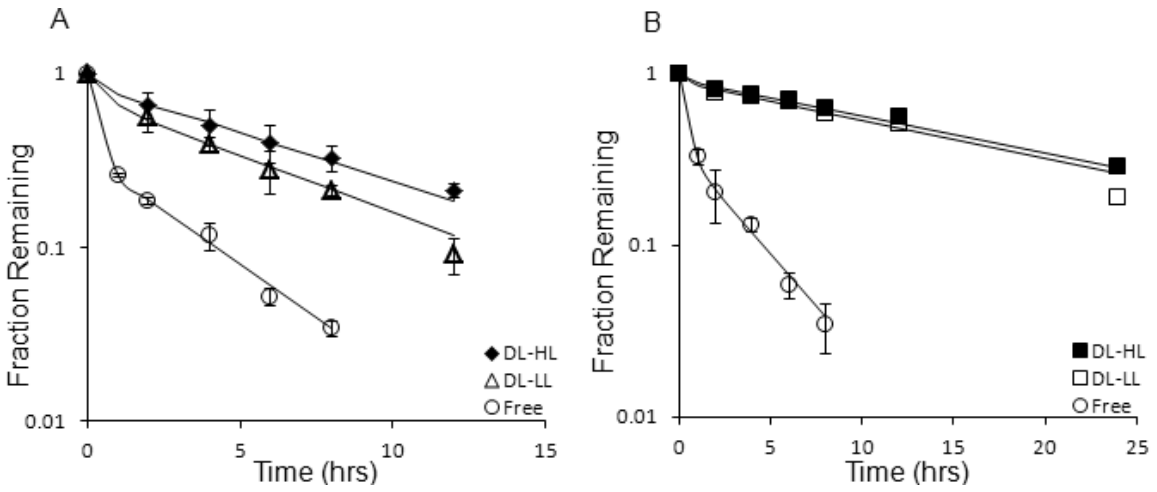

Figure 4.8 Release profiles of Dex across DPPC (A) and DSPC (B) liposomes at high and low lipid concentrations along with the free drug profile determined using dynamic dialysis method. Each of the three profiles in (A) is the average of three independent experiment and the error bars represent the standard deviation. DL stands for drug loaded liposomes. HL and LL represents high and low lipid concentrations respectively.

also fit the DMPC data, the 95% confidence limits for k_m in DMPC were too large (8.2 ± 12 h^{-1}) to allow a reliable estimate of k_m in that system.

Determination of the Intrinsic Permeability Coefficient using Dynamic Dialysis Method

A significant advantage of mathematical modeling of dynamic dialysis data is that it enables the determination of the true apparent release half-life from the nanocarrier – the value that is expected under true sink conditions. Another advantage of the approach for liposomal systems is that when combined with measured liposome/water partition coefficients it enables the calculation of the intrinsic permeability coefficient of the drug from the intrinsic rate constant, k_m. This is possible because both the intra- and extravesicular unbound species concentrations are determined. These are the quantities that constitute the driving force for permeation across the bilayer. Accordingly, the intrinsic permeability coefficient of AR-67 across DSPC bilayers was calculated from the fitted k_m of 44.3 hr^{-1} value at pH 4.2 (Figure 4.2B) to be 3.7 x 10^{-8} cm/sec, using the following relation:

$$k_m = \frac{P_m A}{V_i} \cong \frac{3P_m}{R}$$

where k_m is the intrinsic first-order rate constant for drug release from liposomes, A and R are the area and radius of the liposome, respectively, and V_i is the total intravesicular volume. Permeability coefficients calculated from the fitted k_m values of 2.0 hr^{-1} and 0.43 hr^{-1}, for the release of Dex from DPPC and DSPC liposomes are 1.8 x 10^{-10} cm/s and 8.9 x 10^{-10} cm/s, respectively.

Exploration of the Variable Space - Simulations

Effect of Lipid Concentration: Extravesicular Binding

Model simulations were conducted to show the effect of lipid (*i.e.*, liposome) concentration on the observed release kinetics for drugs with varying binding affinity and a constant intrinsic permeability (Figure 4.9). For these simulations, a constant k_m of 32 hr^{-1} was assumed, corresponding to a situation where, in the absence of significant intravesicular binding, the drug release rate from liposomes would be too fast to measure (recall that k_d for dialysis membrane transport in the experiments discussed previously in this paper was on the order of 1 hr^{-1}). Thus, for K_p=60 (Figure 4.9, left panel), the overall drug release is dialysis membrane rate-limited regardless of lipid concentration and no information regarding the release rate from the nanoparticles can be obtained by dynamic dialysis under these conditions. With higher K_p values (700 and 2440, corresponding to values for Dex in DMPC and AR-67 in DSPC liposomes, respectively), the effect of lipid concentration is more dramatic. This can be attributed to the substantial amount of extravesicular membrane bound drug inside the dialysis tube and the reduction in driving force across the dialysis membrane that accompanies this binding. Figure 4.10A provides estimates of the increases in extravesicular bound fraction accompanying increases in lipid concentration in the dialysis tube for drugs with different partition coefficients. For example, for a drug with moderate binding affinity (K_p=700), almost 70% drug is bound extravesicularly at a lipid concentration of 10 mg/ml. Both Figure 4.9 (center and right panels) and Figure 4.10A illustrate the importance of using low nanoparticle concentrations when the drug binding affinity is high. For example, Figure 4.9 shows

that lipid concentrations <0.5 mg/ml are necessary to minimize the confounding influence of nanoparticle binding within the dialysis tube when the binding affinity is high.

Effect of Intravesicular Binding

Liposomes differ from other matrix type nanoparticles (e.g., solid lipid nanoparticles, polymer micelles, *etc*.) in that there is an aqueous core. The aqueous core concentration of the membrane permeable species, which provides the driving force for drug release, may be substantially reduced by intravesicular membrane binding. Drugs having a high liposome/water partition coefficient (K_p) may be mostly bound to the intravesicular membrane due to the high membrane surface to aqueous core volume ratio. Figure 4.10B illustrates the decrease in intravesicular free drug fraction with an increase in partition coefficient. Notably, this quantity is not affected by the liposome concentration but the free drug fraction for a given K_p does decrease with a decrease in size of the liposome (132). Intravesicular membrane binding as reflected in the value of α_i reduces the effective rate constant ($k_m \cdot \alpha_i$) across the bilayer (Eq. 4.2).

Simulations at a low lipid concentration (0.5 mg/ml) to minimize the impact of extravesicular binding and varying intrinsic rate constants (k_m) are shown in Figure 4.11 at three values of K_p. Consider the curve representing the release profile maximally separated from that of a solution of the free drug in each panel. With an increase in K_p, there is a corresponding systematic increase in the intrinsic rate constant, k_m, or bilayer permeability that can be clearly differentiated from the free drug profile. . In other words, for a drug with low partition coefficient (K_p=52), an apparent half-life of approximately 7 hours is obtained when the intrinsic rate constant (k_m) is about 1 h^{-1}; for a drug with K_p of 700, a similar half-life is obtained with k_m of 10 h^{-1} while for a drug with very high K_p

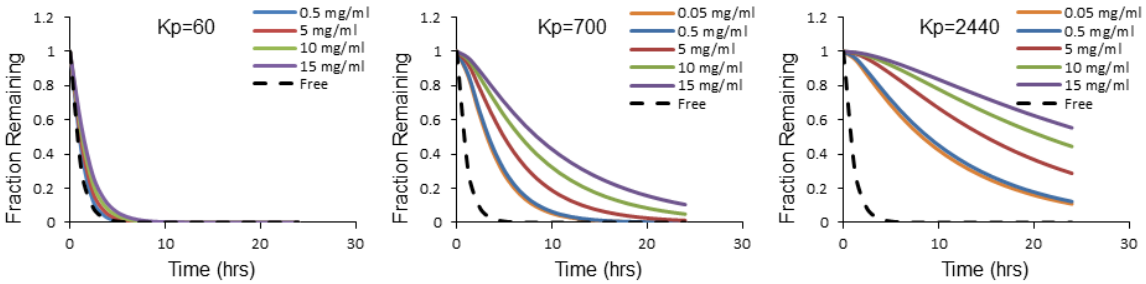

Figure 4.9 Simulations showing the effect of the liposome/water partition coefficient on the observed release kinetics from 90 nm liposomes at varying lipid concentrations (k_m=32).

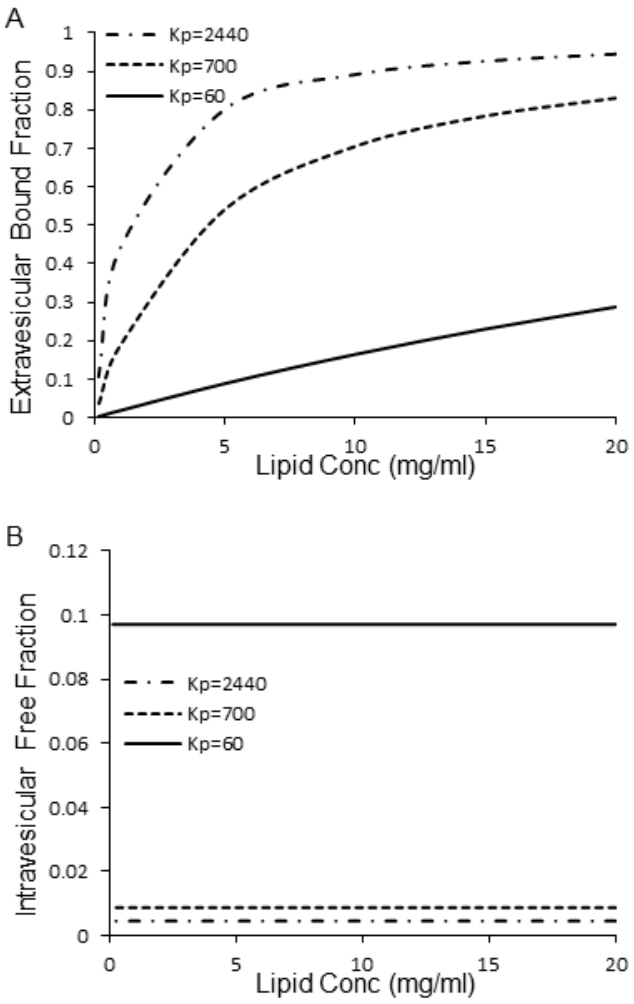

Figure 4.10 Simulations for extravesicular bound and intravesicular free fractions with increasing lipid concentration and different membrane-water partition coefficients in 90 nm liposomes.

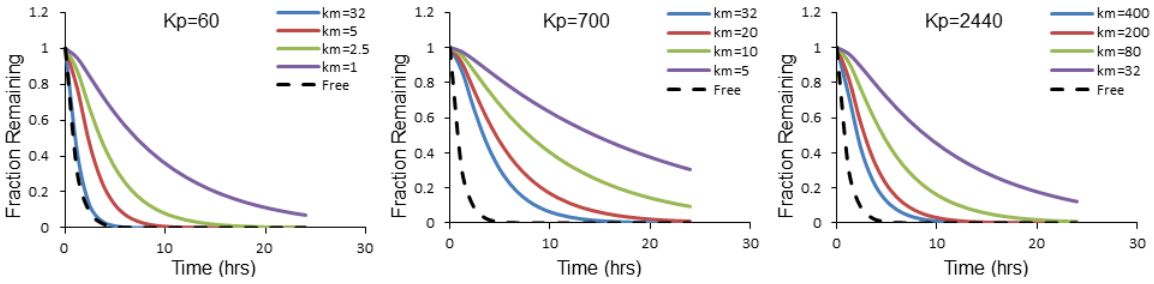

Figure 4.11 Simulations showing the effect of the liposome/water partition coefficient on the observed release kinetics from 90 nm liposomes at varying intrinsic rate constants (Lipid concentration=0.5 mg/ml).

(2440), the same half-life is obtained for a k_m of more than 32 h^{-1}. Thus, in the case of liposomes, a high partition coefficient can be advantageous in slowing the transport rate from liposomes by reducing the intravesicular driving force. If extravesicular binding can be minimized by using a low liposome concentration, dynamic dialysis may still provide a reliable measurement of the effective release rate constant.

The above observations can be used to rationalize why an intrinsic rate constant for liposomal release could be determined for AR-67 in DSPC liposomes but not for Dex in DMPC liposomes. AR-67, a highly hydrophobic compound in its lactone form (pH 4.2), has a significantly higher K_p in DSPC compared to Dex in DMPC (> 3 times greater). Yet, an intrinsic rate constant and permeability coefficient for AR-67 was determined using the same dynamic dialysis method as that failed for Dex in DMPC. One principal reason for this is the lower intravesicular driving force for AR-67 due to its high intravesicular membrane binding. Also, a lower liposome concentration (0.48 mg/ml) was possible for the AR-67 release study as compared to Dex in DMPC (4.6 mg/ml) due to the higher sensitivity of the fluorescent method of analysis employed for AR-67. Therefore, extravesicular binding effects were nearly negligible for AR-67.

The simulated effect of liposome concentration on the dynamic dialysis profiles for AR-67 is shown in Figure 4.12. A lipid concentration of 0.48 mg/ml was a suitable concentration for optimizing the separation of the drug loaded and spiked release profiles. Below this concentration, the profiles did not change significantly but above this concentration slowing of the apparent kinetics was observed along with the decrease in the gap between the drug loaded and spiked profiles

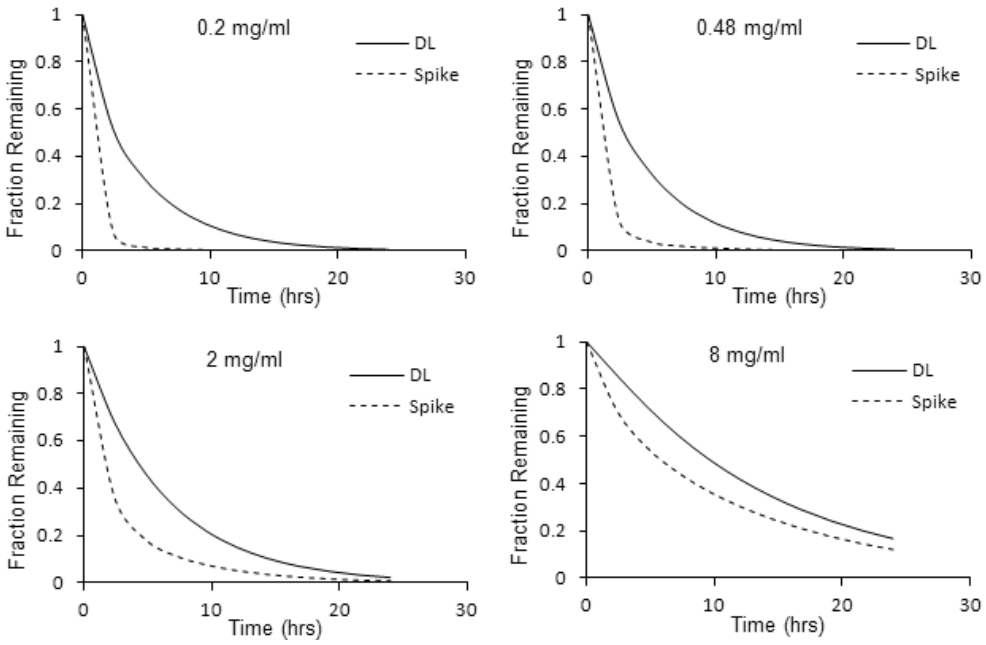

Figure 4.12 Simulations of the effect of lipid concentration on the dynamic dialysis profiles for AR-67 from drug loaded (DL) and blank liposomes of DSPC spiked with the drug (K_p=2440).

Considering the above observations, it follows that before inferring that a given drug release profile obtained by dynamic dialysis truly reflects the rate of release from the nanoparticle formulation and not an artifact due to rate-limiting dialysis membrane transport, perhaps resulting from high extravesicular membrane binding of the drug, one of the following validation experiments should be undertaken: (a) evaluate the profiles obtained from a free drug solution and drug-spiked nanoparticle suspension at the same nanoparticle concentration as the drug-loaded nanoparticle system. Nanoparticle binding effects can be considered negligible at the nanoparticle concentration explored if the kinetic profiles are the same; (b) alternatively, release profiles from drug loaded nanoparticles should be generated at different dilutions and compared with the profile obtained from a free drug solution. If the drug-loaded system release profiles at different dilutions are not significantly different from each other but significantly slower than the free drug profile, then the effect of nanoparticle binding can be ignored and a reliable effective rate constant for nanoparticle release can be determined by application of the appropriate model.

Effect of the Dialysis Membrane

The cellulose ester dialysis membranes employed in these studies had a molecular weight cut-off (MWCO) of 100 kD but membranes having a MWCO up to 1000 kD are available from the manufacturer (Spectrum Labs). Membranes having a MWCO between 12-15 kD or smaller have been commonly used in the literature (181, 194-200). Morino-Bautista and Tam (181) demonstrated that the smaller the pore size (or MWCO), the higher the resistance offered by the membrane to the diffusion of small solutes (specifically, procaine hydrochloride). Thus, the initial rate of diffusion of procaine was 7

times greater across a 10 kD membrane in comparison to a 2 kD MWCO membrane. Considering that the dialysis membrane should be selected with a maximum possible pore size to maximize the rate of diffusion of the drug molecule while serving as a barrier to the carrier, a 1000 kD MWCO may be feasible for nanoparticles in the 100 nm size range.

Three-Dimensional Response Surfaces: Reliability of Results from Dynamic Dialysis

As dictated by the principles of chemical kinetics, the rate determining step governs the rate of an overall reaction. In dynamic dialysis, this principle can be relied upon to unambiguously determine the nanoparticle release rate constant when the rate of transport across the dialysis membrane far exceeds that for nanoparticle release. For liposomes, this situation is most likely realized for polar or ionized drugs that have relatively low membrane permeabilities and negligible membrane/water partition coefficients. In many instances, there may be no single process that is so predominant that it completely determines the rate of drug disappearance from the dialysis chamber, yet there may be sufficient information content in the concentration versus time profile to obtain a reliable rate constant for nanoparticle release even using a simple first-order fit.

In the above paragraphs, the effect of lipid concentration, partition coefficient and the intrinsic rate constant on the observed release kinetics from liposomes using dynamic dialysis was demonstrated. Figs. 4.13A and B systematically define in a 3-dimensional plot the intrinsic liposomal release rate constants and apparent liposomal release half-lives that can be reliably determined by a simple first-order kinetic treatment of dynamic dialysis data as a function of the membrane/water partition coefficient and lipid

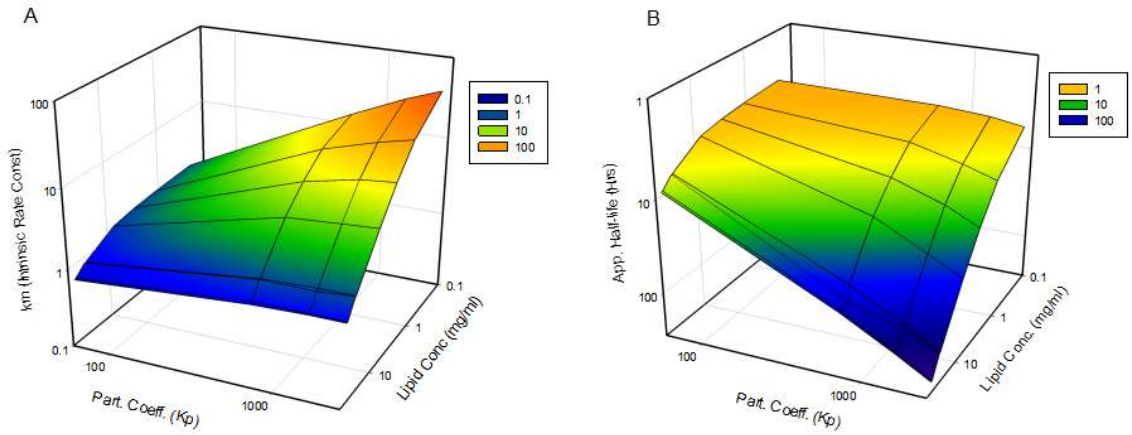

Figure 4.13 Three dimensional surface plots showing the boundary intrinsic rate constants (A) and release half-lives (B) that can be reliably determined in liposomal systems under the given conditions of lipid concentration inside the dialysis tube and the membrane-water partition coefficient of the drug. The values below the surface can be determined by dynamic dialysis and simple first order fit with 80% accuracy. The experimental error is not included and there has been no provision in the simulations for the presence of unencapsulated drug at t=0.

concentration employed in the experiment. The intrinsic rate constant and apparent liposomal release half-life were deemed to be determinable by dynamic dialysis and a first-order treatment if the fitted constant from a first-order fit was within ± 20% of the input value.

Figure 4.13A shows the impact of intra- and extravesicular binding on what intrinsic rate constant can be reliably estimated. If the effects of extravesicular binding can be minimized by using the lowest possible lipid concentration, then a reliable estimate can be obtained even for a drug having a relatively high intrinsic liposomal release rate constant and a high membrane/water partition coefficient by a simple first order model. Figure 4.13B shows the effect of extravesicular binding on the determination of apparent half-lives. With an increase in partition coefficient and lipid concentration, relatively slower apparent rate constants or longer release half-lives are required for the accurate estimation by this method. The values of the intrinsic rate constants and half-lives that can be determined with 80% accuracy using dynamic dialysis and a simple first order model in the absence of experimental error are those below the response surfaces shown in Figs. 4.13A and B. For example, for a drug with a dialysis membrane transport half-life from solution of 0.7 h, a K_p of 60, and at a liposome concentration of 0.2 mg/ml, a minimum half-life of 3.5 hr can be determined with an 80% accuracy by dynamic dialysis using a simple first-order fit.

The simulations shown in Figure 4.13 have not included experimental errors nor have the effects of the presence of a certain fraction of unencapsulated drug at the start of an experiment been taken into account. An appropriate mechanism-based mathematical model treatment, such as that described in this study, would extend the region in which

reliable intrinsic rate constants and apparent release half-lives could be determined from real data. Then, the decision as to reliability should be based on the 95% confidence limits of the parameters of interest.

CONCLUSIONS

In the early literature, dynamic dialysis became a useful and well validated technique for studying protein binding of small molecules because the rate of transport could be correlated to the extent of protein binding. The principle was based on the change in the permeation rate of the small molecule across the dialysis membrane with the change in the free fraction (or fraction bound) inside the dialysis chamber (192, 193). The application of the dynamic dialysis method for determining release kinetics from nanoparticles seems to have grown in popularity in part due to the willingness of investigators to ignore such binding effects. With ever increasing research efforts in the field of nanoparticles as drug delivery systems, it is critical to understand the limitations of this widely adopted dynamic dialysis method for determination of release kinetics. With experiments and simulations, the various scenarios were demonstrated where the interpretation of release data using dialysis can be either straightforward or completely misleading. As shown in this study, consideration of the binding affinity of the drug to the nanoparticles, appropriate control experiments, and suitable mechanism-based mathematical treatment of the data should aid in the judicious use of the dialysis method for determination of the release kinetics from nanoparticles.

CHAPTER FIVE

Enhanced Active Liposomal Loading of a Poorly Soluble Ionizable Drug Using Supersaturated Drug Solutions

INTRODUCTION

Liposomes are attractive delivery systems in cancer therapy because of their potential to passively target solid tumors (33, 44, 170, 201, 202). However, in order for liposomes to be useful from a practical standpoint for antitumor therapy in patients, maximum drug loading and optimization of drug retention and release rates are likely to be necessary (39, 203-205). Liposomal drug loading can be achieved by either passive or active methods. In passive loading, liposomes are formed in the presence of a solution of the drug to be loaded; in active loading, drug internalization occurs into preformed liposomes typically driven by a transbilayer pH gradient which in turn produces a chemical potential gradient, of the unionized, permeable form of the drug across the bilayer. Active loading has been proven to be more effective for achieving higher drug to lipid ratios compared to the passive loading method (39, 44).

Several reports (47, 48, 84, 206-208) on different active loading methods have emphasized the dependence of loading on experimental conditions such as transmembrane pH gradient, membrane-water partitioning, internal buffering capacity, aqueous solubility of the drug, lipid composition, etc. Zucker et al (48) developed a decision tree by computational data mining to qualitatively predict loading efficiency (i.e., low, medium, or high) based on loading conditions and the drug`s physicochemical properties. As described in their model, good aqueous solubility of the drug is one of the requirements for efficient active loading. High drug-to-lipid ratios are more difficult to

achieve for drug candidates exhibiting poor aqueous solubility because the mass flux across the bilayer is governed by the extra-liposomal concentration of the permeating species as well as its permeability coefficient. Extremely low drug solubility reduces the external driving force for liposomal uptake during active loading leading to low final drug-to-lipid ratios.

In this paper, the use of supersaturated drug solutions to facilitate active liposomal loading by the pH-gradient method was explored in order to overcome the aforementioned limitations in actively loading poorly soluble drugs. A highly lipophilic and poorly water soluble camptothecin analogue (AR-67, 7-t-butyldimethylsilyl-10-hydroxycamptothecin) served as a model compound for this study. AR-67 is a novel, blood-stable camptothecin analogue currently in phase II clinical trials in patients with brain cancer (75, 79, 209). It possesses an α-hydroxy-δ-lactone moiety that undergoes pH-dependent chemical hydrolysis to ring-opened carboxylate form (75, 79, 80), a property that can be exploited for active loading. It was demonstrated that active loading coupled with methods to create and maintain drug supersaturation can dramatically enhance drug-to-lipid ratios for this poorly soluble drug. A mathematical model taking into account the various intra- and extra-liposomal ionic and binding equilibria and permeability coefficients has been developed to predict the rate and extent of active drug loading. Quantitative comparison of the experimental results with the predictions from this mechanism-based model should advance understanding of these complex phenomena.

MATERIALS AND METHODS

DSPC (1,2-distearoyl-sn-glycero-3-phosphatidylcholine, >99% purity) and m-PEG DSPE (1,2-distearoyl-sn-glycero-3-phosphoethanolamine-N-[methoxy (polyethylene glycol)-2000] (MW=2806, >99% purity) were purchased as powders from Avanti Polar Lipids (Alabaster, AL). AR-67 (7-t-butyldimethylsilyl-10-hydroxycamptothecin) was obtained from Novartis Pharmaceuticals Corporation (East Hanover, NJ). Dialysis tubes (Float-A-Lyzer®, MWCO: 100 kD) were purchased from Spectrum Laboratories (Rancho Dominguez, CA). Sulfobutyl ether β-cyclodextrin sodium salt (SBE-CD, Captisol®) having an average degree of substitution of 7- sulfobutyl ether residues per β-cyclodextrin molecule was purchased from CyDex Pharmaceuticals, Inc. (Lenexa, Kansas). All other reagents and HPLC grade solvents were purchased from Fisher Scientific (Florence, KY). Deionized water was used for all experiments.

Passive Loading

Liposomes were prepared based on a previously reported method (132). Briefly, DSPC and mPEG-DSPE (95:5 mol%, 32 mg) were dissolved in 2 ml of chloroform. The solvent was evaporated under a stream of nitrogen while rotating the container and the resulting thin film was dried overnight in a vacuum oven at 40°C. For preparation of liposomes at pH 9.5, 2 ml of 100 mM borate buffer (pH 9.5) containing AR-67 (1-1.5 mM) was added to the dried lipid film to give a lipid concentration of 16 mg/ml. After alternate vortexing and heating at 60°C in a water bath to uniformly suspend the lipid, the lipid suspension was extruded 10 times through two stacked 200 nm polycarbonate membranes (GE water and Process Technologies, Trevose, PA) using an extrusion device (Liposofast®,

Avestin, Canada) at 60°C to obtain large unilamellar liposomes. Drug loaded liposomes were allowed to cool to room temperature for 3 hours and stored at 4°C until further use.

Active Loading Methods

Dried DSPC:mPEG-DSPE (95:5 mol%, 120 mg) lipid films, prepared as described above, were hydrated with 2 ml of 0.25 M calcium acetate solution or 0.5 M sodium acetate solution to produce a lipid concentration of 60 mg/ml. Alternate vortexing and heating at 60°C followed by the same extrusion process described above provided unilamellar liposomes. Following their preparation, blank vesicles were allowed to cool to room temperature and dialyzed against 1 L of 0.9% NaCl solution at room temperature for about 2 hours to remove the extravesicular calcium or sodium acetate and create a pH gradient. Active loading was carried out either in the presence of excess solid AR-67 or in the presence of supersaturated AR-67 solutions, at pH 7.5 and at two different temperatures, 37°C and 60°C. Two methods were employed to produce and maintain supersaturated solutions of AR-67, as described below:

Supersaturation Method I

AR-67 was solubilized by adjusting a 0.1 mg/ml suspension to a high pH (10.5-11) by adding 1 M NaOH with continuous stirring followed by readjustment to pH 7.5 by addition of 1 M HCl at either 37°C or 60°C to achieve supersaturation. Thereafter, on each occurrence of precipitation (approximately every 6 hours) pH was again raised to redissolve the precipitated drug followed by readjustment to pH 7.5.

Supersaturation Method II

Aliquots of a filtered (0.2 µm, PVDF syringe filter) 20 mg/ml AR-67 stock solution in 0.1 N NaOH were added into a 2% SBE-CD solution containing HEPES buffer (3 mM)

in 0.9% NaCl and adjusted to pH 7.5 with dilute HCl to produce supersaturated loading solutions at varying total drug concentrations (0.1, 0.2, 0.4 and 0.6 mg/ml). These solutions were at varying degrees of supersaturation ($DS = C/Cs$): 3.8 for 0.1 mg/ml, 7.5 for 0.2 mg/ml, 15.1 for 0.4 mg/ml and 22.7 for 0.6 mg/ml where C is the total supersaturated solution concentration and C_s is the equilibrium solubility of AR-67 in the presence of 2% SBE-CD at pH 7.5. Degrees of supersaturation higher than that represented by a total drug concentration of 0.6 mg/ml could not be sustained over the desired loading period.

Liposomal suspensions (1 mL) in dialysis tubes were dialyzed for 48 hours (supersaturation was maintained for 48 hours by method II) at 37°C in the supersaturated drug loading solutions (200 mL). During loading, 10 µl samples were withdrawn from inside the dialysis tube at various time points and diluted with 900 µl of cold (-25°C) 2:1 v/v methanol:acetonitrile to stop the interconversion between lactone and carboxylate. The samples were stored at -25°C until further analysis by HPLC. Loading studies at the lowest (0.1 mg/ml) (n=3) and highest (0.6 mg/ml) (n=4) drug concentrations in loading solution were repeated to test the reproducibility of the loading process. The loading study at the highest drug loading solution concentration (0.6 mg/ml) was also repeated using 0.5 M sodium acetate (rather than calcium acetate) liposomes to assess the role of the entrapped cation, if any, in the rate and extent of drug loading. The total drug concentration in the liposomal suspension inside the dialysis tube was analyzed for the loading experiments. These concentrations were then fitted to the model (derived in the mathematical model section) to obtain intravesicular drug concentrations. The drug-to-lipid ratios reported were calculated from these intravesicular drug concentrations.

Studies of AR-67 uptake into the dialysis tubes were also carried out in the absence of liposomes at the same pH, with and without cyclodextrin in the bulk loading solution, to determine the rate constants for free and cyclodextrin-complexed drug transport across the dialysis membrane. For determination of k_d (rate constant for the reversible transport of AR-67 across the dialysis membrane), dialysis tubes containing 1 ml of HEPES buffer (3 mM) in 0.9% NaCl adjusted to pH 7.5 with dilute HCl were placed in 200 mL of AR-67 solution (at 0.1, 0.05 and 0.05 mg/ml) in the same buffer solution and the AR-67 concentration inside the tube versus time was monitored. Simultaneous first-order fits of the three experiments were conducted to generate k_d. Two additional uptake experiments (without liposomes) were conducted in the same buffers but also containing 2% SBE-CD at AR-67 concentrations of 0.2 and 0.6 mg/ml to generate K_{dcd} (rate constant for the transport of SBE-CD and SBE-CD/AR-67 complexes across the dialysis membrane).

AR-67 Equilibrium Solubility and SBE-CD Complexation Constants Determinations

The equilibrium solubility of AR-67 was determined at 37°C and pH 6.5, 7.0 and 7.5 in the presence of 0, 1, 2, and 3% SBE-CD to determine the lactone and carboxylate monoanion complexation constants with SBE-CD and to use in calculations of degree of supersaturation achieved in loading solutions. Briefly, 2-4 mg of AR-67 was added to 4 ml of 10 mM MES buffer (pH 6.5) or HEPES buffer (pH 7.0 and 7.5) containing 0, 1, 2 and 3% SBE-CD. The vials were rotated in an incubator at 37°C. At different time points, 1 ml of sample was withdrawn using a needle and syringe and filtered through 0.45 µ PVDF syringe filters (13 mm). A filter adsorption study was carried out and subsequently the first 6-7 drops of filtrate were discarded before collecting filtrate for analysis. Filtrate

was diluted with cold (-25°C) 2:1 v/v methanol: acetonitrile, when required. Three independent samples were analyzed by HPLC at each condition and time point. Equilibrium was considered to have been established when two subsequent time points yielded similar values (8-12 days).

Particle Size Measurements

Particle sizes of blank and drug loaded liposomes were measured by dynamic light scattering (DLS) using a Delsa™ Nano submicron particle size analyzer (Beckman Coulter Inc., Brea, CA) at 25°C. The liposomes were diluted in the same buffer as that used in their preparation.

HPLC Analyses

Samples from equilibrium solubility experiments and liposome loading experiments were analyzed using a previously developed and validated isocratic HPLC method with fluorescence detection (126, 132). Standards for AR-67 carboxylate (0.2-2 μM) were prepared in 10 mM sodium carbonate buffer (pH 10.4) and standards for AR-67 lactone (0.5-2.5 μM) were prepared in acidified methanol. A Waters Alliance 2695 Separations Module coupled to a Waters Scanning Fluorescence Detector (M474) was employed with excitation and emission wavelengths at 380 and 560 nm, respectively. A Waters Symmetry® C18 column (5 μm, 3.9 X 150 mm) and guard column (3.9 X 20 mm) were used with a mobile phase composition of 48% acetonitrile and 52% (v/v) pH 5.5 triethylamine acetate (2%) buffer. The retention times at an injection volume of 10 μl and a flow rate of 1 ml/min were 1.7 and 5.9 min for AR-67 carboxylate and lactone, respectively. Generally, unless otherwise specified, AR-67 concentrations reported in the "Results" section refer to total concentrations considering all drug species.

MATHEMATICAL MODEL

A mathematical model was developed for AR-67 uptake into calcium acetate vesicles, taking into account the chemical equilibria inside and outside the vesicle, mass balance, charge balance, and the transport kinetics of various permeable species across both the dialysis membrane and the liposome bilayer. Built into the model were the concentrations of various components, ionization constants, the different solution complexes present and their association/dissociation constants, binding constants for each species of AR-67 with the lipid bilayer, and permeability coefficients for the transport of permeable species across the dialysis membrane (including all AR-67 species, SBE-CD and AR-67/SBE-CD complexes) and the lipid bilayer (i.e., AR-67 lactone and acetic acid).

AR-67 may exist in a combination of four different species at any given pH (Figure 5.1A). While the lactone (I) is considered to be the therapeutically active form, it exists in reversible equilibrium with its ring-opened carboxylate form under physiological conditions (76, 210). The fraction of the unionized ring-opened (carboxylic acid, II) species has been shown to be negligible in solution (211) and therefore an effective pKa for simultaneous ring-opening and ionization, denoted by K_a $(K_a = K * K_{a1})$ of the E-ring lactone, can be employed. The various equilibria (ionization, complexation, membrane partitioning, etc.) and transport processes governing liposome uptake from the aqueous solution inside the dialysis tube are shown in Figure 5.1B. The concentrations of the various species in the extravesicular solution inside the dialysis tube are also governed by their reversible transport across the dialysis membrane separating the contents within the dialysis tube from the external loading solution. These processes were also built into the mathematical model. The assumptions of the present model are:

(a) the lipid bilayer permeabilities of ionized species are negligible while both neutral and charged drug species cross the dialysis membrane with equal permeability coefficients; (b) SBE-CD and its complexes with AR-67 undergo transport across the dialysis membrane with identical permeability coefficients but liposomal uptake of these species is negligible; and c) an instantaneous equilibrium exists between the various species inside the vesicle during the loading process (126, 132, 187). All of the ionization constants and equilibrium constants for membrane binding of AR-67 were taken from previously published results (126, 132, 187, 212, 213). The permeability value for AR-67 lactone across the liposome was determined from model fitting of experimental data under various loading conditions. The rate constants for free and bound drug transport across dialysis tube were also determined experimentally.

Establishment of the pH gradient

During dialysis of calcium acetate (or sodium acetate) containing vesicles, some of the entrapped acetate is released due to the diffusion of unionized acetic acid across the liposome bilayer, resulting in an increase in the intraliposomal pH. AR-67 uptake is accompanied by efflux of additional acetic acid, resulting in the maintenance of a high intraliposomal pH as a function of time during drug loading.

The changes in acetate concentration in the intra- and extravesicular compartments due to the reversible transport of unionized acetic acid can be described by the following rate equations:

$$\frac{dC_i}{dt} = \frac{3P_m^a}{R}(f_o C_o - f_i C_i) \qquad (5.1a)$$

$$\frac{dC_o}{dt} = \frac{3P_m^a}{xR}(f_i C_i - f_o C_o) \qquad (5.1b)$$

$$f_i = \frac{H_i^+ K_2}{H_i^+ K_2 + K_a^{ac} K_2 + K_a^{ac} Ca_i^{+2}} \qquad (5.1c)$$

$$f_o = \frac{H_o^+}{H_o^+ + K_a^{ac}} \qquad (5.1d)$$

where C_i and C_o are the intra- and extravesicular concentrations of total acetate; f_i and f_o are the intra- and extravesicular fractions of the neutral acetic acid species; $H_i^+$and H_o^+ are the intra- and extravesicular proton concentrations; K_2 is the dissociation constant of the calcium acetate complex; K_a^{ac} (1.78 x 10^{-5}) is the ionization constant of acetic acid; Ca_i^{+2} is the intravesicular calcium concentration; x is the ratio of extravesicular volume (V_o) to the total intravesicular volume (V_i) within the dialysis tube; P_m^a is the permeability coefficient of the neutral acetic acid species; and R is the radius of the vesicles.

Various calcium complexes were considered in the intraliposomal aqueous compartment. The intravesicular concentrations of calcium and its complexes with acetate and hydroxide are given as follows:

$$Ca(Ac)_i^+ = \frac{Ca_i^{2+} Ac_i^-}{K_2} \qquad (5.1e)$$

$$Ca(OH)_i^+ = \frac{Ca_i^{2+} OH_i^-}{K_1} \qquad (5.1f)$$

$$Ca_i^{2+} = \frac{K_1 K_2}{((K_1 K_2) + (K_2 OH_i^-) + (K_1 Ac_i^-))} \frac{C_i 0}{2} \qquad (5.1g)$$

$$Ac_i^- = \frac{K_a^{ac} K_2 C_i}{((H_i^+ K_2) + (K_a^{ac} K_2) + (K_a^{ac} Ca_i^{2+}))} \qquad (5.1h)$$

$$Ac_o^- = \frac{K_a^{ac} C_o}{H_o^+ + K_a^{ac}} \qquad (5.1i)$$

where $Ca(Ac)_i^+$ and $Ca(OH)_i^+$ are intravesicular complexes of calcium with acetate and hydroxide ions respectively; OH_i^- is the intravesicular hydroxide ion concentration; Ac_i^- and Ac_o^- are the intravesicular and extravesicular acetate ion concentrations; and K_1 is the dissociation constant of the calcium hydroxide solution complex. The extravesicular calcium concentration is considered to be negligible.

Substituting Eq. (5.1g) into (5.1h) and simplifying it to the quadratic form,

$$Ac_i^- = \frac{(-B \pm (\sqrt{B^2 - 4AC})}{2A} \qquad (5.1j)$$

where

$$A = 2K_1K_2(H_i^+ + K_a^{ac}) \qquad (5.1j-i)$$

$$B = 2H_i^+K_1\left(K_2{}^2\right) + 2H_i^+OH_i^-\left(K_2{}^2\right) + 2K_a^{ac}K_1\left(K_2{}^2\right) + 2K_a^{ac}OH_i^-\left(K_2{}^2\right) + K_a^{ac}K_1K_2C_i0$$
$$- 2K_a^{ac}K_1K_2C_i \qquad (5.1j-ii)$$

$$C = -2K_a^{ac}K_2{}^2C_i(K_1 + OH_i^-) \qquad (5.1j-iii)$$

Solving Eqs. (5.1a)-(5.1j) combined with the appropriate charge balance equation for the intravesicular compartment using Scientist (Micromath Inc.), the change in intravesicular pH as a function of time due to release of acetic acid can be estimated.

Active Drug Loading Step

Sink conditions inside the liposomes were created by the high intraliposomal pH (which results in conversion of AR-67 lactone to its ring-opened carboxylate mono- and di-anion species) and maintained by acetic acid exchange for the lactone entering the liposome. Intraliposomal membrane binding of AR-67 further contributed to the maintenance of a chemical potential gradient for the lactone. Thus, when liposomes were exposed to a supersaturated AR-67 solution at pH 7.5 the unionized lactone form of the drug permeated from the external solution into the liposomes in response to its concentration

gradient. The mathematical model was utilized to simulate the pH and liposomal AR-67 concentration versus time for varying degrees of supersaturation of the drug loading solution.

Details of the model development are presented below and the relevant constants used in simulations are given in Table 5.1. The equations were solved using Scientist® (Micromath Scientific Software, St. Louis, MO) software.

$$\frac{d(I_t^i)}{dt} = k_m(I_o^w - I_i^w) \qquad (5.2a)$$

$$\frac{d(I_t^o)}{dt} = \frac{k_m}{x}(I_i^w - I_o^w) + k_d(I_b - I_o^w) + k_d(III_b - III_o^w) + k_{dcd}(I_bCD_b - I_oCD_o) + k_{dcd}(III_bCD_b - III_oCD_o) \qquad (5.2b)$$

$$\frac{d(CD_t)}{dt} = k_{dcd}\,(CD_b - CD_o) + k_{dcd}(I_bCD_b - I_oCD_o) + k_{dcd}(III_bCD_b - III_oCD_o) \qquad (5.2c)$$

$$I_t = \frac{I_t^i}{x} + I_t^o \qquad (5.2d)$$

where, I_t^i is the total intravesicular drug concentration and I_t^o is the total extravesicular drug concentration; $I_i^w$and I_o^w are the intravesicular and extravesicular aqueous concentrations of the lactone form (permeable species) of the drug, respectively; III_o^w, I_oCD_o, III_oCD_o are the extravesicular free carboxylate, lactone/SBE-CD complex, and carboxylate monoanion/SBE-CD complex concentrations, respectively; and I_b, III_b, I_bCD_b, $III_{bo}CD_b$ are the free lactone, free carboxylate, lactone/SBE-CD complex, and carboxylate monoanion/SBE-CD complex concentrations in the bulk loading solution, respectively. k_m is the rate constant for lactone transport through the given lipid bilayer and x is the ratio of extravesicular to intravesicular volume in the dialysis tube, as

described before. k_d and k_{dcd} are the rate constants for the free drug and cyclodextrin complexed drug (or free cyclodextrin) across the dialysis membrane, respectively. The intrinsic permeability coefficient, P_m , is related to the rate constant for lactone transport by $P_m = k_m * V_i/A = k_m * R/3$ where R and A are the radius and area of the liposome, respectively.

The mass balance of total drug inside the liposomes is

$$I_t^i = \frac{I_i^w + III_i^w + IV_i^w}{a} + \frac{I_i^m + III_i^m + IV_i^m}{b} \left(a = \frac{V_i}{V_i^w};\ b = \frac{V_i}{V_i^m} \right) \qquad (5.2e)$$

where I_i^w, III_i^w, IV_i^w are internal aqueous concentrations of lactone, carboxylate monoanion and carboxylate dianion, respectively; I_i^m, III_i^m, IV_i^m are internal membrane bound concentrations of lactone, carboxylate monoanion and carboxylate dianion, respectively; a and b are volume ratios to account for the differences in aqueous and membrane volumes with respect to the total intravesicular volume; V_i is the total liposomally entrapped aqueous volume plus the lipid volume in the inner bilayer leaflet of liposomes in the suspension; V_i^w and V_i^m are the volumes of the inner aqueous compartment and inner monolayer in each vesicle, respectively.

Substituting,

$$I_t^i = \frac{I_i^w + \frac{K_a^w\, I_i^w}{H_i^+} + \frac{K_a^w\, K_{a2}^w\, I_i^w}{(H_i^+)^2}}{a} + \frac{K_{p1} I_i^w + K_{p2} III_i^w + K_{p3} IV_i^w}{b} \qquad (5.2f)$$

where K_a^w and K_{a2}^w are the ionization constants of AR-67 in the aqueous phase and K_{p1}, K_{p2}, K_{p3} are the membrane/water partition coefficients of the lactone, carboxylate monoanion and carboxylate dianion, respectively. The values of all these parameters ($K_a^w, K_{a2}^w, K_{p1}, K_{p2}, K_{p3}$) have been determined previously (126, 132, 187, 213).

Expressing the total intravesicular concentration in terms of free aqueous lactone concentration,

$$I_t^i = I_i^w \left\{ \frac{1 + \frac{K_a^w}{H_i^+} + \frac{K_a^w K_{a2}^w}{(H_i^+)^2}}{a} + \frac{K_{p1} + \frac{K_{p2} K_a^w}{H_i^+} + \frac{K_{p3} K_a^w K_{a2}^w}{(H_i^+)^2}}{b} \right\} \qquad (5.2g)$$

$$I_t^i = I_i^w \{a_i + b_i\} \ldots \left(a_i = \frac{1 + \frac{K_a^w}{H_i^+} + \frac{K_a^w K_{a2}^w}{(H_i^+)^2}}{a};\ b_i = \frac{K_{p1} + \frac{K_{p2} K_a^w}{H_i^+} + \frac{K_{p3} K_a^w K_{a2}^w}{(H_i^+)^2}}{b} \right) \qquad (5.2h)$$

The intravesicular aqueous unbound concentration of lactone can be described in terms of total intravesicular concentration;

$$I_i^w = ubi\ (I_t^i) \ldots \left(ubi = \frac{1}{a_i + b_i} \right) \qquad (5.2i)$$

where ubi is the intravesicular unbound fraction of the drug.

Now, considering the extravesicular drug equilibrium with cyclodextrin and the mass balance of the total drug in the bulk loading solution,

$$I_t^o = \frac{I_o^w + III_o^w + I_o CD_o + III_o CD_o}{c} + \frac{I_o^m + III_o^m}{d} \left(c = \frac{V_o}{V_o^w};\ d = \frac{V_o}{V_o^m} \right) \qquad (5.3a)$$

where, I_t^o is the total extravesicular drug concentration, I_o^w and III_o^w are unbound extravesicular aqueous concentrations of lactone and carboxylate monoanion, respectively; $I_o CD_o$ and $III_o CD_o$ are the aqueous concentrations of lactone and carboxylate monoanion complexes with SBE-CD; I_o^m and III_o^m are the membrane bound extravesicular drug concentrations, respectively; c and d are volume ratios to account for

the differences in aqueous and membrane volume with respect to the total extravesicular volume in the dialysis tube; V_o is the extravesicular aqueous volume along with the volume of lipid in the outer bilayer leaflet of suspended liposomes in the dialysis tube; V_o^m is the volume of the outer monolayer in each vesicle and V_o^w is the volume of the extravesicular aqueous compartment in the dialysis tube.

Note: In the mass balance of extravesicular drug concentrations, only lactone and carboxylate monoanion species are considered because the extravesicular pH was maintained at pH 7.5 where the concentration of carboxylate dianion species is assumed to be negligible (pka_2^w=8.67).

$$I_o^w + CD_o \xrightarrow{K_{cd1}} I_oCD_o \ldots \left(I_oCD_o = K_{cd1}(I_o^w)(CD_o)\right) \qquad (5.3b)$$

$$III_o^w + CD_o \xrightarrow{K_{cd2}} III_oCD_o \ldots \left(III_oCD_o = K_{cd2}(III_o^w)(CD_o)\right) \qquad (5.3c)$$

where, CD_o is the free extravesicular concentration of SBE-CD and K_{cd1} and K_{cd2} are the complexation constants of AR-67 lactone and carboxylate monoanion with SBE-CD, respectively (experimentally determined in this study).

Substituting Eqs. (5.3b and 5.3c) into Eq. (5.3a),

$$I_t^o = \frac{I_o^w + III_o^w + K_{cd1}(I_o^w)(CD_o) + K_{cd2}(III_o^w)(CD_o)}{c} + \frac{I_o^m + III_o^m}{d} \qquad (5.3d)$$

$$I_t^o = \frac{I_o^w + \frac{K_a^w I_o^w}{H_o^+} + K_{cd1}(I_o^w)(CD_o) + \frac{K_{cd2}K_a^w I_o^w CD_o}{H_o^+}}{c} + \frac{K_{p1}I_o^w + K_{p2}\frac{K_a^w I_o^w}{H_o^+}}{d} \qquad (5.3e)$$

$$I_t^o = I_o^w \left\{ \frac{1 + \frac{K_a^w}{H_o^+} + K_{cd1}(CD_o) + \frac{K_{cd2}K_a^w CD_o}{H_o^+}}{c} + \frac{K_{p1} + K_{p2}\frac{K_a^w}{H_o^+}}{d} \right\} \qquad (5.3f)$$

$$I_t^o = I_o^w \left\{ \frac{\left(1 + \frac{K_a^w}{H_o^+}\right) + CD_o\left(K_{cd1} + \frac{K_{cd2}K_a^w}{H_o^+}\right)}{c} + \frac{K_{p1} + K_{p2}\frac{K_a^w}{H_o^+}}{d} \right\} \qquad (5.3g)$$

Considering the mass balance of extravesicular total cyclodextrin,

$$CD_t = CD_o + I_o CD_o + III_o CD_o \qquad (5.3h)$$

where CD_t is the total concentration of extravesicular cyclodextrin.

$$CD_t = CD_o + K_{cd1}(I_o^w)(CD_o) + K_{cd2}\frac{K_a^w}{H_o^+}(I_o^w)(CD_o) \qquad (5.3i)$$

$$CD_o = \frac{CD_t}{1 + K_{cd1}(I_o^w) + K_{cd2}\frac{K_a^w}{H_o^+}(I_o^w)} \qquad (5.3j)$$

Substituting eq. 5.3j into 5.3g,

$$I_t^o = I_o^w \left\{ \frac{\left(1 + \frac{K_a^w}{H_o^+}\right) + \frac{CD_t}{1 + K_{cd1}(I_o^w) + K_{cd2}\frac{K_a^w}{H_o^+}(I_o^w)}\left(K_{cd1} + \frac{K_{cd2}K_a^w}{H_o^+}\right)}{c} + \frac{K_{p1} + K_{p2}\frac{K_a^w}{H_o^+}}{d} \right\} \qquad (5.3k)$$

Rearranging and simplifying it to the quadratic form,

$$I_o^w = \frac{(-B_1 \pm (\sqrt{{B_1}^2 - 4A_1C_1})}{2A_1} \qquad (5.3l)$$

where,

$$A_1 = \left(1 + \frac{K_a^w}{H_o^+}\right) K_{cd1} + \left(1 + \frac{K_a^w}{H_o^+}\right)\left(\frac{K_{cd2} K_a^w}{H_o^+}\right) + \frac{K_{p1} + (K_{p2}\frac{K_a^w}{H_o^+})}{d} K_{cd1} c$$

$$+ \frac{K_{p1} + (K_{p2}\frac{K_a^w}{H_o^+})}{d} c\left(\frac{K_{cd2} K_a^w}{H_o^+}\right) \qquad (5.3l - i)$$

$$B_1 = \left(1 + \frac{K_a^w}{H_o^+}\right) + \left(K_{cd1} + \frac{K_{cd2} K_a^w}{H_o^+}\right) CD_t + \frac{K_{p1} + (K_{p2}\frac{K_a^w}{H_o^+})}{d} c - I_t^o K_{cd1} c$$

$$- I_t^o c\left(\frac{K_{cd2} K_a^w}{H_o^+}\right) \qquad (5.3l - ii)$$

$$C_1 = -I_t^o c \qquad (5.3l - iii)$$

Similarly, considering the mass balance in the bulk loading solution,

$$I_t^b = I_b + III_b + I_b CD_b + III_b CD_b \qquad (5.4a)$$

where, I_t^b is the total drug concentration in the bulk loading solution, I_b and III_b are unbound bulk aqueous concentrations of lactone and carboxylate monoanion, respectively; $I_b CD_b$ and $III_b CD_b$ are the aqueous concentrations of lactone and carboxylate monoanion complexes with SBE-CD in the bulk.

$$I_t^b = I_b + \frac{K_a^w I_b}{H_o^+} + K_{cd1}(I_b)(CD_b) + K_{cd2}\left(\frac{K_a^w I_b}{H_o^+}\right)(CD_b) \qquad (5.4b)$$

$$I_t^b = I_b\left\{(1 + \frac{K_a^w}{H_o^+}) + CD_b(K_{cd1} + \frac{K_{cd2} K_a^w}{H_o^+})\right\} \qquad (5.4c)$$

Considering the mass balance of total cyclodextrin in the bulk loading solution,

$$CD_{tb} = CD_b + I_b CD_b + III_b CD_b \qquad (5.4d)$$

where, CD_{tb} is the total cyclodextrin concentration in the bulk loading solution.

$$CD_{tb} = CD_b + K_{cd1}(I_b)(CD_b) + K_{cd2}\frac{K_a^w}{H_o^+}(I_b)(CD_b) \qquad (5.4e)$$

$$CD_b = \frac{CD_{tb}}{1 + K_{cd1}(I_b) + K_{cd2}\frac{K_a^w}{H_o^+}(I_b)} \qquad (5.4f)$$

Substituting eq. 5.4f into 5.4c,

$$I_t^b = I_b\left\{\left(1 + \frac{K_a^w}{H_o^+}\right) + \left(\frac{CD_{tb}}{1 + K_{cd1}(I_b) + K_{cd2}\frac{K_a^w}{H_o^+}(I_b)}\right)\left(K_{cd1} + \frac{K_{cd2}K_a^w}{H_o^+}\right)\right\} \qquad (5.4g)$$

Rearranging and simplifying it to the quadratic form,

$$I_b = \frac{(-B_2 \pm (\sqrt{{B_2}^2 - 4A_2C_2})}{2A_2} \qquad (5.4h)$$

where,

$$A_2 = \left(1 + \frac{K_a^w}{H_o^+}\right)K_{cd1} + \left(1 + \frac{K_a^w}{H_o^+}\right)\left(\frac{K_{cd2}K_a^w}{H_o^+}\right) \qquad (5.4h - i)$$

$$B_2 = \left(1 + \frac{K_a^w}{H_o^+}\right) + \left(K_{cd1} + \frac{K_{cd2}K_a^w}{H_o^+}\right)CD_{tb} - I_t^b K_{cd1} - I_t^b\left(\frac{K_{cd2}K_a^w}{H_o^+}\right) \qquad (5.4h - ii)$$

$$C_2 = -I_t^b \qquad (5.4h - iii)$$

<u>Charge Balance</u>

$$\frac{H^+ + 2Ca^{2+} + Ca(OH)^+ + Ca(Ac)^+ - Ac^- - OH^-}{a} - III^- - 2IV^{2-} = 0 \qquad (5.4i)$$

Eqs. (5.1a)-(5.1j), (5.2a-5.2i) (5.3a)-(5.3l) and (5.4a)-(5.4i) constitute the comprehensive set of equations used to model active drug loading into calcium acetate-containing liposomes. (Eqs. (5.1a)-(5.1j) describe the establishment of the pH gradient due to acetic

acid transport and Eqs. (5.2a-5.2i, 5.3a-5.3l and 5.4a-5.4i) account for active drug loading as a function of time.

Experimentally, the pH gradient was established in a separate step where 1 ml of liposome was dialyzed against 1000 ml of 0.9% NaCl solution. The drug loading step was then carried out in 200 ml of supersaturated drug solution following the pH gradient step. However, for the purposes of modeling, the equations governing the pH gradient were solved simultaneously with drug loading equations.

Sodium Acetate Vesicles

Similarly, while using the sodium acetate-containing vesicles instead of calcium acetate-containing vesicles, the equations remain the same except that the equilibria involving calcium are absent. Sodium acetate (NaAc) dissociates completely in water.

$$NaAc \rightarrow Na^+ + Ac^- \qquad (5.5a)$$

$$Na^+ = C_i0 \qquad (5.5b)$$

where C_i0 is the total initial acetate concentration (t=0).

$$f_i = \frac{H_i^+}{H_i^+ + K_a^{ac}} \qquad (5.5c)$$

and f_i is the fraction of unionized acetic acid.

Charge Balance

$$\frac{H^+ + Na^+ - Ac^- - OH^-}{a} - III^- - 2IV^{2-} = 0 \qquad (5.5d)$$

Table 5.1 Values of the constants used in the model simulation

Parameter	Values	Parameter	Values
a	1.08 [#]	K_{cd1}	9788 (±820) M^{-1} [&]
b	12.86 [#]	K_{cd2}	1385 (±170) M^{-1} [&]
c	1.0272 [#]	K_1	0.05 M [*]
d	39.15 [#]	K_2	0.066 M [*]
x	3.2118 [#]	K_a^{ac}	1.78E-5 M [*]
K_a^w	3.4E-7 M [$]	k	1.77E5 hr^{-1} [$]
K_{a2}^w	2.7E-9 M [$]	k_m	287 (±43) hr^{-1} [¥]
K_{p1}	2443 [$]	k_d	0.71(±0.06) hr^{-1} [¥]
K_{p2}	141 [$]	k_{dcd}	0.33(±0.04) hr^{-1} [¥]
K_{p3}	73 [$]		

[#]From the calculations described in the mathematical model section; [$] from references (126, 131, 132, 187, 212, 213), [&] Avg. ± 95% CI (determined in this study); [*]calculated using Chemist® (Microsoft Scientific Software), [¥] from model fitting of experimental data in this study (Avg. ± 95% CI).

RESULTS

Liposome Characterization

The particle size of blank liposomes was in the range of 180-190 nm, with a polydispersity index in the range of 0.075-0.087, indicating monodisperse formulations. Passive and active loading of liposomes with AR-67 did not alter the particle size significantly as drug loaded liposomes exhibited particle sizes within the range of 175-185 nm, polydispersity index of 0.080-0.091. The extrusion procedure employed in this study was previously shown by ^{31}P-NMR to produce unilamellar vesicles (141).

Passive Loading

Based on the pH-solubility profile of AR-67 (Figure 5.2), passive loading could not be successfully carried out with the lactone form of the drug due to its extremely poor aqueous solubility at pH 4.2 (1.11×10^{-4} mg/ml). In order to overcome the limitations of low solubility at pH 4.2, passive loading at pH 9.5 was carried out. Despite an improvement in solubility of about four orders of magnitude, the drug-to-lipid ratio achieved was only 3×10^{-5}. The low drug-to-lipid ratio achieved by passive loading led to consideration of the active loading method.

Preliminary Active Loading Studies

At high intravesicular pH, lactone (I) undergoes ring-opening and ionization to give carboxylate monoanion (III) and dianion forms (IV), providing sink conditions for uptake. Preliminary active loading of AR-67 into calcium acetate vesicles in the presence of excess solid at 37°C resulted in a drug-to-lipid ratio of only 0.0016 even after 70 hours (Figure 5.3A). Model simulations also predicted a very slow uptake under these conditions due to the low solubility of AR-67 at this temperature. In order to expedite the

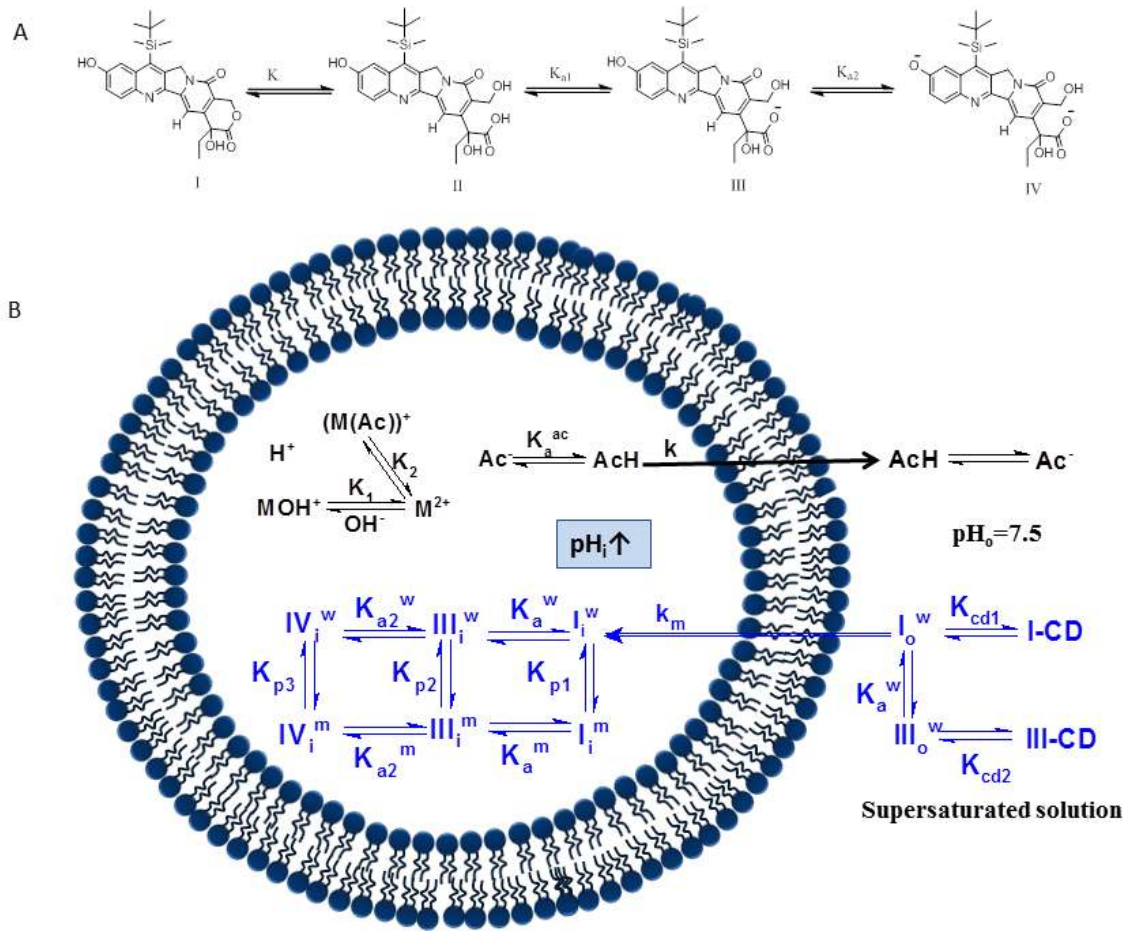

Figure 5.1 (A) Equilibria between AR-67 lactone (I), AR-67 carboxylic acid (II), AR-67 carboxylate monoanion (III) and dianion (IV). (B) Possible chemical equilibria inside and outside the liposomes and transport processes during active drug loading in calcium acetate liposomes.

K_a^{ac} is the dissociation constant for acetic acid; k is the rate constant for acetic acid transport; K_1 and K_2 are the dissociation constants of calcium hydroxide and calcium acetate complexes respectively. M is calcium metal ion, I_i^w, III_i^w, IV_i^w refer to intravesicular lactone, monoanion and dianion form of AR-67 respectively; I_i^m, III_i^m, IV_i^m are corresponding intravesicular membrane bound species. Ka^w and Ka_2^w are ionization constants of AR-67 in water and Ka^m and Ka_2^m are ionization constants of membrane bound AR-67. K_{p1}, K_{p2} and K_{p3} are bilayer water partition coefficients for lactone, monoanion and dianion form of AR-67 respectively, km is release rate constant of AR-67 through bilayer. I_o^w and III_o^w are extravesicular lactone and monoanion form of AR-67 respectively; I-CD and III-CD are their corresponding cyclodextrin complexes in the extravesicular supersaturated drug solution. K_{cd1} and K_{cd2} are the binding constants of lactone and monoanion AR-67 with SBE-CD. The subscripts i and o denote intravesicular and extravesicular, respectively; superscripts w and m refer to water and membrane phases, respectively. Note: Dialysis tube is not shown in the figure but was considered in the development of the mathematical model.

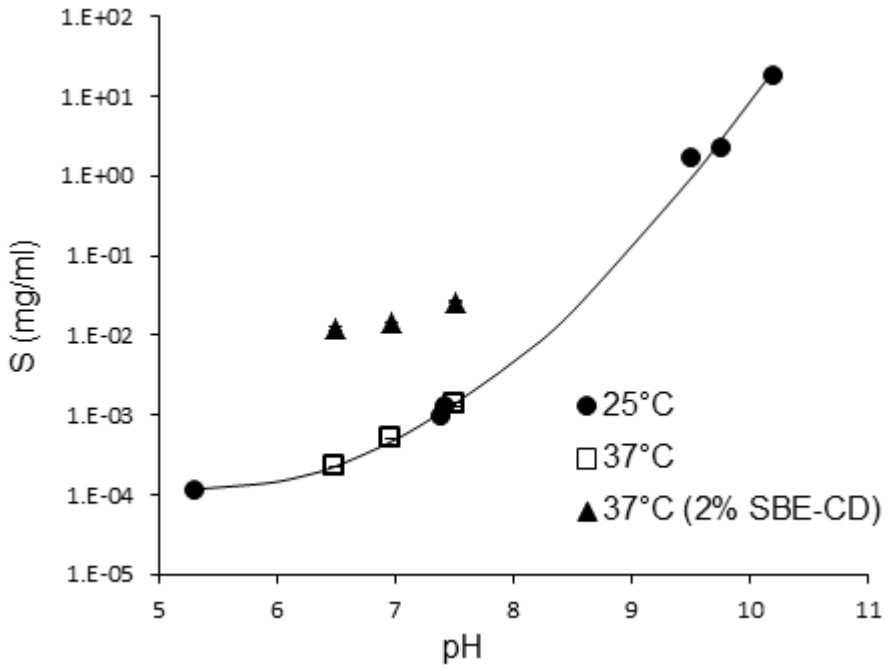

Figure 5.2 pH-solubility profile of AR-67 in aqueous solution at 25℃ (●) from ref [27] and solubility data generated in this study at 37℃ and pH 6.5, 7.0 and 7.5 at 0% SBECD (□) and at 2% SBECD (▲). Solubility data at 37℃ are averages of three independent determinations; the error bars are buried in the symbol itself.

uptake process, active loading in the presence of excess solid was also carried out at 60°C (i.e., above the gel→liquid crystalline phase transition temperature of DSPC of 55°C) as shown in Figure 5.3B. The intraliposomal pH-gradient stability was compromised at this high temperature, as evident from the significant increase in the fraction of intraliposomal lactone as a function of time (Figure 5.3B inset). The pH gradient was much more stable at 37°C, as shown by the inset in Figure 5.3A, although some drift in the fraction of lactone was apparent over the 70 hour time frame of these studies.

To overcome the low solubility problems and subsequent low loading encountered using the active loading method even in the presence of excess solid, supersaturated solutions were produced by the pH adjustment method (Method I) and liposome uptake was monitored from these solutions at either 37°C or 60°C. Loading from supersaturated solutions increased dramatically compared to the results obtained in the presence of excess solid without supersaturation, as shown by the results in both Figures. 3A and B. Interestingly, the rate and extent of loading from the supersaturated drug solution was lower at 60°C (Figure 5.3B) compared to 37°C (Figure 5.3A) and at 60°C, the fraction of lactone increased rapidly as a function of time, exceeding 0.5 after 5 hrs (Figure 5.3B). Liposomal concentrations of AR-67 also peaked at 5 hours at 60°C and gradually declined thereafter, consistent with the evidence of instability in the pH gradient as monitored by the fraction of intraliposomal lactone. At 37°C, the fraction of lactone remained relatively stable and below 0.2 over at least 96 hours (Figure 5.3A inset), indicating that the high intraliposomal pH was maintained. Consistent with this result, the liposomal uptake of AR-67 from the supersaturated solution at 37°C continued to increase over the entire 120 hr duration of the loading experiment (Figure 5.3A).

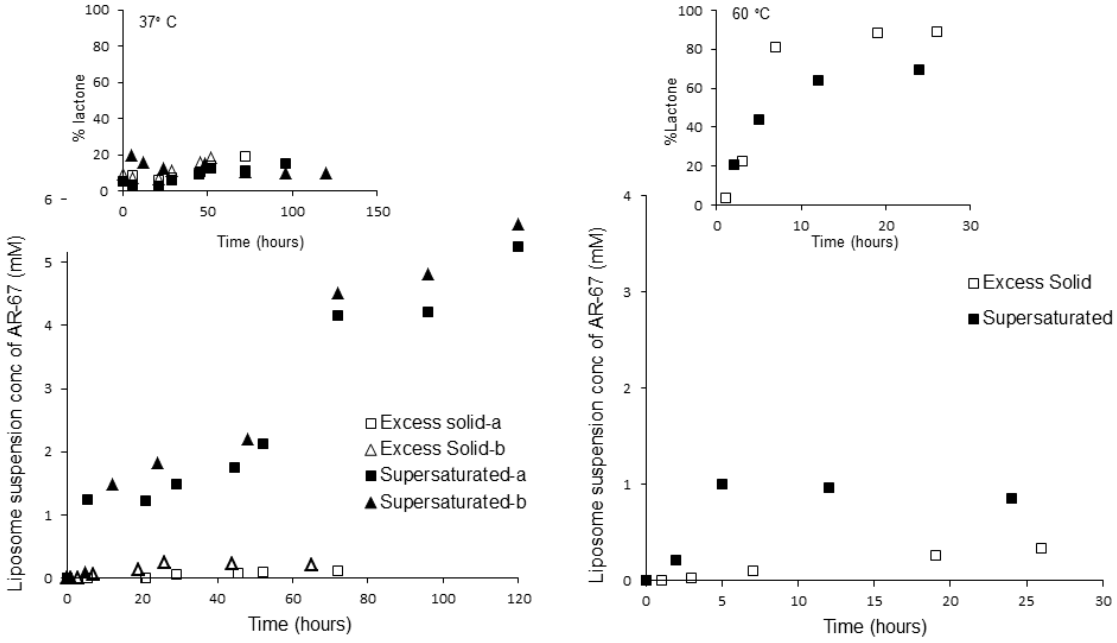

Figure 5.3 Active loading in 0.25 M calcium acetate liposomes at pH 7.5 and 37°C (A) or 60°C (B) in the presence of excess solid and from supersaturated AR-67solutions (Method I). Inset shows intraliposomal % lactone during loading. a and b denotes replicates for the experiments at 37ºC.

Maintenance of Supersaturation

The solubility profiles of AR-67 at pH 6.5, 7.0 and 7.5 with increasing concentrations of the cyclodextrin ([CD]) are shown in Figure 5.4. The linear solubility profiles indicate that 1:1 complexes predominate. Assuming [CD]>> S_o and carboxylate dianion is negligible in the pH 6.5-7.5 region, complex formation constants for the neutral lactone (K_{cd1}) and carboxylate monoanion (K_{cd2}) were calculated from the following equation (185):

$$S = S_o(1 + K_a 10^{pH} + K_{cd1} CD + K_{cd2} CD K_a 10^{pH}) \qquad (5.6)$$

where S_o is the intrinsic solubility of lactone. A linear least-squares fit of the data in Figure 5.4 to the above equation yielded K_{cd1} =9788 (±820) M^{-1} and K_{cd2} =1385 (±170) M^{-1} (the values in the bracket are ± 95% S-plane confidence intervals).

Creating a supersaturated drug solution significantly increased the drug loading achievable but to maintain the supersaturation achieved by the pH adjustment method (Method I), frequent re-dissolution of precipitates formed over time by raising and then lowering the pH was required - a tedious and poorly reproducible process. Incorporation of a low (2%) concentration of SBE-CD into the pH 7.5 supersaturated solutions produced by the pH adjustment method was found to dramatically inhibit drug precipitation. The equilibrium solubility of AR-67 at pH 7.5 in the presence and absence of 2% SBE-CD was determined to account for the increase in the equilibrium solubility that would result from the complexation of AR-67 with SBE-CD and to assess the degree of supersaturation that could be achieved in loading solutions containing 2% SBE-CD. The equilibrium solubilities of AR-67 (± SD) were experimentally determined to be 1.35 ± 0.07 μg/ml and 26.5 ± 0.2 μg/ml in the absence and presence of 2% SBE-CD,

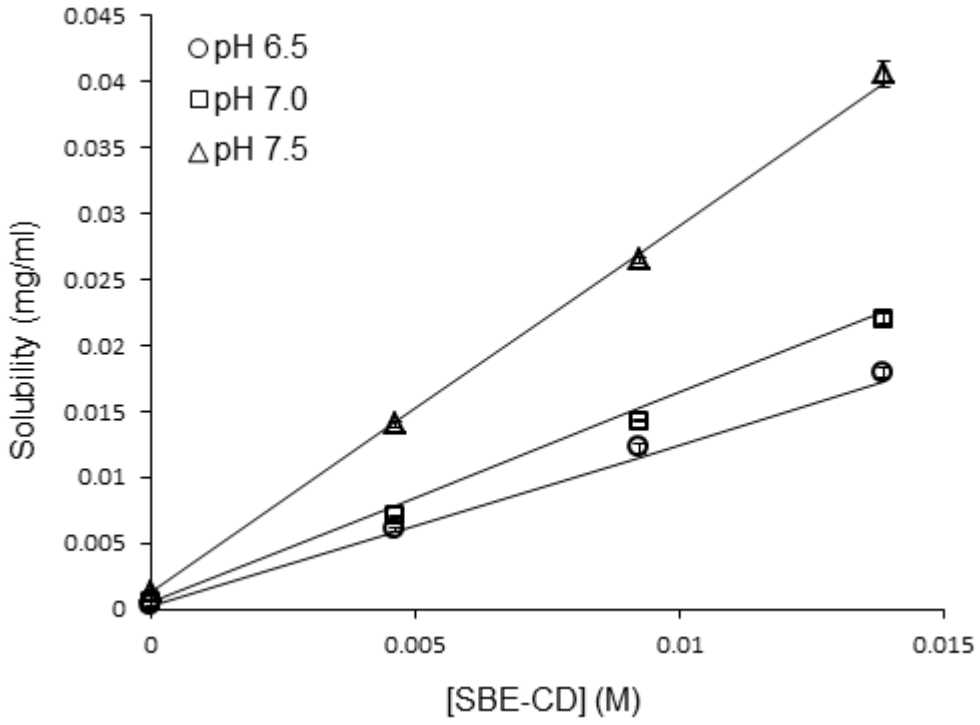

Figure 5.4 Plots of equilibrium solubility of AR-67 at 37°C as a function of SBE-CD concentration in buffered aqueous solutions at pH 6.5, 7.0 and 7.5. Each value is the average of three independent determinations; error bars are the standard deviations. Straight lines are least squares fits using Eq. 5.6.

respectively, at a pH of 7.5 at 37°C. Total supersaturated solution concentrations achieved by pH adjustment and maintained in the presence of 2% SBE-CD ranged from 0.1-0.6 mg/ml. Figure 5.5 depicts the degree of supersaturation achieved in different loading solutions after normalizing to the appropriate equilibrium solubility value. The equilibrium solubilities of AR-67 at pH 7.5 with and without 2% SBE-CD were significantly different ($p<0.05$). Dramatic increases in concentrations of the permeable, free lactone were possible using this method (Method II).

Active Loading from Drug Solutions Varying in Degree of Supersaturation

Active loading of AR-67 in liposomes using an acetate pH gradient method was carried out in supersaturated loading solutions containing different drug concentrations (0.1, 0.2, 0.4 and 0.6 mg/ml). Evidently, an increase in total drug concentration and a corresponding increase in lactone concentration in the loading solution resulted in increased intravesicular loading (Figure 5.6).

Furthermore, a linear relationship was observed between the extent of loading and loading time with slopes that increased linearly with the drug concentration in the loading solution. This linearity is demonstrated in Figure 5.7, where liposome suspension concentration at 48 hr are plotted versus the drug concentration in the loading solution. The highest intraliposomal drug-to-lipid ratio of 0.17 was achieved when the drug concentration of 0.6 mg/ml was used in the external loading solution. Furthermore, the intraliposomal carboxylate fraction was found to remain above 0.86 in all cases (Figure 5.8), indicating that the high intraliposomal pH was stable over the entire time frame of the loading experiments. Studies at the lowest (0.1 mg/ml) (n=3) and highest (0.6 mg/ml)

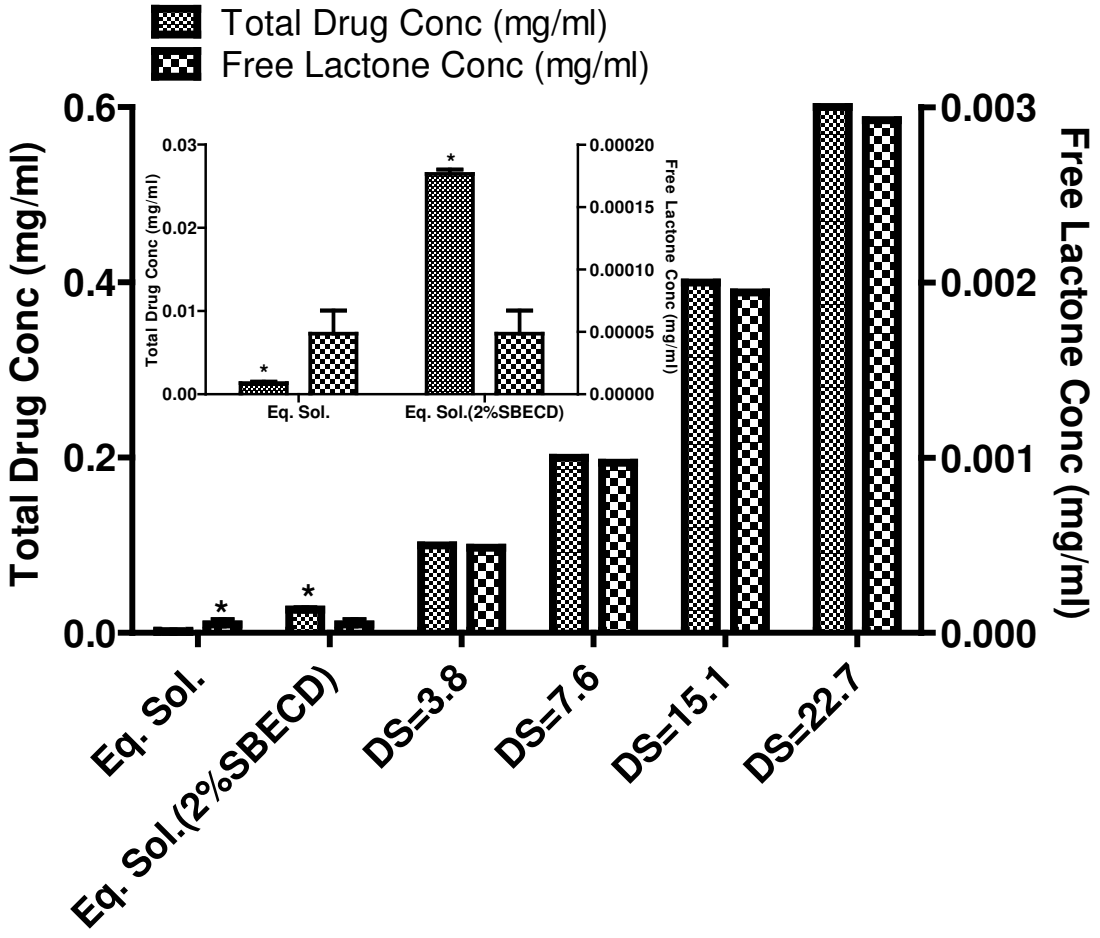

Figure 5.5 Enhancement of the total drug solubility and corresponding lactone concentration at pH 7.5 in the presence of 2% SBE-CD at equilibrium and in supersaturated solutions of varying degree. (Degree of supersaturation was calculated with respect to equilibrium solubility in 2% SBE-CD). * denotes the two values are significantly different from each other ($p<0.05$).

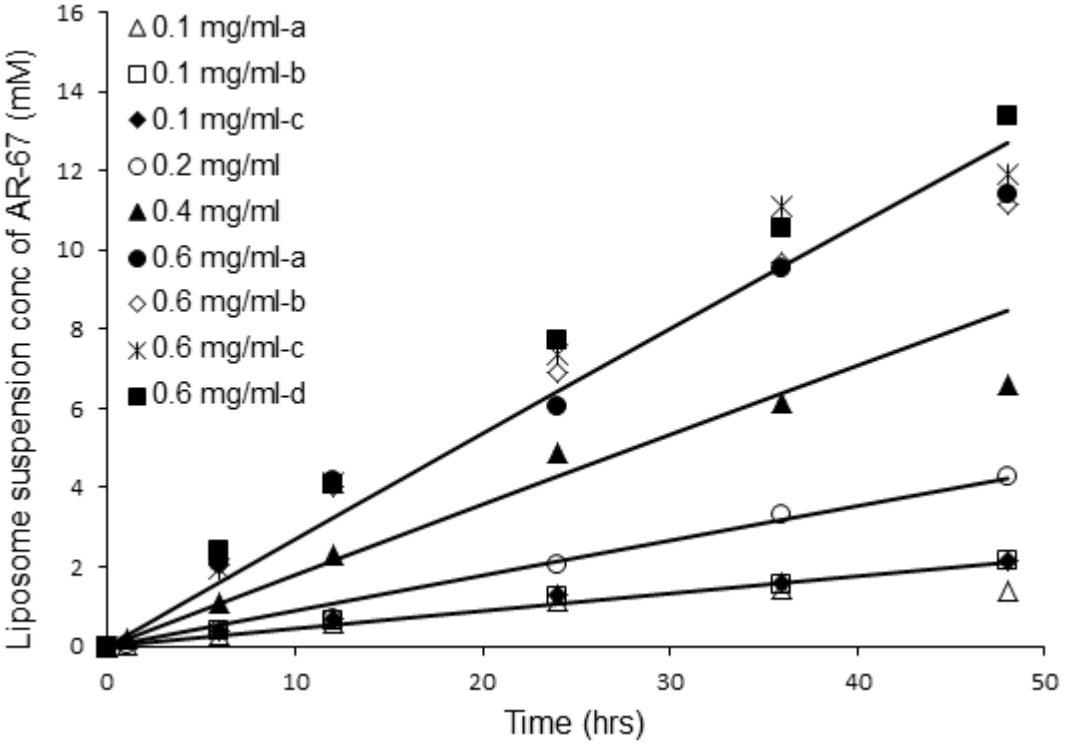

Figure 5.6 Liposome suspension concentrations of AR-67 versus time during active loading in calcium acetate-containing liposomes in supersaturated loading solutions (Method II) at different drug concentrations (0.1, 0.2, 0.4 and 0.6 mg/ml) at 37°C. Solid lines are the least-squares fits using the active loading model (Eqns. 5.2a-5.2d).

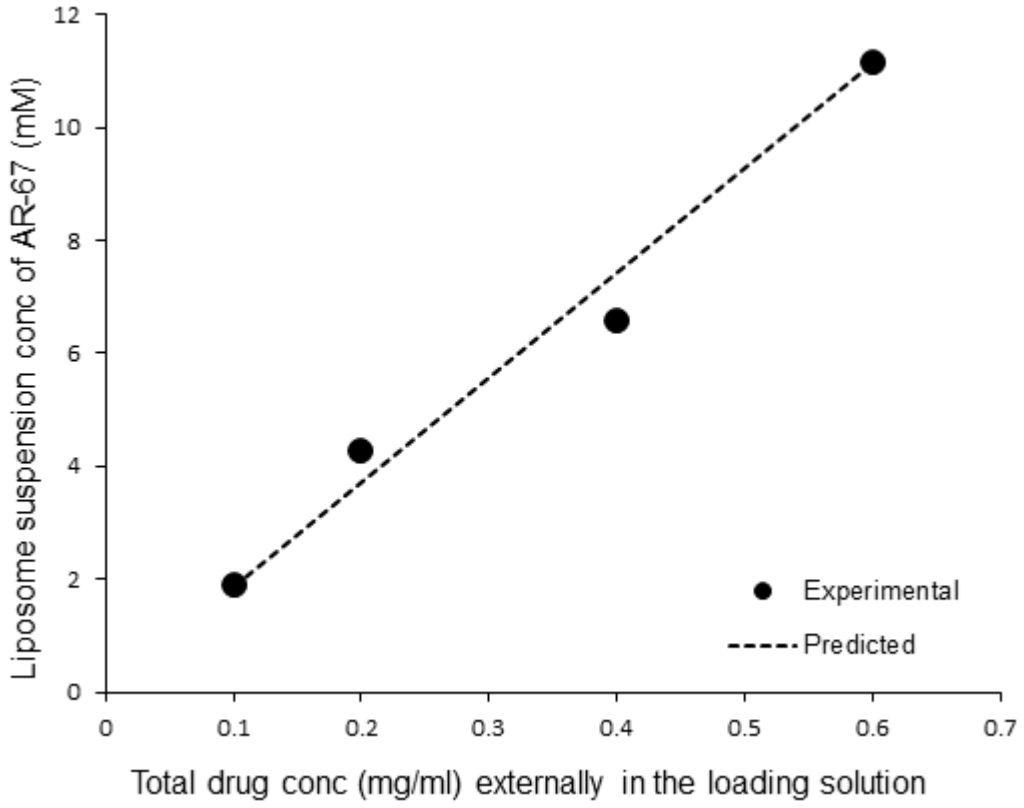

Figure 5.7 Experimental and predicted relationship between liposome drug loading upto 48 hours and 37°C and total drug concentration in the external supersaturated loading solution.

(n=4) loading solution concentrations were repeated and the results were found to be reproducible.

Drug-to-lipid ratios obtained in all drug loading experiments described above are summarized in Table 5.2.

Effect of counter ions on loading

The active loading experiments reported above were carried out in liposomes prepared from 0.25 M calcium acetate. Active loading of AR-67 was also carried out in liposomes prepared in 0.5 M sodium acetate using supersaturation Method II at the highest solution concentration of drug (0.6 mg/ml) to determine the role of the entrapped counter ion on loading. No significant difference was found in either the rate or extent of loading in sodium acetate vs. calcium acetate containing vesicles at various time points up to 48 hours (Figure 5.9).

Model Predictions

Dialysis experiments in the absence of liposomes were necessary to obtain the reversible first-order rate constants for the transport of AR-67 in either its lactone and carboxylate forms (k_d) and SBE-CD or SBE-CD/AR-67 complexes (k_{dcd}) across the dialysis membrane. The values found for k_d and k_{dcd} are shown in Table 5.1 with their 95% confidence limits generated from a total of five independent concentration versus time profiles as described in the methods section. The values obtained for k_d and k_{dcd} in the absence of liposomes within the dialysis tube were assumed to be the same when liposomes were present.

Table 5.2 Drug/Lipid ratios for liposome formulations of AR-67 under passive and active loading conditions

Initial extravesicular solution drug conc. (mg/ml)	Loading type/Conditions	Lipid Conc# (mM)	AR-67 conc. (mM) in the liposome suspension	Drug/Lipid ratio
0.8	Passive/ pH 9.5	18.0	5.3E-4	3.0E-5
0.00135	Active/Excess Solid	67.4	0.11	0.0016
0.1*	Active/ Supersaturated	67.4	1.91±0.44	0.027±0.006
0.2	Active/ Supersaturated	67.4	4.26	0.060
0.4	Active/ Supersaturated	67.4	6.58	0.089
0.6*	Active/ Supersaturated	67.4	11.95±0.99	0.170±0.015

For calculation of lipid concentration, normalized molecular weight of lipid was used, DSPC: mPEG-DSPE 95:5 mol%, Mol. Wt.= (0.95*Mol. Wt. of DSPC)+(0.05*Mol. Wt. of mPEG-DSPE)

* Replicate experiments were conducted under these two extreme loading conditions to test the reproducibility of the loading method. Averages of three (at 0.1 mg/ml) and four (at 0.6 mg/ml) loading experiments are reported along with standard deviations. Drug/lipid ratios were calculated based on intravesicular drug concentrations.

The permeability coefficient for AR-67 lactone (permeable species) was determined from model fitting at different loading conditions (total external drug concentration of 0.1, 0.2, 0.4 and 0.6 mg/ml) to be $2.13 \times 10^{-7} \pm 0.38$ cm/s (95% confidence interval). Simulations can be performed, using the determined permeability value, to predict the loading as a function of the degree of supersaturation. While some of the constants and parameters (aqueous and membrane bound ionization constants of the drug, membrane partition coefficients of each species) employed in these model simulations were from previously published experimental studies from our lab (126, 132, 187), the permeability coefficient of the lactone was the only fitted parameter generated from the liposome loading data, as the rate constants for free and bound drug across the dialysis membrane were determined from separate experiments. Figure 5.6 shows the model fitting of the experimental data demonstrating the linear increase in intravesicular drug concentrations with time. The slopes of the fits increased linearly with drug concentration consistent with the model prediction indicated by the dashed line in Figure 5.7. The model simulations also gave identical results with sodium and calcium acetate liposomes for the liposomal concentration vs. time (Figure 5.9) indicating that the nature of the intraliposomal cation (i.e., Na^+ vs. Ca^{++}) was inconsequential for loading.

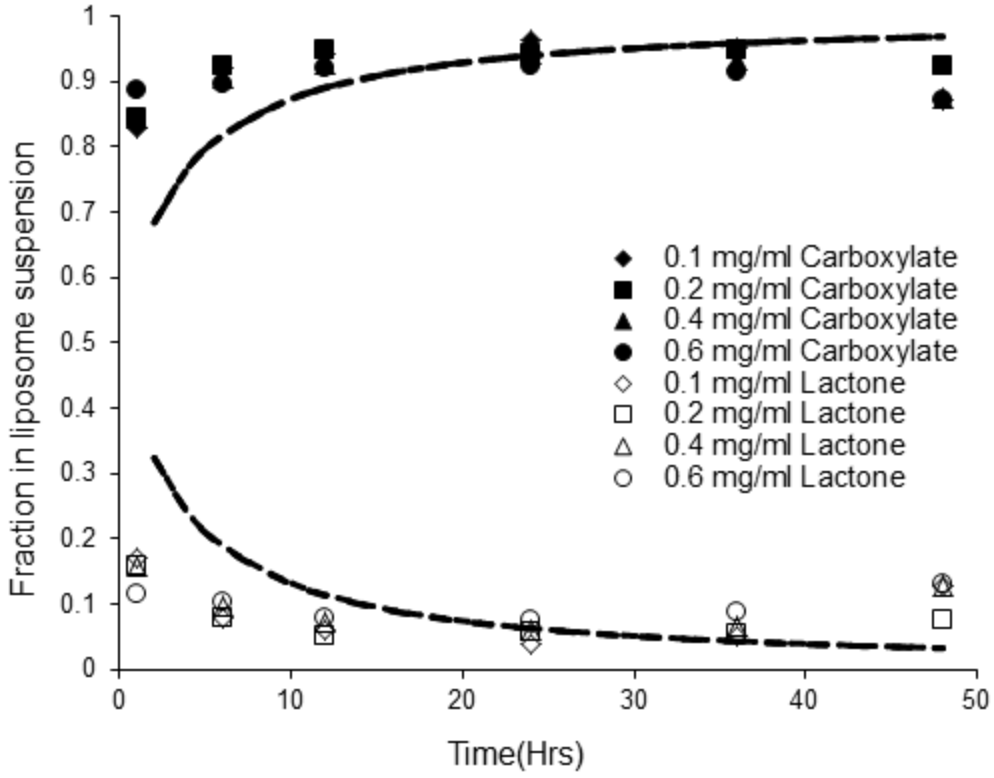

Figure 5.8 Liposomal suspension fraction of carboxylate and lactone versus time during active loading in calcium acetate-containing liposomes in supersaturated loading solutions (Method II) at different total drug concentrations (0.1, 0.2, 0.4 and 0.6 mg/ml) at 37°C. The points are the experimental data and the lines are the model simulations.

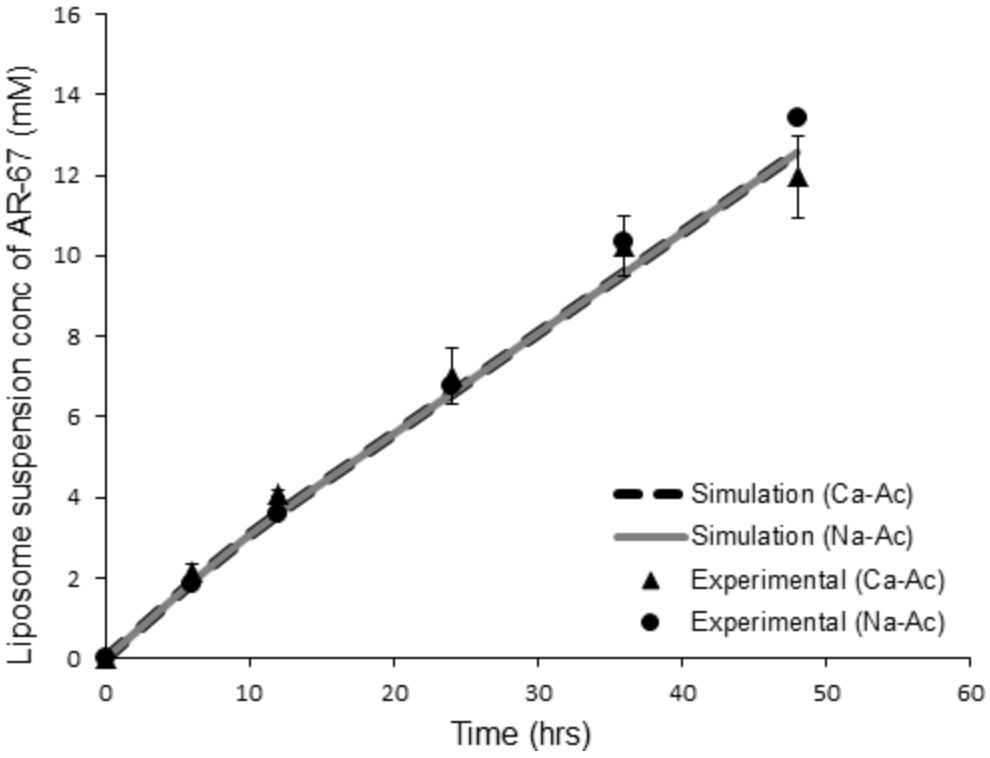

Figure 5.9 Comparison of active loading in 0.5 M sodium acetate and 0.25 M calcium acetate-containing liposomes in the presence of supersaturated solutions (Method II) containing 0.6 mg/ml AR-67 concentration at 37°C.

DISCUSSION

Liposomal delivery of antitumor agents is highly desirable to passively target these drugs to tumor tissues and minimize unwanted side effects (214). Achieving high liposomal loading may be particularly challenging for new, highly lipophilic antitumor agents exhibiting very low water solubility. AR-67, a novel camptothecin analogue that is currently in clinical studies, serves as an example and was therefore chosen as a model drug for this study.

Passive Loading

The intraliposomal drug concentrations achieved by passive loading, the conventional method of drug loading into liposomes, depends on entrapped aqueous volume, lipid concentration, and the solubility and partition coefficient of the drug (48). For the lipid concentration (16 mg/ml) employed in this study, the entrapped aqueous volume can be estimated to be ~ 6.4%. Passively loading liposomes using AR-67 solutions at a low pH of 4.2 was not feasible due to the poor drug solubility at this pH. An attempt to improve drug uptake by carrying out passive loading at a higher pH of 9.5, where an aqueous solubility of 0.8 mg/mL could be achieved (Table 5.2), resulted in a very low drug to lipid ratio (D/L=$3x10^{-5}$). Theoretically, based on the solubility at pH 9.5 and the aqueous entrapped volume, a D/L of ~$3x10^{-3}$ can be estimated with no contribution of intraliposomal membrane binding. The much lower loading ratio achieved may reflect poor permeation of the hydrophilic dianionic species which predominates at pH 9.5 through the lipid film layers during the hydration step prior to vesicle formation. Moreover, based on the profile for AR-67 membrane binding versus pH (126) and its pH-solubility profile (185), there exists an interplay between solubility and membrane

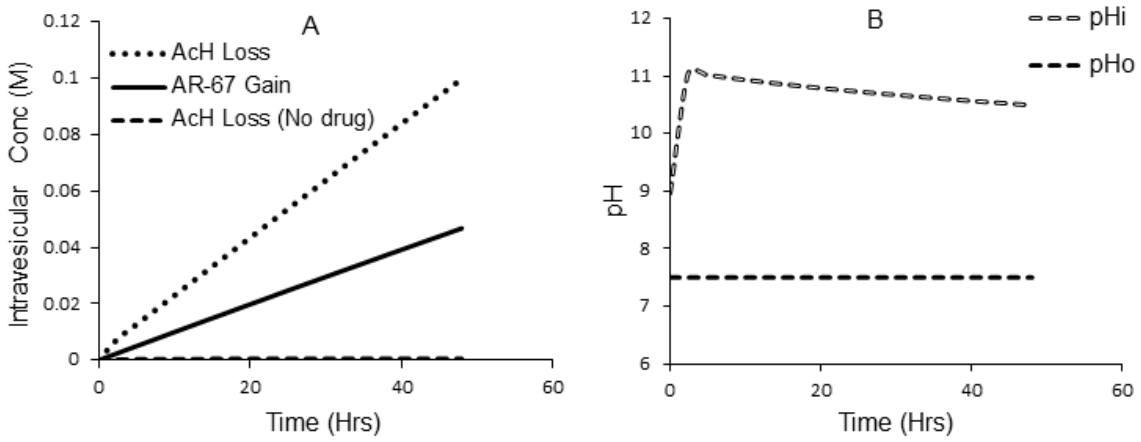

Figure 5.10 Model simulations for different intraliposomal and extraliposomal species. (A) Loss of intraliposomal acetic acid and corresponding intraliposomal AR-67 gain during active loading along with comparison of acetic acid loss in the absence of drug; (B) Intravesicular and extravesicular pH during active loading of drug in 0.25 M calcium acetate liposomes at 37°C.

partitioning with changes in pH. While the solubility of AR-67 increases from $1.11x10^{-4}$ mg/ml at pH 4.2 to 0.8 mg/ml at pH 9.5, the bilayer/water partition coefficient decreases from 2443 ± 230 at pH 4.1 to 57 ± 5 at pH 9.5 (212). Thus, in terms of passive loading, the advantage of increased solubility at high pH is offset in part by decreased membrane binding.

Active Loading

Active loading is primarily driven by a chemical potential gradient across the bilayer as given by Eq. 5.7.

$$Flux\ \alpha\ P_m(C_{free}^{out} - C_{free}^{in}) \qquad (5.7)$$

where P_m is the intrinsic permeability coefficient for the unionized species, C_{free}^{out} is the free concentration of the unionized species in the external medium and C_{free}^{in} is the free intraliposomal concentration of the same species assuming that only the unionized species is permeable.

Enhancement of the External Driving Force for Active Loading

To enhance liposome loading of AR-67, a pH-gradient active loading approach was explored in which a high intraliposomal pH was created by preparing liposomes in the presence of high concentrations of either calcium acetate or sodium acetate. As indicated in Eq. 5.7, the driving force for active loading of AR-67 is the external to internal free lactone concentration gradient. Partial release of acetic acid creates a high intraliposomal pH resulting in a reduction in C_{free}^{in}, providing sink conditions for liposomal uptake of AR-67. Eq. 5.7 also indicates that the rate of uptake (flux) can be increased by enhancing the trans-membrane permeability of the drug, for example, by increasing temperature. Under conditions in which C_{free}^{out} is limited by the equilibrium solubility of AR-67, it was

reasoned that maintaining this concentration by conducting drug loading in the presence of excess solid would be beneficial. Therefore, active loading studies were initially conducted in the presence of excess solid drug at 37°C, although model predictions suggested that this approach would have limited success due to the very low equilibrium solubility of the drug. Slow uptake was indeed observed at 37°C, as shown by the data in Figure 5.3A. To increase P_m (and perhaps AR-67 solubility) loading experiments were also conducted at 60°C, as above the phase transition temperature for DSPC (55°C), the liposome bilayer is in a more permeable liquid crystalline form (131). This resulted in a modest increase in uptake rate (Figure 5.3B) but as illustrated by the inset in Figure 5.3B, the fraction of the intraliposomal lactone species which is dominant only at a lower pH increased dramatically with time at 60°C indicating that within 5-10 hrs the pH gradient had dissipated. Previous reports (215, 216) have confirmed losses in pH gradients during active loading in cholesterol free liposomes above the phase transition temperature attributed to membrane destabilization, leading to a decline in loading with time. Dissipation of pH gradients above the phase transition temperature may be attributable to increased permeability of hydrochloric acid, hydrogen ions, or ion pairs, etc. (215, 217-220). Liposomes containing 40-50% cholesterol may be more resistant to these effects due to stabilization of bilayers by cholesterol above the phase transition (206, 221, 222).

In an attempt to overcome the limitations in liposomal uptake imposed by the low aqueous solubility of AR-67, which results in a low driving force (c*f.*, Eq. 5.7), supersaturated drug solutions of AR-67 was created, first simply by pH adjustment (Method I). Supersaturation increased the aqueous concentration of the drug, including free lactone, and dramatically enhanced liposomal uptake rates at both 37°C (Figure

5.3A) and 60°C (Figure 5.3B), although the aforementioned dissipation in pH gradient and a resulting decline in drug loading now became clearly evident at 60°C. Because Method I was ineffective in maintaining supersaturation over a prolonged period, the use of SBE-CD to inhibit nucleation and crystal growth was evaluated. Previously, 20% SBE-CD had been shown to inhibit the crystallization of 2 mg/ml supersaturated solutions of AR-67 after reconstitution from lyophiles for at least three days (185). Here, 2% solution concentrations of SBE-CD were employed to minimize the fraction of lactone present in inclusion complexes while maintaining high supersaturated concentrations. As demonstrated in Table 5.2 and Figure 5.5, supersaturated solution concentrations as high as 0.6 mg/ml were maintained using this approach, resulting in substantial increases in drug loading at 37°C, with D/L ratios as high as 0.17 (Table 5.2) and with no apparent dissipation in the pH gradient (Figure 5.8).

Mechanism-Based Mathematical Model Development

A mathematical model was developed to explore intraliposomal properties that may be important both for loading and drug release and to predict drug loading under various conditions. A key assumption in the model is that the driving force for drug uptake is the transbilayer concentration gradient of the free lactone. The model incorporates the experimentally determined ionization and membrane binding constants of each species of the drug along with equilibrium constants for the formation of cyclodextrin complexes of AR-67 lactone and its ring-opened monoanion. The incorporation of the permeability coefficients enables the prediction of rates of drug uptake, representing an important advance in comparison to previous models (223-225).

Experimental data generated at various loading concentrations (0.1, 0.2, 0.4 and 0.6 mg/ml) were fitted to the developed model to determine the permeability coefficient of the lactone under active loading conditions. The intrinsic permeability value for AR-67 lactone obtained in this study from k_m (see Table 5.1) is $2.13 \times 10^{-7} \pm 0.38$ cm/s, which lies between a previously reported experimental value determined from liposomal release studies by Joguparthi et al (212) and a predicted value using the "barrier-domain" solubility diffusion model (130, 212).

While one would expect the permeability coefficient to be the same for both uptake and release the determination of the driving forces (lactone concentration gradient) governing drug uptake or release rates is not trivial. If the driving force is not determined accurately, the permeability coefficient obtained by experiment will also be inaccurate. Estimating the driving force governing drug release requires determination of the aqueous concentration of free lactone inside the liposome, which depends on the intraliposomal pH and membrane binding of each AR-67 species inside the liposome. AR-67 is extensively bound intraliposomally due to its high membrane binding coefficients and the high membrane surface to volume ratio inside the liposomes [19, 20]. The driving force for drug uptake is somewhat easier to determine, although one must either analyze the free lactone concentration or use a mathematical model that includes transport across the dialysis membrane to obtain the steady-state extravesicular lactone concentration inside the dialysis tube. In the present study, the dialysis membrane did partially contribute to the overall barrier for drug-loading but reliable estimation of the intrinsic permeability coefficient of AR-67 was still possible. The extravesicular free lactone concentration at steady-state was 2.4 times lower than the free lactone concentration in the bulk solution

outside the dialysis tube due to the resistance of the dialysis membrane barrier. In the absence of this barrier, a maximum increase of ~2.5 fold in the rate of loading might have been achievable. It can be expected that using a dialysis membrane of higher molecular weight cut-off would have had some benefit, but much less than this maximum.

Differences in the uptake rate and extent of AR-67 loading up to 48 hours into calcium acetate-containing liposomes under various loading conditions can be accurately predicted by the mathematical model using the permeability value determined for AR-67 (Eqs. 5.2a-5.2d) as illustrated in Figures 5.6 and 5.7. Simulations using the same model were conducted to further explore the role of intraliposomal acetate in establishing the pH gradient. A high intraliposomal pH is produced by the transbilayer concentration gradient of acetic acid, which is a highly permeable weak acid (P_m^a=1.6 (± 0.2)x10^{-4} cm/s across DSPC bilayers (131)). Figure 5.10B shows the simulated increase in intraliposomal pH during the initial dialysis step to remove unentrapped buffer (Eqs. 5.1a-5.1j). This high intraliposomal pH is maintained by the continuous transport of acetic acid from inside the vesicles in exchange for incoming lactone. Figure 5.10A shows the direct relationship between acetate loss and intraliposomal drug loading. For each molecule of lactone internalized, two molecules of acetic acid are lost due to the predominance of the AR-67 dianion at this intraliposomal pH. Model predictions of the fractions of lactone and carboxylate in the liposome suspension during the course of loading compare favorably to the experimental observations except at the initial time points. In the initial stages of loading, the contribution of the extravesicular drug concentration to the total suspension concentration is relatively high and the discrepancy in this early region may be attributable to the fact the solution initially introduced into the dialysis tube is a poorly

buffered dilute calcium acetate solution in 0.9% NaCl that may have a higher initial pH than the bulk loading solution. The model assumes a constant extravesicular and bulk pH of 7.5. Also, there may be some error associated with quenching the carboxylate to lactone conversion during sample preparation and prior to HPLC analysis. In their validation of an analytical method for the determination of the lactone and carboxylate concentrations in mouse plasma, Horn et al. reported a carboxylate to lactone conversion of about 3.7% prior to sample analysis [44]. Nevertheless, experimental analysis of both lactone and carboxylate fractions during drug loading under different conditions revealed relatively stable, high intraliposomal carboxylate fractions, indicative of a high intraliposomal pH.

The high intraliposomal pH demonstrated in both simulations and experimentally in this study results in a low intravesicular fraction of free lactone (I), caused by base-catalyzed ring-opening of the lactone to its carboxylate form (III and IV) at the high intraliposomal pH. Internal membrane binding further reduces the intraliposomal lactone concentration, creating intraliposomal sink conditions. The uptake rate during active loading is therefore primarily governed by the extravesicular driving force (i.e., free lactone concentration enhanced by supersaturation to varying degrees). These increases in drug loading with higher lactone concentrations in the supersaturated loading solutions are illustrated in Figures. 5.5 and 5.6. Experimentally, the maximum drug-to-lipid ratio demonstrated within 48 hours was 0.17. However, as mentioned previously, the rate of loading may have been modestly enhanced by using a dialysis membrane of higher molecular weight cut-off to increase dialysis membrane transport rates. Model simulations predict that a very high extent of loading (D/L of 0.8) could be achieved at equilibrium, provided

supersaturation could be maintained for a prolonged period of time. Also, loading may be further enhanced by intraliposomal precipitation of the calcium salt of AR-67, as governed by its solubility product (226). While the model developed herein does not consider possible intraliposomal salt precipitation, the rates of uptake and extent of loading within 48 hrs would not have been affected by this possibility because intraliposomal sink conditions were maintained throughout this time frame even in the absence of salt precipitation. No significant difference could be detected between the rate and extent of loading at 48 hours from 0.6 mg/ml supersaturated drug concentrations when liposomes prepared in 0.5 M sodium acetate were employed rather than those containing 0.25 M calcium acetate (Figure 5.9). This further suggests that the enhanced active loading is mainly dependent upon establishment and maintenance of the pH gradient leading to intraliposomal sink conditions and increases in the external driving force by supersaturation.

Active loading in response to a transmembrane chemical gradient is dependent upon the properties of the individual drug (208). Zucker et al. suggested an aqueous solubility of 1.9 mM to be a reasonable solubility for active drug loading (48). While the aqueous solubility of a drug is important, it is the concentration of the unionized permeable species that provides the driving force for active loading (*cf*., Eq. 5.7). A detailed analysis of the factors responsible for the maximum liposome loading achieved by others (39, 41, 44, 46-48, 84, 206, 208, 227) using the active loading technique is difficult, but the evidence suggests that reasonable loading required either a moderate solubility of the unionized species, or, in some cases, the authors may have unknowingly created supersaturated solutions during loading. In the present study, achieving the high drug to

lipid ratio of 0.17 clearly required a combination of the transmembrane pH gradient approach and supersaturation.

CONCLUSIONS

A novel method of active loading was developed for a poorly soluble model compound, AR-67, a third generation potent camptothecin analogue, using supersaturated drug solutions along with a high intraliposomal pH produced by a transmembrane acetate gradient. Maintenance of supersaturation was aided by use of a cyclodextrin (SBE-CD) to inhibit drug crystallization during loading. Furthermore, a mechanism-based mathematical model was developed to understand the loading process, assuming that the driving force for drug uptake across the membrane is the concentration gradient of the free unionized species. Loading was mainly driven by the establishment of a pH gradient (high pH inside) produced by the loss of acetic acid, intraliposomal drug ionization, and internal membrane binding of the drug leading to near intraliposomal sink conditions. Improved liposome loading of AR-67 was achieved by developing a novel method for creating and maintaining supersaturation of this hydrophobic, water insoluble drug during the active loading process. The model was successful in fitting the rates of drug-loading (up to 48 hours, period of time supersaturation was maintained using SBE-CD) at several degrees of supersaturation to obtain a single intrinsic membrane permeability coefficient. The developed model can be used to further predict the rate and extent of loading under different loading conditions. This proposed loading methodology may be useful in meeting the formulation challenges presented by the increasing number of poorly soluble anticancer agents emerging from drug discovery.

CHAPTER SIX

Optimization of Liposome Release Kinetics of a Corticosteroid Phosphate Based on pH and Lipid Composition

INTRODUCTION

Dexamethasone (Dex) acts as an anti-inflammatory and immunosuppressive agent by inhibiting the production of pro-inflammatory cytokines. Since inflammatory responses play an important role in tumor progression and metastasis, dexamethasone was shown to enhance the anti-tumor efficacy of certain chemotherapeutic agents. Wang et al. found in pre-clinical studies that pre-treatment with Dex significantly enhanced the antitumor activity of carboplatin and gemcitabine and increased their tumor accumulation (90-92). These observations were further supported by phase II randomized clinical studies (228) and Dex has been proposed as an adjuvant (chemoprotectant and/or chemosensitizer) in cancer chemotherapy to reduce some of the associated side effects (nausea, hematotoxicity) and increase the efficacy of antitumor drugs. Although Dex has numerous therapeutic applications, its use is limited by the side-effects such as immunosuppression, hyperglycemia etc. (229, 230). In addition, due to its rapid clearance from the body, frequent high doses are required to achieve efficacy which in turn causes serious side effects (84). This leads to the demand for a targeted and sustained delivery of dexamethasone to maximize its therapeutic potential and minimize the side effects. It was in fact demonstrated that a sustained delivery over 3-4 days was more effective compared to the 1-day pre-treatment in reducing the carboplatin induced hematologic toxicity (231-233).

Liposomal drug delivery systems play an important role in targeted delivery of anti-tumor agents (20). The steady-state drug concentration at the site of action is a function of the local input and elimination rates. Thus, the rate of drug release from the formulation is an important factor governing the availability of drug at the target site (52). There may be a need to modulate drug release rates based on the tumor type and size in order to provide safe and efficacious concentrations at the tumor site. As a result, it would be highly desirable to design formulations with tunable and predictable drug release rates that can be tailored according to the therapeutic requirement. Generally, drug release half-lives of approximately 24 hours or more are needed so that liposomes retain a majority of their drug payload prior to reaching their maximum accumulation at the tumor site (234-236). Previously, half-lives of dexamethasone (Dex) in liposomes varying in lipid composition were determined. The longest half-life obtained was in DSPC, a densely packed phospholipid that is in its gel state at 37C and therefore more highly resistant to permeability than shorter chain lipids, but the half-life was only 14 hours..

Due to the higher permeability and poor solubility of dexamethasone, the water soluble 21-phosphate prodrug was considered. Along with the advantage of enhanced solubility, the phosphate prodrug of Dex is ionizable, thus allowing the exploration of pH as a formulation variable to tailor its release kinetics. As reported in chapter five for AR-67 and in previous publications from this laboratory (189, 237), lipid bilayer permeabilities of neutral drug species are often orders-of-magnitude higher than their ionized species. Therefore, the release kinetics of liposome encapsulated ionizable drugs can potentially be controlled by modulating the intravesicular pH, providing that the intravesicular pH can be maintained at the desired value. Previous studies have shown that maintaining

intravesicular pH in the alkaline region can be challenging due to the dissipation of the pH gradient due to CO_2 uptake into liposomes under physiological conditions (126). However, phosphate prodrugs possess the advantage of having a low first pKa (~2) and consequently do not require an alkaline pH for ionization (133).

In addition to pH control, the barrier properties of the bilayer can be altered by varying the lipid composition. The effect of bilayer chain density on permeability has been taken into account in the barrier domain model (131, 189). The decrement in permeability due to chain ordering in this model depends exponentially on the ratio of solute size to bilayer free surface area. The relationship between trans-bilayer transport and bilayer free surface area has been tested for small solutes (61, 62, 122, 131, 189, 237, 238) while the present study offers the opportunity to test the applicability of the theory to larger drug-like molecules.

A fundamental understanding of the physicochemical factors governing drug transport across lipid bilayers is essential to predict the release kinetics from liposome formulations. The key for both tunability and predictability is the development of quantitative mathematical models that will take into account the physicochemical properties of the drug and the bilayer membrane along with the intraliposomal and external local environments.

The goal of the present study was to develop a mechanism-based mathematical model of drug release kinetics to account for the physicochemical properties of the drug (e.g., ionic equilibria, membrane binding, etc.), the barrier properties of the bilayer membrane, and the intraliposomal pH microenvironment. The hypothesis was that liposomal release rates could be prolonged significantly by modulating the intravesicular pH and entrapping the

drug in the membrane impermeable ionized form. In addition, changes in the free surface area of the bilayer brought about by changing the lipid composition were expected to further affect the trans-bilayer solute permeability. This study explores liposomal delivery systems of a corticosteroid phosphate, dexamethasone phosphate (Dex-P), that provide a range of release half-lives. Such information will also be useful in extending previously developed quantitative relationships between lipid bilayer permeability and factors such as intravesicular pH, lipid composition, and permeant size to larger molecules having a size more typical of most drugs.

MATERIALS AND METHODS

Dexamethasone sodium phosphate USP (Dex-P) was purchased from Spectrum Chemical Mfg. Corp, New Brunswick, NJ and dexamethasone (Dex) (≥98%, powder) was purchased from Sigma-Aldrich Co., St. Louis, MO. Lipids (DSPC (1,2-distearoyl-sn-glycero-3-phosphatidylcholine, >99% purity), DPPC (1,2-dipalmitoyl-*sn*-glycero-3-phosphocholine, >99% purity), DMPC (1,2-dimyristoyl-*sn*-glycero-3-phosphocholine, >99% purity), m-PEG DSPE (1,2-distearoyl-sn-glycero-3-phosphoethanolamine-N-[methoxy (polyethylene glycol)-2000]), m-PEG DPPE (1,2-dipalmitoyl-*sn*-glycero-3-phosphoethanolamine-N-[methoxy(polyethylene glycol)-2000]) and m-PEG DMPE (1,2-dimyristoyl-*sn*-glycero-3-phosphoethanolamine-N-[methoxy(polyethylene glycol)-2000])) were purchased as powders from Avanti Polar Lipids (Alabaster, AL). Dialysis tubes (Float-A-Lyzer®, MWCO: 100 kD) were purchased from Spectrum Laboratories (Rancho Dominguez, CA). HPLC grade solvents and other chemicals were purchased from Fisher Scientific (Florence, KY).

Determination of ionization constant

The second ionization constant of Dex-P was determined at room temperature by the pH-titration method. Dexamethasone sodium phosphate USP (Dex-P) solution (4 ml) at about 4 mM in deionized water was titrated with 8 mM HCl solution under continuous stirring and pH was monitored after each addition. Plots of pH versus volume of titrant added were fitted to the following implicit equation.

$$H^+ + \frac{C_{drug} V_o\, P}{V_o + V_a} = \frac{C_{HCl}\, V_a}{V_o + V_a} + \frac{K_w}{H^+} + \frac{K_{a2}}{K_{a2} + H^+} \frac{C_{drug} V_o\, P}{V_o + V_a} \qquad (6.1)$$

where V_o is the initial volume of Dex-P solution and V_o is the volume at each titration point. K_w is the ion product of water and K_a is the second ionization constant of Dex-P. P is the purity of the drug. The data was also analyzed by plotting the change in pH/ml of acid added Vs volume of titrant added.

Determination of Critical Aggregation Concentration (CAC)

Fluorescence Method

CAC of dexamethasone sodium phosphate USP (Dex-P) was determined by the fluorescence method using pyrene (Sigma) as a probe molecule and a Varian Cary Eclipse spectrofluorometer with a 10 mm path length quartz cuvette. Excitation was at a wavelength of 335 nm and the emission spectrum was recorded from 350-500 nm. The excitation slid width was maintained at 5 nm and emission slit width at 1.5 nm, at a slow setting. Pyrene was dissolved in acetone to give 0.1mg/ml concentration, 65-100µl of this solution was added to blank test tubes and acetone was then evaporated under nitrogen. To these test tubes, 2 ml of different concentrations (0-85 mM) of Dex-P solution was added and vortexed. Data were acquired using Cary Eclipse software from Varian at 25°C.

Solubility Method

Dexamethasone sodium phosphate USP (Dex-P) solutions were made from 0.01-0.5M concentration range. Excess Dex was added to each solution and equilibrated at 25°C for 48 hours. After equilibration, the suspensions were filtered using 13 mm 0.45µ PVDF syringe filters (Fisherbrand) and the first 10 drops were discarded to minimize possible effects of filter adsorption. Successive 10 drop fractions were collected and compared to ensure that filter adsorption had no effect on the results. The filtrates were diluted with mobile phase (32:68 acetonitrile:aqueous buffer containing 2% triethylamine acetate) before analysis by HPLC.

Liposome Preparation

Dex-P loaded liposomes for transport experiments were prepared based on a previously reported method (127). Briefly, DMPC: mPEG DMPE, DPPC: mPEG DPPE or DSPC: mPEG-DSPE (95:5 mol%, 80 mg) were separately dissolved in about 2 ml of chloroform. The solvent was evaporated under a stream of nitrogen and the resulting film was dried overnight in a vacuum oven. The lipid film (DMPC, DPPC and DSPC) was hydrated with 2 ml of buffer (50 mM glycine buffer at pH 2 or 50 mM citrate buffers at pH 3, 4, 5 and 6)) containing dexamethasone sodium phosphate (Dex-P) (2-3 mM) to give a lipid concentration of 40 mg/ml. The pH of the drug solutions were adjusted back to the desired pH after Dex-P addition before hydrating the lipid films. After alternate vortexing and heating in a water bath at a temperature above the phase transition temperature of the respective lipids to uniformly suspend the lipid, the suspension was extruded 10 times through two stacked 100 nm polycarbonate membranes using an extruder at 30°C, 50°C and 60°C for DMPC, DPPC and DSPC, respectively, to obtain unilamellar liposomes

(141). Liposomes were allowed to cool to room temperature for 3 hours and used for release studies. Particle sizes of Dex-P loaded liposomes were measured at 25°C by dynamic light scattering (DLS) using a Delsa™ Nano submicron particle size analyzer (Beckman Coulter Inc., Brea, CA). The liposomes were diluted in the same buffer as that used in their preparation.

Determination of Liposomal Drug Release Kinetics

Dex-P loaded liposomes were separated from free drug by passing through a Sephadex® G25 column pre-equilibrated in the same buffer as that used in the preparation of liposomes. Drug loaded liposome suspensions (0.1-0.5 ml) were added to the Sephadex column, eluted with 2-5 ml of buffer, and eluting fractions were analyzed for drug and lipid concentration.

The liposome containing eluent fractions were diluted in the same buffer (if needed), introduced into a dialysis tube (Float-a-lyzer, MWCO (Molecular Weight Cut Off) 100 kD, Spectrum Laboratories), immersed into a 1000 ml of aqueous reservoir (sink conditions) containing the same pH buffer as that used for the liposome preparation and dialyzed at 37°C. Since some of the release studies were monitored for several days, 0.05% sodium azide was added to the buffers to inhibit microbial growth. Total drug concentration in the tube was monitored versus time by HPLC by withdrawing 50-100 µl samples from inside the dialysis tube at various time points and diluting with an appropriate volume of methanol. The kinetics of disappearance of free Dex-P from solution (800 µM) from the dialysis tube was also studied in a similar fashion.

HPLC Analysis of Dex and Dex-P

Samples from solubility studies (for pKa_2 determination) and liposome release studies were analyzed using an isocratic HPLC method with UV detection. A Waters Alliance 2695 Separations Module coupled to a UV detector (Waters 996, Photodiode Array Detector) was employed with wavelength of maximum absorption at 240 nm. A Waters Symmetry® C18 column (5 µm, 3.9 X 150 mm) and guard column (3.9 X 20 mm) were used with a mobile phase composition of 32% acetonitrile and 68% (v/v) pH 5.5 triethylamine acetate (2%) buffer. The retention times at an injection volume of 10 µl and a flow rate of 1 ml/min were about 2.3 and 6.4 min for Dex-P and Dex, respectively. Four independent standards for Dex-P (100-800 µM) in water and Dex (100-800 µM) in methanol were prepared. The relative standard deviation for the response factor was less than 3%.

Lipid Analysis

Lipids were analyzed using HPLC and ELSD (Evaporative Light Scattering Detector) as reported previously (126). Briefly, separation was done using an Allsphere™ silica column (Grace Davison Discovery Sciences, Deerfield, IL) (5 µ, 4.6X150 mm) with a guard column (Allsphere silica, 5µ, 7.5 X 4.6mm). A linear gradient method was used; mobile phase A was 80% chloroform: 19.5% methanol: 0.5% (v/v) ammonium hydroxide solution (28-30%) and mobile phase B consisted of 80% methanol: 19.5% water and 0.5% (v/v) ammonium hydroxide. Each run began with 100% (v/v) mobile phase A, changing to 80% mobile phase A: 20% mobile phase B at 3 min, maintaining the composition (80%A: 20%B) until 7 min and changing back to 100% mobile phase A at 14 min. The total run time was 15 min at a flow rate of 1 ml/min with the following

ELSD settings: gain, 8; pressure, 3.4 bar; and temperature, 40°C. The sample compartment temperature was maintained at 4°C and the column was at ambient temperature. Standards were in mobile phase A and log-log plots of peak area versus concentration were linear. Aliquots of drug loaded liposomes (10-20 µl) for lipid analysis were transferred to test tubes, dried under nitrogen, and stored at -20°C until further analysis. For analysis, the dried lipid films were re-constituted in mobile phase A. Lipid concentration was evaluated versus time during the course of transport studies in representative DPPC liposomes at various pH values.

DATA ANALYSES

Equilibrium pH-Permeability Model

Dex-P is n amphiphilic, ionizable drug that can exist as three different species depending on the pH (Figure 6.1). A mathematical model to explain the pH dependent permeability of a solute across the liposome and its evaluation by dynamic dialysis method was developed in chapter five and in previous publications from this laboratory (126, 132). A similar model with some modifications has been adopted and explained here. The model takes into account the ionization, membrane binding, and transport of possible permeable species. Instantaneous equilibrium between the various species is assumed both within and outside the liposomes. The model considers the internal and external volume in the liposomal suspension along with the volume occupied by the aqueous (inner and outer) and membrane phases (inner and outer leaflets of the bilayer), the membrane/water partition coefficients of the various drug species and the fractions bound inside and outside the liposomes. The kinetics of release of the encapsulated drug from the liposomes and the transport of free drug across the dialysis membrane into a sufficiently

large volume of dialysate to ensure sink conditions in the reservoir are incorporated into the rate equations. Samples taken from inside the dialysis tube at various time points were analyzed for the total Dex-P remaining.

Two types of models were considered in the pH-permeability studies of Dex-P (Figure 6.2). The membrane-water partition coefficient of the monoanionic species was found to be either small (DMPC) or negligible (DPPC and DSPC) in the lipid systems used for release studies (Chapter three). Therefore, initially, the following mathematical model (Model I) that ignored binding of the drug to the liposomal membrane was employed.

Model I

$$I_i^t = I_i + II_i + III_i \qquad (6.2)$$

$$I_i^t = I_i \left(1 + \frac{K_{a1}}{H_i} + \frac{K_{a1}K_{a2}}{H_i^2}\right) \qquad (6.3)$$

$$I_i = \frac{I_i^t}{1 + \frac{K_{a1}}{H_i} + \frac{K_{a1}K_{a2}}{H_i^2}} \qquad (6.4)$$

Similarly,

$$I_o = \frac{I_o^t}{1 + \frac{K_{a1}}{H_o} + \frac{K_{a1}K_{a2}}{H_o^2}} \qquad (6.5)$$

$$\frac{d(I_t^i)}{dt} = -k_m^a(I_i - I_o) - k_m^b(II_i - II_o) - k_m^c(III_i - III_o) \qquad (6.6)$$

$$\frac{d(I_t^o)}{dt} = \frac{k_m^a}{x}(I_i - I_o) + \frac{k_m^b}{x}(II_i - II_o) + \frac{k_m^c}{x}(III_i - III_o) - (k_{on} + k_d)I_t^o + \frac{k_{on}}{K}D_m \qquad (6.7)$$

$$\frac{d(D_m)}{dt} = k_{on}\alpha_o D_o - \frac{k_{on}}{K}D_m \qquad (6.8)$$

where, I_t^i and I_t^o are the total intravesicular and extravesicular drug concentrations (in molar); k_m and k_d are the rate constants for drug transport across the lipid bilayer and dialysis membrane, respectively, and x is the ratio of extravesicular to intravesicular volume in the dialysis tube. I_i, II_i, III_i and I_o, II_o, III_o are the intravesicular and extravesicular neutral, monoanion and dianion concentrations, respectively. D_m is the drug concentration bound to the dialysis membrane; k_{on} and k_{off} are the association and dissociation constants for binding of drug to the dialysis membrane $\left(K = k_{on}/k_{off}\right)$.

Model II

Model I was inadequate for explaining the release data obtained in DPPC and DSPC liposomes for Dex-P. As a result, a more elaborate model (Model II) that took into account the binding of different species to the liposome membrane was considered.

$$I_i^t = \frac{I_i^w + II_i^w + III_i^w}{a} + \frac{I_i^m + II_i^m + III_i^m}{b} \qquad (6.9)$$

$$I_i^t = \frac{I_i^w(1 + \frac{K_{a1}^w}{H_i} + \frac{K_{a1}^w K_{a2}^w}{H_i^2})}{a} + \frac{I_i^w(K_{p1} + \frac{K_{p2}K_{a1}^w}{H_i} + \frac{K_{p3}K_{a1}^w K_{a2}^w}{H_i^2})}{b} \qquad (6.10)$$

$$Let\ \frac{I_i^w(1 + \frac{K_{a1}^w}{H_i} + \frac{K_{a1}^w K_{a2}^w}{H_i^2})}{a} = a_i\ , \frac{I_i^w(K_{p1} + \frac{K_{p2}K_{a1}^w}{H_i} + \frac{K_{p3}K_{a1}^w K_{a2}^w}{H_i^2})}{b} = b_i, \frac{1}{a_i + b_i}$$

$$= ubi,$$

$$I_i^w = ubi\ I_i^t \qquad (6.11)$$

$$II_i^w = ubi\ I_i^t\ \frac{K_{a1}^w}{H_i} and\ III_i^w = ubi\ I_i^t\ \frac{K_{a1}^w K_{a2}^w}{H_i^2}$$

where a and b are volume ratios to account for the differences in aqueous and membrane volumes with respect to the total intravesicular volume

Similarly,

$$I_o^w = ubo\ I_o^t \qquad (6.12)$$

$$II_o^w = ubo\ I_o^t\ \frac{K_{a1}^w}{H_o} and\ III_o^w = ubo\ I_o^t\ \frac{K_{a1}^w K_{a2}^w}{H_o^2}$$

$$Let\ \frac{I_o^w\left(1 + \frac{K_{a1}^w}{H_o} + \frac{K_{a1}^w K_{a2}^w}{H_o^2}\right)}{c} = a_o, \frac{I_o^w\left(K_{p1} + \frac{K_{p2}K_{a1}^w}{H_o} + \frac{K_{p3}K_{a1}^w K_{a2}^w}{H_o^2}\right)}{d} = b_o,$$

$$\frac{1}{a_o + b_o} = ubo$$

where K_a^w and K_{a2}^w are the ionization constants of Dex-P in the aqueous phase and K_{p1}, K_{p2}, K_{p3} are the membrane/water partition coefficients of the neutral, monoanion and dianion, respectively.

$$\frac{d(I_t^i)}{dt} = -k_m^a(I_i^w - I_o^w) - k_m^b(II_i^w - II_o^w) - k_m^c(III_i^w - III_o^w) \qquad (6.13)$$

$$\frac{d(I_t^o)}{dt} = \frac{k_m^a}{x}(I_i^w - I_o^w) + \frac{k_m^b}{x}(II_i^w - II_o^w) + \frac{k_m^c}{x}(III_i^w - III_o^w) - (k_{on} + k_d)\ I_t^o + \frac{k_{on}}{K} D_m \qquad (6.14)$$

$$\frac{d(D_m)}{dt} = k_{on}\alpha_o D_o - \frac{k_{on}}{K} D_m \qquad (6.15)$$

where I_i^w, II_i^w, III_i^w are the unbound aqueous intravesicular neutral, monoanion, and dianion concentrations, respectively, while I_o^w, II_o^w, III_o^w are the unbound aqueous extravesicular neutral, monoanion, and dianion concentrations, respectively. In the present study, the pH was assumed to remain constant and not change due to ionization of the drug because the buffer concentration (50 mM) was about 1000-fold higher than the drug concentration (40-60 μM).

The apparent permeability at each pH can be expressed as:

$$P_{app} = P_I f_{ub}^I + P_{II} f_{ub}^{II} + P_{III} f_{ub}^{III} \qquad (6.16)$$

where P_I, P_{II} and P_{III} represent the permeability coefficients of the unionized, monoanion and dianion Dex-P with f_{ub} representing the fraction unbound for each species. The dianion was assumed to be membrane impermeable (P_{III}=0). Substituting the terms for the fraction unbound of the unionized and monoanionic species from Eq. 6.11, the apparent permeability coefficient of Dex-P can be expressed as:

$$P_{app} = P_I \frac{1}{a_i + b_i} + P_{II} \frac{K_{a1}^w}{H_i} \frac{1}{a_i + b_i} \qquad (6.17)$$

$$(\frac{1}{a_i + b_i} = ubi = f_{ub}^I)$$

Bilayer Free Surface Area-Permeability model

Historically, passive permeability through lipid bilayers has been described by the "bulk solubility diffusion" model that assumes the membrane to be homogenous and isotropic, resembling a bulk hydrocarbon solvent. According to this model, permeability is given as:

$$P_o = \frac{K_{m/w}\, D_m}{h_m} \qquad (6.18)$$

where P_o is the permeability coefficient, $K_{m/w}$ and D_m are the membrane/water partition coefficient and diffusion coefficient across the membrane, respectively, and h_m is the membrane thickness. However, unlike bulk solvents, lipid bilayers are heterogeneous, interfacial and anisotropic systems. The lipid bilayer can be roughly divided into three regions: an ordered, polar interfacial head group region, a highly ordered hydrocarbon chain region and a relatively disordered hydrocarbon chain region towards the center of the bilayer (189). As permeant moves across the bilayer, it encounters variations in the barrier environment. For very small polar molecules the transport is primarily governed by a distinct region within the bilayer interior (i.e. the highly ordered chain region).

Solubility diffusion theory fails to account for the effects of lipid bilayer chain order on the permeability coefficient of a permeant. Xiang and Anderson have addressed this issue by introducing a scaling factor that must be applied to permeability prediction from solubility-diffusion theory. The permeability coefficient for small molecules, according to this new "barrier-domain" solubility diffusion model is

$$P_m = \frac{K_{barrier/water} * D_{barrier}}{h_{barrier}} = f * P_o \qquad (6.19)$$

where $K_{barrier/water}$ and $D_{barrier}$ are the partition coefficients from water into and diffusion coefficient of the permeant within the barrier domain, respectively, and $h_{barrier}$ is the barrier thickness. Thus, P_m is the product of P_o from solubility-diffusion theory and a scaling factor f, the permeability decrement due to chain ordering effects (61, 131).

The permeability decrement factor, f can be defined in terms of the two-dimensional packing structure of the bilayer, as characterized by the free surface area per lipid molecule, a_f, and cross-sectional area of the permeant, a_s, as follows (61, 131):

$$f = f_o exp\left(-\lambda\, a_s/a_f\right) \qquad (6.20)$$

where f_o and λ are constants independent of permeant size and bilayer packing structure. Thus, the scaling factor that accounts for the decrease in permeability due to chain ordering is exponentially dependent on the ratio of permeant size to the free surface area of the membrane. It was proposed that non-spherical solutes orient their long axes along the bilayer normal and the permeation across the bilayer occurs with the creation of a free volume with a cross-sectional area equal to or greater than the minimum cross-sectional area of the diffusing permeant. Alternative models have employed a power law in permeant volume instead of the minimum cross-sectional surface area to rationalize the molecular size dependence of membrane permeability (131, 239). Mitragotri et al. also

analyzed the size selectivity of solute permeability in lipid bilayers using scaled-particle theory. They evaluated the relative contributions of both partitioning and diffusion processes across the ordered chain region and suggested the dependence of each on the solute size and bilayer parameters (168).

RESULTS

Dex-P and Liposome Characterization

The state of ionization is important for rationalizing the pH dependent liposome permeability of Dex-P. The accurate determination of pKa values less than about 2 by the potentiometric method is challenging. However, Derendorf et al. calculated a pKa_1 of 1.9 by studying the partition coefficient of Dex-P as a function of pH. This value was therefore assumed in the present study. The value of pKa_2 of Dex-P, as determined by pH-titration method and fitting the data to Eq. 6.1, was 6.27 ± 0.13 (Figure 6.5), which is in good agreement with the reported value of 6.4 (133). Although the experimental determination of pKa2 was performed at room temperature, the temperature sensitivity for phosphate pKa values is known to be insignificant where d(pKa)/dT for pKa_1 is about 0.0044 and for pKa_2, it is -0.0028 (240, 241). This suggests a change in pKa_1 of 0.05 and pKa_2 of -0.03 units with change in temperature from 25 to 37°C (240, 241).

Figure 6.3 shows the change in fluorescence emission spectra of pyrene (excitation at 335 nm) in increasing concentrations of Dex-P solution (0-84 mM). The ratio of the first vibrational band (372 nm), the highest energy vibrational band, to that of the vibrational band at 383 nm is considered to be an index of polarity of its environment. In water the ratio (I1/I3) is around 1.6-1.8, in ethanol about 1.1, and in hydrocarbon solvents around 0.57-0.61. Left inset shows the ratio of I1/I3 of pyrene as a function of Dex-P

concentration. In the presence of micelle forming systems at concentrations below the CMC, the intensity of the highest energy vibrational band normalized against the intensity of third peak decreases. There was a sharp breakpoint at the CAC (34 mM) and above the CAC the ratio was constant. As an additional confirmation of CAC values, the intensity of the excimer peak (at 475 nm) relative to first peak (IE/I1) was plotted against the Dex-P concentration and was observed to show a peak at CAC concentration (Figure 6.3 right inset).

The critical aggregation concentration (CAC) of Dex-P determination, by solubility method (Figure 6.4) gave an apparent value of ~120 mM with no sharp deflection point observed in the solubility curve. The inset of Figure 6.4 shows the rise in solubility of Dex even at lower concentrations of Dex-P (<50 mM) suggesting smaller aggregate (dimer, trimer etc.) formations prior to true aggregation.

Dex-P loaded liposomes of DMPC, DPPC and DSPC prepared at different pH values exhibited particle sizes in the range of 87-102 nm, with polydispersity indices in the range of 0.06-0.09, indicating monodisperse formulations. The drug and lipid concentrations during release studies at different pH values were determined using previously developed and validated HPLC methods. For the analysis of Dex-P, samples were taken from inside the dialysis tube at various time points, diluted with methanol and analyzed for both, Dex-P and its hydrolytic product, Dex. There was no degradation of Dex-P observed during the time period of transport studies at any pH. Based on the literature,, the half-life Dex-P at pH 4.06 and 70°C is about 4.6 days (242). Flynn and Lamb studied solvolysis of several corticosteroid phosphates and found that the nature of the steroid nucleus has little effect on the monoanion hydrolysis rate constant. They

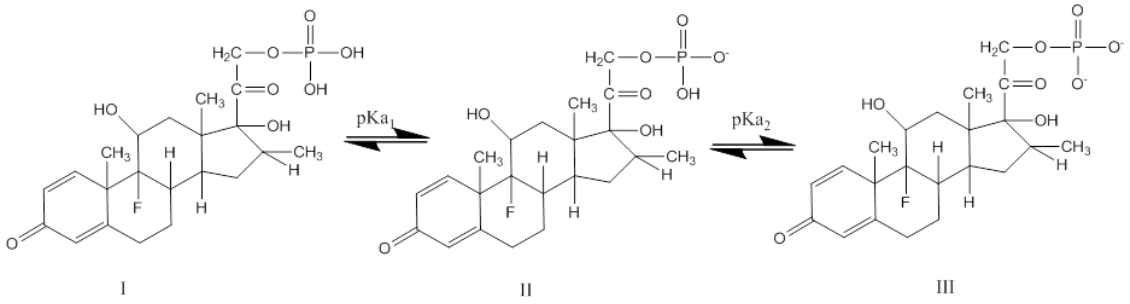

Figure 6.1 Equilibria between neutral, unionized Dex-P (I), its monoanion (II) and dianion (III). pKa1 and pKa2 are the first and second ionization constants, respectively.

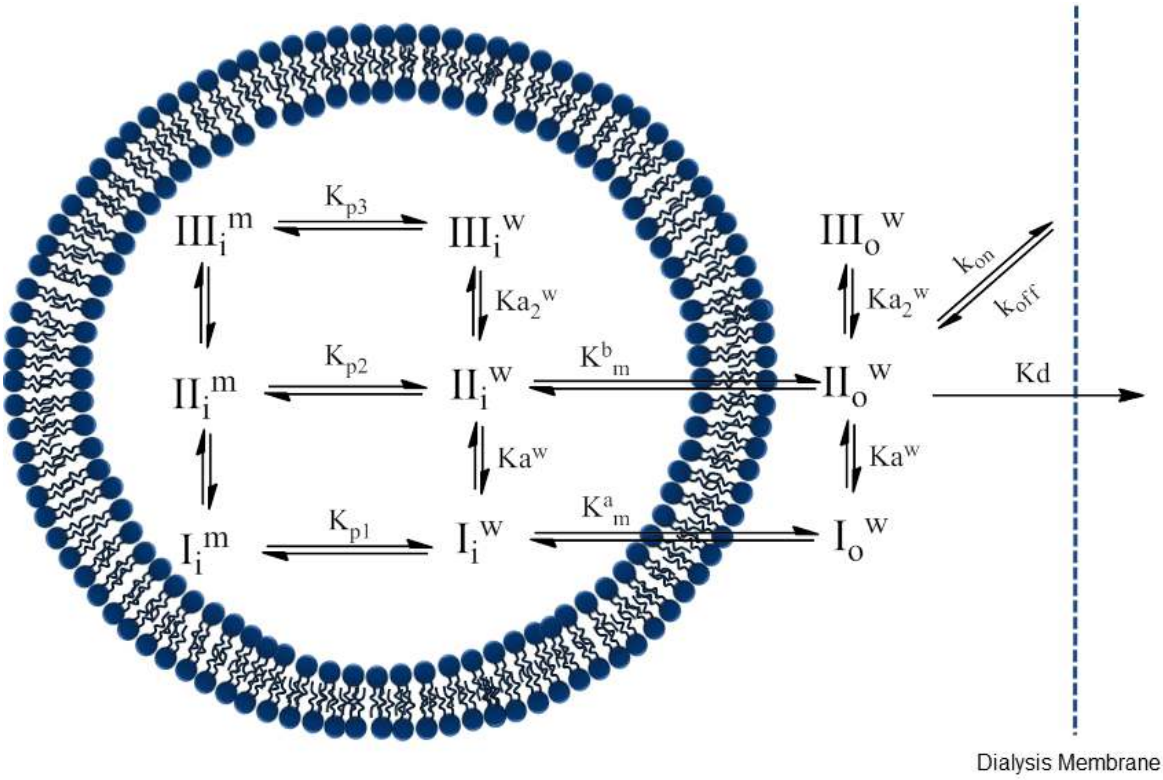

Figure 6.2 The pH-permeability model considered to explain Dex-P liposomal release profiles at different pH values determined by dynamic dialysis (model II).

I, II and III refer to the unionized, monoanion and dianion concentrations of Dex-P, respectively. Subscripts *i* and *o* refer to the intravesicular and extravesicular compartments. Superscripts *m* and *w* refer to the membrane and aqueous phases. The binding parameters (K_{p1}, K_{p2} and K_{p3}) were assumed to be negligible in model I.

suggested that stability data for methylprednisolone-21-phosphate could be considered to be representative of related steroid phosphates as well (242). Therefore, using the activation energy reported for methylprednisolone-21-phosphate, the half-life for hydrolysis of Dex-P at pH 3.32 and 37°C should be about 347 days, well beyond the time frame of the present studies.

The lipid concentration in the dialysis tube during the transport studies was in the range of 0.6-2.0 mg/ml. Shown in Figure 6.9 are DPPC concentration versus time profiles during transport studies at pH 2, 3, 4, 5 and 6. Table 6.2 shows the parameters from regression analysis at each pH along with 95% C.I for slope and intercept. The % coefficient of variation for the determination of initial value (t=0) was 8-20% and the slope was not significantly different from zero ($P>0.05$). Therefore, the total concentration of lipid remained constant during the release studies. Additionally, previous studies on stability of saturated phosphatidylcholines (DSPC and natural soybean PC) have shown that the half-life of degradation is greater than 3 months at pH 9 and 40°C and more than 2 months for DMPC at pH 4 and 30°C (142, 143, 243, 244). Although in the same order of magnitude, a small increase in hydrolysis rate constant (K_{obs}) from 3.2 x 10^{-4} hr^{-1} to 4.7 x 10^{-4} hr^{-1} was reported with increase in fatty acid chain length of liposomes from C_{12} (DLPC) to C_{18} (DSPC) at pH 4 and 30 °C (245, 246).

The membrane water partition coefficient of Dex-P monoanion was previously determined by equilibrium dialysis for DMPC, DPPC and DSPC liposomes (pH 4) to be 62 ± 8, 2 ± 4 , 6 ± 2, respectively. In addition, the study of Dex-P binding at different pH values in DMPC liposomes showed significant binding of the neutral form (241 ± 38) relative to the ionized species.

Kinetics of Drug Release from Liposomes at Different pH

The kinetics of free drug disappearance from dialysis tubes (100 kD) that were used in the pH-permeability studies was evaluated. Previous dynamic dialysis studies for release of Dex from liposomes indicated free drug binding to the dialysis membrane. Therefore, the kinetics of free Dex-P disappearance from aqueous solutions during dynamic dialysis was evaluated for a sufficient time to capture the effect of binding to the dialysis membrane, if present. Figure 6.6 indicates that a biphasic profile was observed for Dex-P disappearance from solution very similar to that observed for Dex. The similarity in the biphasic profiles for free Dex and Dex-P despite the differences in their physicochemical properties suggests membrane binding rather than partitioning into the membrane. The rate and equilibrium constants obtained from the fitting of free drug profiles were used in modeling the transport of Dex-P from liposomes.

The concentration versus time profiles for the release of Dex-P from DPPC and DSPC liposomes at different pH values are shown in Figure 6.7. Concentration versus time profiles for Dex-P release from drug loaded liposomes at all pH values (pH 2, 3, 4, 5 and 6) were simultaneously fit to equations 6-8 (Model I) to obtain the rate constants for permeation of the neutral and monoanionic species (with the assumption that the di-anion is impermeable) and the apparent pKa_1 of Dex-P. The second ionization constant was fixed because all the pH values explored were below pKa_2. The values of pKa_1 obtained from the simultaneous fitting of the pH dependent transport data across DPPC and DSPC were 2.8 (95% CI of 2.6-3.3) and 3.4 (95% CI of 3.3-3.6), respectively.

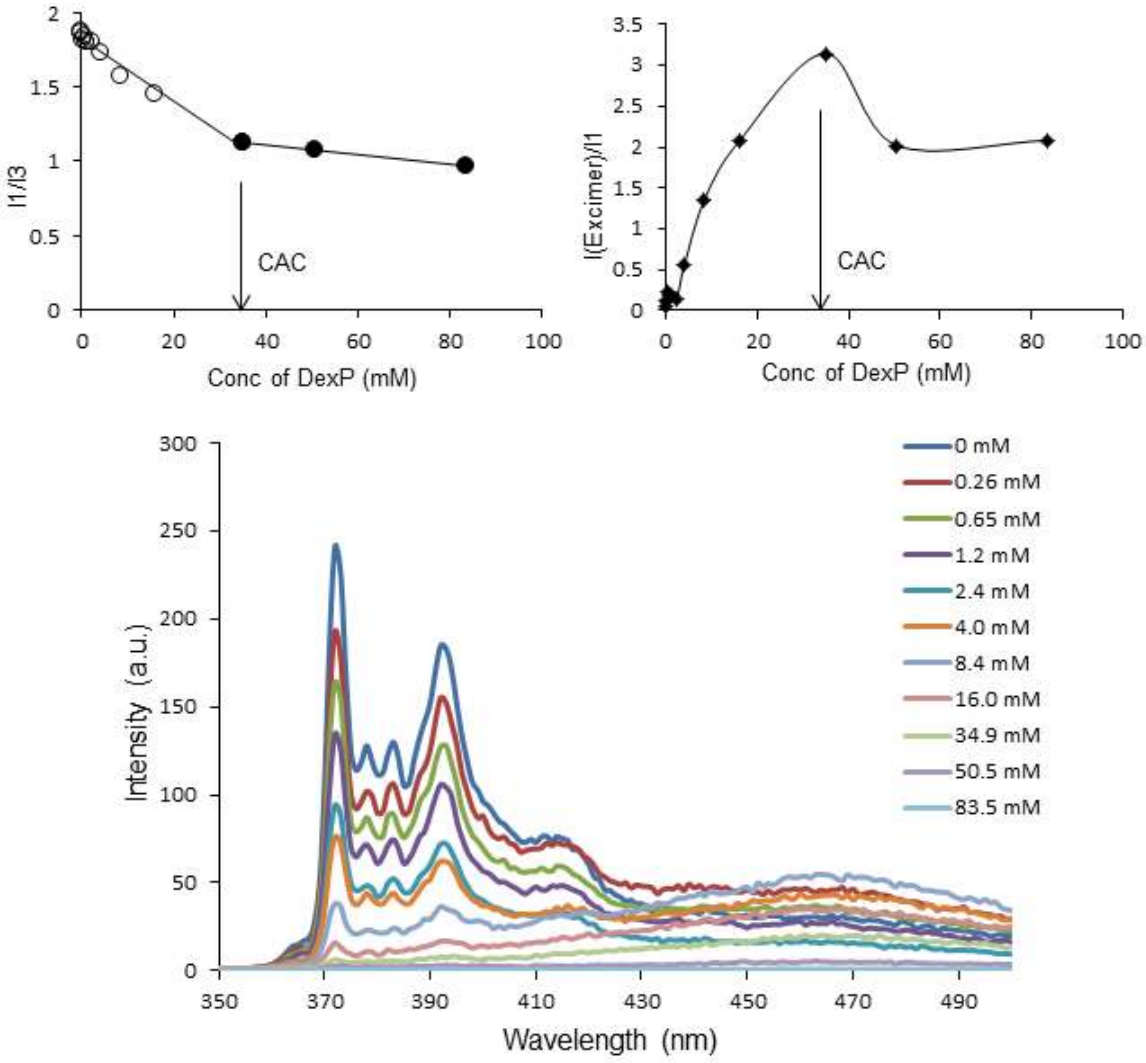

Figure 6.3 Fluorescence spectra of pyrene recorded at increasing concentrations of Dex-P and the corresponding decrease in peak intensity at 372 and 383 nm The inset shows the breakpoint when the ratio of the I1/I3 is plotted against the Dex-P concentration and a peak when the ratio of excimer peak (475 nm) relative to first peak is plotted against the Dex-P concentration.

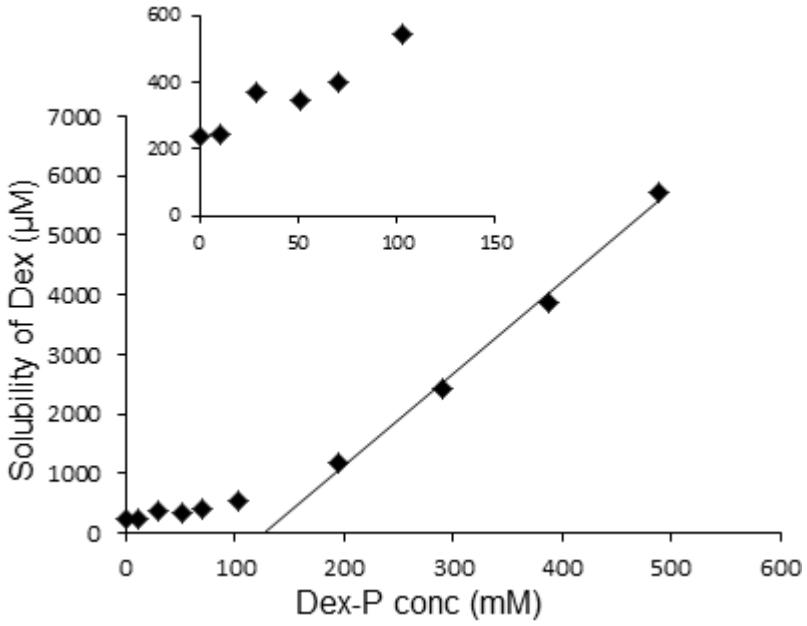

Figure 6.4 Solubility of Dex with increasing concentrations of Dex-P at 25°C. The inset shows the magnified view of the region between 0-100 mM Dex-P.

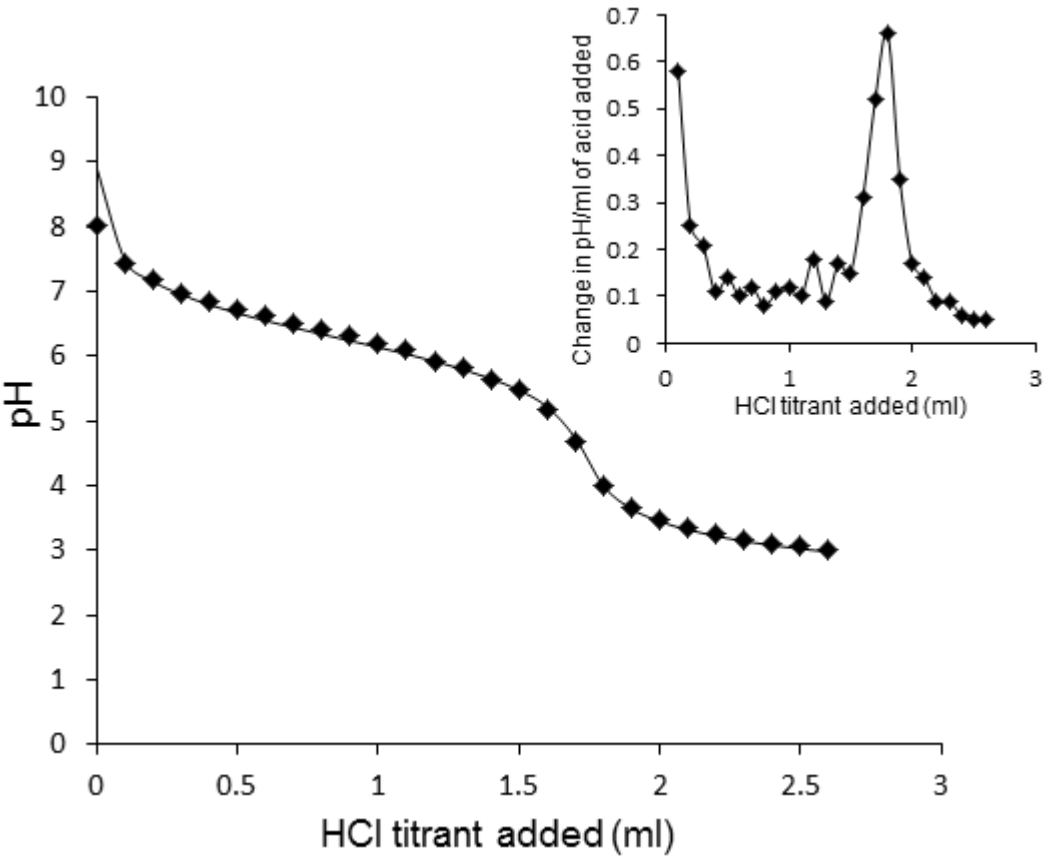

Figure 6.5 Change in pH of a 4 mM Dex-P solution on addition of HCl titrant. The data points are the experimental recording while the solid line is the model predictions on solving Eq. 6.1. Inset shows the ratio of the change in pH per ml of acid against the volume of HCl and the peak in the plot corresponds to the half-equivalence point.

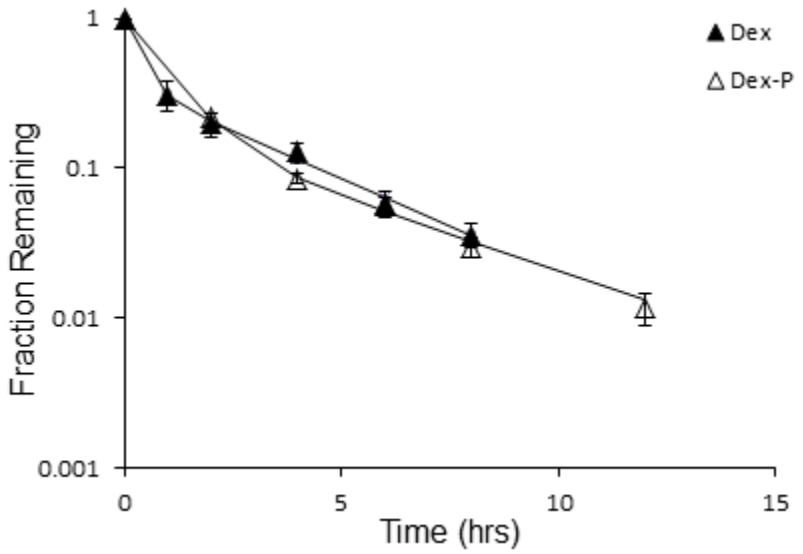

Figure 6.6 Fractions of initial amount of Dex-P in solution remaining in the dialysis tube with time. Error bars are the standard deviations from the replicate experiments (n=3). The kinetics of free Dex is also shown for comparison.

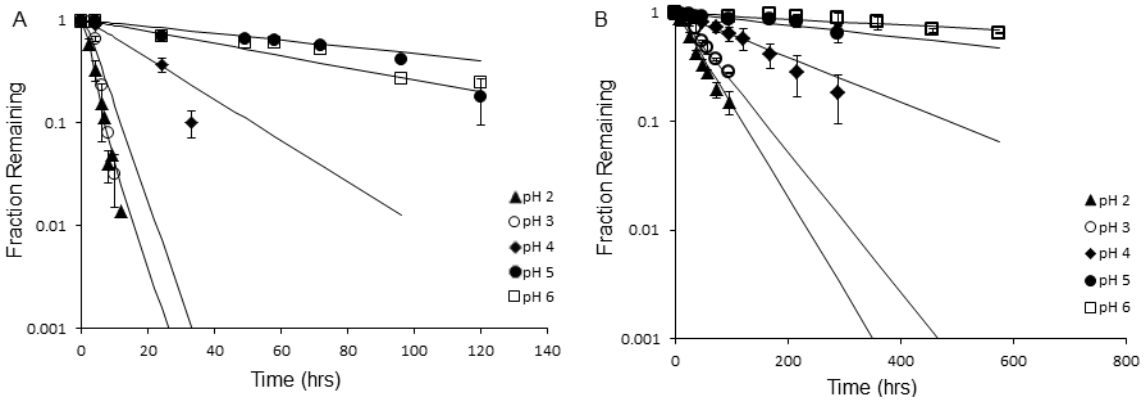

Figure 6.7 Fraction of Dex-P remaining (mean ± S.D) in dialysis tubes containing Dex-P loaded liposomes at pH values of 2, 3, 4, 5 and 6. Solid lines are simultaneous fits based on the equilibrium pH-permeability model (Eqs. 6.13-6.15). Error bars are the standard deviations from the replicate (n=2) experiments (A) DPPC (B) DSPC.

The apparent permeability constants (calculated from apparent first order rate constants) at each pH from transport data across DPPC and DSPC liposomes were plotted versus pH. The pH-permeability profiles of Dex-P from DPPC and DSPC liposomes shown in the log-linear plot in Figure 6.8 indicate an upward shift in first pKa, from 1.9 to 2.8 in DPPC and to 3.4 in DSPC liposomes.

Since previous studies on membrane binding of Dex-P in DMPC liposomes indicated significant binding of the neutral form, inclusion of a term for neutral species binding to account for the apparent shift in pKa was considered. Model II including a binding parameter was used to simultaneously fit the release data at different pH values with the first and second ionization constants fixed at 1.9 and 6.4, respectively. Rate constants for the transport of the neutral and monoanionic Dex-P species, k_m^a and k_m^b, in DPPC were 4.2 ± 1.8 and 9 ± 3 x 10^{-3} hr^{-1} (95% C.I.) while in DSPC the values were 0.54 ± 0.14 and 8 ± 2 x 10^{-4} hr^{-1}, respectively. The intrinsic permeability coefficients of the neutral Dex-P across DPPC and DSPC were calculated to be 1.74 (±0.74) x 10^{-9} cm/s and 2.24 (±0.59) x 10^{-10} cm/s (95% C.I.), respectively. The partition coefficients of the neutral form, obtained from the fitting were 42 ± 35 and 186 ± 68 (95% C.I.) in DPPC and DSPC respectively.

Quantitative Relationship between Permeability and Chain Ordering (Free Surface Area)

Transport data for Dex-P at pH 4 were available for unilamellar vesicles composed of DMPC, DPPC and DSPC, as shown in Figure 6.10. The apparent half-lives obtained were 1.2, 10.8 and 169 hours, respectively. These lipids varied in their acyl chain length and bilayer chain density, which also brought about changes in phase structure (gel or

liquid crystalline phase). At 37°C, DMPC (Tm of 23°C) is in a disordered liquid-crystalline phase, DPPC is in a gel phase but very close to its phase transition temperature (T_m of 41°C) and DSPC is in the highly ordered gel phase (T_m of 55°C). The chain ordering can be quantified in terms of surface density or free surface area, as demonstrated earlier (122, 131). To test the dependence of apparent permeability of Dex-P on the order parameter, the log of apparent permeability was plotted versus the inverse of free surface area and a linear dependence was observed (Figure 6.11). A least-squares fit of the data gave a slope of -0.53 and correlation coefficient of 0.99.

Table 6.1 shows the observed half-lives for release obtained at various pH values and different liposome compositions. The experimental half-life for Dex-P release from liposomes ranged from 1.2 h at pH 4 in DMPC liposomes to 892 hours at pH 6 in DSPC liposomes. The broad range of release kinetics was obtained by modulation of two formulation variables in liposomes i.e. pH and lipid composition.

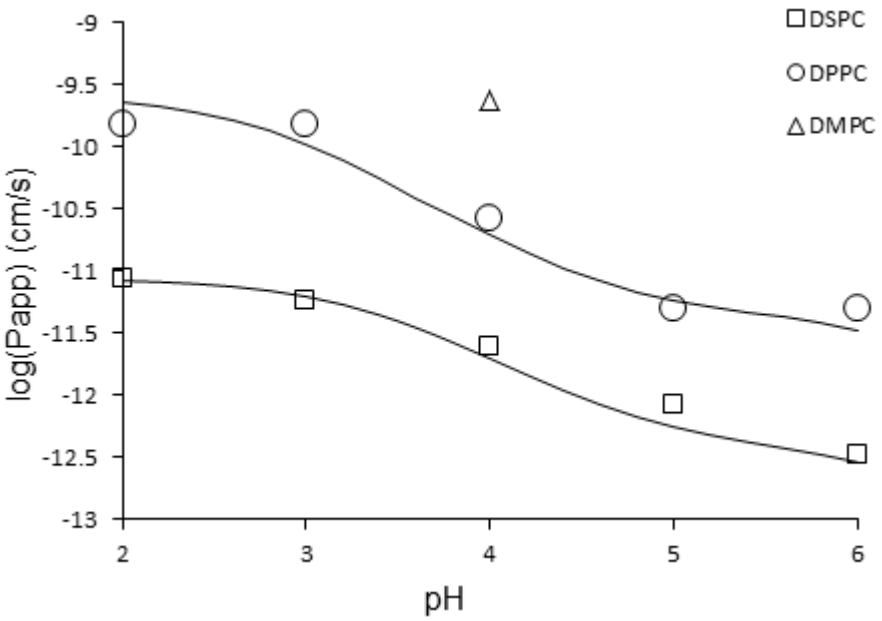

Figure 6.8 Log of apparent permeability of Dex-P vs pH across DMPC, DPPC and DSPC liposomes at 37°C. The solid lines for DPPC and DSPC represent the predicted values based on model II and Eq. 6.17.

Table 6.1 The half-life ($t_{1/2}$) for liposome retention of Dex-P as a function of liposome composition and intraliposomal pH

Liposome	**pH**	**Retention Half-life (hrs)***
DMPC	4	1.2 ± 0.05
DPPC	2	1.9 ± 0.1
DPPC	3	2.2 ± 0.3
DPPC	4	10.8 ± 2.3
DSPC	2	32 ± 2
DSPC	3	48 ± 3
DPPC	5	58 ± 9
DPPC	6	58 ± 5
DSPC	4	169 ± 6
DSPC	5	579 ± 82
DSPC	6	892 ± 78

*The values are mean ± Std. Dev.

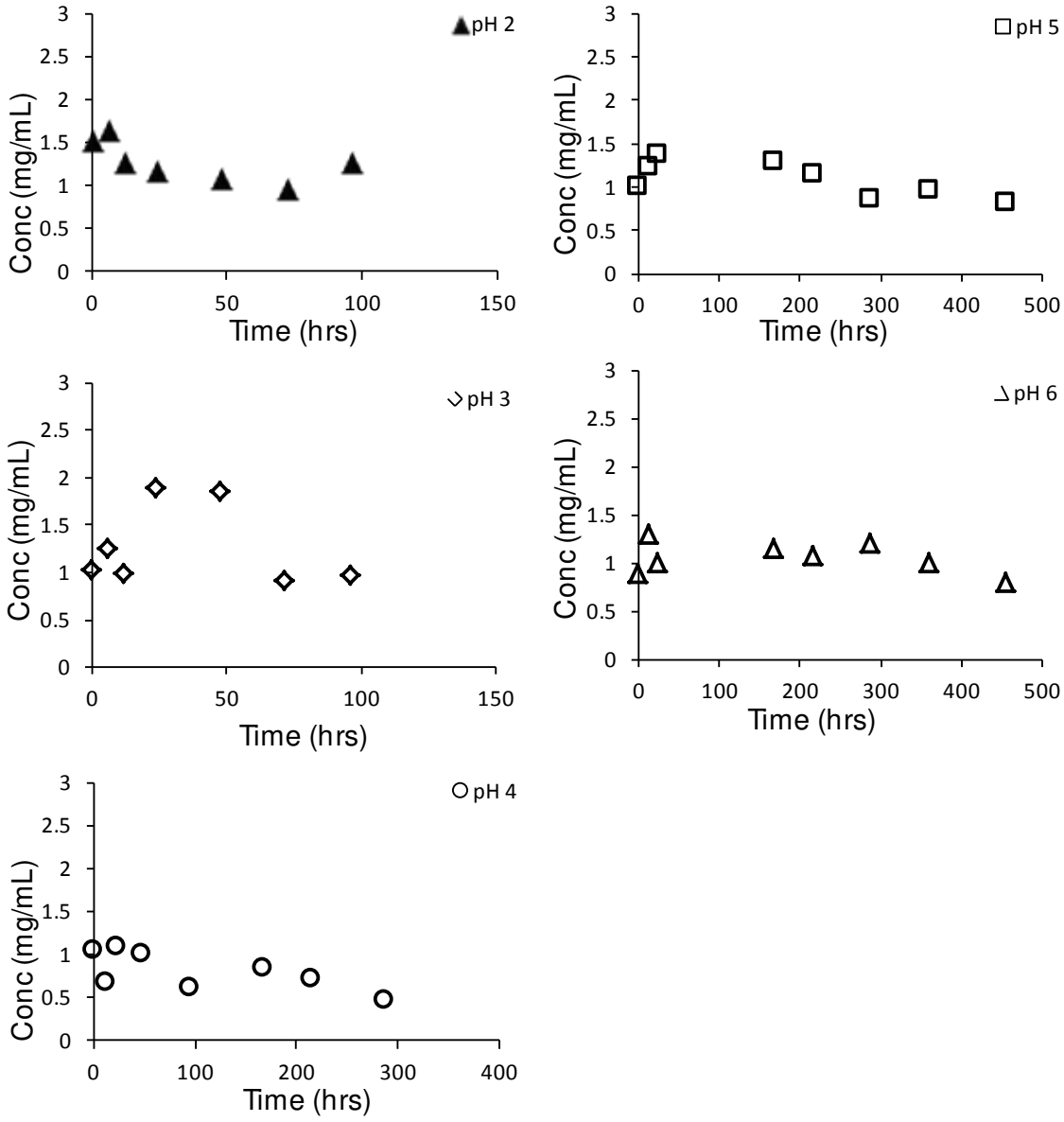

Figure 6.9 Concentration-time profiles for DPPC liposomes at pH 2, 3, 4, 5 and 6 during transport studies of Dex-P by dynamic dialysis.

Table 6.2 Regression analyses of lipid concentration Vs time data at different pH of release studies

pH	Slope (95% C.I)	Intercept (95% C.I.)	P value (Is slope significantly non-zero?)
2	-0.0041 (-0.0101 to 0.0019)	1.429 (1.131 to 1.726)	0.1368 (>0.05)
3	-0.0020 (-0.0153 to 0.0113)	1.338 (0.675 to 2.002)	0.7134 (>0.05)
4	-0.0015 (-0.0030 to 0.00005)	0.961 (0.739 to 1.184)	0.0566 (>0.05)
5	-0.0008 (-0.0017 to 0.00001)	1.245 (1.034 to 1.456)	0.0529 (>0.05)
6	-0.0003 (-0.0012 to 0.0006)	1.109 (0.8828 to 1.335)	0.4300 (>0.05)

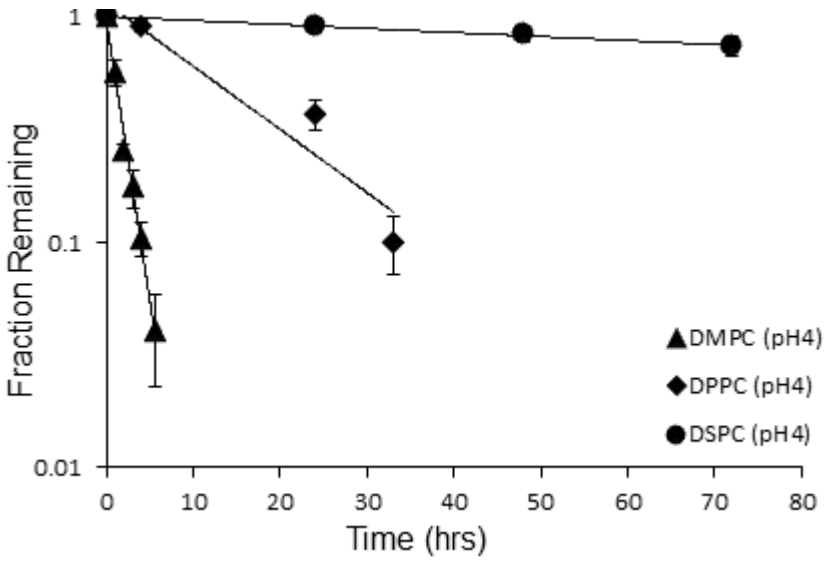

Figure 6.10 Fraction of Dex-P remaining in dialysis tube from DMPC, DPPC and DSPC liposomes at pH 4. Error bars are the standard deviations from replicate experiments (n=2).

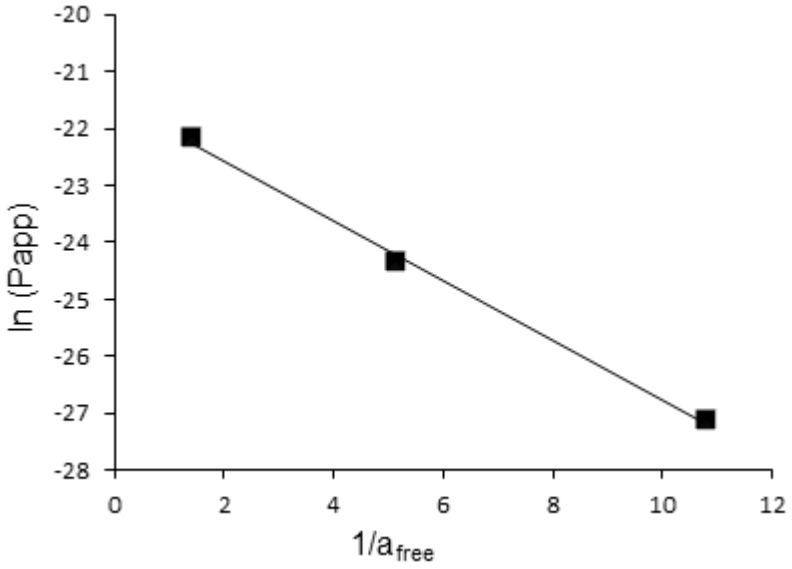

Figure 6.11 Dependence of the natural logarithm of apparent permeability of Dex-P on the inverse of free surface area of the liposome bilayer. Points represent permeability coefficients in DMPC, DPPC, and DSPC.

DISCUSSION

Liposomes hold the promise of enhancing the therapeutic index of drugs by reducing the toxicity and increasing drug efficacy (20). To accomplish the goal of selectively delivering the drug to the target site, the drug needs to remain entrapped inside the liposomes while the nanoparticles are circulating in the blood and then release once at the target site. Even at the site of action, drug release should ideally be optimized as per the therapeutic need. Therefore, there is a great need for the ability to tune the release kinetics of drugs from liposomes in response to the therapeutic requirement. Depending on the therapeutic need, half-lives ranging from a few hours to several days may be required. To meet this end, quantitative relationships that could provide predictive capability based on the drug and delivery vehicle properties would be highly desirable. Such a universal quantitative model would also greatly enhance mechanistic understanding of release kinetics from the delivery system. In this study, two simple liposomal formulation variables, pH and phospholipid chain length were explored to obtain a range of release kinetics. The mathematical modeling of the release data enables an understanding of the release kinetics under different conditions and the ability to design systems having a predetermined release rate.

CAC Determination

Hydrophobic solutes or compounds having a large surface area of exposed organic groups or aromatic rings have a tendency to self-associate in water at higher concentration. As opposed to molecules containing flexible chains that organize into typical micellar structures above a particular critical concentration, organic compounds containing rigid aromatic fused rings rather have a more diffuse concentration range

where they associate to a different extent (247, 248). Also, such molecules do not form the typical micellar structures but rather form aggregates due to stacking of the rigid aromatic rings. The critical concentration for aggregate formation is often referred to as Critical Aggregation Concentration (CAC) instead of Critical Micelle Concentration (CMC) (249).

Pyrene is a very common fluorescent probe used in the determination of CMC of amphiphiles owing to the dependence of its emission characteristics on the polarity of its environment (250). As the concentration of aggregate forming agent (Dex-P) increases, pyrene molecules experience a more hydrophobic environment than water due to premicellar aggregates and a lowering of the intensity ratio (I1/I3) is observed (Figure 6.3 inset, below CAC). Above the CAC, with increase in Dex-P concentration there is no increase in monomer concentration and the ratio of the pyrene intensity peaks (I1/I3) is constant due to incorporation of pyrene into the hydrophobic region of micelles or aggregates (250, 251).

Excited pyrene monomers form an excimer complex with a ground state pyrene monomer and show an emission peak at 475 nm. Pyrene excimer formation is a concentration dependent phenomenon in organic solution. Owing to the low solubility of pyrene in water, pyrene excimer formation is not observed in pure water. Solubilization of pyrene by micelle forming agents allows excimer formation in aqueous solution. The measurement of excimer emission as a function of surfactant concentration allows the determination of aggregation number of micelles (252). As the concentration of micelle forming agent increases, IE/I1 ratio increases owing to movement of pyrene molecules from premicellar aggregates to micelles resulting in a rise in average occupancy of

pyrene molecules in micelles. Above the CAC, the number of micelles increases causing the lowering of an average occupancy and thereby lowering the probability of excimer formation and hence the decrease in IE/I1 ratio (253).

The CMC of methylprednisolone-21-phosphate has been reported by surface tension measurements to be 0.017 M (242), which is on the same order of magnitude as the CAC for Dex-P of 0.034 M as determined by the fluorescence method. However, Shah et al have determined the CAC of Dex-P to be 0.0034 mol/kg at 25 °C by measuring the electrical conductivities of increasing concentrations of the drug solution (254). The reported value is about ten times lower than that determined for Dex-P in our study by fluorescence method. The differences in these various techniques probably reflect the different properties being probed where conductivity may be more sensitive to very small aggregates. Additionally, Flynn and Lamb also used the conductivity method for the study of CMC of methylprednisolone-21-phosphate at pH 7.5 at various temperatures including 25 °C but did not find a sharp break point and obtained a range of 0.01 to 0.02 M between which the CMC values lies (242).

The CAC determined by the solubility method is only an apparent value because of the curvature in the solubility curve instead of distinct discontinuity and therefore differs significantly from the value obtained by fluorescence method. Since the solubility method does not allow for direct calculation of the monomer concentration, the presence of premicellar aggregates complicates the data interpretation. If the aggregates formed are sufficiently large, containing more than 20 monomers, a simple monomer-micelle model adequately describes the equilibria. Such systems are characterized by a distinct sharp break point in plots of any properties versus its concentration. However, steroidal

molecules, such as Dex-P, are known to form pre-micellar aggregates prior to true aggregation resulting in curvature rather than a distinct break-point in the plots (255) as seen in Figure 6.4 and the inset highlighting the increase in Dex solubility even at lower Dex-P concentration (~50 mM).

For drugs with a smaller hydrophilic portion relative to their hydrophobic portion, a trend of decreasing CMC or CAC values with an increase in temperature has been observed (256). In particular, the CAC of Dex-P was found to increase with temperature and was attributed to greater dehydration of polar head groups than those of hydrophobic groups leading to repulsion between them and difficulty in aggregation (254). Based on this, the CAC of Dex-P at 37°C would be expected to be higher than that determined at 25°C. Although the CAC values at lower pH where the free acid predominates was not investigated, the low solubility of Dex-P at low pH would preclude the determination (242).

The present studies were conducted at concentrations well below the determined CAC value of 34 mM or even 3.4 mM as reported by Shah et al. The Dex-P conc. range in loading and release studies were less than 1 mM. Also, since the release studies were conducted at 37 °C and the CAC of Dex-P is known to increase with temperature, it further ensures the absence of aggregates in the transport experiments. Additionally, the release studies at different pH values were conducted at much lower concentrations (<1 mM) because structural resemblance between the corticosteroid phosphates and the surface active bile acids raises the possibility of mixed micellization and potential bilayer disruption at higher concentrations (257, 258). This could also be a likely explanation for

inefficient loading of Dex-P by passive loading methods despite its high water solubility, as observed in our and other studies (259, 260).

pH Dependence of Bilayer Permeability Coefficients

The method of pH adjustment to modulate bilayer transport of ionizable drugs was studied long back by Xiang and others, mostly for small molecules such as α and β-naphthoic acids (238), p-toluic acid and their analogues (189, 237) etc., where they also demonstrated a quantitative relationship between pH and permeability. However, mostly with the goals of understanding the barrier properties of the bilayers, they studied the pH-permeability relationship in an attempt to explore the pH region where the flux of the highly permeable carboxylic acids was membrane controlled and changed several orders of magnitude (189, 237, 238).

The pH-gradient strategy has also been explored and applied to a great extent for active loading of weak acids and bases in liposomes but the approach of intravesicular pH modification has not been explored as much for the retention of large-drug like molecules for the purpose of achieving controlled or tunable release. Joguparthi et al. developed the pH-permeability model for drug permeability in liposomes for a hydrophobic model drug, AR-67, a camptothecin analogue (126). Since this can be a very valuable and simple formulation approach for the modulation of release kinetics of both hydrophobic and hydrophilic ionizable compounds, there is a need to extend the applicability of the relationship to more drugs having structural diversity. Here, this effect was demonstrated for a hydrophilic steroidal compound, Dex-P.

The bilayer properties were assumed to be independent of pH in the range explored in this study (pH 2-6) based on the previous studies from this laboratory. Xiang et al.

showed there was no change in apparent permeability with change in pH for α-D-glucose across DHPC and DPPC bilayers and for acetamide across egg-lecithin bilayers, both non-ionizable compounds, indicating pH-independence of the barrier properties of the bilayers (189). Additionally, Joguparthi et al. found no change in barrier properties of DSPC liposomes at pH 4.1 and 9.5 by comparing the permeability of ^{14}C-thiourea to that reported previously (126).

At a given pH, an ionizable drug exists partially in its neutral and ionized forms, depending upon the ionization constants. The change in apparent permeability with pH can be attributed to different permeability coefficients of the neutral and ionic species and changes in the relative fractions of those species with pH. The bilayer permeability of the neutral form of Dex-P could not be determined directly from experiments due to the low pKa_1 of 1.9 and the lipid stability concerns that would arise in conducting transport studies at pH values below the pKa (142, 243, 244). However, the permeability of the neutral species could be estimated from the simultaneous model fitting of the release profiles at various pH values. Since the rate constant for the monoanion was more than 500 fold smaller than that for the neutral species, the permeability of the monoanion and dianion was assumed to be negligible. Transport of ionic species across liposome bilayers is energetically unfavorable due to the tremendous energetic penalty incurred in their transfer from water into the non-polar hydrocarbon-like region in the bilayer (62). Although the permeability of monoanion was about 500 fold smaller than the unionized species, the difference is smaller compared to that obtained between neutral and ionized species of some small carboxylic acids (189, 261). This can be attributed to the

possibility of ion pair transport through the membrane, although the evidences for it have not been explored here.

Model I was inadequate in satisfactorily describing the data in Figure 6.8 and therefore model II which considers the intra and extra-vesicular membrane binding of the different species was tested. The membrane binding of Dex-P has been described in detail in chapter three. Although the binding of Dex-P mono-anion (at pH 4) was negligible in DPPC and DSPC liposomes, based on the pH-partition profile in DMPC, the binding of neutral Dex-P in DPPC and DSPC could not be neglected. Considering the binding of the neutral species accounted for the shift in the pKa observed from the pH-permeability profile when no binding was considered. The bilayer membrane transport is primarily governed by the concentration gradient of the aqueous free neutral species. The simultaneous binding and ionization deplete the free aqueous concentration of permeable, neutral species that is the driving force for the transport of drug across the liposome. Owing to the large intraliposomal surface-to-volume ratio, there is significant intraliposomal binding of a drug even for low partition coefficient values. The depletion of the free neutral drug, attributed to binding and ionization, therefore needs to be taken into account for accurate determination of the permeability coefficient. Thus, the retention of the weak acid drugs in liposome would depend upon the pKa of the drug, membrane partitioning of the neutral and ionized species and the intraliposomal pH.

The fitting of the pH-permeability data of Dex-P to model II suggested the membrane partition coefficients of the unionized neutral Dex-P to be 42 ± 35 and 186 ± 68 (95% C.I.) in DPPC and DSPC, respectively. The predicted higher partition coefficient in DSPC liposomes as compared to DPPC is in contrast to the expected dependence of

membrane partition coefficients on free surface area, as reported in the literature (55, 121, 122) and chapter three. Since DPPC has a smaller acyl chain length and a lower chain density leading to a higher free surface area as compared to DSPC, the partition coefficient would be expected to be higher in DPPC. However, the large 95% confidence intervals of the predicted partition coefficients are quite large, thus complicating the interpretation of these results. One of the reasons for the wide confidence intervals is the low pKa_1 of Dex-P and the absence of permeability data at pH values below pKa_1. Considering the release profiles shown in Figure 6.7, the experimental pH values mainly explore the pH region where the drug is predominantly in the monoanionic form. Moreover, the profiles at pH 2 and pH 3 were not significantly different from each other and in DPPC they very similar to the profile observed for free Dex-P. More reliable data at low pH may require the use of a different transport method.

Quantitative Relationship between Permeability and Free Surface Area

Depending on the properties of the permeant, the rate-limiting or barrier region for liposomal release may differ. If the polarity of solute is sufficient to establish the bilayer membrane as rate-limiting, then it might be reasonable to expect a dependence of the permeability coefficient on the available free surface area of the bilayer. Indeed, Xiang and Anderson discovered using acetic acid as a model solute that the bilayer free-surface area was a "universal" variable that quantitatively related solute permeability to chain packing in both liquid-crystalline and gel phases (122, 131). They further demonstrated the dependence of the permeability decrement ($f=P_m/P_o$), a factor that accounts for the effects of chain ordering, on the inverse of the bilayer free surface area for several short-chain monocarboxylic acids (61). Thus, it has long been demonstrated that the effects of

bilayer packing on trans-bilayer transport can be rationalized in terms of a dependence of permeability on the two-dimensional packing structure, as characterized by the free surface area per lipid molecule, a_{free}. However, there has been no systematic attempt to test such a quantitative relationship using larger drug-like molecules. Such a quantitative model could provide a significant contribution by enhancing the predictive capability for drug release across liposomal delivery systems.

The effects of lipid chain packing in gel and liquid crystalline lipid bilayers on permeability was investigated for the larger solute Dex-P by measuring its release kinetics from DMPC, DPPC and DSPC liposomes at pH . As shown in Figure 6.11, the natural logarithm of P_{app} was found to correlate linearly with the inverse of the bilayer free surface area. The slope is the measure of the sensitivity of the apparent permeability of Dex-P on bilayer chain density. Particularly noteworthy is the finding that the apparent permeability coefficient for Dex-P across gel phase DSPC bilayers is 16-fold smaller than that across co-existing gel-liquid crystalline phase DPPC bilayers, which in turn is 9-fold smaller than that across the liquid crystalline DMPC bilayer. In other words, the apparent permeability across highly ordered gel phase of DSPC is nearly 2 orders-of-magnitude smaller than that across the disordered liquid crystalline bilayer of DMPC, demonstrating a significant role of bilayer chain ordering on solute transport.

In chapter three, the concept of surface density or free surface area and its effect on membrane partition coefficients was explained. A similar relationship was observed here with apparent permeability of Dex-P across the liposomes. However, the degree of changes in apparent permeability with decrease in free surface area is higher than that observed for partitioning as demonstrated by the steeper slope of -0.5 for apparent

permeability versus a slope of -0.2 for partitioning of Dex-P (Chapter Three). This is attributed to the requirement for passage of solute across the bilayer for permeation as opposed to partitioning and thereby a higher sensitivity to the chain density. In partitioning, depending on the nature of the solute and its location and specific interactions with the bilayer, there may be only partial insertion of the solute into the bilayer. For permeation, the solute has to travel from one side of the bilayer to the other and may encounter a large penalty in free energy for insertion into the highly ordered barrier domain. Thus, the permeation process probes a different region of bilayer than the partitioning process. Additionally, variations in free surface area have an additional effect on solute diffusivity in lipid bilayers which does not affect solute partitioning. Both the barrier domain/water partition coefficient and the diffusion coefficient within the barrier domain may be functions of a_{free} and have a combined effect on trans-bilayer permeability.

CONCLUSIONS

A range of liposome release rates for Dex-P corresponding to half-lives from 1 hour to 892 hours were obtained by varying the lipid composition and the intravesicular pH. Changes in bilayer free surface area by varying the lipid composition and intravesicular pH are the simple formulation variables that can be exploited to tune drug release kinetics. Moreover, the ability to quantitatively relate the permeability across liposomes to physicochemical factors and bilayer barrier properties can be tremendously helpful in tailoring the release kinetics as per the therapeutic need. Although the free surface area was varied in this study by using lipids of different acyl chain length, it can also be modified by changing the temperature and inclusion of different percentages of

cholesterol in the bilayer. The prediction of permeability of a drug molecule across the bilayer is also relevant for the mechanistic understanding of the drug absorption process.

CHAPTER SEVEN

Conclusions and Future Directions

In the design of liposomal delivery systems, predictive strategies are needed to maximize drug loading and optimize drug retention regardless of the physicochemical properties of the drug. Drug candidates that are either highly hydrophobic or hydrophilic may pose particular challenges in their formulation design and for such compounds the optimization of both loading and release kinetics, if achieved at all, is usually done empirically. It would be highly beneficial to have a universal, comprehensive mathematical model relating the drug and bilayer properties to the rate and extent of loading and release kinetics in liposomes. In view of this objective, one of the principal goals of this work was to explore the factors affecting the bilayer partitioning, loading and permeability of model solutes using mechanism-based mathematical models to predict these processes in liposomes based solely on the structure of the solute, composition of the lipid membrane, and the local environmental conditions.

The investigation of the influence of liposome composition on membrane partitioning behavior of two solutes differing in physicochemical properties demonstrated a quantitative relationship between bilayer/water partitioning and the bilayer chain ordering (free surface area). Thus, knowledge of the membrane partition coefficient of a particular drug in a given phospholipid bilayer would enable the prediction of the same quantity in another bilayer varying, for example, in lipid chain length solely from the difference in bilayer free surface area. Relationships between solute structure and lipid bilayer membrane binding, if sufficiently comprehensive, would not only be useful for determining how much of a drug of interest would be bound to a liposomal membrane,

which is an essential term in understanding and modeling both drug loading and release, but it would also be an important piece of the puzzle in understanding how drugs distribute in vivo. However, a more comprehensive set of compounds with diverse size, structure and properties needs to be evaluated to establish universally applicable structure-binding relationships.

To properly design nanoparticle release kinetics, one must have the right mathematical models to describe drug release as well as proper methods to test those models. The analysis of the dynamic dialysis method for the determination of release kinetics from nanoparticles as conducted in this work should greatly enhance understanding of the central mechanisms involved in dynamic dialysis and provide the ability to evaluate the reliability of data generated by this method. The proposed mathematical models will enable the deconvolution of the true release rate constant from the apparent kinetics where drug binding effects and/or dialysis membrane transport may be partially contributing.

The novel active loading method developed in this study using supersaturated drug solutions should be valuable in overcoming formulation challenges associated with the liposomal delivery of poorly soluble, ionizable anticancer agents. In terms of drug release kinetics, the *a priori* design of liposomal release kinetics may play an important role in the selection of optimal systems tailored to specific tumor types. Mechanistic understanding of the thermodynamic and kinetic factors governing the trans-bilayer activity gradient of a drug is the key to predicting its release kinetics. It was shown that a varying range of release kinetics from few hours to several days can be obtained by modulation of formulation variables such as intraliposomal pH and bilayer barrier

properties. A quantitative relationship between membrane permeability, the intraliposomal microenvironment, and bilayer chain ordering was demonstrated. However, the connection between mechanistic models for in vitro release in aqueous buffers and the in vivo release kinetics from the same systems in the systemic circulation and local tumor environment has not yet been established. Mechanism-based models such as those developed in this study should also be beneficial in understanding and minimizing differences between in vitro and in vivo behavior of drug-loaded liposomes when such differences emerge.

In the near term, evaluation of the in vivo performance of optimized liposomal formulations in order to test the applicability of models based on in vitro observations to in vivo behavior should be considered. The long term goal would be to evaluate the applicability of such binding, loading and release models with a diverse set of compounds varying in size and structure in order to contribute towards the ultimate vision of establishing global, comprehensive mathematical models that can predict in vitro drug loading and both in vitro and in vivo release kinetics of various liposomally loaded drugs.

REFERENCES

1. P.A. McCarron and M. Hall. Pharmaceutical nanotechnology. Encyclopedia of Nanoscience and Nanotechnology. 8:469-487 (2004).
2. I. Brigger, C. Dubernet, and P. Couvreur. Nanoparticles in cancer therapy and diagnosis. Advanced Drug Delivery Reviews:631-651 (2002).
3. S. Marchesan and M. Prato. Nanomaterials for (Nano)medicine. ACS Medicinal Chemistry Letters:147-149 (2013).
4. R. Misra, S. Acharya, and S.K. Sahoo. Cancer nanotechnology: application of nanotechnology in cancer therapy. Drug Discovery Today. 15:842-850 (2010).
5. S.R. Qureshi, Y.P. Sahni, S.K. Singh, M.A. Bhat, A.A. Dar, and S.A. Quadri. Application of nanotechnology in cancer treatment. J Pharm Res Opin. 1:37-41 (2011).
6. S.P. Sahane, A.K. Nikhar, S. Bhaskaran, and D.R. Mundhada. Nanotechnology in cancer chemotherapy. Int J Pharm Technol. 4:2085-2099 (2012).
7. A.Z. Wang, R. Langer, and O.C. Farokhzad. Nanoparticle delivery of cancer drugs. Annu Rev Med. 63:185-198 (2012).
8. C.C. Anajwala, G.K. Jani, and S.M.V. Swamy. Current trends of nanotechnology for cancer therapy. Int J Pharm Sci Nanotechnol. 3:1043-1056 (2010).
9. R.G. Aswathy, B. Sivakumar, D. Brahatheeswaran, S. Raveendran, T. Ukai, T. Fukuda, Y. Yoshida, T. Maekawa, and D.N. Sakthikumar. Multifunctional biocompatible fluorescent Carboxymethyl cellulose nanoparticles. J Biomater Nanobiotechnol. 3:254-261 (2012).
10. D. Gyawali, M. Palmer, R.T. Tran, and J. Yang. Progress of nanobiomaterials for theranostic systems. Biomed Mater Diagn Devices:435-476 (2012).
11. S. Kuroda, T. Yokoyama, J.O. Tam, A.W. Scott, L.L. Ma, M. Shanker, J. Jin, C. Goerlich, D. Willcutts, J.A. Roth, K. Sokolov, K.P. Johnston, and R. Ramesh. Multifunctional tumor-targeted nanoparticles for lung cancer. Pulm Nanomed:15-44 (2013).
12. D. Wang, J. Tang, Y. Wang, S. Ramishetti, Q. Fu, K. Racette, and F. Liu. Multifunctional Nanoparticles Based on a Single-Molecule Modification to Treat Drug-Resistant Cancer. Mol Pharmaceutics:Ahead of Print.
13. H. Yan, M. Guo, and K. Liu. Multifunctional magnetic hybrid nanoparticles as a nanomedical platform for cancer-targeted imaging and therapy. Biomed Sci, Eng Technol:283-300 (2012).
14. S. Acharya and S.K. Sahoo. PLGA nanoparticles containing various anticancer agents and tumour delivery by EPR effect. Advanced Drug Delivery Reviews. 63:170-183 (2011).

15. K. Greish. Enhanced permeability and retention (EPR) effect for anticancer nanomedicine drug targeting. Methods Mol Biol (Totowa, NJ, U S). 624:25-37 (2010).

16. H. Maeda. Macromolecular therapeutics in cancer treatment: The EPR effect and beyond. Journal of Controlled Release. 164:138-144 (2012).

17. S. Modi, J.P. Jain, A.J. Domb, and N. Kumar. Exploiting EPR in polymer drug conjugate delivery for tumor targeting. Curr Pharm Des. 12:4785-4796 (2006).

18. L. Basile, R. Pignatello, and C. Passirani. Active targeting strategies for anticancer drug nanocarriers. Curr Drug Delivery. 9:255-268 (2012).

19. Q. Tu, Y. Zhang, R. Liu, J.C. Wang, L. Li, N. Nie, A. Liu, L. Wang, W. Liu, L. Ren, X. Wang, and J. Wang. Active drug targeting of disease by nanoparticles functionalized with ligand to folate receptor. Curr Med Chem. 19:3152-3162 (2012).

20. D.B. Fenske and P.R. Cullis. Liposomal nanomedicines. Expert Opinion on Drug Delivery. 5:25-44 (2008).

21. G. Gregoriadis. Liposomes as drug carriers. Pharm Int. 4:33-37 (1983).

22. D.G. Lasic. Liposomes in drug delivery. Surfactant Sci Ser. 62:447-476 (1996).

23. R.K. Scheule and S.H. Cheng. Liposome delivery systems. Gene Ther:93-112 (1996).

24. M. Brandl. Liposomes as drug carriers: a technological approach. Biotechnol Annu Rev. 7:59-85 (2001).

25. P.R. Kulkarni, J.D. Yadav, and K.A. Vaidya. Liposomes: a novel drug delivery system. Int J Curr Pharm Res. 3:10-18 (2011).

26. M. Schneider. Liposomes as drug carriers: 10 years of research. Drug Targeting, Proc Symp:119-134 (1985).

27. A.A. Gabizon. Stealth liposomes and tumor targeting: one step further in the quest for the magic bullet. Clinical Cancer Research. 7:223-225 (2001).

28. D. Papahadjopoulos and A.A. Gabizon. Sterically stabilized (Stealth) liposomes: Pharmacological properties and drug carrying potential in cancer. Liposomes Tools Basic Res Ind:177-188 (1995).

29. P. Srinath and P.V. Diwan. Stealth liposomes - an overview. Indian J Pharmacol. 26:179-184 (1994).

30. A. Chonn and P.R. Cullis. Recent advances in liposome technologies and their applications for systemic gene delivery. Advanced Drug Delivery Reviews. 30:73-83 (1998).

31. P. Goyal, K. Goyal, S.G.V. Kumar, A. Singh, O.P. Katare, and D.N. Mishra. Liposomal drug delivery systems - Clinical applications. Acta Pharm (Zagreb, Croatia). 55:1-25 (2005).

32. Y. Malam, M. Loizidou, and A.M. Seifalian. Liposomes and nanoparticles: nanosized vehicles for drug delivery in cancer. Trends Pharmacol Sci. 30:592-599 (2009).

33. V.P. Torchilin. Recent advances with liposomes as pharmaceutical carriers. Nat Rev Drug Discovery. 4:145-160 (2005).

34. B. Ansell. Future directions in lipid therapies. Adv Ther. 19:61-72 (2002).

35. D. Zucker, A.V. Andriyanov, A. Steiner, U. Raviv, and Y. Barenholz. Characterization of PEGylated nanoliposomes co-remotely loaded with topotecan and vincristine: relating structure and pharmacokinetics to therapeutic efficacy. Journal of Controlled Release. 160:281-289 (2012).

36. Y. Barenholz. Doxil - The first FDA-approved nano-drug: Lessons learned. Journal of Controlled Release. 160:117-134 (2012).

37. Y. Barenholz and D. Peer. Liposomes and other assemblies as drugs and nano-drugs: From basic and translational research to the clinics. Journal of Controlled Release. 160:115-116 (2012).

38. Y. Barenholz and D. Peer. Liposomes, lipid biophysics, and sphingolipid research: from basic to translation research. Chem Phys Lipids. 165:363-364 (2012).

39. Y. Barenholz. Relevancy of drug loading to liposomal formulation therapeutic efficacy. J Liposome Res. 13:1-8 (2003).

40. J.A. Crommelin Daan and G. Storm. Liposomes: from the bench to the bed. J Liposome Res. 13:33-36 (2003).

41. P.R. Cullis, L.D. Mayer, M.B. Bally, T.D. Madden, and M.J. Hope. Generating and loading of liposomal systems for drug-delivery applications. Advanced Drug Delivery Reviews. 3:267-282 (1989).

42. F. Szoka, Jr. and D. Papahadjopoulos. Comparative properties and methods of preparation of lipid vesicles (liposomes). Annu Rev Biophys Bioeng. 9:467-508 (1980).

43. P.J. Gaillard, C.C.M. Appeldoorn, and J. Rip. Advanced active liposomal loading of poorly water-soluble active substances, (to-BBB Holding B.V., Neth.).2012, p. 38pp.

44. J. Gubernator. Active methods of drug loading into liposomes: recent strategies for stable drug entrapment and increased in vivo activity. Expert Opin Drug Del. 8:565-580 (2011).

45. Y. Barenholz. Doxil-the first FDA-approved nano-drug: from an idea to a product. Handbook of Harnessing Biomaterials in Nanomedicine:335-398,, 334 plates (2012).

46. Y. Barenholz. Amphipathic weak base loading into preformed liposomes having a transmembrane ammonium ion gradient: from the bench to approved Doxil. Liposome Technology (3rd Edition). 2:1-25 (2007).

47. S. Clerc and Y. Barenholz. Loading of amphipathic weak acids into liposomes in response to transmembrane calcium acetate gradients. Biochim Biophys Acta. 1240:257-265 (1995).

48. D. Zucker, D. Marcus, Y. Barenholz, and A. Goldblum. Liposome drugs' loading efficiency: A working model based on loading conditions and drug's physicochemical properties. J Control Release. 139:73-80 (2009).

49. D.D. Lasic, B. Ceh, M.C.A. Stuart, L. Guo, P.M. Frederik, and Y. Barenholz. Transmembrane gradient driven phase transitions within vesicles: lessons for drug delivery. Biochimica et Biophysica Acta, Biomembranes. 1239:145-156 (1995).

50. V. Joguparthi and B.D. Anderson. Liposomal delivery of hydrophobic weak acids: enhancement of drug retention using a high intraliposomal pH. J Pharm Sci. 97:433-454 (2007).

51. D.C. Drummond, C.O. Noble, Z. Guo, K. Hong, J.W. Park, and D.B. Kirpotin. Development of a Highly Active Nanoliposomal Irinotecan Using a Novel Intraliposomal Stabilization Strategy. Cancer Research. 66:3271-3277 (2006).

52. M.J.W. Johnston, S.C. Semple, S.K. Klimuk, K. Edwards, M.L. Eisenhardt, E.C. Leng, G. Karlsson, D. Yanko, and P.R. Cullis. Therapeutically optimized rates of drug release can be achieved by varying the drug-to-lipid ratio in liposomal vincristine formulations. Biochimica et Biophysica Acta, Biomembranes. 1758:55-64 (2006).

53. W.C. Zamboni, A.C. Gervais, M.J. Egorin, J.H.M. Schellens, E.G. Zuhowski, D. Pluim, E. Joseph, D.R. Hamburger, P.K. Working, G. Colbern, M.E. Tonda, D.M. Potter, and J.L. Eiseman. Systemic and tumor disposition of platinum after administration of cisplatin or STEALTH liposomal-cisplatin formulations (SPI-077 and SPI-077 B103) in a preclinical tumor model of melanoma. Cancer Chemotherapy and Pharmacology. 53:329-336 (2004).

54. J.F. Nagle, J.C. Mathai, M.L. Zeidel, and S. Tristram-Nagle. Theory of passive permeability through lipid bilayers. J Gen Physiol. 131:77-85 (2008).

55. L.R. De Young and K.A. Dill. Partitioning of nonpolar solutes into bilayers and amorphous n-alkanes. Journal of Physical Chemistry. 94:801-809 (1990).

56. A. Finkelstein. Water and Nonelectrolyte Permeability of Lipid Bilayer Membranes. J Gen Physiol. 68:127-135 (1976).

57. Y. Katz and J.M. Diamond. A Method for measuring nonelectrolyte partition coefficients between liposomes and water. J Membrane Biol. 17:69-86 (1974).

58. A. Finkelstein and A. Cass. Permeability and electrical properties of thin lipid membranes. Nature. 52:145-171 (1968).

59. E. Orbach and A. Finkelstein. The nonelectrolyte permeability of planar lipid bilayer membranes. J Gen Physiol. 75:427-436 (1980).

60. A. Walter, D. Hastings, and J. Gutknecht. Weak acid permeability through lipid bilayer membranes. Role of chemical reactions in the unstirred layer. J Gen Physiol. 79:917-933 (1982).

61. T.-X. Xiang and B.D. Anderson. Influence of chain ordering on the selectivity of dipalmitoylphosphatidylcholine bilayer membranes for permeant size and shape. Biophys J. 75:2658-2671 (1998).

62. T.-X. Xiang and B.D. Anderson. Liposomal Drug Transport: A Molecular Perspective from Molecular Dynamics Simulations in Lipid Bilayers. Advanced Drug Delivery Reviews. 58:1357-1378 (2006).

63. T.-X. Xiang, X. Chen, and B.D. Anderson. Transport methods for probing the barrier domain of lipid bilayer membranes. Biophys J. 63:78-88 (1992).

64. D.W. Deamer and J. Bramhall. Permeability of lipid bilayers to water and ionic solutes. Chem Phys Lipids. 40:167-188 (1986).

65. T.-X. Xiang and B.D. Anderson. Permeability of Acetic Acid Across Gel and Liquid-Crystalline Lipid Bilayers Conforms to Free-Surface-Area Theory. Biophys J. 72:223-237 (1997).

66. A.C. Chakrabarti and D.W. Deamer. Permeability of lipid bilayers to amino acids and phosphate. Biochimica et Biophysica Acta, Biomembranes. 1111:171-177 (1992).

67. T.-X. Xiang and B.D. Anderson. Substituent contributions to the permeability of substituted p-toluic acids in lipid bilayer membranes. J Pharm Sci. 83:1511-1518 (1994).

68. I. Henriksen, S.A. Sande, G. Smistad, T. Agren, and J. Karlsen. In vitro evaluation of drug release kinetics from liposomes by fractional dialysis. Int J Pharm. 119:231-238 (1995).

69. N. Chidambaram and D.J. Burgess. A novel in vitro release method for submicron sized dispersed systems. AAPS pharmSci. 1:E11 (1999).

70. Y. Zambito, E. Pedreschi, and G. Di Colo. Is dialysis a reliable method for studying drug release from nanoparticulate systems?-A case study. International journal of pharmaceutics(2012).

71. P.M. Rowe. Camptothecins: new enthusiasm for an old drug [news]. Lancet. 347:892 (1996).

72. C.H. Takimoto and S.G. Arbuck. The Camptothecins. In B.A. Chabnerand D.A. Longo (eds.), Cancer Chemotherapy and Biotherapy, Lippincott-Raven Publishers, Philadelphia, 1996, pp. 463-484.

73. T.G. Burke. Chemistry of the camptothecins in the bloodstream. Drug stabilization and optimization of activity. Annals of the New York Academy of Sciences. 803:29-31 (1996).

74. I.F. Pollack, M. Erff, D. Bom, T.G. Burke, J.T. Strode, and D.P. Curran. Potent topoisomerase I inhibition by novel silatecans eliminates glioma proliferation in vitro and in vivo. Cancer Research. 59:4898-4905 (1999).

75. D. Bom, D.P. Curran, S. Kruszewski, S.G. Zimmer, J.T. Strode, G. Kohlhagen, W. Du, A.J. Chavan, K.A. Fraley, A.L. Bingcang, L.J. Latus, Y. Pommier, and

T.G. Burke. The novel silatecan 7-tert-butyldimethylsilyl-10-hydroxycamptothecin displays high lipophilicity, improved human blood stability, and potent anticancer activity. J Med Chem. 43:3970-3980 (2000).

76. D. Bom, D.P. Curran, J. Zhang, S.G. Zimmer, R. Bevins, S. Kruszewski, J.N. Howe, A. Bingcang, L.J. Latus, and T.G. Burke. The highly lipophilic DNA topoisomerase I inhibitor DB-67 displays elevated lactone levels in human blood and potent anticancer activity. Journal of Controlled Release. 74:325-333 (2001).

77. T.G. Burke, P.J. Houghton, D. Bom, D. Wu, S. Kruszewski, Y. Pommier, G. Kohlhagen, R. Perez-Soler, S.G. Zimmer, L.J. Latus, A.J. Charvan, and D.P. Curran. The Novel Silatecan DB-67 Displays High Lipophilicity, Improved Human Blood Stability and Potent Anticancer Activity in Vitro and in Vivo. Proc Am Assoc Cancer Research. 41:213 (2000).

78. T.G. Burke, A.K. Mishra, M.C. Wani, and M.E. Wall. Lipid bilayer partitioning and stability of camptothecin drugs. Biochemistry. 32:5352-5364 (1993).

79. S.M. Arnold, J.J. Rinehart, E. Tsakalozou, J.R. Eckardt, S.Z. Fields, B.J. Shelton, P.A. De Simone, B.K. Kee, J.A. Moscow, and M. Leggas. A phase I study of 7-t-Butyldimethylsilyl-10-hydroxycamptothecin in adult patients with refractory or metastatic solid malignancies. Clinical Cancer Research. 16:673-680 (2010).

80. T.G. Burke, T.-X. Xiang, B.D. Anderson, and L.J. Latus. Recent advances in camptothecin drug design and delivery strategies. Camptothecins in cancer therapy2005, pp. 171-190.

81. E.D. Adane, Z. Liu, T.-X. Xiang, B.D. Anderson, and M. Leggas. Pharmacokinetic Modeling to Assess Factors Affecting the Oral Bioavailability of the Lactone and Carboxylate Forms of the Lipophilic Camptothecin Analogue AR-67 in Rats. Pharm Res. 29:1722-1736 (2012).

82. W.L. Furman, C.F. Stewart, C.A. Poquette, C.B. Pratt, V.M. Santana, W.C. Zamboni, L.C. Bowman, M.K. Ma, F.A. Hoffer, W.H. Meyer, A.S. Pappo, A.W. Walter, and P.J. Houghton. Direct translation of a protracted irinotecan schedule from a xenograft model to a phase I trial in children. J Clin Oncol. 17:1815-1824 (1999).

83. V.M. Santana, W.C. Zamboni, M.N. Kirstein, M. Tan, T. Liu, A. Gajjar, P.J. Houghton, and C.F. Stewart. A pilot study of protracted topotecan dosing using a pharmacokinetically guided dosing approach in children with solid tumors. Clinical Cancer Research. 9:633-640 (2003).

84. Y. Avnir, R. Ulmansky, V. Wasserman, S. Even-Chen, M. Broyer, Y. Barenholz, and Y. Naparstek. Amphipathic weak acid glucocorticoid prodrugs remote-loaded into sterically stabilized nanoliposomes evaluated in arthritic rats and in a beagle dog: a novel approach to treating autoimmune arthritis. Arthritis & Rheumatism. 58:119-129 (2008).

85. U. Naumann, S. Durka, and M. Weller. Dexamethasone-mediated protection from drug cytotoxicity: association with p21WAF1/CIP1 protein accumulation? Oncogene. 17:1567-1575 (1998).

86. M. Banciu, M.H. Fens, G. Storm, and R.M. Schiffelers. Antitumor activity and tumor localization of liposomal glucocorticoids in B16 melanoma-bearing mice. J Control Release. 127:131-136 (2008).

87. M. Banciu, J.M. Metselaar, R.M. Schiffelers, and G. Storm. Liposomal glucocorticoids as tumor-targeted anti-angiogenic nanomedicine in B16 melanoma-bearing mice. J Steroid Biochem Mol Biol. 111:101-110 (2008).

88. A.M. Gorman, U.A. Hirt, S. Orrenius, and S. Ceccatelli. Dexamethasone pre-treatment interferes with apoptotic death in glioma cells, *Neuroscience (Oxford)*, Vol. 962000, pp. 417-425.

89. M. Leggas, K.L. Kuo, F. Robert, G. Cloud, M. deShazo, R. Zhang, M. Li, H. Wang, S. Davidson, and J. Rinehart. Intensive anti-inflammatory therapy with dexamethasone in patients with non-small cell lung cancer: effect on chemotherapy toxicity and efficacy. Cancer chemotherapy and pharmacology. 63:731-743 (2009).

90. H. Wang, M. Li, J.J. Rinehart, and R. Zhang. Dexamethasone as a chemoprotectant in cancer chemotherapy: hematoprotective effects and altered pharmacokinetics and tissue distribution of carboplatin and gemcitabine. Cancer Chemotherapy and Pharmacology. 53:459-467 (2004).

91. H. Wang, M. Li, J.J. Rinehart, and R. Zhang. Pretreatment with dexamethasone increases antitumor activity of carboplatin and gemcitabine in mice bearing human cancer Xenografts: in vivo activity, pharmacokinetics, and clinical implications for cancer chemotherapy. Clinical Cancer Research. 10:1633-1644 (2004).

92. H. Wang, Y. Wang, E.R. Rayburn, D.L. Hill, J.J. Rinehart, and R. Zhang. Dexamethasone as a chemosensitizer for breast cancer chemotherapy: potentiation of the antitumor activity of adriamycin, modulation of cytokine expression, and pharmacokinetics. International Journal of Oncology. 30:947-953 (2007).

93. P. Kallinteri, G. Antimisiaris Sophia, D. Karnabatidis, C. Kalogeropoulou, I. Tsota, and D. Siablis. Dexamethasone incorporating liposomes: an in vitro study of their applicability as a slow releasing delivery system of dexamethasone from covered metallic stents. Biomaterials. 23:4819-4826 (2002).

94. T. Rodgers, H.M. Jones, and M. Rowland. Tissue lipids and drug distribution: Dog versus rat. J Pharm Sci. 101:4615-4626 (2012).

95. T. Rodgers and M. Rowland. Mechanistic approaches to volume of distribution predictions: understanding the processes. Pharm Res. 24:918-933 (2007).

96. T. Rodgers and M. Rowland. Physiologically based pharmacokinetic modelling 2: predicting the tissue distribution of acids, very weak bases, neutrals and zwitterions. J Pharm Sci. 95:1238-1257 (2006).

97. S. Nagar and K. Korzekwa. Commentary: Nonspecific protein binding versus membrane partitioning: it is not just semantics. Drug Metab Disp. 40:1649-1652 (2012).

98. S. Takegami, K. Kitamura, T. Funakoshi, and T. Kitade. Partitioning of anti-inflammatory steroid drugs into phosphatidylcholine and phosphatidylcholine-cholesterol small unilamellar vesicles as studied by second-derivative spectrophotometry. Chemical & Pharmaceutical Bulletin. 56:663-667 (2008).

99. C. Pereira-Leite, C. Nunes, J.L. Lima, S. Reis, and M. Lucio. Interaction of celecoxib with membranes: the role of membrane biophysics on its therapeutic and toxic effects. J Phys Chem B. 116:13608-13617 (2012).

100. P. Poulin and F.P. Theil. Prediction of pharmacokinetics prior to in vivo studies. 1. Mechanism-based prediction of volume of distribution. J Pharm Sci. 91:129-156 (2002).

101. C. Peetla, A. Stine, and V. Labhasetwar. Biophysical interactions with model lipid membranes: applications in drug discovery and drug delivery. Mol Pharm. 6:1264-1276 (2009).

102. K. Balon, B.U. Riebesehl, and B.W. Muller. Drug liposome partitioning as a tool for the prediction of human passive intestinal absorption. Pharm Res. 16:882-888 (1999).

103. M.M.B. Ribeiro, M.N. Melo, I.D. Serrano, N.C. Santos, and M.A.R.B. Castanho. Drug-lipid interaction evaluation: why a 19th century solution? Trends Pharmacol Sci. 31:449-454 (2010).

104. R. Collander. The permeability of Nitella cells to non-electrolytes. Physiol Pl. 7:420-445 (1954).

105. E. Overton. Ueber die allgemeinen osmotischen Eigenschaften der Zelle, ihre vermutlichen Ursachen und ihre Bedeutung fur die Physiologie. Vjschr Naturforsch Ges Zurich. 44:88-135 (1899).

106. A. Leo, C. Hansch, and D. Elkins. Partition coefficients and their uses. Chem Rev. 71:525-616 (1971).

107. K.J. Schaper. Absorption of ionizable drugs: nonlinear dependence on log P, pKa, and pH-quantitative relationships. Quant Struct Act Relat. 1:13-27 (1982).

108. J.A. Marqusee and K.A. Dill. Solute partitioning into chain molecule interphases: monolayers, bilayer membranes, and micelles. J Chem Phys. 85:434-444 (1986).

109. J.K. Seydel. Octanol-water partitioning versus partitioning into membranes. Methods Princ Med Chem. 15:35-50 (2002).

110. T.X. Xiang and B.D. Anderson. Molecular distributions in interphases: statistical mechanical theory combined with molecular dynamics simulation of a model lipid bilayer. Biophys J. 66:561-572 (1994).

111. R.P. Austin, A.M. Davis, and C.N. Manners. Partitioning of Ionizing Molecules between Aqueous Buffers and Phospholipid Vesicles. J Pharm Sci. 84:1180-1183 (1995).

112. A. Avdeef, K.J. Box, J.E.A. Comer, C. Hibbert, and K.Y. Tam. pH-metric logP 10. Determination of liposomal membrane-water partition coefficients of ionizable drugs. Pharm Res. 15:209-215 (1998).

113. A. Loidl-Stahlhofen, T. Hartmann, M. Schottner, C. Rohring, H. Brodowsky, J. Schmitt, and J. Keldenich. Multilamellar liposomes and solid-supported lipid membranes (TRANSIL): screening of lipid-water partitioning toward a high-throughput scale. Pharm Res. 18:1782-1788 (2001).

114. R.P. Austin, P. Barton, A.M. Davis, R.E. Fessey, and M.C. Wenlock. The thermodynamics of the partitioning of ionizing molecules between aqueous buffers and phospholipid membranes. Pharm Res. 22:1649-1657 (2005).

115. R. Fruttero, G. Caron, E. Fornatto, D. Boschi, G. Ermondi, A. Gasco, P.-A. Carrupt, and B. Testa. Mechanisms of liposomes/water partitioning of (p-methylbenzyl)alkylamines. Pharm Res. 15:1407-1413 (1998).

116. B.I. Escher, R.P. Schwarzenbach, and J.C. Westall. Evaluation of liposome-water partitioning of organic acids and bases. 1. Development of a sorption model. Environ Sci Technol. 34:3954-3961 (2000).

117. S.H. White and W.C. Wimley. Peptides in lipid bilayers: structural and thermodynamic basis for partitioning and folding. Curr Opin Struct Biol. 4:79-86 (1994).

118. R.W. Tejwani, M.E. Davis, B.D. Anderson, and T.R. Stouch. Functional group dependence of solute partitioning to various locations in a DOPC bilayer: I. A comparison of molecular dynamics simulations with experiment J Pharm Sci. 100:2636-2646 (2011).

119. R.W. Tejwani, M.E. Davis, B.D. Anderson, and T.R. Stouch. An atomic and molecular view of the depth dependence of the free energies of solute transfer from water into lipid bilayers. Mol Pharmaceutics. 8:2204-2215 (2011).

120. E. Sikorska, E. Ilowska, D. Wyrzkowski, and A. Kwiatkowska. Membrane structure and interactions of peptide hormones with model lipid bilayers. Biochim Biophys Acta. 1818:2982-2993 (2012).

121. L.R. De Young and K.A. Dill. Solute partitioning into lipid bilayer membranes. Biochemistry. 27:5281-5289 (1988).

122. T.X. Xiang and B.D. Anderson. Phospholipid surface density determines the partitioning and permeability of acetic acid in DMPC:cholesterol bilayers. Journal of Membrane Biology. 148:157-167 (1995).

123. N. Matubayasi, W. Shinoda, and M. Nakahara. Free-energy analysis of the molecular binding into lipid membrane with the method of energy representation. J Chem Phys. 128:195107/195101-195113 (2008).

124. R.W. Tejwani, T.R. Stouch, and B.D. Anderson. Substituent effects on the ionization and partitioning of p-(aminoethyl)phenols and structurally related compounds: Electrostatic effects dependent on conformation. J Pharm Sci. 98:4534-4544 (2009).

125. T.-X. Xiang, Z.-Q. Jiang, L. Song, and B.D. Anderson. Molecular dynamics simulations and experimental studies of binding and mobility of 7-t-butyldimethylsilyl-10-hydroxycamptothecin (DB-67) and its 20(S)-4-aminobutyrate ester in DMPC membranes. Mol Pharmaceutics. 3:589-600 (2006).

126. V. Joguparthi and B.D. Anderson. Liposomal delivery of hydrophobic weak acids: enhancement of drug retention using a high intraliposomal pH. J Pharm Sci. 97:433-454 (2008).

127. S. Modi, T.-X. Xiang, and D. Anderson Bradley. Enhanced Active Liposomal Loading of a Poorly Soluble Ionizable Drug Using Supersaturated Drug Solutions. J Control Release. 162:330-339 (2012).

128. K. Taniguchi, N. Yamazawa, K. Itakura, K. Morisaki, and S. Hayashi. Partition characteristics and retention of anti-inflammatory steroids in liposomal ophthalmic preparations. Chemical & Pharmaceutical Bulletin. 35:1214-1222 (1987).

129. C. Matos, C. Moutinho, and P. Lobao. Liposomes as a Model for the Biological Membrane: Studies on Daunorubicin Bilayer Interaction. Journal of Membrane Biology. 245:69-75 (2012).

130. T.X. Xiang and B.D. Anderson. Influence of chain ordering on the selectivity of dipalmitoylphosphatidylcholine bilayer membranes for permeant size and shape. Biophys J. 75:2658-2671 (1998).

131. T.-X. Xiang and B.D. Anderson. Permeability of acetic acid across gel and liquid-crystalline lipid bilayers conforms to free-surface-area theory. Biophys J. 72:223-237 (1997).

132. V. Joguparthi, T.-X. Xiang, and B.D. Anderson. Liposome transport of hydrophobic drugs: gel phase lipid bilayer permeability and partitioning of the lactone form of a hydrophobic camptothecin, DB-67. J Pharm Sci. 97:400-420 (2008).

133. H. Derendorf, P. Rohdewald, G. Hochhaus, and H. Moellmann. HPLC determination of glucocorticoid alcohols, their phosphates and hydrocortisone in aqueous solutions and biological fluids. Journal of Pharmaceutical and Biomedical Analysis. 4:197-206 (1986).

134. R.P. Austin, P. Barton, A.M. Davis, C.N. Manners, and M.C. Stansfield. The effect of ionic strength on liposome-buffer and 1-octanol-buffer distribution coefficients. J Pharm Sci. 87:599--607 (1998).

135. H.D. Baeuerle and J. Seelig. Interaction of charged and uncharged calcium channel antagonists with phospholipid membranes. Binding equilibrium, binding enthalpy, and membrane location. Biochemistry. 30:7203-7211 (1991).

136. C. Matos, J.L.C. Lima, S. Reis, A. Lopes, and M. Bastos. Interaction of antiinflammatory drugs with EPC liposomes: Calorimetric study in a broad concentration range. Biophys J. 86:946-954 (2004).

137. A. Seelig, P.R. Allegrini, and J. Seelig. Partitioning of local anesthetics into membranes: surface charge effects monitored by the phospholipid head-group. Biochimica et Biophysica Acta, Biomembranes. 939:267-276 (1988).

138. P. Smejtek, S. Wang, and A.W. Barstad. Adsorption of ionized and neutral pentachlorophenol to phosphatidylcholine membranes. Biochimica et Biophysica Acta, Biomembranes. 905:213-221 (1987).

139. P.G. Thomas and J. Seelig. Binding of the calcium antagonist flunarizine to phosphatidylcholine bilayers: Charge effects and thermodynamics. Biochem J. 291:397-402 (1993).

140. M.R. Moncelli, L. Becucci, and R. Guidelli. The intrinsic pKa values for phosphatidylcholine, phosphatidylethanolamine, and phosphatidylserine in monolayers deposited on mercury electrodes. Biophys J. 66:1969-1980 (1994).

141. T.-X. Xiang and B.D. Anderson. Development of a combined NMR paramagnetic ion-induced line-broadening/dynamic light scattering method for permeability measurements across lipid bilayer membranes. J Pharm Sci. 84:1308-1315 (1995).

142. M. Grit, N.J. Zuidam, and D.J.A. Crommelin. Analysis and hydrolysis kinetics of phospholipids in aqueous liposome dispersions. Liposome Technol (2nd Ed). 1:455-486 (1993).

143. N.J. Zuidam, H.K.M.E. Gouw, Y. Barenholz, and D.J.A. Crommelin. Physical (in)stability of liposomes upon chemical hydrolysis: the role of lysophospholipids and fatty acids. Biochimica et Biophysica Acta, Biomembranes. 1240:101-110 (1995).

144. F. Martinez and A. Gomez. Thermodynamics of partitioning of some sulfonamides in 1-octanol-buffer and liposome systems. J Phy Org Chem. 15:874-880 (2002).

145. M.M. Saket, K.C. James, and I.W. Kellaway. Partitioning of some 21-alkyl esters of hydrocortisone and cortisone. Int J Pharm. 21:155-166 (1984).

146. H. Yamamoto and H.M. Liljestrand. Partitioning of Selected Estrogenic Compounds between Synthetic Membrane Vesicles and Water: Effects of Lipid Components. Environ Sci Technol. 38:1139-1147 (2004).

147. R.W. Tejwani and B.D. Anderson. Influence of intravesicular pH drift and membrane binding on the liposomal release of a model amine-containing permeant. J Pharm Sci. 97:381-399 (2008).

148. P. Saveyn, J. Cocquyt, M. De Cuyper, and P. Van der Meeren. Evaluation of the Interaction of Propranolol with 1,2-Dimyristoyl-sn-glycero-3-phosphocholine (DMPC) Liposomes: The Langmuir Model. Langmuir. 24:6007-6012 (2008).

149. J.-H. Kwon, H.M. Liljestrand, L.E. Katz, and H. Yamamoto. Partitioning Thermodynamics of Selected Endocrine Disruptors between Water and Synthetic Membrane Vesicles: Effects of Membrane Compositions. Environ Sci Technol. 41:4011-4018 (2007).

150. G.M. Pauletti and H. Wunderli-Allenspach. Partition coefficients in vitro: artificial membranes as a standardized distribution model. European Journal of Pharmaceutical Sciences. 1:273-282 (1994).

151. S.E. Wright, J.C. White, and L. Huang. Partitioning of teniposide into membranes and the role of lipid composition. Biochimica et Biophysica Acta, Biomembranes. 1021:105-113 (1990).

152. M. Luxnat and H.J. Galla. Partition of chlorpromazine into lipid bilayer membranes: the effect of membrane structure and composition. Biochimica et Biophysica Acta, Biomembranes. 856:274-282 (1986).

153. Z. Fisar, K. Fuksova, and M. Velenovska. Binding of imipramine to phospholipid bilayers using radioligand binding assay. Gen Physiol Biophys. 23:77-99 (2004).

154. M. Ikonen, L. Murtomaeki, and K. Kontturi. Studying the interactions of drugs and hydrophobic model membranes using contact angle goniometry. Colloids and Surfaces, B: Biointerfaces. 71:107-112 (2009).

155. S. McLaughlin. The electrostatic properties of membranes. Annu Rev Biophys Biophys Chem. 18:113-136 (1989).

156. S.G.A. McLaughlin, G. Szabo, and G. Eisenman. Divalent ions and the surface potential of charged phospholipid membranes. J Gen Physiol. 58:667-687 (1971).

157. M. Fernandez-Vidal, S.H. White, and A.S. Ladokhin. Membrane Partitioning: "Classical" and "Nonclassical" Hydrophobic Effects. Journal of Membrane Biology. 239:5-14 (2011).

158. W.C. Wimley and S.H. White. Membrane partitioning: Distinguishing bilayer effects from the hydrophobic effect. Biochemistry. 32:6307-6312 (1993).

159. M. Arrowsmith, J. Hadgraft, and I.W. Kellaway. Thermodynamics of steroid partitioning in dimyristoylphosphatidylcholine liposomes. Biochim Biophys Acta, Lipids Lipid Metab. 750:149-156 (1983).

160. A.M.S. Ahmed, F.H. Farah, and I.W. Kellaway. The thermodynamics of partitioning of phenothiazines between phosphate buffer and the lipid phases of cyclohexane, n-octanol and DMPC liposomes. Pharm Res:119-124 (1985).

161. H.R. Lozano and F. Martinez. Thermodynamics of partitioning and solvation of ketoprofen in some organic solvent/buffer and liposome systems. Rev Bras Cienc Farm. 42:601-613 (2006).

162. M.R. Wenk, T. Alt, A. Seelig, and J. Seelig. Octyl-β-D-glucopyranoside partitioning into lipid bilayers: thermodynamics of binding and structural changes of the bilayer. Biophys J. 72:1719-1731 (1997).

163. C.M. Avila and F. Martinez. Thermodynamics of partitioning of benzocaine in some organic solvent/buffer and liposome systems. Chemical & Pharmaceutical Bulletin. 51:237-240 (2003).

164. T.-X. Xiang, Z.-Q. Jiang, L. Song, and B.D. Anderson. Molecular dynamics simulations and experimental studies of binding and mobility of 7-t-

butyldimethylsilyl-10-hydroxycamptothecin (DB-67) and its 20(S)-4-aminobutyrate ester in DMPC membranes Mol Pharmaceutics. 3:589-600 (2006).

165. G.A. Golden, R.T. Rubin, and R.P. Mason. Steroid hormones partition to distinct sites in a model membrane bilayer: direct demonstration by small-angle X-Ray diffraction. Biochimica et Biophysica Acta, Biomembranes. 1368:161-166 (1998).

166. R. Vijayan and P.C. Biggin. A steroid in a lipid bilayer: localization, orientation, and energetics. Biophys J. 95:L45-L47 (2008).

167. H. Yamauchi, Y. Takao, M. Abe, and K. Ogino. Molecular interactions between lipid and some steroids in a monolayer and a bilayer. Langmuir. 9:300-304 (1993).

168. S. Mitragotri, M.E. Johnson, D. Blankschtein, and R. Langer. An analysis of the size selectivity of solute partitioning, diffusion, and permeation across lipid bilayers. Biophys J. 77:1268-1283 (1999).

169. L. Mei, Z. Zhang, L. Zhao, L. Huang, X.-L. Yang, J. Tang, and S.-S. Feng. Pharmaceutical Nanotechnology for Oral Delivery of Anticancer Drugs. Advanced drug delivery reviews(2012).

170. T. Musacchio and V.P. Torchilin. Recent developments in lipid-based pharmaceutical nanocarriers. Frontiers in Bioscience, Landmark Edition. 16:1388-1412 (2011).

171. L. Zhang, F.X. Gu, J.M. Chan, A.Z. Wang, R.S. Langer, and O.C. Farokhzad. Nanoparticles in Medicine: Therapeutic Applications and Developments. Clinical Pharmacology & Therapeutics (New York, NY, United States). 83:761-769 (2008).

172. J.L. Arias. Drug targeting strategies in cancer treatment: an overview. Mini-Reviews in Medicinal Chemistry. 11:1-17 (2011).

173. H. Maeda, H. Nakamura, and J. Fang. The EPR effect for macromolecular drug delivery to solid tumors: Improvement of tumor uptake, lowering of systemic toxicity, and distinct tumor imaging in vivo. Advanced Drug Delivery Reviews:71-79 (2013).

174. V. Torchilin. Tumor delivery of macromolecular drugs based on the EPR effect. Advanced Drug Delivery Reviews. 63:131-135 (2011).

175. J.D. Byrne, T. Betancourt, and L. Brannon-Peppas. Active targeting schemes for nanoparticle systems in cancer therapeutics. Advanced Drug Delivery Reviews. 60:1615-1626 (2008).

176. N. Maurer, D.B. Fenske, and P.R. Cullis. Developments in liposomal drug delivery systems. Expert Opinion on Biological Therapy. 1:923-947 (2001).

177. S. Loew, A. Fahr, and S. May. Modeling the release kinetics of poorly water-soluble drug molecules from liposomal nanocarriers. Journal of Drug Delivery:376548, 376510 pp (2011).

178. L. Zeng, L. An, and X. Wu. Modeling drug-carrier interaction in the drug release from nanocarriers. Journal of Drug Delivery:370308, 370315 pp (2011).

179. S.J. Wallace, J. Li, R.L. Nation, and B.J. Boyd. Drug release from nanomedicines: selection of appropriate encapsulation and release methodology. Drug Delivery and Translational Research. 2:284-292 (2012).

180. M.Y. Levy and S. Benita. Drug release from submicronized o/w emulsion: a new in vitro kinetic evaluation model. Int J Pharm. 66:29-37 (1990).

181. G. Moreno-Bautista and K.C. Tam. Evaluation of dialysis membrane process for quantifying the in vitro drug-release from colloidal drug carriers. Colloids and Surfaces, A: Physicochemical and Engineering Aspects. 389:299-303 (2011).

182. D. Friedman and S. Benita. A mathematical model for drug release from O/W emulsions: application to controlled-release morphine emulsions. Drug Development and Industrial Pharmacy. 13:2067-2085 (1987).

183. C. Washington. Evaluation of non-sink dialysis methods for the measurement of drug release from colloids: effects of drug partition. Int J Pharm. 56:71-74 (1989).

184. C. Washington. Drug release from microdisperse systems: a critical review. Int J Pharm. 58:1-12 (1990).

185. T.-X. Xiang and B.D. Anderson. Stable supersaturated aqueous solutions of silatecan 7-t-butyldimethylsilyl-10-hydroxycamptothecin via chemical conversion in the presence of a chemically modified beta -cyclodextrin. Pharm Res. 19:1215-1222 (2002).

186. R. Margalit, R. Alon, M. Linenberg, I. Rubin, T.J. Roseman, and R.W. Wood. Liposomal drug delivery: thermodynamic and chemical kinetic considerations. Journal of Controlled Release. 17:285-296 (1991).

187. V. Joguparthi, S. Feng, and B.D. Anderson. Determination of intraliposomal pH and its effect on membrane partitioning and passive loading of a hydrophobic camptothecin, DB-67. Int J Pharm. 352:17-28 (2008).

188. S. Modi and D. Anderson Bradley. Bilayer Composition, Temperature, and Speciation Effects on Partitioning of Dexamethasone and its 21-phosphate: The Role of Bilayer Chain Ordering. Pharm Res(2013).

189. T.X. Xiang, Y.H. Xu, and B.D. Anderson. The barrier domain for solute permeation varies with lipid bilayer phase structure. Journal of Membrane Biology. 165:77-90 (1998).

190. P.K. Gupta, C.T. Hung, and D.G. Perrier. Quantitation of the release of doxorubicin from colloidal dosage forms using dynamic dialysis. J Pharm Sci. 76:141-145 (1987).

191. G. Purohit, T. Sakthivel, and A.T. Florence. The interaction of cationic dendrons with albumin and their diffusion through cellulose membranes. Int J Pharm. 254:37-41 (2003).

192. M.C. Meyer and D.E. Guttman. Dynamic dialysis as a method for studying protein binding. I. Factors affecting the kinetics of dialysis through a cellophane membrane. J Pharm Sci. 59:33-38 (1970).

193. M.C. Meyer and D.E. Guttman. Dynamic dialysis as a method for studying protein binding. II. Evaluation of the method with a number of binding systems. J Pharm Sci. 59:39-48 (1970).

194. M.R. Aji Alex, A.J. Chacko, S. Jose, and E.B. Souto. Lopinavir loaded solid lipid nanoparticles (SLN) for intestinal lymphatic targeting. European Journal of Pharmaceutical Sciences. 42:11-18 (2011).

195. S. Essa, J.M. Rabanel, and P. Hildgen. Characterization of rhodamine loaded PEG-g-PLA nanoparticles (NPs): Effect of poly(ethylene glycol) grafting density. Int J Pharm. 411:178-187 (2011).

196. B.D. Kurmi, V. Gajbhiye, J. Kayat, and N.K. Jain. Lactoferrin-conjugated dendritic nanoconstructs for lung targeting of methotrexate. J Pharm Sci. 100:2311-2320 (2011).

197. R.C. Nagarwal, P.N. Singh, S. Kant, P. Maiti, and J.K. Pandit. Chitosan nanoparticles of 5-fluorouracil for ophthalmic delivery: characterization, in-vitro and in-vivo study. Chemical & Pharmaceutical Bulletin. 59:272-278 (2011).

198. J. Wang, B. Chen, J. Chen, X. Cai, G. Xia, R. Liu, P. Chen, Y. Zhang, and X. Wang. Synthesis and antitumor efficacy of daunorubicin-loaded magnetic nanoparticles. International Journal of Nanomedicine. 6:203-211 (2011).

199. T. Wang, C. Zhang, X.-J. Liang, W. Liang, and Y. Wu. Hydroxypropyl-β-cyclodextrin copolymers and their nanoparticles as doxorubicin delivery system. J Pharm Sci. 100:1067-1079 (2011).

200. J.A. Zhang, T. Xuan, M. Parmar, L. Ma, S. Ugwu, S. Ali, and I. Ahmad. Development and characterization of a novel liposome-based formulation of SN-38. Int J Pharm. 270:93-107 (2004).

201. D.D. Lasic. Recent developments in medical applications of liposomes: sterically stabilized liposomes in cancer therapy and gene delivery in vivo. J Control Release. 48:203-222 (1997).

202. A. Puri, K. Loomis, B. Smith, J.-H. Lee, A. Yavlovich, E. Heldman, and R. Blumenthal. Lipid-based nanoparticles as pharmaceutical drug carriers: from concepts to clinic. Crit Rev Ther Drug Carrier Syst. 26:523-580 (2009).

203. Y. Barenholz. Liposome application: problems and prospects. Curr Opin Colloid Interface Sci. 6:66-77 (2001).

204. A. Gabizon, D. Goren, R. Cohen, and Y. Barenholz. Development of liposomal anthracyclines: from basics to clinical applications. J Control Release. 53:275-279 (1998).

205. D.B. Fenske, A. Chonn, and P.R. Cullis. Liposomal nanomedicines: an emerging field. Toxicol Pathol. 36:21-29 (2008).

206. S.A. Abraham, K. Edwards, G. Karlsson, N. Hudon, L.D. Mayer, and M.B. Bally. An evaluation of transmembrane ion gradient-mediated encapsulation of topotecan within liposomes. J Control Release. 96:449-461 (2004).

207. G. Haran, R. Cohen, L.K. Bar, and Y. Barenholz. Transmembrane ammonium sulfate gradients in liposomes produce efficient and stable entrapment of amphipathic weak bases. Biochim Biophys Acta. 1151:201-215 (1993).

208. T.D. Madden, P.R. Harrigan, L.C.L. Tai, M.B. Bally, L.D. Mayer, T.E. Redelmeier, H.C. Loughrey, C.P.S. Tilcock, L.W. Reinish, and P.R. Cullis. The accumulation of drugs within large unilamellar vesicles exhibiting a proton gradient: a survey. Chem Phys Lipids. 53:37-46 (1990).

209. News-Medical.Net. Arno AR-67 Phase II clinical study for glioblastoma meets pre-defined interim goals. Retrieved from http://www.news-medical.net/news/20110623/Arno-AR-67-Phase-II-clinical-study-for-glioblastoma-meets-pre-defined-interim-goals.aspx.

210. E.D. Adane, Z. Liu, T.-X. Xiang, B.D. Anderson, and M. Leggas. Factors Affecting the In Vivo Lactone Stability and Systemic Clearance of the Lipophilic Camptothecin Analogue AR-67. Pharm Res. 27:1416-1425 (2010).

211. J. Fassberg and V.J. Stella. A kinetic and mechanistic study of the hydrolysis of camptothecin and some analogues. J Pharm Sci. 81:676-684 (1992).

212. V. Joguparthi. Physicochemical approaches to enhance the liposomal loading and retention of hydrophobic weak acids2007, p. 325.

213. V. Joguparthi and B.D. Anderson. Effect of cyclodextrin complexation on the liposome permeability of a model hydrophobic weak acid. Pharm Res. 25:2505-2515 (2008).

214. L.A. Lopez-Barcons, J. Zhang, G. Siriwitayawan, T.G. Burke, and R. Perez-Soler. The novel highly lipophilic topoisomerase I inhibitor DB67 is effective in the treatment of liver metastases of murine CT-26 colon carcinoma. Neoplasia (Ann Arbor, MI, U S). 6:457-467 (2004).

215. N. Dos Santos, K.A. Cox, C.A. McKenzie, F. van Baarda, R.C. Gallagher, G. Karlsson, K. Edwards, L.D. Mayer, C. Allen, and M.B. Bally. pH gradient loading of anthracyclines into cholesterol-free liposomes: enhancing drug loading rates through use of ethanol. Biochim Biophys Acta. 1661:47-60 (2004).

216. N. Dos Santos, L.D. Mayer, S.A. Abraham, R.C. Gallagher, K.A.K. Cox, P.G. Tardi, and M.B. Bally. Improved retention of idarubicin after intravenous injection obtained for cholesterol-free liposomes. Biochim Biophys Acta. 1561:188-201 (2002).

217. T.-H. Chou, S.-C. Chen, and I.M. Chu. Effect of composition on the stability of liposomal irinotecan prepared by a pH gradient method. J Biosci Bioeng. 95:405-408 (2003).

218. L.-A. Tai, Y.-C. Wang, and C.-S. Yang. Heat-activated sustaining nitric oxide release from zwitterionic diazeniumdiolate loaded in thermo-sensitive liposomes. Nitric Oxide. 23:60-64 (2010).

219. J. Gutknecht. Proton/hydroxide conductance and permeability through phospholipid bilayer membranes. Proc Natl Acad Sci U S A. 84:6443-6446 (1987).

220. J. Gutknecht and A. Walter. Transport of protons and hydrochloric acid through lipid bilayer membranes. Biochim Biophys Acta. 641:183-188 (1981).

221. A.S. Taggar, J. Alnajim, M. Anantha, A. Thomas, M. Webb, E. Ramsay, and M.B. Bally. Copper-topotecan complexation mediates drug accumulation into liposomes. J Control Release. 114:78-88 (2006).

222. S.A. Abraham, K. Edwards, G. Karlsson, S. MacIntosh, L.D. Mayer, C. McKenzie, and M.B. Bally. Formation of transition metal-doxorubicin complexes inside liposomes. Biochim Biophys Acta, Biomembr. 1565:41-54 (2002).

223. B. Ceh and D.D. Lasic. A rigorous theory of remote loading of drugs into liposomes: transmembrane potential and induced pH-gradient loading and leakage of liposomes. J Colloid Interf Sci. 185:9-18 (1997).

224. B. Ceh and D.D. Lasic. A rigorous theory of remote loading of drugs into liposomes. Langmuir. 11:3356-3368 (1995).

225. D.D. Lasic, B. Ceh, M.C.A. Stuart, L. Guo, P.M. Frederik, and Y. Barenholz. Transmembrane gradient driven phase transitions within vesicles: lessons for drug delivery. Biochim Biophys Acta. 1239:145-156 (1995).

226. S. Modi, T.X. Xiang, and B.D. Anderson. Application of a theoretical model to delineate the factors governing the active loading of AR-67 in ca-acetate loaded liposomes, *AAPS Annual Meeting and Exposition*, New Orleans, Louisiana, USA, 2010, p. Poster Presentation.

227. S. Clerc and Y. Barenholz. A quantitative model for using acridine orange as a transmembrane pH gradient probe. Anal Biochem. 259:104-111 (1998).

228. J. Rinehart, S. Arnold, G. Kloecker, A. Lim, M.-A. Zaydan, T. Baeker, G. Maheshwari Jewraj, H. Carloss, S. Slone, B. Shelton, J. Croley, E. Kvale, M. Brooks, and M. Leggas. Phase II randomized trial of carboplatin and gemcitabine with or without dexamethasone pre-treatment in patients with Stage IV non-small cell lung cancer. Cancer chemotherapy and pharmacology(2013).

229. M. Barel, O.A.B. Perez, V.A. Giozzet, A. Rafacho, J.R. Bosqueiro, and S.L. do Amaral. Exercise training prevents hyperinsulinemia, muscular glycogen loss and muscle atrophy induced by dexamethasone treatment. European Journal of Applied Physiology. 108:999-1007 (2010).

230. J. Vardy, K.S. Chiew, J. Galica, G.R. Pond, and I.F. Tannock. Side effects associated with the use of dexamethasone for prophylaxis of delayed emesis after moderately emetogenic chemotherapy. British Journal of Cancer. 94:1011-1015 (2006).

231. M. Leggas, K.-L. Kuo, F. Robert, G. Cloud, M. de Shazo, R. Zhang, M. Li, H. Wang, S. Davidson, and J. Rinehart. Intensive anti-inflammatory therapy with dexamethasone in patients with non-small cell lung cancer: effect on chemotherapy toxicity and efficacy. Cancer Chemotherapy and Pharmacology. 63:731-743 (2009).

232. J. Rinehart, L. Keville, J. Measel, A.M. Spiekerman, and K. Burke. Corticosteroid alteration of carboplatin-induced hematopoietic toxicity in a murine model. Blood. 86:4493-4499 (1995).

233. J.J. Rinehart and L.R. Keville. Reduction in carboplatin hematopoietic toxicity in tumor bearing mice: comparative mechanisms and effects of interleukin-1β and corticosteroids. Cancer Biotherapy & Radiopharmaceuticals. 12:101-109 (1997).

234. A. Gabizon and F. Martin. Polyethylene glycol-coated (pegylated) liposomal doxorubicin. Rationale for use in solid tumours. Drugs. 54 Suppl 4:15-21 (1997).

235. K.J. Harrington. Liposomal cancer chemotherapy: current clinical applications and future prospects. Expert Opinion on Investigational Drugs. 10:1045-1061 (2001).

236. S.M. Moghimi, A.C. Hunter, and J.C. Murray. Long-circulating and target-specific nanoparticles: Theory to practice. Pharmacological Reviews. 53:283-318 (2001).

237. T.-x. Xiang and B.D. Anderson. Substituent Contributions to the Transport of Substituted p-Toluic Acids across Lipid Bilayer Membranes. J Pharm Sci. 83:1511-1518 (1994).

238. T.-X. Xiang and B.D. Anderson. The Relationship Between Permeant Size and Permeability in Lipid Bilayer Membranes. J Membrane Biol. 140:111-122 (1994).

239. J. Nitsche and G. Kasting. Permeability of Fluid-Phase Phospholipid Bilayers: Assessment and Useful Correlations for Permeability Screening, Dermal Absorption and Other Applications. Journal of Pharmaceutical Sciences(2013).

240. K.J. Ellis and J.F. Morrison. Buffers of constant ionic strength for studying pH-dependent processes. Methods Enzymol. 87:405-426 (1982).

241. N.E. Good and S. Izawa. Hydrogen ion buffers. Methods Enzymol. 24:53-68 (1972).

242. G.L. Flynn and D.J. Lamb. Factors influencing solvolysis of corticosteroid-21-phosphate esters. J Pharm Sci. 59:1433-1438 (1970).

243. M. Grit and D.J. Crommelin. Chemical stability of liposomes: implications for their physical stability. Chem Phys Lipids. 64:3-18 (1993).

244. M. Grit, W.J.M. Underberg, and D.J.A. Crommelin. Hydrolysis of saturated soybean phosphatidylcholine in aqueous liposome dispersions. J Pharm Sci. 82:362-366 (1993).

245. N.J. Zuidam, R. De Vrueh, and D.J.A. Crommelin. Characterization of liposomes. Liposomes (2nd Edition):31-78 (2003).

246. N.J. Zuidam, E. Van Winden, R. De Vrueh, and D.J.A. Crommelin. Stability, storage, and sterilization of liposomes. Liposomes (2nd Edition):149-165 (2003).

247. P. Mukerjee. Micellar properties of drugs. Micellar and nonmicellar patterns of self-association of hydrophobic solutes of different molecular structures. Monomer fraction, availability, and misuses of micellar hypothesis. J Pharm Sci. 63:972-981 (1974).

248. P. Mukerjee and J.R. Cardinal. Solubilization as a method for studying self-association: solubility of naphthalene in the bile salt sodium cholate and the complex pattern of its aggregation. J Pharm Sci. 65:882-886 (1976).

249. K. Konno, T. Jinno, and A. Kitahara. Solubility, critical aggregating or micellar concentration, and aggregate formation of nonionic surfactants in nonaqueous solutions. Journal of Colloid and Interface Science. 49:383-389 (1974).

250. G. Basu Ray, I. Chakraborty, and S.P. Moulik. Pyrene absorption can be a convenient method for probing critical micellar concentration (cmc) and indexing micellar polarity. Journal of Colloid and Interface Science. 294:248-254 (2006).

251. K. Kalyanasundaram and J.K. Thomas. Environmental effects on vibronic band intensities in pyrene monomer fluorescence and their application in studies of micellar systems. Journal of the American Chemical Society. 99:2039-2044 (1977).

252. N.J. Turro and P.L. Kuo. Pyrene excimer formations in micelles of nonionic detergents and of water-soluble polymers. Langmuir. 2:438-442 (1986).

253. M.C. Rei, P.J.G. Coutinho, E.M.S. Castanheira, and M.E.C.D.R. Oliveira. C12E7-DPPC mixed systems studied by pyrene fluorescence emission. Progress in Colloid & Polymer Science. 123:83-87 (2004).

254. A. Shah, A.M. Khan, M. Usman, R. Qureshi, M. Siddiq, and S.S. Shah. Thermodynamic characterization of dexamethasone sodium phosphate and its complex with DNA as studied by conductometric and spectroscopic techniques. Journal of the Chilean Chemical Society. 54:134-137 (2009).

255. B.D. Anderson, R.A. Conradi, and K. Johnson. Influence of premicellar and micellar association on the reactivity of methylprednisolone 21-hemiesters in aqueous solution. J Pharm Sci. 72:448-454 (1983).

256. B.A. Cicciarelli, J.A. Elia, T.A. Hatton, and K.A. Smith. Temperature Dependence of Aggregation and Dynamic Surface Tension in a Photoresponsive Surfactant System. Langmuir. 23:8323-8330 (2007).

257. M. Cardenas, K. Schillen, V. Alfredsson, R.-D. Duan, L. Nyberg, and T. Arnebrant. Solubilization of sphingomyelin vesicles by addition of a bile salt. Chemistry and Physics of Lipids. 151:10-17 (2008).

258. T. Igarashi, Y. Shoji, and K. Katayama. Anomalous solubilization behavior of dimyristoylphosphatidylcholine liposomes induced by sodium dodecyl sulfate micelles. Analytical Sciences. 28:345-350 (2012).

259. G.A. Koning, R.M. Schiffelers, M.H.M. Wauben, R.J. Kok, E. Mastrobattista, G. Molema, T.L.M. ten Hagen, and G. Storm. Targeting of angiogenic endothelial cells at sites of inflammation by dexamethasone phosphate-containing RGD peptide liposomes inhibits experimental arthritis. Arthritis & Rheumatism. 54:1198-1208 (2006).

260. U. Rauchhaus, F.-W. Schwaiger, and S. Panzner. Separating therapeutic efficacy from glucocorticoid side-effects in rodent arthritis using novel, liposomal delivery of dexamethasone phosphate: long term suppression of arthritis facilitates interval treatment. Arthritis Research & Therapy. 11:No pp given (2009).

261. J. Gutknecht and D.C. Tosteson. Diffusion of weak acids across lipid bilayer membranes: effects of chemical reactions in the unstirred layers. Science. 182:1258-1261 (1973).

VITA

Sweta Modi

EDUCATIONAL INSTITUTIONS AND DEGREES

Master of Science (Pharmaceutics), National Institute of Pharmaceutical Education and Research (NIPER), India. Thesis: Synthesis and characterization of poly(ester-anhydride) as drug carriers for anticancer agents.	2003-2005
Bachelors in Pharmacy, NDMVPS College of Pharmacy, Nasik, India	1998-2002

PROFESSIONAL POSITIONS

Summer Intern at Pfizer Inc, Groton, CT, USA	06/2010-08/2010
Research Scientist at Nicholas Piramal India Ltd., India	06/2005-07/2007

PROFESSIONAL HONORS

- Formulation Design and Development (FDD) section travelship to attend the 2012 AAPS Annual Meeting and Exposition, Chicago, US.
- 2011-2012 American Foundation for Pharmaceutical Education (AFPE) Pre-Doctoral Fellowship
- 2012 The Pharmaceutical Research and Manufacturers of America (PhRMA) Pre-Doctoral Fellowship
- Selected to represent University of Kentucky at GPEN 2012 at Melbourne, Australia (GPEN Sponsorship)
- Graduate Student Incentive Award (For recipients of nationally competitive fellowship of more than $10,000)
- U Kentucky Research Assistantship (2008-2012)
- U Kentucky Graduate School Travel Award (2010, 2011, 2012) for attending AAPS
- U Kentucky Teaching Assistantship (2007-2008)
- NIPER Fellowship (Jul 2003 – May 2005)
- Second prize in oral presentation at Graduate Student Interdisciplinary Conference 2011
- Third prize in poster presentation at Rho Chi Research Day 2011

PUBLICATIONS

Sweta Modi, Tian-Xiang Xiang and Bradley D Anderson, Enhanced Active Loading of Poorly Soluble Ionizable Drugs into Liposomes Using Supersaturated Drug Solution, ***J. Controlled Release*** 162 (2) (2012) 330-339.

Sweta Modi, Jay Prakash Jain, Abraham J. Domb, Neeraj Kumar**,** Exploiting EPR for tumor targeting in polymer drug conjugate delivery, ***Current Pharmaceutical Design*** 12(36) (2006) 4785-4796.

Sweta Modi, Jay Prakash Jain, Abraham J. Domb, Neeraj Kumar, Copolymers of pharmaceutical grade lactic acid and sebacic acid: Drug release behavior and biocompatibility, ***Eur. J. Pharm. Biopharm***., 64(3) (2006) 277-286.

Sweta Modi, J.P. Jain, and Neeraj Kumar**,** Synthesis, characterization and degradation of poly(ester-anhydride) for particulate delivery, ***Israel J. Chem.***, 45(2005) 401-409.

Jay Prakash Jain, **Sweta Modi**, Abraham J. Domb and Neeraj Kumar**,** The role of polyanhydrides as localized drug carrier, ***J. Controlled Release*** 103 (2005) 541-563.

Jay Prakash Jain, Vrushali Waknis, **Sweta Modi**, M.N.V. Ravikumar and Neeraj Kumar**,** Trapping EPR for polymer drug conjugate delivery, ***Drug Delv. Tech.*** 5(3) (2005) 65-69.

Jay Prakash Jain, **Sweta Modi**, and Neeraj Kumar**, "**Hydroxy fatty acid based polyanhydride as drug delivery system: Synthesis, characterization, *in vitro* degradation, drug release and biocompatibility" ***J. Biomed. Mater. Res A.*** 84(3) (2008) 740-52.